Toxicology and Cellular Interactions of Polymer-based Nanocarriers for Pulmonary Drug Delivery

NASHWA MOSTAFA MAHMOUD OSMAN

Thesis submitted in partial fulfillment of the requirements of Liverpool John Moores University for the degree of Doctor of Philosophy

November 2020

Table of Contents

List of Tables

List of Figures

List of Abbreviations

7-AAD	7-Aminoactinomycin D
AB	Alamar blue assay
AD	Aerodynamic diameter
ALI	Air-liquid interface
ARDS	Acute respiratory distress syndrome
CF	Cystic fibrosis
CLSM	Confocal laser scanning microscopy
COPD	Chronic obstructive pulmonary disease
CTAB	Hexadecyltrimethylammonium bromide
DCM	Dichloromethane
DOTAP	1,2-dioleoyl-3-trimethylammoniumpropane
DVA	Divinyl adipate
EPR	Enhanced permeability and retention effect
FBS	Fetal bovine serum
FC	Flow cytometry
FITC	Fluorescein isothiocyanate
FSC	Forward scatter characteristics
Inh1	Dynasore hydrate
Inh2	Genistein
Inh3	Cytochalasin-D
Inh4	Nocodazole
Inh5	EIPA
Inh6	Methyl-β-cyclodextrin
Inh7	Chlorpromazine
LCC	liquid-covered culture
LDH	Lactate dehydrogenase
MC	Macrophage clearance
MCC	Mucociliary clearance/escalator
MP	Microparticle

NC	Negative control/untreated cells
NP	Nanoparticle
NPMPs	Nanoparticle in microparticle composite
NR	Nile red
NSCLC	Non-small cell lung cancer
PF68	Poloxamer188
QSAR	Quantitative structure–activity relationships
Tg	Glass transition temperature
THF	Tetrahydrofuran
TJs	Tight junctions
Tm	Melting temperature
w/o	Water-in-oil
w/o/w	Water-in-oil-in-water
TB	Tuberculosis
PEG	Polyethylene glycol
MFI	Median Fluorescence Intensity
TEER	Transepithelial electrical resistance
PG	*PG*A-co-PDL
PL	*PLGA*
CS	chitosan
PVA	Polyvinyl alcohol
DAPI	4',6-diamidino-2-phenylindole
DSC	Dynamic scanning colorimetry
***PLGA*, *PL*A, *PG*A**	Poly (lactide-co- glycerol), poly (Lactic acid), poly (glycolide) polymers
JC-1 dye	5,5,6,6’-tetrachloro-1,1’,3,3’ tetraethylbenzimi-dazoylcarbocyanine iodide
BSA	Bovine serum Albumin
SSC	Side scatter characteristics
LT-26	LysoTracker® Green DND-26
SFL	Simulated lung fluid

MT	MitoTracker™ Green
P*app*	Apparent permeability coefficient
ΔΨm	Mitochondrial membrane potential
MW	Molecular Weight
mPTP	Mitochondrial permeability transition pore
LPS	Lipopolysaccharide
DMAB	Didodecyl dimethyl ammonium bromide
SCLC	Small cell lung cancer
PC	Positive control/treated cells
PEG	Polyethylene-glycol polymer
RES	Reticuloendothelial system
ROS	Reactive oxygen species
AF488	Alexa Flour®488-Phalloidin
H_2DCFDA	2′,7′-Dichlorofluorescin diacetate
CM	Complete media/medium containing 10% FBS
DW	Purified water
SEM	Scanning electron microscopy
SFM	Serum free media/medium
TEM	Transmission electron microscopy
N*P*-NR	Nanoparticles labelled with Nile Red
PDI	Polydispersity index
w/v	Weight/volume
PMA	Phorbol 12-myristate 13-acetate
w/w	Weight/weight
PBS	Phosphate buffer saline
GPC	Gel permeation chromatography

List of Publications and Awards

Publications:

- **Osman NM**, Sexton DW, Saleem IY. Toxicological assessment of nanoparticle interactions with the pulmonary system. Nanotoxicology.14(1):21-58. 2020.
- Kaneko K., **Osman N**., Carini V., Scagnetti G., Saleem I. Overview of the Advantages and Disadvantages of Different Mucosal Sites for the Delivery of Nanoparticles. In: Muttil P., Kunda N. (eds) Mucosal Delivery of Drugs and Biologics in Nanoparticles. AAPS Advances in the Pharmaceutical Sciences Series, vol 41. Springer, Cham, 2020.
- **Osman N**, Kaneko K, Carini V, Saleem I. Carriers for the targeted delivery of aerosolized macromolecules for pulmonary pathologies. Expert Opinion on Drug Delivery.15(8):821-34. 2018
- N. Basar, O. A. Oridupa, K.J. Ritchie, L. Nahar, **N. M. Osman**, A. S., H. Kushiev, A. Kan, S.D. Sarker. Comparative Cytotoxicity of Glycyrrhiza glabra Roots from Different Geographical Origins against Immortal Human Keratinocyte (HaCaT), Lung Adenocarcinoma (A549) and Liver Carcinoma (He*PG*2) Cells. J Phytotheraphy Research.29 (6):944-948. 2015.

Oral/ Poster Presentations and Conference proceedings (4-page abstract):

- **Osman N M,** G. A. Hutcheon, Darren Sexton, I. Y. Saleem. Size and Charge Dependent Inflammatory Response of Polymeric Nanocarriers. CRS. NY (2018).

- **Osman N M:** Nanomedicine: Toward tailoring the future of medicines- FAMELAB- LJMU-2017.

- **Osman N M**, G. A. Hutcheon, Darren Sexton, I. Y. Saleem. *In-Vitro* Pulmonary Cytotoxicity of Novel Polymeric Nanocarriers for Drug Delivery'. Pulmonary Drug Delivery (PDD), Turkey, (2017).

- **Osman N M**, G. A. Hutcheon, Darren Sexton, I. Y. Saleem. *In-vitro* Cytotoxicity of Novel Polymeric Nano Carriers for Pulmonary Drug Delivery. AAPS. (2016).

- **Osman N M**, G. A. Hutcheon, Darren Sexton, I. Y. Saleem. *In-vitro* Cytotoxicity of Nano Carriers of A Novel Polymer For Pulmonary Drug Delivery. BSNM. (2016).

- **Osman N M**, G. A. Hutcheon, Darren Sexton, I. Y. Saleem. Comparative Nanotoxicology of Novel Polymeric Nanocarriers with Different Surface Charge against Human Lung Epithelial Cells. Drug Delivery to the Lung (DDL) (2016).

- **Osman N M**, K. Sin, J. Jaffer, K. Ritchie, I. Y. Saleem, G. A. Hutcheon (2015):'' Degradation of *PLGA* and *PGA-co-PDL* Polymeric Carriers in Simulated Lung Fluid for Pulmonary Drug Delivery''. UK and Ireland Controlled Release Society (2015).

- **Osman N**, Hilal M, Mohamed S, Dawood A, Ritchie K, Saleem I, & Hutcheon G. *In-vitro* Stability and Degradation of *PLGA* and *PGA-co-PDL* Microparticles for Pulmonary Drug Delivery. DDL Conference (2015).

- Adel A. Mohamed, **Osman N M**, Imran Y. Saleem, Gillian A. Hutcheon'' Dioleoyltrimethylammoniumpropane (DOTAP) modified poly (glycerol

adipate-co-ω-pentadecalactone) *PGA-co-PDL* nanocarrier for pulmonary delivery''. INTERREG IV A 2Sea Training School; UoG-AAPS Chapter Conference (2014).

These publications contributed to the science pool with reviewing the up to date knowledge regarding the generated NPs types so far, the nanotoxicological potentials of pharmaceutical, environmental, and occupational NPs with a focus on the mucosal contact and pulmonary route of delivery. I had presented many oral and poster presentations to present my findings to the scientific community and challenge some of the commonly employed assay with a recommendation to improve the methods to accommodate for the NPs interference possibilities. I had provided few evidences and cases where NPs interference with the assays have to be suspected and evaluated.

Awards, Funding, and Honors:

- **3MT Thesis Winner in 2018**: I won the 3MT Thesis competition where the PhD students are challenged to present their PhD research to public audience only in 3 minutes. I won the best oral presentation prize (£ 200) for School of Pharmacy and Bimolecular Sciences-LJMU.
- **Travel Award from Pulmonary Drug Delivery (PDD) in 2017**: to attend the PDD conference in Turkey (£ 500).
- ***PG*R Travel Fund Award in 2016:** from Faculty of Science to attend Controlled Release Society conference (£ 375).
- **Best Oral Presentation in 2011:** 2nd Young Researchers Conference, Egypt. I won the best oral presentation award in delivering my MSc research to scientific audience (EG 1000).

- Moderator: The Faculty Research Seminar Day, 2019 (LJMU)
- Associate Fellow of the Higher Education Academy (UK)
- Member of Royal Society of Chemistry (MRSC)
- Member of British Toxicology Society (BTS)
- Member of British Society Nanomedicine (BSNM)
- Member of Controlled Release Society (CRS)
- Member of American Association of Pharmaceutical Scientists (AAPS).

Acknowledgement

I would like to express my sincere gratitude to Allah for providing me with guidance and support to overcome all the obstacles in my PhD path. I would like to thank my parents who without their endless support and dua'a (prayer) I could not have completed my PhD. I would like to thank my brothers and sisters (Susan, Mohamed, Hossam, Khalid, Amal) for their endless care of me during my PhD. I would like to thank my husband, Carl Werbisky, for his understanding and continued support during my PhD.

I would like to thank my supervisor Prof Imran Saleem for his continued guidance, support, encouragement and motivation during my PhD. I am very grateful for his constant support in guiding my PhD project and writing-up my thesis. I would like to thank my co-supervisor Dr Darren Sexton for his constant support and kind guidance. I would like to thank all my group of Formulation and Drug Delivery, Biology and Imaging Labs in LJMU for their continued support and guidance. I would like to thank Dr Neill Liptrott, Dr Helen Box, Dr Paul Curley and all his research group in the Nanomedicine Lab, University of Liverpool (Faculty of Medicine) for their kind co-operation to use the lab facilities and their kind support to perform the permeability studies. I would like to thank my Egyptian mentors; Dr Abdelwahab Dawood, Dr Maha Hilal, Dr Sohier Soliman for their continuous support and encouragement during this PhD (Faculty of Medicine, Sohag University, Egypt).

I would like to thank all my friends and lab colleagues for their kind support and encouragement during this PhD.

Finally, I would like to say; without everyone's love and care, I could not have made it through.

Abstract

The attractiveness and enhanced applications of nanoparticles (NPs) stem from their exceptional properties at the nanoscale size, i.e., 1-1000 nm, they may exhibit nano-specific toxicological concerns. Hence, the toxicological assessment of NPs and their interactions within biological systems are investigated and continuously evolving to ensure their safety at the nanoscale.

This project explored the nanotoxicology potential of NPs fabricated from two polymers; *PGA-co-PDL*(*PG*), and *PLGA* (*PL*). NPs of different sizes and charges were successfully formulated; 200 nm (*PL* and *PG*; to explore chemistry effect), 500 nm and 800 nm (*PG* only; to explore size effect), and with different charges; negatively-charged using PVA as emulsifier, and positively charged NPs using DOTAP as emulsifier (to explore surface charge effect) via emulsification-solvent evaporation methods.

A stability and degradation studies were evaluated in different biological media. All NPs showed better stability in SFM than CM. *PL* NPs showed faster degradation with acidic pH changes, while *PG* NPs showed slower degradation with an alkaline pH slowly decreasing toward the neutrality by the end of 28 days. This denoted better suitability of *PG* NPs for lung delivery with lower acidic changes.

A nanotoxicological screen evaluation by a variety of *in vitro* assays (viability by alamar blue assay, reactive oxygen species by H_2DCFDA reagent and Deep Red ROS assay, mitochondrial membrane potential ($\Delta\Psi m$) by JC-1 dye, cell membrane integrity by LDH Total and Release, cell death; apoptosis and necrosis, caspases activation, inflammatory potentials (IL-8, IL-2, IL-4, IL-6, IL-10, IL-17a, TNF-α, INF-ɣ), and genotoxicity potential by COMET alkaline gel electrophoresis assay) of all NPs

were investigated. The NPs showed cytotoxicity that was dependent on the physicochemical nature of the NPs where *PG* showed biocompatible cellular responses that can be compared to *PL* at low concentrations as similar or better. The size increase was associated with a limited uptake for the larger sized NPs resulting in lower cytotoxicity at low concentrations to smaller NPs, however, higher cytotoxicity was observed at high concentrations. In addition, negatively charged NPs were reported to be more cytotoxic than their positive counterparts that were correlated to the larger size of positive NPs after dispersion in media that was associated with limited uptake.

The underlaying cytotoxicity mechanisms after these NPs exposure demonstrated involvement of ROS, lowering ΔΨm, release or decrease of LDH, apoptosis, caspases activation (Caspase 8 > caspases 3/7 > caspase 9), inflammatory potential (IL-8, IL-6, TNF-α, INF-ɣ), but no genotoxicity was detected. However, there were many challenges on the application of different assays that required optimization to improve the accuracy of the results and ensure the results measured were due to NPs interactions with the cells (to exclude NP interferences). These were addressed and validated.

In addition, the integrity of the epithelial barrier was investigated *in vitro* using Calu-3 polarized tight monolayers grown under ALI to mimic *in vivo* epithelial lung exposure. The internalisation and uptake mechanisms were investigated under 4 ^{o}C, and 37 ^{o}C temperatures with the use of a group of pharmacological inhibitors to cover a wide range of endocytic mechanisms after 1 hr exposure to NPs. A visual confirmation and subcellular trafficking for NPs were performed using confocal microscopy. All NPs didn’t show any impairment of tight junctions (TJs). All NPs sowed active endocytic uptake via caveolin, clathrin and macropinocytosis. Visual confirmation of

internalisation and co-localisation with lysosomes and mitochondria that confirmed the vesicular transport and possible therapeutic potentials to target subcellular targets. This indicated the potential therapeutic targeting of these NPs to subcellular targets such as lysosomes and mitochondria.

Overall, these studies had explored the potential safe use of these polymeric NPs for lung delivery. *PG* showed better profile of slower degradation (can be used for sustained formulations), of less acidic changes (less risk of acidity and inflammatory stimulation), and biocompatible profile that can be explored for *in vivo* lung delivery. The different sizes of NPs have shown potential use for lung delivery where the small sized NPs can be used for targeting deep lung while the larger size can be aimed for vaccine targeting to allow macrophages uptake.

1. General Introduction

1.1. Pulmonary Route for Nanoparticle Drug Delivery:

Respiratory diseases occupy four of the top ten conditions associated with global mortality; chronic obstructive pulmonary disease (COPD), lower respiratory tract infections, lung cancer, and Tuberculosis. Together they represent one sixth of global deaths and is expected to increase to one fifth in the next five years (1). Hence, the respiratory diseases have a huge health burden. Scientists are actively trying to tackle the respiratory problems with novel formulation approaches to intensify local and systemic drug delivery purposes based on its immense health implication. Nano-enabled pulmonary drug delivery is a very active area of research with successful translation to pharmaceutical and clinical uses overcoming both pharmaceutical and clinical challenges. Although the attractiveness and enhanced applications of these nanoparticles (NPs) stem from their exceptional properties at the nanoscale size, i.e., 1-1000 nm, they exhibit completely different physicochemical profiles and, subsequently, toxicological profiles from their parent bulk materials. Hence, the toxicological assessment and the clinical evaluation of NPs interactions within biological systems are continuously evolving to ensure their safety at the nanoscale.

1.1.1. Pulmonary System Structure and Functions:

The respiratory system is a complex vital organ that has two structurally different regions; conducting (upper) and respiratory (lower) part (Figure. 1.1. A) (2, 3). The conducting airways start from the mouth/nose, followed by the trachea and extending to approximately 17 generations, based on the Weibel's lung model (4), until reaching the respiratory bronchioles with progressive narrowing in length and diameter (5). The lining epithelium is pseudo-stratified ciliated with tight junctions, with abundant mucous glands, which secret mucous that is responsible for the air filtration, humidity, and acts with the motile cilia to provide mucociliary clearance/escalator

(MCC) (Figure. 1.1. B). The epithelial thickness is approximately 60 µm and lined with a thick mucus layer with a cover layer of a lung surfactant (6). Diseases affecting the conducting airways, i.e., asthma, CF, COPD, impair the respiratory functions by developing pulmonary hypertension and aggravating the bronchoconstriction and congruently, impairing the conventional treatments. Hence, improving the efficiency of NPs drug delivery to the lungs and/or the drug absorption by NPs. The respiratory airways are distal to the terminal bronchioles consisting of the respiratory bronchioles and alveolar ducts ending in alveolar sacs (18-25 generations).

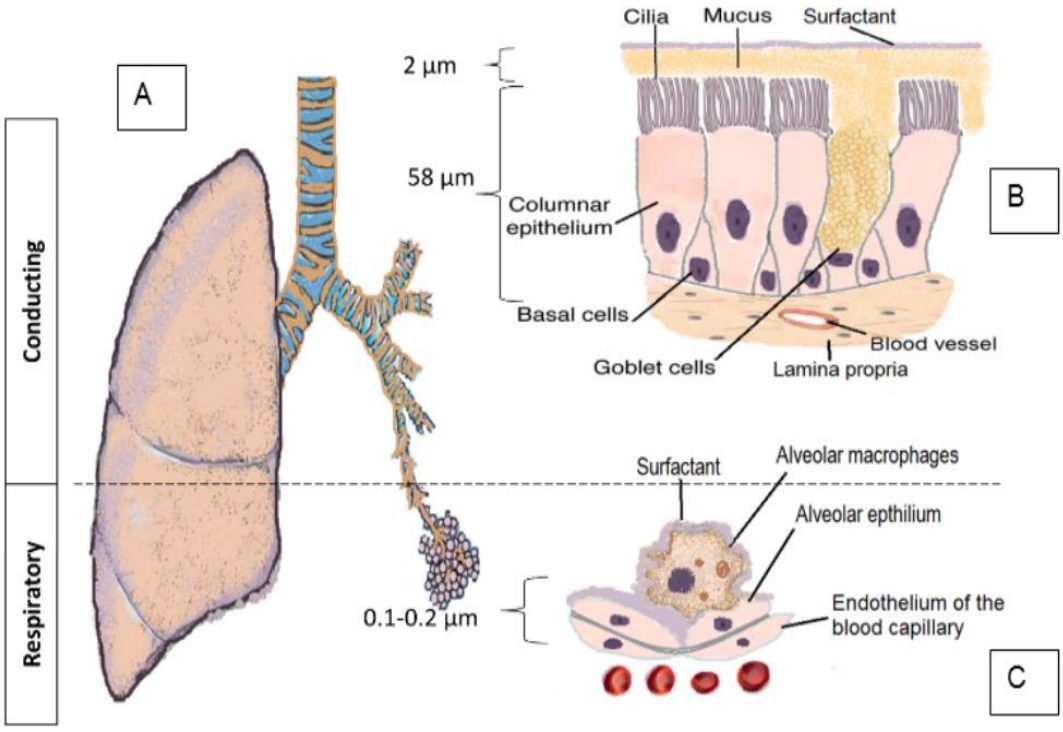

Figure. 1.1. Lung structure and epithelial differences: (A) Respiratory system structure, (B) Conducting region epithelium, and (C) Respiratory region and air-blood barrier (Reprinted with permission (35)).

The alveolar lining consists of two main cell types (Figure. 1.1. C): Alveolar type I, which is the main cell type, involved in the alveolar air-blood barrier, and the alveolar cell type II, which is responsible for secreting lung surfactant. It has a plethora of immune cells rich in macrophages that are responsible for clearance and eliminating

particles (7). The lining epithelium is very thin, 0.1-0.2 µm, with a fluid lining thickness of 70 nm. The alveolar epithelium has tight and gap junctions and shows high permeability. Diseases affecting the respiratory region are very common debilitating conditions, such as infections, tuberculosis, emphysema, lung fibrosis, lung cancer, acute distress and pulmonary oedema.

1.1.2. Rational, Advantages, and Limitations of Drug Delivery via the Lungs:

Pulmonary route for drug delivery offers many advantages over other routes of drug administrations but has its own limitations (summarized in Table. 1.1). The pulmonary system is an attractive route for local drug delivery due to its unique structural features that can permit minimal off-target systemic interactions and less side effects. This can be of a great importance to target agents which have high systemic toxicity to be limited to local lung targets e.g. lung cancer and chemotherapeutics (7).

Pulmonary drug delivery offers many advantages to improve patient compliance, and quality of life in the management and / or treatment of lung cancer, asthma, COPD, infections and other lung chronic conditions. Direct lung administration enhances the therapeutic efficiency, with higher local concentrations achieved with lower doses, frequency and is non-invasive (8). The large surface area of the respiratory epithelium (up to ~140 m^2 in adults), its dense vasculature, and ultra-thin respiratory air barrier (compared to the thick enteric epithelial barrier, ~25 µm) offers fast systemic delivery as an alternative route to IV in case of targeting systemic drugs via the lungs. The lungs are in continuous exposure to the fast heart-lung circulation (~5 L/minute), bypassing the hepatic metabolism with a limited proteolytic capacity (better option for systemic delivery of aerosolized macromolecules, such as proteins/peptides, and gene therapy) achieving almost near or equal IV bioavailability (9).

Notwithstanding these considerable advantages of inhalation, deposition of the drug is rapidly cleared by MCC and MC, limiting its effective residence time and concentrations. The difficulty in achieving drug deposition deep into the lungs is due to the physical branching and narrowing with off-target binding limiting its efficiency. Drug particle damage during the aerosolization process carries another challenge for successful lung delivery. Hence, NPs offer great promises to improve the lung drug delivery, including polymeric NPs. These NPs are composed from biodegradable and biocompatible materials and offer better control of physicochemical characteristic such as size, shape, charge. Furthermore, they can be tailored to improve the pharmacokinetics and the aqueous solubility of hydrophobic drugs, enhance stabilizations or protection of the active agent against enzymatic degradation, and offer the feasibility of functionalization and surface coating with targeting moieties (10).

Table. 1.1. Advantages and limitations of the pulmonary route for drug delivery, and strategies to overcome these limitations (11).

Advantages pulmonary delivery	Limitations of pulmonary route	Strategies to overcome the limitations
• Wide surface area of the respiratory part; ~ 140 m^2, compared with the conducting airway; merely 2-3 m^2, allows for greater contact surface area for drug action (12) offering high bioavailability and fast action.	• The pulmonary airways undergo progressive narrowing that traps particles away from the deep alveoli (13).	• Nanomedicine strives to design NPs with tuneable NP size that can target either upper airways with large sized particles or the lower airways with small sized particles (14).
• Epithelial thickness reduced to submicron (0.2 µm) from approximately 60 µm in the conducting areas, accompanied with thinning of lining fluid layer (from 8 µm to 70 nm) (5).	• The internal humidity affects the hygroscopic particles favouring their size increase, impaction away from the respiratory areas, and early clearance.	• The internal humidity is being employed to overcome the NPs aerosols impaction in the upper airways using small size NPs that grow in size by hygroscopicity to be inhaled then trapped in the lower airways (15) (16).
• Respiratory epithelium is densely vascularised (5 L/min) with fast drug distribution and circulation (17). Highly permeable to small hydrophilic molecules, water and macromolecules and dependent on physicochemical properties, for example, lipophilicity, size, molecular weight (inversely affecting the absorption), etc.	• The lining epithelium very tight and is especially thick in conducting region with very thick mucus layer and lung surfactants, representing a challenge for the inhaled particles to penetrate (9).	• Tuning the physicochemical NPs properties to enhance drug permeability: various absorption, mucoadhesive and mucopenetrating functionalization, tight junction modulators and permeation enhancers are employed to overcome the mucous layers, tight junctions and epithelial barrier. • The use of cationic particles that increase the NP-epithelial interaction (14).

Continued. Table. 1.1. Advantages and limitations of the pulmonary route for drug delivery, and strategies to overcome these limitations **(11)**.

Advantages pulmonary delivery	Limitations of pulmonary route	Strategies to overcome the limitations
• Non-invasive, with lower dose and dose fraction compared to other routes of administration, improving the patient compliance and decrease the potential side effects (18).	• The effective MCC eliminates inhaled particles representing a challenge (19).	• NP engineering to design the size very small to escape upper airway impaction. • The use of mucous penetrating, absorption enhancers (20) • Coating with hydrophilic polymers, e.g., PEG, or lung surfactants (21). • Hygroscopic particles (16).
• High pulmonary bioavailability stems from the epithelial properties and no hepatic first pass metabolism, with limited local metabolism allowing efficient drug delivery.	• The macrophages clearance (MC) phagocytising inhaled particles (22).	• To overcome the phagocytic clearances, various mechanisms can be employed such as optimal size above or below the phagocytic capacity; large porous particles, hollow particles or trojan particles, swellable or hygroscopic particles, shielding the NPs with PEG or other shielding polymers (16, 23). • That could be stimulated to induce the immune response and for the vaccination (24-27)
• Pulmonary drug administration proved successful in delivering local treatments for respiratory problems as asthma, COPD, lung cancer and lung infections etc. as well as systemic diseases through delivery of	• Pulmonary system is affected by many diseases that decrease the airflow limiting the efficiency of the aerosol delivery to deep lung (28).	• Different aerosol delivery devices that can be used to adjust the rate of flow and deposition with the lung conditions • Fabrication of NPs from safe biodegradable and biocompatible materials with surface

Continued. Table. 1.1. Advantages and limitations of the pulmonary route for drug delivery, and strategies to overcome these limitations **(11)**

Advantages pulmonary delivery	Limitations of pulmonary route	Strategies to overcome the limitations
delivery of therapeutic molecules as protein/peptide or gene delivery, hormonal therapy or vaccines (19).	• Potential NP toxicity and Inflammation (11).	functionalization to enhance drug delivery efficacy (8). • Full NPs characterizations and nanotoxicological: NPs carefully investigated to be biocompatible and biodegradable to exclude any adverse effects from toxicity or inflammatory effects (29, 30)

1.2. Nanoparticles as Promising Drug Delivery Vehicles:

NPs are fuelling the development of a novel class of medicines retaining engineered NPs for various theranostic applications such as analytical nano-devices, novel nanotherapeutics, drug delivery and targeting nanocarriers, tissue engineering, clinical and toxicological applications. All these applications are under the umbrella of *Nanomedicine*.

Due to their nanosize, NPs can easily penetrate the cellular barriers and migrate to the site of action and cross-different types of biological barriers (31, 32). In addition, NPs can enhance pharmaceutical properties such as drug stability, dissolution rate, and bioavailability; especially important for poorly soluble and hydrophobic drugs (33). NPs have versatile capacities to encapsulate different types of molecules; not only drugs, but also macromolecules (34-36), biopharmaceuticals (37, 38), nucleic acids and gene therapeutics (39-42). They efficiently allow for multidrug or combinational therapy targeting (43-46) achieving synergistic, or multi-targeting, or theranostic applications. Functionalized NPs can deliver the active substance intracellularly (47). Furthermore, NPs could be modulated with mechanisms to target only the diseased tissue or cells, either passively, through the enhanced permeability and retention effect (EPR) (increased local blood supply tends to pool the NPs as in case of tumour sites), or actively, through targeting molecules like antibodies (here the tumour cells selectively intake the NPs) (48, 49). In addition, NPs can be equipped with mechanisms to allow the control of drug release, i.e., sustained or slow release, pulsatile or stimuli-responsive release (50-52). The release profile from these carriers can be tuned by enhancing their physicochemical properties (32). These mechanisms would boost the drug bioavailability at the site of action, bypassing the hepatic metabolism, lowering the off-target systemic side-effects and improving the therapeutic efficacy, patient

compliance, and health outcomes. NPs delivered systemically showed better circulatory distribution profiles and less aggregation compared to microparticles (51, 53, 54).

Recently, biodegradable polymers appeared very attractive for pharmaceutical applications, fuelling the development of drug delivery systems due to their biocompatibility, biodegradability, diversity and versatility of physicochemical properties, and ease of fabrication and functionalization (10, 55-58). Although nanomedicines enhance the drug efficacy and reduce toxicity, potential risks and unique challenges may occur due to the exceptional properties of their engineered nanomaterials. This has led to the development of a new branch of science, known as *Nanotoxicology*, to understand, determine, and regulate the main factors underlying the toxicological concerns of nanomaterials (32, 59, 60).

1.2.1. Biodegradable Polymers for Nanoparticles Fabrication:

Biodegradable polymers are fuelling the advances in NP drug delivery and other biomedical applications (Figure. 1.2), i.e., tissue engineering, development of drug delivery devices, gene therapy, overcoming biocompatibility, invasive application and removal processes (61, 62).

There is a continuous evolution to tailor polymeric materials to suit a variety of target applications, delivery approaches, and various tissues, and to develop new polymers to conquer the current and emerging pharmaceutical and clinical challenges.

The ideal biodegradable polymers should achieve a wide range of criteria (62-64):

- They are easy to synthetize and purify, and can be scaled-up,
- They are versatile or flexible to be used by different fabrication methods,
- They have long-shelf life,

- Their biodegradation time and behaviour should suit the required application, the resultant products should be easily eliminated and non-toxic to the body,
- They are flexible; easily functionalized to suit different applications
- They are versatile to load a variety of drugs; hydrophilic, hydrophobic, macromolecules and genes,
- They are biocompatible; however the biocompatibility is not an inherent property but depends on the nature of the biological environment at the target site, and the physicochemical properties of the fabricated device such as polymer chemistry; chain and monomeric structure, crystallinity, MW, solubility, size, shape, surface area, impurities and any adjuvants used, degradation process.

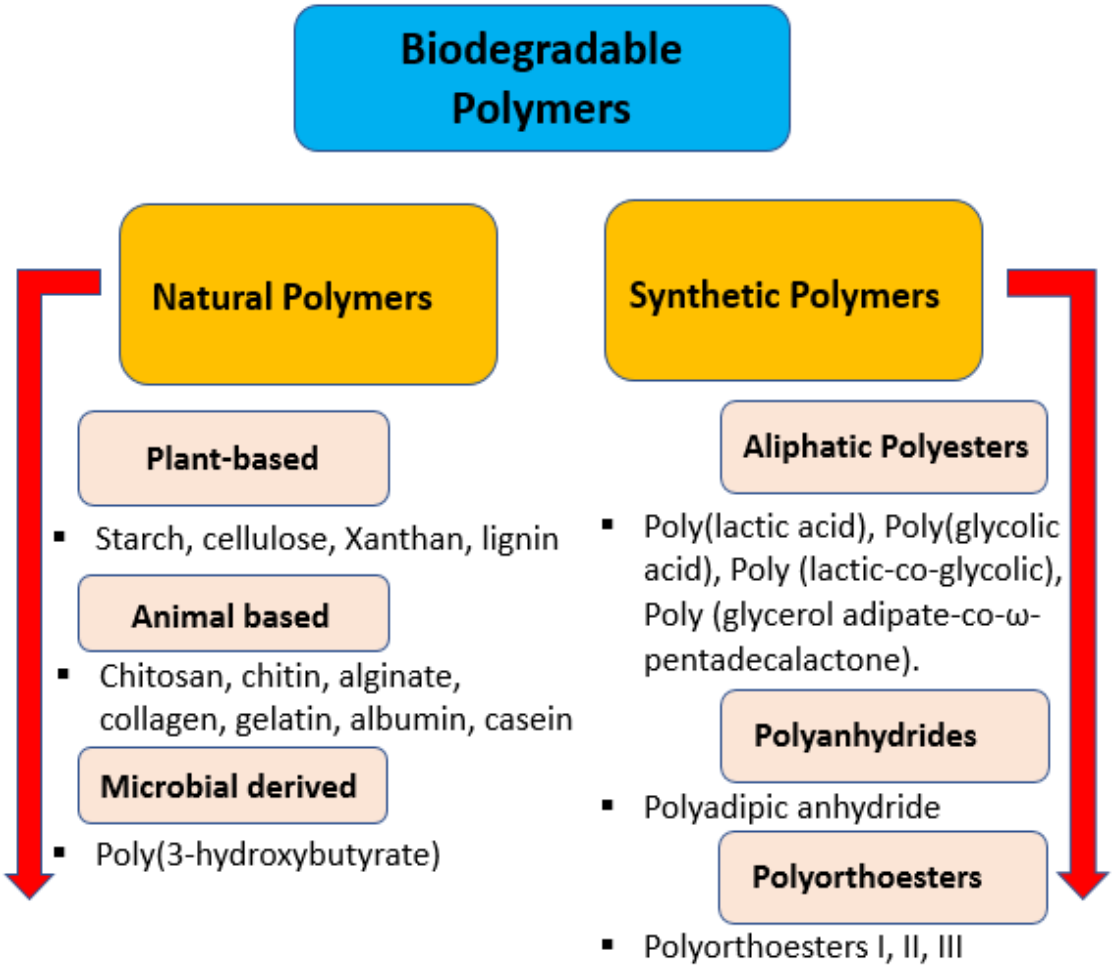

Figure. 1.2. Biodegradable polymers for drug delivery purposes (64).

Natural biodegradable polymers mostly undergo enzymatic degradation that will vary according to the site of application and its abundance of enzymes. They have some disadvantages such as a costly process of production and purification, their inherent bioactivity and immunogenicity (63, 64). Synthetic biodegradable polymers are widely used for fabrication of NPs due to many advantages they offer. The synthetic polymers can be easily synthesized with high purity (61). They are very versatile in nature that allows for modification of their physicochemical properties that permit a variety of pre- or post-synthetic alterations. Their biodegradability and general biocompatibility render them safe for use in many applications. The degradation profile can be easily tuned with subsequent easy elimination of the degraded products (61).

Poly α-esters are a wide group of synthetic polymers that are commonly used in various biomedical application for NPs formulations, for example, poly (Lactic-co-glycolic acid) (*PLGA*), poly (Lactic acid) (*PLA*), poly (glycolide), *PGA* (Figure. 1.3). They are synthetized via ring-opening condensation polymerization and possess a hydrolytic labile ester linkage that causes them to undergo bulk erosion (63, 65).

PGA is one of the earliest polymers to be investigated as biodegradable suture (DEXON $_{VR}$), tissue scaffolds, and bone screws due to its high tensile strength (Figure. 1.3). *PGA* has fast degradation and insolubility in common solvents (dichloromethane, acetone, chloroform, tetrahydrofuran) made it difficult to be used for drug delivery devices and NPs formulations. *PGA* degrades by hydrolytic degradation to glycine and glycolic acid that can be excreted through the kidneys or further oxidized in Krebs cycle to water and carbon dioxide and eliminated via the lungs. However, *PGA* degradation with accumulation of glycolic acid at the site of action has resulted in increased local acidity and induction of undesirable inflammatory response, limiting its use (64, 66).

PLA is produced from polymerization of lactic acid that can be naturally derived from starch and sugarcane (Figure. 1.3). It is found in three isoforms either poly L-lactide, (*PLLA*), poly D-lactide (*PDLA*) or a mixture of both (*PDLLA*) due to its chirality. *PL*A are very hydrophobic (limited cell adhesion) due to the free methyl groups and degrade slower over time compared to *PGA*. *PL*A degradation time depends on the MW and the racemic form, with longer chains of high MW are very slow degrading (can take up to few years). Co-blending *PLA* with other polymers such as *PGA* (*PLGA*), PEG, caprolactone, and shortening its polymer structure lowered its crystallinity, increased their degradation time and improved its hydrophobicity. *PLA* has been used for systemic NPs or microparticles (MPs) and topical drug delivery (64).

PLGA (Figure. 1.3) is a co-polyester polymer that is formed from ring-opening polycondensation of the both; *PG*A and *PL*A to improve upon their characters (67). It has versatile abilities to tune its MW (4-240 KDa, by controlling the polymeric chain length), degradation rate (slow to fast degrading) and hydrophobicity, crystallinity (amorphous to crystalline) by controlling the polymerization conditions and monomeric ratios. *PLGA* degradation can be altered by changing the monomeric ratio of its two polymers, for example *PLGA* 75:25 ratio (75% lactic acid to 25% glycolic acid) shows very slow degradation compared to *PLGA* 50:50 that shows the fastest degradation with the fastest drug release and hence very appealing for NPs drug formulations. The hydrophobicity is due to the methyl groups of lactide residues. *PLGA* has a Tg and low Tm in the range of 40-60 ^{o}C, hence in physiological temperature it retains its rigid chain structure (56, 64, 68).

PLGA is soluble in a wide range of solvents either chlorinated (for more lactide content) or fluorinated (more glycolide content) solvents. *PLGA* undergoes hydrolysis of its ester linkages and the rate is dependent on its monomeric ratio, the higher the

lactides the slower the degradation rate. The terminal end of the polymer can be either free carboxylic acid or ester capped that is slower degrading than the former. *PLGA* can be functionalized covalently and non-covalently with other polymers to produce a wide range of matrices to assist in stealth effects, controlled release or stimuli-responsive, and targeting. This versatile nature of *PLGA* has made it a very attractive candidate for many biomedical applications as biodegradable sutures, implants and prosthetic devices, tissue engineering, and very recently formulating many NPs, microparticles (MP), other drug carriers and successful loading of different drugs and macromolecules that many of them have been approved by the FDA for clinical use (68-70).

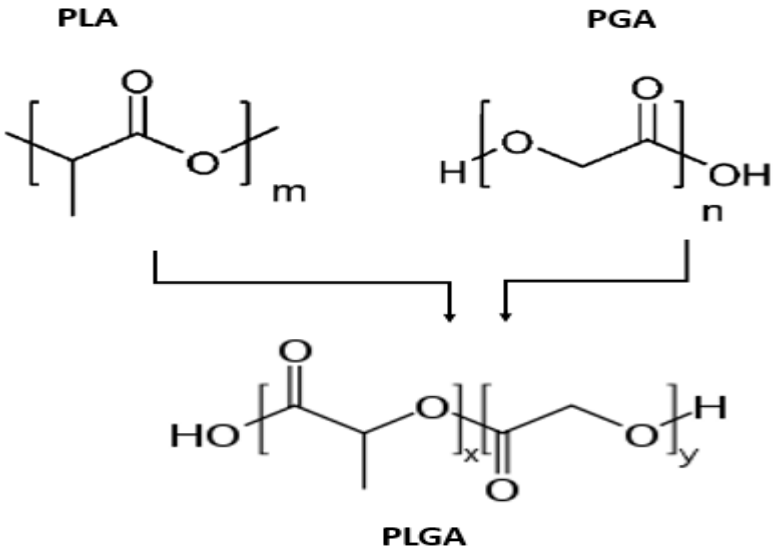

Figure. 1.3. *PGA*, *PLA*, and *PLGA* structure; *x:* units of lactic acid and *y:* units of glycolic acid.

Upon *PLGA* degradation, original monomers (lactate and glycolate) are among the common by-products of many cellular metabolic reactions. D-lactides are excreted without further metabolism through the kidneys, while L-lactide are further metabolized to pyruvate that enters Krebs cycle. Glycolate can be excreted directly via the kidneys or further oxidized to either glyoxylates, glycine, serine or pyruvate. These monomers will be oxidized by Krebs cycle to CO_2 and water that will be easily

eliminated via the lungs and the kidneys hence minimal toxicity (71). The main drawbacks of *PLGA* as a polymer in fabricating NPs are the bulk hydrolytic degradation, accumulation of acidic monomers causing a reduction of local pH at the site of drug action. This affects the stability of pH-sensitive drugs and the long degradation with repeated doses and local acidity promoting an inflammatory response (68).

Thus, novel materials are under development to improve upon the physicochemical properties of *PLGA.* Poly (glycerol adipate-co-ω-pentadecalactone) (*PG*A-co-PDL) is such a new polymer that has been developed and characterized in-house in LJMU laboratory and under intensive investigations for drug delivery purposes. *PGA-co-PDL* is enzymatically prepared from equimolar quantities of three monomers namely (Figure. 1.4); glycerol, divinyl adipate, and ω-pentadecalactone that are catalysed via the lipase from Candida antarctica through a ring opening polycondensation reaction (72).This polymerization reaction condenses the primary hydroxyl groups of the glycerol and spares the secondary hydroxyl group that is functional for possible covalent or hydrogen bonding with a drug molecule and increases slightly its hydrophilicity. This reaction can be altered with different ratios and mixture of different chemical monomers allowing of versatile nature of the produced polymer (73).

PGA-co-PDL can undergo hydrolytic degradation releasing its monomers including adipic acid that are less acidic than glycolic and lactic acids. It has successfully been formulated into NPs, MPs, and drug conjugates for lung delivery with good aerosolization performance and deep lung delivery (34, 72, 74-78). It has successfully encapsulated many small drugs and macromolecules, i.e., ibuprofen, dexamethasone phosphate, bovine serum albumin, pneumococcal protein, gene

delivery, and vaccine; showing very promising results for treating lung diseases and vaccine delivery (23, 25, 34, 38, 74, 77, 79-81).

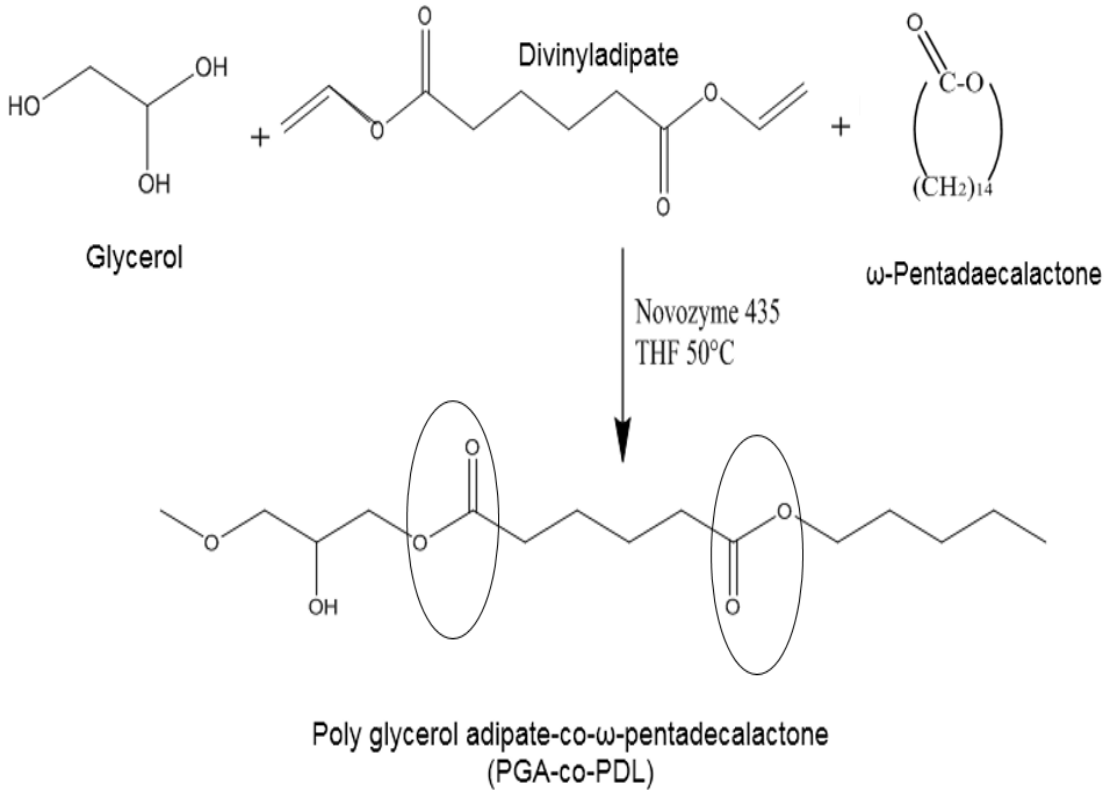

Figure. 1.4. Chemical synthesis and structure of *PGA-co-PDL*.

1.2.2. Methods of Polymeric Nanoparticle Formulations:

The polymeric NPs can be formulated by various methods that can be tailored for the desired drug encapsulation or adsorption e.g. emulsification solvent-evaporation methods; single or double emulsions, solvent displacement, coacervation, and salting out. Emulsification solvent evaporation are the most employed method for preparing polymeric NPs. Figure. 1.5. represents a schematic diagram of the emulsification solvent evaporation methods; single or double. These methods emulsify the polymer dissolved in a suitable organic phase (immiscible with water) into aqueous phase (containing a suitable surfactants) under high sheering stress (to reduce the droplet size) then followed by a solvent removal process i.e. evaporation (82).

Single emulsion (SE) method (oil in water or O/W); the oil/organic phase containing the polymer (with or without the drug) is solubilized into an organic volatile solvent e.g. dichloromethane, chloroform, or ethyl acetate. Then, it is emulsified into an aqueous phase; water that contains a suitable emulsifier, under either sonication or homogenization shearing stress. The emulsion will subsequently be subjected to the removal of the solvent by the evaporation process during a continuous stirring process resulting in hardening of the NPs outer shell and encapsulating the drug within. NPs are then isolated by a centrifugation-wash processes (to remove any excess surfactants) and subsequent characterization of NP size, zeta potential, and shape. This method can be used to encapsulate hydrophobic/oil soluble drugs. However, SE method can't be used for hydrophilic drugs (drug leakage), poor entrapment and difficult to scale-up (83, 84).

Double emulsion (DE) method (water in oil in water or W/O/W); This method can be used to encapsulate both hydrophilic drugs such as proteins and hydrophobic drugs. It allows production of larger size NPs. The drug is dissolved in aqueous phase and then added to the polymer dissolved in organic phase to form the primary emulsion (W/O). This is then followed by addition to another aqueous phase (with a surfactant) using two steps of sheering stress prior solvent removal process and NPs isolation. The main disadvantages are the larger NPs size with polydispersity, requiring two steps homogenization, the leakage of hydrophilic drugs in the aqueous phase, and difficult to scale-up (83, 84).

SE and DE allow tuning NP size by altering the parameters: the volume of aqueous phase, emulsifier concentrations, organic solvent type and concentration, power of sonication and homogenization, polymer mass, stirring rate, and temperature (85). However, the main drawbacks in addition to those mentioned above are the agglomeration of the NPs after the ultracentrifugation, batch to batch variability,

polydispersity of the produced NPs, unsuitable for some solvent-sensitive molecules (38, 84).

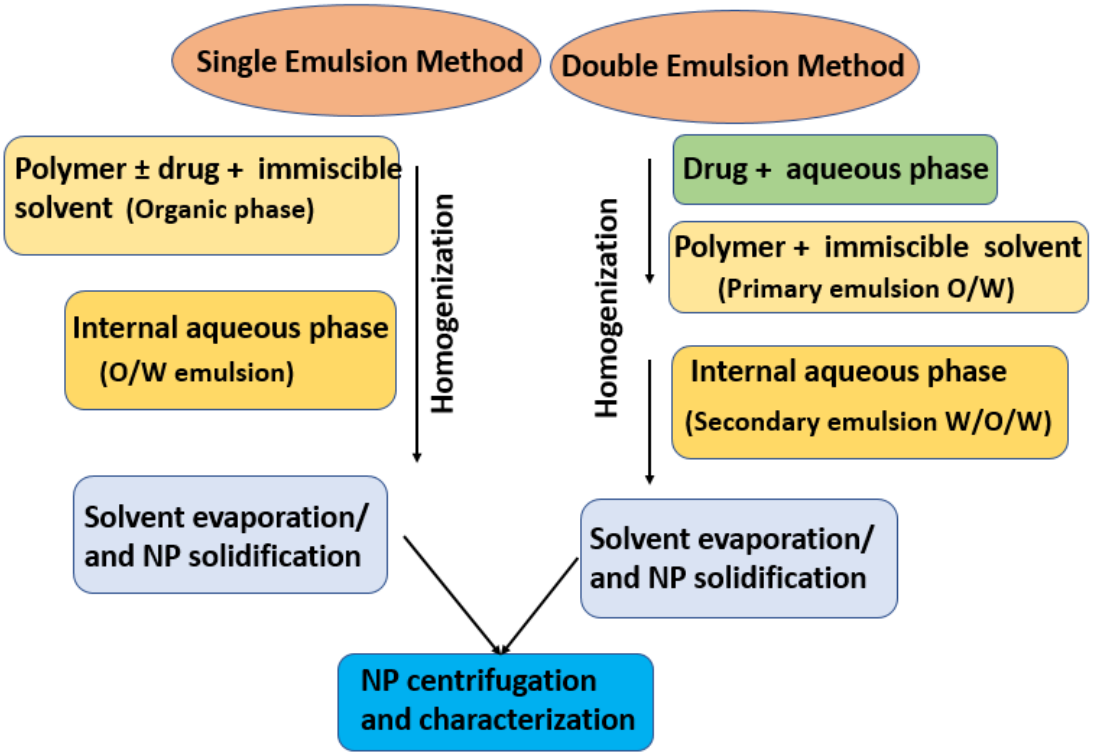

Figure. 1.5. Schematic diagram of SE and DE methods of NP fabrication.

1.3. Aerosol Drug Delivery of Nanoparticles to the lungs:

There is burgeoning interest in NP drug delivery to the lungs via aerosols. NP aerosols can localize the drug topically in the lungs with enhanced pharmacokinetic properties in terms of retention and direct local action in the treatment and management of lung diseases, compared to other routes of administration. This limits the systemic off-target side effects. Moreover, lung delivery can be used as a systemic portal for drug delivery with better patient compliance and enhanced therapeutic efficiency (32, 86, 87). The USFDA has approved a liposomal (ARIKAYCE®) amikacin suspension for the treatment of Mycobacterium avium complex (MAC) lung disease via nebulization as the first NP based-drug aerosol delivery (88). A list of aerosolized nanomedicines

approved for lung delivery or in the preclinical/clinical trial stages is provided in Table. 1.2.

Polymeric NPs show progressively improved profiles that can be better alternatives for inhalation delivery. Polymeric NPs can be formulated into dry powders and pMDIs with the possibility for self-administration and better patient compliance. Polymeric NPs can be easily co-blended with various molecules and other materials generating immense potentials, e.g., polymeric lipid hybrids (8, 43, 89, 90).

Table. 1.2. Examples of aerosolized nanomedicines to target the lung or systemic targets.

Active drug/molecule	NP carrier	Indication/disease	Type of study
Quercetin	*PLGA* NP coated with magnetic (Fe3O4) NPs	Lung cancer	*In vitro* using A549 lung cancer model, and *in vivo* mice studies (152)
Amodiaquine	*PLGA* NP functionalized with PEI	NSCLC	*In vitro* lung study using 2D; H4006, H358, H2122, H460 and H157 NSCLC cell lines and A549 spheroids (91)
Rifampicin, isoniazid, pyrazinamide	*PLGA* NPs coated with PEG and chitosan	TB	*In vitro* bacterial sensitivity assay using *M.tb* H37Rv, and *in vivo* C57Bl/6 female mice (92).
Quinacrine	*PLGA* NPs	Lung cancer	*In vitro* study using A549 cell lines (93)
Ciprofloxacin	*PLGA* NPs	Pseudomonas aeruginosa and CF	*In vitro* study using Calu-3 cells and CF bronchial epithelial cells (CFBE41o^{-})
Tobramycin	*PLGA* NPs coated with PEG	Lung infections and CF	*In vitro* using A549 cell lines and against P. aeruginosa and B. cepacia biofilms (94).
2-methoxyestradiol	*PLGA* coated with chitosan NPMPs	Lung cancer	*In vivo* rat lung model (95).
docetaxel	*PLGA* NPs functionalized with Poloxamer (*PLX*-188)	Lung cancer	*In vitro* A549 cell line and *in vivo* using rat cancer lung model (96).

Continued. **Table. 1.2**. Examples of aerosolized nanomedicines to target the lung or systemic targets.

Active drug/molecule	NP carrier	Indication/disease	Type of study
Gene delivery: siRNA Knockout	*PLGA* NPs functionalized with DOTAP and further made into NPMPs	Lung cancer	*In vitro* using H1299 stably expressing EGFP (97).
Sorafenib	*PLGA* NPs	Lung cancer	*In vitro* lung cancer:A549, H4006, H460, H358, H157; and human embryonic kidney cells HEK 293 (98) .
Resveratrol complexed with sulfobutylether-β-cyclodextrin	*PLGA* NPs	Lung cancer	*In vitro* A549, H358, H460, H4006, H157; and human embryonic kidney cells HEK-293 (99).
Afatinib	*PLGA* NPs	Lung cancer	*In vitro* using A549, H460, 3D tumour spheroid (100).
Human IgG (as a model antibody)	*PLGA* NPMPs	Vaccine delivery	*In vitro* sustained release study (101).
Gene delivery: cmRNA ^{hCFTR}	*PLGA* NPs coated with chitosan	CF	*In vitro* study using CFBE41o− and 16HBE14o- cells, ex-vivo using human whole blood assay, and *in vivo* using CFTR deficient mice models (102).
Bovine serum albumin as a model protein	*PGA-co-PDL* NPMPs	Vaccine delivery	*In vitro* using A549 and dendritic cell lines (103, 104)
Resveratrol	*PGA-co-PDL* NPMPs	Lung cancer	*In vitro* using Calu-3 cell lines (105).

Continued. **Table. 1.2.** Examples of aerosolized nanomedicines to target the lung or systemic targets.

Active drug/molecule	NP carrier	Indication/disease	Type of study
Gene Targeting: miRNA (reduce gene IRAK1 expression)	*PGA-co-PDL* coated with DOTAP NPs	COPD	*In vitro* using A549 cell model (79).
Pneumococcal surface protein A (PspA)	*PGA-co-PDL*NPMP	Pneumococcal vaccine	*In vitro* using dendritic cell lines and *in vivo* mouse assay (25, 106)
Paclitaxel	Polymeric lipid hybrid: PEG_{5000}-DSPE micelles	Lung cancer	*In vivo* using Sprague–Dawley rats study (107)
Insulin	Chitosan NPMPs Insulin-loaded lipid into chitosan NPMPs	Diabetes	*In vitro* (108-110) using Calu-3 and A549 lung cell lines and *in vivo* using rat model (111).
Gene delivery: Akt1 siRNA	PEI NP	Lung Cancer	*In vivo* study using K-ras (LA1) mice as lung cancer model (112).
Doxorubicin	poly (isobutyl cyanoacrylate) (BIPCA) NPs	Lung cancer	*In vitro* study using H460 lung cancer cells and (MH-S) alveolar macrophage (114).
Doxorubicin	PEGylated PAMAM dendrimers NPs	Lung cancer	*In vitro* A549 lung model (115).
Gene delivery: tumour suppressor gene on Akt on a recombinant plasmid DNA	Glycosylated PEI NPs	Lung cancer	*In vivo* using K-*ras* null mice lung cancer model (116).

1.3.1. Nanoparticle Aerosol Generation and Deposition into the Lungs:

Inhalation drug delivery is attained via respirable-sized aerosol particles. The aerosol is described as suspended solid or liquid particles stabilized in a gaseous phase (117). There are three widely recognised aerosols-generating devices: Nebulizers (118, 119), metered dose inhalers (MDI) (117), dry powder inhalers (DPI) (120, 121).

The aerosols are described by their aerodynamic diameter (AD) which is the diameter of a unit density sphere having the same settling velocity in the air to the particle of interest (122). The aerosols that have an inhalable size are of an AD smaller than 10 µm and classified as coarse particles (> 2 µm), fine particle fraction (0.1-2 µm), and ultrafine particle fraction (< 0.1 µm). The AD range of the pharmaceutical aerosols is between 1-5 µm (123). A major limitation for NPs lung deposition as a dry powder is their AD is smaller than the optimal size for aerosol deposition; 1-5 µm and they have low mass (124). Consequently, the delivery of NPs as a single/monodisperse NP aerosol to the lungs is almost impossible as they are removed from the lungs upon expiration. Hence, many formulations and delivery strategies have been proposed to overcome this limitation, including formulating NPs in a bigger microparticle carrier , delivering NPs aggregates either pure or with excipient carriers such as lactose or L-leucine, or freeze-dried or pre-spray dried in large porous or hollow carriers in DPI, or delivering the NPs as micron-sized agglomerates using nebulization/pMDI that achieves a temporary increase in their AD favouring their lung deposition (Oswald ripening) (80, 125-127). Recently, effervescent particles technology that involve spray-drying into effervescent excipients have shown better aerosolization and faster release of NPs upon dissolution in aqueous media (128-130). NPs drug delivery via DPI is claimed to be superior than nebulization/pMDI in being more controlled and stable spherical particles, enhanced loading, and aerosolization performance (17, 57). The physicochemical properties of

aerosol NPs represent an active multi-disciplinary research to develop particles that are non-toxic, have efficient loading and target-delivery vehicle, stable, safe and fit for purpose, and good aerosolisation performance (131).

NPs aerosol deposition into the lungs is a multifactorial dependent process and primarily depends on the physicochemical properties of NP aerosol (Table. 1.3.), the aerosol generating device; carrier medium; air (Nebulizers, DPI), or a propellant (Table.1.4), and lastly the underlying lung condition factors (19, 132, 133). The deposition of inhaled particles into pulmonary targets is known to be through the following mechanisms either: impaction, gravitational settling, interception, and Brownian diffusion (Figure. 1.6). Charged particles are exposed to another force depositing them into the airways known as electrostatic precipitation (10, 19).

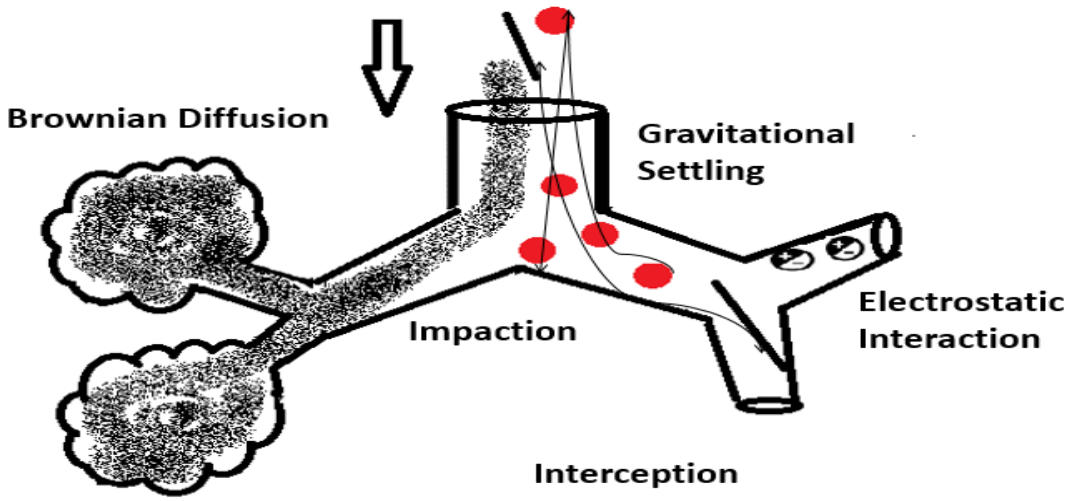

Figure. 1.6. Mechanisms of NPs deposition in the airways (Reprinted with permission (3)). NPs size and other physicochemical properties determine NP deposition: NP with AD >5 μm deposits in the conducting airways via impaction (NPs deposited at sites of air flow directional changes); NPs with AD = 1 - 5 μm deposit in the bronchoalveolar regions via sedimentation; NPs AD <1 μm persist air suspended (can be exhaled) and deposit via Brownian diffusion; interception for fibre NP; and electrostatic interaction for charged NPs (19, 132, 133).

Table. 1.3. NP physicochemical Factors affecting the NPs aerosol deposition in the lungs (8, 11).

NP physicochemical factors NP deposition	Effect on lung deposition
Size	• 5-10 µm AD aerosols impact in the upper airways and prone to MCC • 1-5 µm aerosols sediment in the deeper airways and prone to MCC and MC mechanisms • Below 1 µm aerosols undergo diffusion in the deepest airways • Less phagocytic uptake, < 0.5 µm are not recognized by macrophages • Cohesive/adhesive agglomerates that are difficult to be dispersed
Shape	• Spherical particles are commonly employed as easier fabrication methods. • High aspect ratio/ fibre-like NPs deposited by interception. This was adapted from pathological example of asbestos.
Charge	• Cationic coated NPs are deposited by the electrostatic interception. • Longer residence or membrane bound time • Corona formation
Density	• NPs deposition in the deepest regions is inversely relate to the particle density. • Hollow particle with lower density and larger size is better deposited than small dense solid particles
Chemistry	• Hydrophobicity of NP increases drug absorption but strong hydrophobic NPs will increase the retention time. • Small molecular weight (MW) hydrophilic particles will be absorbed faster than the larger molecules. • High MW particles are less epithelial permeable in the alveolar epithelium
Solubility	• The readily soluble particles will be less prone to clearance than insoluble particles that will be trapped either by the MCC or MC. • Poor soluble particles with size over 6 µm are cleared faster with majority of deposited particles cleared within 24 hrs post deposition.

Table. 1.4. Aerosol generating device factors affecting the NPs aerosol deposition in the lungs (19).

Device factors	Effect on lung deposition
Nebulizers	• Commonly used device in hospital settings, newer nebulizers also used by patients in community setting • FPF ranging from 60-80% • Deliver mixes of drugs in one shot • Effective in lower inspiratory flow 6-8 L/min • ~ 10 % dose is deposited, various patient training techniques as to breathe deeply and breath-holding can increase the deposition to 17% • Main concerns are the negative effect on the formulation structure integrity, the carrier or the drug or macromolecules that may be damaged due to the nebulization forces. New generations of nebulizers such as vibrating mesh technologies, that deliver more uniform particles increasing the deep lung deposition and maintain the formulation integrity are being developed and used. Further details can be found in (18).
MDI	• Common portable device and used by COPD, asthma patients. • ~ 20% of the dose deposited with minimal inspiratory flow rate is necessary ~ 20 L/min. • The formulation integrity is achieved with producing inhalable aerosols and using a propellant. • The main issue that might render the treatment unsuccessful in some patients is the lack of coordination. • Not suitable for delivery of high doses, biologicals and long-term storage due to loss of stability or degradation. • New MDI have been developed allowing less patient effort to actuate, such as Autohaler® and Easybreath®; with enhanced lung deposition and less inspiratory volumes required (18).
DPI	• DPIs have superior advantages over the other devices based on more stable powder formulation • DPIs are breath-actuated removing the actuation/coordination • DPIs have similar deposition rate to the MDIs. • Size, inspiratory flow, humidity and temperature influence the DPI aerosol performance • An inspiratory flow rate of at least 30 l/min is necessary for aerosol generation. • Difficult use in debilitating conditions, elderly, and children associated with low inspiratory force

Challenges for NP aerosolization: NP aerosol deposition is not a straightforward process and needs extensive optimization of the formulation. NP pharmaceutical formulation and therapeutic performance must be worthwhile. Translation from benchtop to the clinics is faced with issues, such as, the dose- and dosage-form defining problems (134), the shelf-life, the scalability, the ease and safe of the use, and the cost (57, 135).

1.4. Inhaled Nanoparticle Pharmacokinetics and Toxicity:

Once deposited, polymeric NPs interact with a group of biological barriers starting from the surfactant layer, mucous, epithelial cells, vascular endothelium, and interacting with different molecular and cellular structures in the biological environments prior to exerting a drug response (7).

For successful pulmonary delivery, NPs must be absorbed and transported to their targets faster than the rate of their clearance and degradation (19). Upon contact of NPs with the fluid environment of the barrier site, a layer of proteins and other molecules of that fluid medium will adhere to the NPs giving a new identity to the NPs that can influence its safety and efficacy of the treatment (136). This may lead to NPs aggregates and more prone to phagocytic uptake, or the physicochemical properties may change implicating variations in their kinetic behaviour limiting their effect and/or intensifying their toxicity (137-140). A stealth/shielding technique for NPs are currently designed to limit the effect of protein corona (141). After traversing the lung surfactant and mucous layers, NPs will be internalized by the lung epithelium where they can be transported mainly via the transcytosis pathways (142). Locally delivered NPs are designed to have longer lung retention (3), which can elicit local NPs toxicity as well as the possibility of NPs escape through the thin alveolar epithelium to systemic circulation producing off-target side effects (11, 143) (Figure. 1.7).

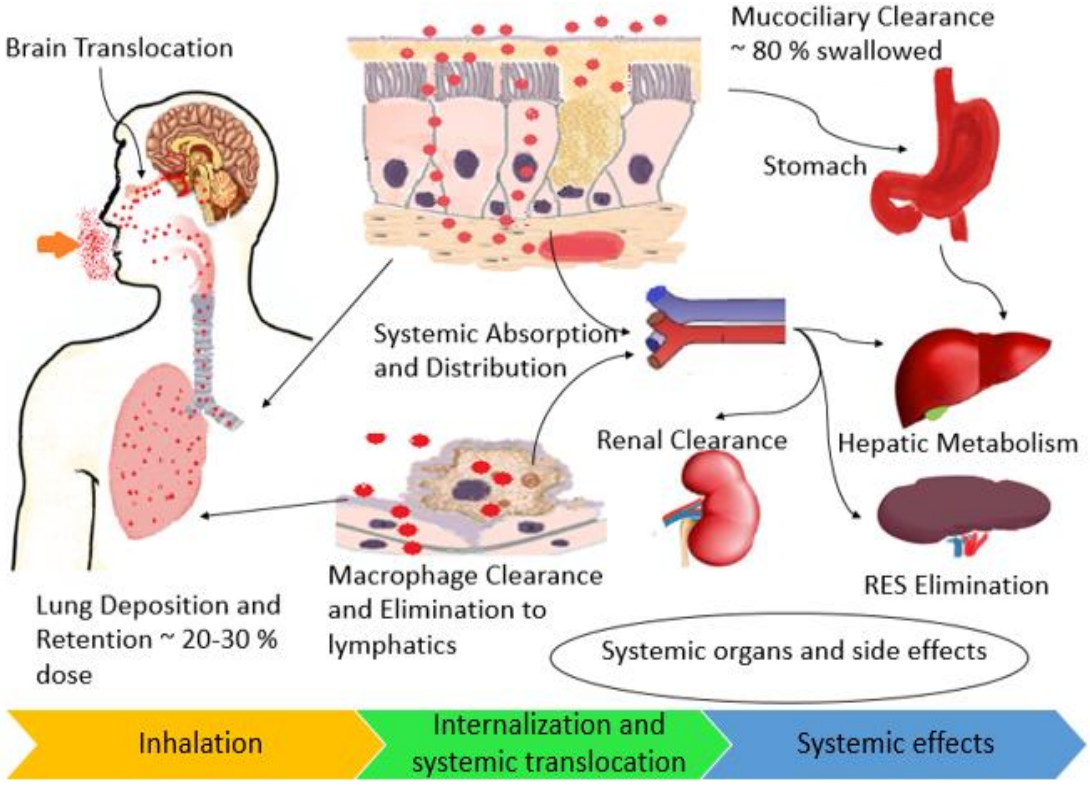

Figure. 1.7. Pharmacokinetics of inhaled NPs and their potential toxicity (Reprinted with permission (11)).

Systemically targeted NPs delivered via inhalation traverse the air-blood barrier to be delivered to the systemic targets by EPR effect or actively targeted by '*homing*' antibodies (143, 144).

NP metabolism and clearance have shown many variations. With the use of lung delivery for both systemic and local delivery, the low metabolizing activity will increase the pulmonary retention of NPs and prolong their action (13). This could be advantageous, where the lung acts as a stable reservoir for NPs sustained delivery and clearance. However, the full lung metabolizing capacity is not fully understood with little information known about any enzyme induction or inhibition apart from smoking; a well-known lung metabolizing inducer (145), the lung enzymatic inhibition could increase the potential clinical side effects, and toxicity of locally delivered NPs (13).

NPs elimination from the lung can be attributed to their dissolution/solubility in the interstitial fluid or physically eliminated by MCC or MC (144). The biodegradable NPs products will eventually be cleared by the renal system. The renal clearance is limited to a size lower than 8 nm for NP or its degrading by products (146). The physical clearance of NPs in the upper airways is achieved via the faster MCC (to be coughed or swallowed). NPs swallowed into the stomach will undergo faecal clearance or reabsorption to the systemic circulation and renal clearance. In the lower airways, the slower MC (to reticuloendothelial system (RES): Liver, spleen, bone, and others) may entrap these NPs resulting in an inflammatory reaction upon exceeding the macrophages ability to digest (13). NPs can be drained to local lymphatics and lymph nodes delivered by MC and different antigen presenting cells such as dendritic cells (DCs) or sole NPs drainage to lymphatics. From lymphatics, NPs can travel to the systemic circulation and end up in RES where further chemical digestion or physical retention will occur that may elicit off-target side effects (147). However, this was exploited to target therapies to treat these organs such as liver cancer and liver infections (148).

Although the enhanced properties of NPs stem from their exceptional physicochemical properties they still require optimization of the NP formulation and evaluation of nanotoxicological effects prior to the intended route of entry (149-152). Thus, a nanotoxicological evaluation on a single NP case should be assessed covering the nanocarrier physicochemical properties, nanocarrier-drug formulation factors, with *in vitro/in vivo* evaluation prior to clinical trials. Recently applying *in silico* models after *in vitro* studies was successful to predict the *in vivo* kinetics of gold aerosolized NPs (149, 153).

In a study performed by Chen *et. al.*, (2017) (154), they investigated alternative strategies to lower the systemic toxicity of yuanhuacine an anticancer agent when administered orally or IV to target lung tumours. They evaluated the efficiency of two *PLGA* NPs formulations prepared via emulsification-solvent evaporation method: *PLGA* NPs loaded with the drug (Yh/*PLGA* NPs), and *PLGA* NPs loaded with the drug and functionalized hierarchical targeting strategy (Yh/M*PLGA* NPs) to target lung cancer *in vitro* and *in-vivo*. The two NPs were of ~ 150 nm in size, zeta potential was negative for Yh/*PLGA* NPs, while it was negative for Yh/M*PLGA* NPs in neutral pH and turned positive in the acidic pH (using histidine coating to aid in lysosomal escape via proton sponge theory (155, 156), lysosomal pH 4.5–5.5), and shape was spherical for both. Both formulations were tested *in vitro* using A459 lung cell lines; Yh/M*PLGA* NPs showed better inducer of cell cycle arrest, higher uptake, active internalisation via clathrin endocytosis, better inducer of higher mitochondrial depolarization, apoptosis and higher production of cytochrome C. Furthermore, via confocal visualisation; functionalised NPs showed lysosomal colocalization, lysosomal escape, targeting the mitochondria and more apoptosis than the non-functionalized Yh/*PLGA* NPs, and both showed better therapeutic performance than the free drug. Hence, the value of *in vitro* methods to optimize the formulation, uncovering the mechanistic relationship of NPs and cellular interaction, and minimizing the use of animals. The authors chose the most effective formulation (Yh/M*PLGA* NPs) to optimize as a dry powder inhalation (1-5 µm) dosing for animal testing as well as IV solution. *In vivo*, the authors compared the efficiency of targeting the lung tumour via two routes of administration: local inhalation or IV using male Sprague-Dawley rats (154). The authors evaluated the plasma blood concentrations (via blood Sampling), lung, liver, spleen, kidney and reproductive organs (as tissue homogenates) after the two different routes of administration. The IV

route showed higher blood concentration, higher concentration in liver, spleen, kidney and reproductive organs and low lung concentrations. However, the inhalation (via intratracheal insufflator) had shown the highest local lung concentration and longer lung residence, lower blood levels, lower concentrations in liver, spleen, kidney and reproductive organs with faster blood elimination. The authors concluded the experiments with a successful optimization of a dry powder formulation for inhalation. The formulation was multitargeting strategy, targeting the lung delivery by suitable aerosols size (NPMPs), targeting the tumour by specific ligands, and targeting intracellular mitochondrial shutdown as anticancer strategy. The inhalation delivery was superior and safer than the IV route for targeting lung pathology. However, the authors did not comment about any signs of distress or inflammatory response either local or systemic that may have occurred following the different administration routes or the survival rate of the animals following the exposure prior to their sacrifice or Sampling intervals that might suggest good tolerance for the two administrations with better therapeutic performance for the inhalation delivery.

1.4.1. Nanoparticle Interactions at Cellular and Molecular Levels:

NP drug delivery aims to deliver the cargo to certain cells, or more specifically, to certain subcellular locations, to exert a response dependent on its enhanced ability to cross biological barriers. Cellular uptake is mediated by various mechanisms, passive or carrier-mediated or endocytosis. For NP-mediated drug delivery, nanocarriers are of high MW are mostly subjected to vesicular transport or endocytosis (157, 158). Endocytosis pathways involve pinocytosis and phagocytosis processes (Figure. 1.8).

The physicochemical characters, primarily particle size, are very critical parameter to determine the subsequent uptake process (159).

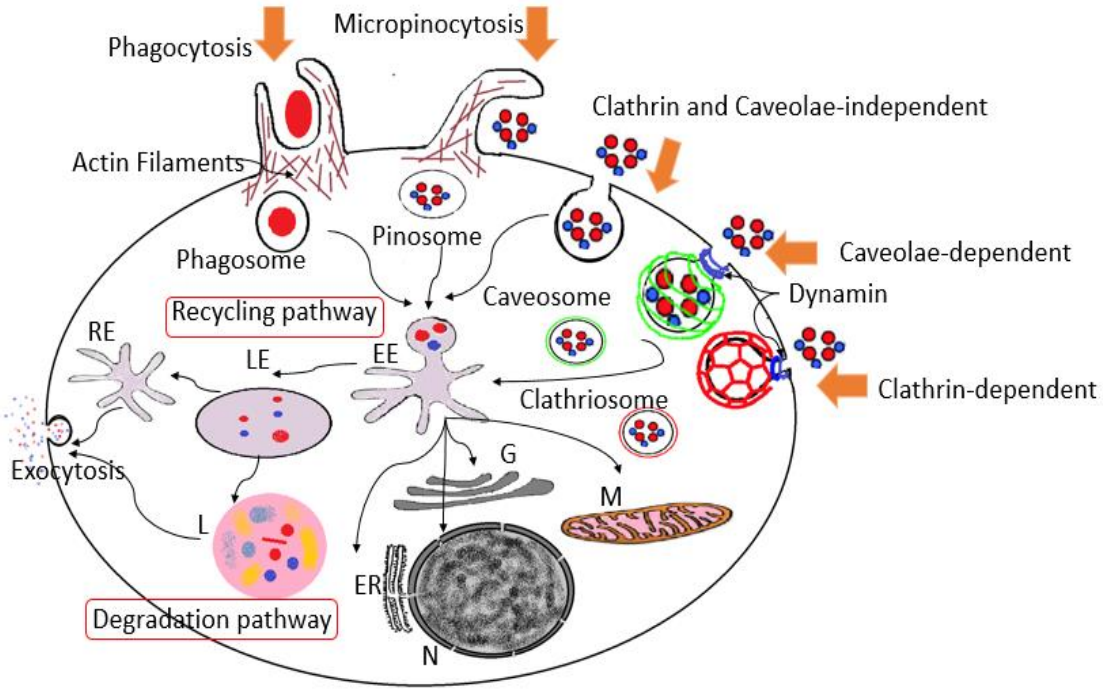

Figure. 1.8. Main uptake mechanism of NPs and the endocytic pathways. (EE: Early Endosome-low pH, LE: Late endosome-low pH, ER: Endoplasmic reticulum, L: Lysosome-very acidic, N: Nucleus, M: Mitochondria, G: Golgi, RE: Recycle endosome) (Reprinted with permission (11)).

Phagocytosis or 'cell eating' is the process of engulfing large sized particles/ debris, dead cells, bacteria or viruses found in the extracellular environment, with the aim to dispose unwanted materials. It is executed by professional phagocytes, such as macrophages or neutrophils or eosinophils. It's largely triggered by opsonization of the unwanted materials by antibodies or complement proteins (i.e., antibodies: IgG, IgA, IgM, Fcɣ, complement proteins [C3, C4, C5], serum proteins that can be found in protein corona; fibronectin, C-reactive protein, type-I collagen) prior to binding to surface receptors (such as Fc, complement) initiating cellular recognition. Engulfing nonopsonized materials by identifying certain molecular patterns (i.e., mannose, C-type lectins such as Dectin-1or -2, scavenger receptors or fructose receptors, apoptotic receptors: TIM-1, TIM-4, stabilin-2, and BAI-1) also exists (160). Hence, shielding

NPs with stealth polymers such as PEG reduces the opsonization process, evades the RES recognition, and increase the lifespan of NPs.

Many studies conducted *in vitro* and *in vivo* have demonstrated that MC is size-dependent where NP with a size range below 0.5 µm showed limited clearance but those with size above 1 µm had higher clearance, more than those of size above 6 µm (161-163). In addition to size, the shape and surface properties of the NPs have influence on the MC. Particle shape showed an effect on the initial contact and subsequent progress into phagocytosis (164, 165). For example, rod or fiber-like NP are very challenging for phagocytosis resulting in frustrated macrophages (166).

After triggering, signalling cascade Rho family GTPases stimulate cell membrane actin filaments condensation into pseudopodia that zipper up enclosing the foreign material forming the characteristic cupping. The vacuole closes around the target by the actin constrictions and very recently it has been discovered with the activation of session protein GTPase dynamin 2, it is released into the cytoplasm (167, 168). Once enclosed in a phagosome, it is then fused with the lysosomes that starts digesting with acidic hydrolase (such as lipases and esterases, proteases, phosphatases, and nucleases) under acidic pH (159, 169, 170).

Pinocytosis or ‘cell drinking’ is the cellular uptake of small sized particles and fluids, and subcategorized into macropinocytosis, clathrin-dependent, caveolin-dependant and clathrin- and caveolin-independent mechanisms.

Macropinocytosis process uptakes a large volume of extracellular fluids (0.5-10 µm) upon activation by growth factors initiating signalling cascade of Rho family GTPase (171). Unlike phagocytosis, the actin filaments condense into membranous protrusions or rufflings around the target and collapse to fuse with the cell membrane

generating large macropinosomes that can be partly dependent on dynamin2 or its variants for scission (172). It is involved in diverse functions, such as immune recognition, cell migration, disposing unwanted materials, and Sampling fluids and nutrients from the extracellular environment and ending with lysosomal degradations (173, 174).

Clathrin-dependent endocytosis is the most characterized endocytosis process as far it's the most active and constitutively present in all types of cells (175). Its role is essential for the cellular haemostasis for nutrients and macromolecule transport such as cholesterol via low density lipoproteins (LDL receptors), and iron via transferrin (Tfn receptors) that are considered as markers for this route of uptake, serum proteins, membranous ion pumps. It has a crucial role in cellular communication during organogenesis, cell signalling regulation by controlling and downregulation of receptor levels, synaptic neuronal transmission (Ca+2-gated channels regulation, recycling of neurotransmitter vesicles), reabsorption of serum proteins after filtration in kidney tubules (176, 177). It is membranous invaginations mediated through clathrin triskelia that coat or cage the incoming vesicles (178). It is initiated by a binding of certain ligands to surface receptors at clathrin-nucleation sites/pits with subsequent clathrin-1 protein assembly with the adaptor/assembly protein complexes into clathrin coated lattices. Dynamin GTPase scission mechanism proceeds around the vesicle neck. Clathrisome disassemble its coatings prior to fusion with the endolysosmes. The molecules/particles size ranges from ~100-200 nm (175).

Caveolin-dependent endocytosis is a process of internalisation of small particles and fluids through membrane invaginations as flask-shaped vesicles. It is commonly abundant in endothelial linings facilitating the extravasation of serum proteins and nutrients to the surrounding tissues. Caveolae are triggered through certain

receptors, i.e., serum albumin gp60. Subsequent signalling cascade through Src tyrosine kinase activates phosphorylation and formation of Caveolin-1; a dimeric protein that forms a coating of caveolin striations around certain cholesterol/sphingolipids-rich bindings on the inner membrane layer. Caving-in or invaginating membranous vesicles ensues with the contraction of dynamin and dynamin arrangement by the actin cytoskeleton forming caveosomes (178). Caveosomes have neutral pH and bypass the lysosomes protecting its package from degradation with subcellular smooth ER and cytosolic delivery. This route has been used by some pathogens and bacteria to evade lysosomal degradation (179), and has been under investigations to enhance NPs internalisation (180). Caveolae have many biological roles; lipid and cholesterol haemostasis, regulating some cellular cascades, regulating endothelial NO synthase, transcellular transport of serum albumin and nutrients (181, 182). Caveolae involve transport small fluid vesicles of ~80 nm (173).

Clathrin and caveolin-independent endocytosis are many processes and yet they are negatively described as being independent to the aforementioned cornerstone molecules in other endocytosis processes. They involve Lipid rafts that are highly organized lipid clusters and cholesterol rich that exist on the cell membrane exerting endocytosis uptake in absence of clathrin, caveolin and/or dynamin but mostly requires actin polymerization. Examples are Flotillin, endophilins, clathrin-independent carriers (CLIC/GEEC) pathways have been recently discovered and full understanding is under research (169, 183).

The size of NPs is suitable for many uptake and endocytosis mechanisms where NP size around 100 - 200 nm are endocytosed via clathrin or caveolin mediated pathway while NP size > 250 nm up to 3 µm occur via macropinocytosis and phagocytosis (159,

184). However, there are many examples of larger or smaller NPs uptaken by various endocytic mechanisms (159, 184).

Post uptake; NPs containing vesicles will be fused with lysosomes directly or via the early endosome (EE) where a low pH digestive activity can take place degrading the NPs. Endosomes can release the cargo to the cytosol or continue maturing to late endosomes (more acidic, pH~ 5). The late endosomes can digest or eliminate the waste or fuse with the lysosomes for further digestion. The lysosomal digestion carries many potentials of biodegradable NPs for drug delivery if the drug can tolerate the harsh environment. Otherwise, lysosomal/endosomal escape strategies will require optimisation to deliver drugs and genes to subcellular targets i.e., cell organelles (185), nucleus (186, 187) and mitochondria (188-190). Endosomes have a complex machinery that allows for NP vesicular sorting, digestion and degradation, and waste-exocytosis and recycling as well as initiating cellular death in case of toxic NP overload (191-193). Some NPs can be found without vesicles in the cytoplasm (143) and their uptake can be passively across the lipid bilayer.

1.4.1.1. Proposed Mechanisms of Nanoparticle Interactions and Toxicity:

NP toxicity is one of the hot topic areas due to the novelty of the materials that render the NP with unique physicochemical properties. These exceptional properties are not only tremendously critical for their efficacy but also for their toxicity with partly or completely dose independent. Cellular injury might vary from trivial reversible injuries recovered by the efficient repair mechanisms to severe or irreversible injuries inducing cell death or long term adverse effects (149). Various intersecting toxic mechanisms have been reported upon exposure to various types of NPs, or even to the same chemical structure NP with variable physiochemical properties (Figure. 1.9). However, there is no agreed solid background as to which is the single and most critical

parameter for NP toxicity, for example, is it the size only, or the chemical composition, or the mass? Unlike the same bulk counterparts, the mass dose is not critical for the toxicity (apart from being overtly overdosed that would generate toxicity anyway) and the full identity of physicochemical properties of the NPs is critical. Hence, NP characterization is necessary prior to their testing and drawing conclusions.

Most of generated information about the nanotoxicity are based on the *in vitro* methods due to the novelty of NPs. Although most of the *in vitro* research pool is based on lung cell lines exposure to suspended NPs and that is due to the expensive nature and the extreme difficulty to achieve aerosolization exposures to *in vitro* cell lines.

The value of the initial *in vitro* step is establishing the relationship between the NP physicochemical identity to biological or toxicological responses, uncovering the underlying mechanisms, a possible high throughput screening, developing *in silico* predictive modelling, and reducing the use of animals (194). The *in vivo* based experiments are inhalation exposure but with varied routes of delivery, i.e., oral- or nasal-delivery, whole body exposure, intratracheal instillation or cannulation. These studies will provide solid frameworks to understand the toxicity of NPs aerosols on the lung due to the novelty of the aerosolized NPs.

Cell membrane disruption are commonly reported due to NPs surface chemistry or functionality and shape, and could be mediated via various mechanisms (Figure. 1.9) (149, 195). Cell membrane could be directly damaged when the NPs interact with the lipid bilayer. For example, cationic NPs are more cytotoxic to cells due to their interactions with the negatively charged cell membrane altering, depolarizing or damaging the membrane i.e. thinning, pore formations and erosions (158, 196-199). The anionic and neutral NPs are also reported to affect the cell

membrane through the electrostatic repulsion with the lipids causing membrane pores and lipid leakage (200, 201). Inorganic NPs are commonly affecting the cell membrane through the ion shedding/release mechanisms that interact and damage the lipid bilayer (202, 203). Cell membrane damage could be indirectly following NP internalisation due to subcellular organelles damage, e.g. endolysosomes (204, 205), or cytoskeleton affection disrupting the major functional proteins, e.g. F-actin and α- or β-tubulins, which are involved in cellular shape, motility, adhesion, transport, and cellular division and proliferation (206). PEGylated NPs were found to reduce the surface chemistry effects (207).

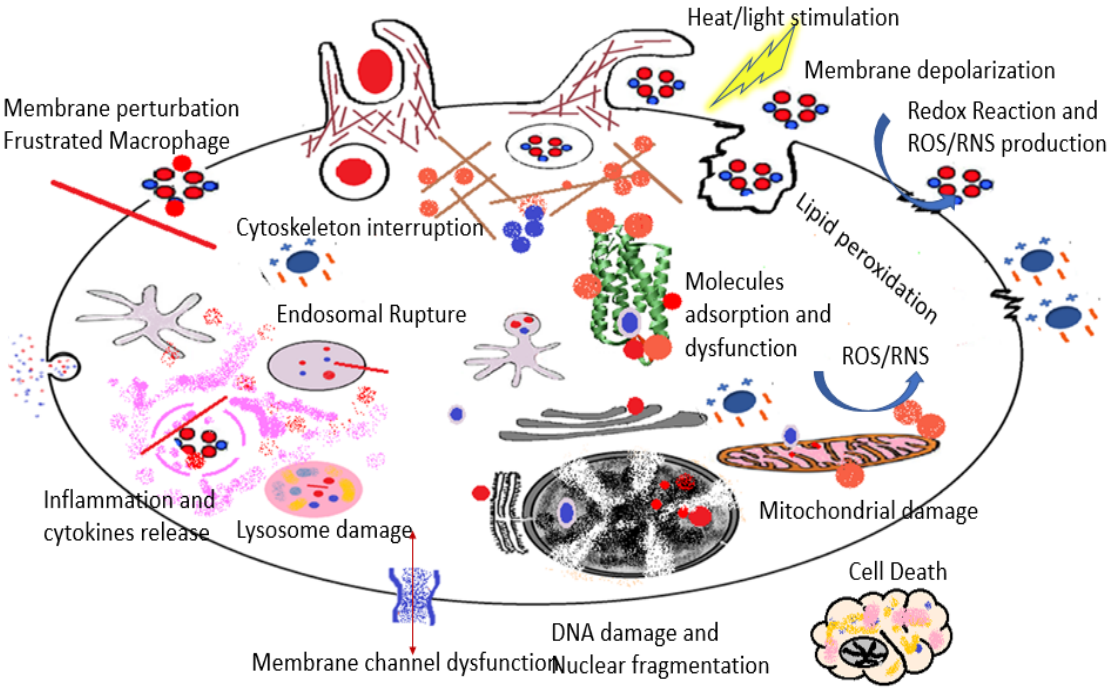

Figure. 1.9. NP cellular uptake and interactions with different mechanisms of cytotoxicity (Reprinted with permission (11)).

Spherical and smooth surfaced NPs are considered less toxic from the high aspect ratio NPs, e.g. rod or fibre-like NPs. Cytotoxicity was lowered by lowering the aspect ratio of NPs in alveolar macrophage (J774A.1) (208). Macrophages have less-

efficient clearing for NPs with rod or fibre-like shape, as they are very challenging for phagocytosis resulting in frustrated macrophages (166).

The use of stimuli responsive NPs that can be stimulated by internal stimuli such as local pH or certain molecules such as Reactive Oxygen Species (ROS), or external stimuli such as temperature, magnetic field or radiation (209) can damage the cell membrane on stimulation, that are aimed therapeutically to the target diseased cells such as tumours.

Oxidative stress: ROS have many fundamental functions in controlling many physiological and pathological cellular process such as cell signalling, growth and cell differentiation, allergy, and inflammation (210-212). ROS generated mainly through the oxidative respiration in the mitochondria but can be generated as by-products from other oxidative processes such as lipid or protein oxidation. ROS include superoxide anion (O_2^-), hydrogen peroxides (H_2O_2), hydroxyl radicals (OH^-) (213). When ROS production exceeds the cellular ability to inhibit, this induces what is called oxidative stress where excess free radicals will react with the cellular components, proteins, membranes, inflammation, lipid peroxidation, mitochondrial shutdown, molecular and DNA damage, and eventually cell death, either through the apoptosis if its less severe insult or through necrosis with severe toxic insults (149, 200). NPs can generate the ROS/oxidative stress by directly affecting the mitochondria or impairing the enzymes (that lower the ROS), reacting with the transition metals inside the cell such as Fe^{2+} and Cu^+ (Haber-Weiss reactions) (Figure. 1.9) (214) .

Almost all types of NPs demonstrate toxicity that is linked to the production of ROS and this could be determined by measuring free radicals and anti-oxidant levels

such as GSH levels (215-219). However, ROS production was exploited as a therapeutic mechanism to induce cell death for tumours (210, 220-222).

Cell organelles damage and mitochondrial shutdown: NPs ability to interact with the cellular components and induce membrane damage and ROS will suggest potential toxicity on the mitochondria (Figure. 1.9). Direct NP-mitochondria interaction instigate mitochondrial membrane depolarization, damage, and leakage were observed with many types of NPs; organic or non-organic (189). Lysosomal damage either by chemical sponge theory or physical needle-like shaped NPs rupturing the lysosome and releasing Ca^{2+} from the endoplasmic reticulum with eventually loss of control of mitochondrial permeability. The mitochondrial damage with loss of energy production and exhausting antioxidant capacities end in high ROS, nuclear and DNA damage, and membrane disruption (149, 223). Mitochondrial targeting is exploited to deliver therapeutics to cells with defective mitochondria or to simply targeting the mitochondrial knockout in cancer therapies (224-227).

DNA damage and mutagenicity: This could be direct NP genotoxic effect or indirect effect through the induction of inflammation, inflammatory mediators or ROS, molecular and organelle damage (228, 229) (Figure. 1.9). Due to the high surface energy of the NPs, DNA as any other biological molecule is subjected to surface adsorption. This binding will induce both conformational and functional deformity of these biomolecules. *PLGA* NPs of positively-charged (Hexadecyltrimethylammonium bromide (CTAB) cationic modified, 78 nm size) showed higher cytotoxicity associated with high ROS production, and genotoxicity potentials (chromosomal aberrations detected by micronucleus assay) than the negatively-charged (bare *PLGA*) or neutrally-charged (coating with PEG) *PLGA* NPs (80 nm, 82 nm size respectively). These effects

were more pronounced on 16HBE14o- cells than L5178Y mouse lymphoma and TK6 human B-lymphoblastoid cell lines (230).

PLGA-PEO NPs (average size ~ 160 nm, zeta potential: negatively charged) didn't show any genotoxicity potentials on TK6 lymphoblastoid cells and human peripheral blood cells as genotoxicity models using both comet and micronucleus assays. This confirmed that not only the physicochemical properties of NPs Play a role in their NP-cellular interactions but also the cell lines show an effect on the outcomes of this interaction (231, 232).

Inflammation: Upon 'foreign body' recognition in the airways (stimulating the pattern recognition receptors (PRRs)), phagocytosis and antigen presenting by macrophages and other inflammatory recruits to stimulate the inflammatory response by cytokines such as IL-6, IL-8, TNF-α, IL-1β or by ROS (233), or other signalling mediators (234, 235) (Figure. 1.9). More inflammatory cells are recruited to the site such as neutrophils, eosinophils or adaptive (B-, T- cells) lymphocytes and trigger inflammation via signalling pathways such as MAPK, JAK-STAT, and most commonly NF-κß pathways (234, 235). NF-kß signalling pathway is implicated in many inflammatory responses, immunity, and survival/death signalling (235). This is a physio-pathological reaction which in excess or persistence could predispose to autoimmune disease, long term diseases such as asthma, COPD, or CF, and lung cancer (149).

Hence, for lung delivery, the inflammatory potential of NP drug delivery should be determined. Nano-based lung delivery aims to deliver a nanosized particles or micronized NPs (NPMPs) (delivering a size below or larger than the alveolar macrophages phagocytic range; 1-3 μm) to bypass the MC (20, 106). When the MC

unresolved or persistent due to NP physicochemical potentials, NPs agglomerates or their prolonged pulmonary retention (due to slow degradation or elimination) or repeated exposures, inflammatory response would be evoked. Acute excessive or recurrent inflammatory lung reaction can predispose to chronic inflammatory response that can aggravate current lung pathologies (234). It has been known from the pathogenesis of lung silicosis that following inhalation of particulate foreign bodies (free crystalline silica, long fibres, and not biodegradable), these fibres were trapped longer due to defective clearance with subsequent inflammatory induction and development of lung diseases (234). Therefore, the multiple parameters of NPs physicochemical characteristics Play a role in inflammation induction (236). Changing the polymeric ratio or co-blending of *PLA* and *PLGA* to increase the size and prolong the degradation time (to act as a reservoir), Thomas *et. al.*, investigated aerosolized NPs ((size <500 nm, or > 500 nm), porous NPs of smooth surface, and negatively-charged) loaded hepatitis B surface antigen (HBsAg) as a vaccine model *in vitro* and *in vivo*. The higher *PLA* content NPs were of larger size (~1 µm), more hydrophobic, and were more preferentially internalized by rat alveolar macrophages with more production of cytokines: IL-2, IFN-ɣ (237). Calu-3 cell viability showed all NPs were biocompatible and well tolerated at low concentrations. *In vivo* inhalation in rats, NPs with higher composition of *PLA* showed longer lung residence, stronger IgA secretory titres denoting successful mucosal and humeral immune induction. However, there was no evaluation of the local lung or general inflammatory/distress indicators.

Another example, *PLGA* NPs encapsulating ovalbumin (as a model antigen (OVA)) and functionalized with lipopolysaccharides ((LPS), as a chemoattractant, as a pathogen mimicking) (LPS/OVA/*PLGA*) (238) were compared to the non-functionalized OVA/*PLGA* NPs (size 100-400 nm, using PVA); functionalized NPs

were preferentially internalized by the dendritic cells as antigen presenting cells (DCs, DC2.4 cell line) and stimulated the adaptive immunity CD8+ T cells with inducing IFN-γ cytokines release more than soluble LPS, OVA solution, OVA/*PLGA* NPs and blank *PLGA* NPs. Furthermore, in wild-type macrophages neither deficient in NLRP3 nor caspase-1, LPS/OVA/*PLGA* NPs showed preferential internalisation and production of IL-1β that indicated the inflammasome activation. LPS/OVA/*PLGA* NPs achieved stimulating PRRs in macrophages and DCs via two mechanisms: activating Toll-like receptors (TLRs) via LPS (triggers TLR4) that activated NF-kβ proinflammatory pathway, or through NOD-like receptors (NLRs) via *PLGA* NPs (NLRP3) activating the inflammasome complex that induced caspase-1 to activate pro IL-1β. Hence tuning the physicochemical properties of *PLGA* NPs increased the immunogenicity of the encapsulated antigen (239).

Similarly, Kunda *et.al*., had successfully formulated *PGA-co-PDL*NPs (~ 300 nm and negatively charged) with surface adsorption of Pneumococcal surface protein A (PspA4Pro) as a vaccine against Streptococcus pneumoniae infection. The NPs were incorporated in MPs to achieve a respirable size (~1.7 µm) via spray-drying. *PGA-co-PDL* NPMPs were biocompatible and well tolerated at low concentrations against A549, -16HBE14o-, and JAWS II DCs cell lines (38). The authors had ensured that the stability and the functional integrity of the antigen were preserved after successful loading into NPs. Furthermore, these potential carriers had been further investigated by Rodrigues *et al*., (25) *in vivo* using female specific-pathogen-free (SPF) BALB/c mice animal model via administration to the lung as nasal instillation (PspA NPMPs) or vis SC injection of the purified protein (PspA solution). Lung administered vaccine had showed lower serum IgG levels to SC after the first dose. This could indicate a slower primary immune response for lung delivery. However, the inhaled route had showed

more robust secondary immune response, higher serum IgG titres, better and earlier infection control post-challenge with bacterial strains. BALF had shown higher antibody IgG and cytokines titre (IFN-γ, IL-1β, IL-5, IL-6, IL-10, IL-17A, KC/CXCL1, MCP-1/CCL2, MIP-2/CXCL2 and TNF-α). The PspA solution was nasally instilled and induced negligible response. The NPMPs empty were nasally instilled and showed lower BALF bacterial load post-challenge and reduced the proinflammatory cytokines indicating a non-specific immune stimulation. The PspA/NPMPs showed better therapeutic performance and increased the lung immunogenicity of the adsorbed antigen. The authors had evaluated the survival rate, local lung inflammatory, and systemic immune response to ensure the welfare of the animals were preserved denoting the safety of the formulation.

Cell death mechanisms are the final fate after any irreversible cytotoxic or stress insult. Cell death is referred to either programmed cell death known as apoptosis, and unprogrammed cell death known as necrosis (Figure. 1.9). NPs can induce complex cell death mechanism with many intersecting activations of different death pathways with a physicochemical dependant manner (240). NPs can trigger many intrinsic and extrinsic pathways and induce apoptosis, autophagy, lysosomal-induced cell death either through inducing external cellular or internal damage that is unrepairable and progress to cell death. The uncontrolled cell death or necrosis is commonly a passive accidental cell death due to energy failure or simply bursting in response to severe acute insult (193, 241). Necrosis is usually evaluated by the release of intracellular markers such as LDH release. While the apoptosis is usually evaluated by measuring cellular signals such phosphatidylserine or protein expression such as caspases enzymes such as caspases 3/7, 8 or 9 that have major roles in the downstream of programmed cell deaths (242, 243). Very recently, the Nomenclature Committee on Cell Death had

adopted new considerations to replace the old cell death classification to the new adopted and emerging mechanisms provided by many studies that have discovered variable mechanisms of the programmed cell death such as apoptosis, autophagy, ferroptosis, pyroptosis, necroptosis, paraptosis, lysosomal-induced, autoimmune-induced, and many others. These processes have different fundamental mechanisms with different underlying biological and histological picture of the cell death (240, 241).

1.4.1.2. NPs Physicochemical-Dependant Toxicity Determinants:

Nanoparticle size and surface area: NPs have intrinsic properties that Play a role in their beneficial advantages as well as their toxicity (Figure. 1.10 and Table. 1.5). Lowering the size to nanoscale (1-1000 nm) is associated with increasing the surface area for the same mass or volume. This explains their high reactivity and strong adsorption properties that Plays both roles in facilitating their biomolecular interaction and NP-NP interactions (aggregating/agglomerating) as well as their toxicity (244). For lung delivery, delivering nanoscale size is to achieve better crossing of the biological barrier and to evade both MCC and MC.

For targeting the deep and lower lung airways, is achieved by controlling NP size. Lung deposition for particles < 3 μm AD has 50-60% deposition in the deep airways via both sedimentation and diffusion. Particles in the diffusion range (< 1 μm AD) have the highest deposition efficiency in the deep narrow distal airways (132, 245). To increase the deposition with evading MCC, NP size is optimized in a range that facilitates their mucosal clearance escape. However, the effective mucosal mesh formed by entangling mucin fibres and other glycoprotein inducing highly viscous and tight mesh pores (100 nm-few micrometre range) can effectively trap a lot of inhaled NPs (246, 247). Hence, the new strategies to functionalize NPs with a variety of surface

coatings such as mucoadhesive and mucopenetrative materials to increase the mucosal penetration ability of NPs (7, 248-250) .

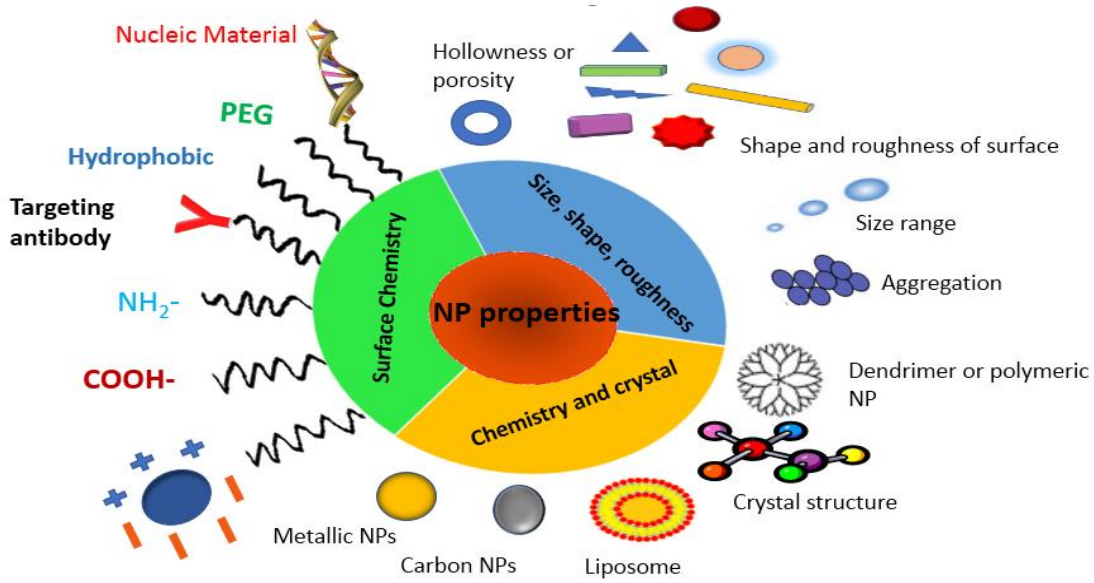

Figure. 1.10. Nanoparticle physiochemical properties (Reprinted with permission (11)).

Nanoparticle surface chemistry: NPs with specific charge, surface coatings or modifications are intentionally designed to achieve some pharmaceutical or therapeutic targets such as increasing the stability of the formulation, increasing the efficiency of protein adsorption with cationic NPs (23, 74), reducing the immune system recognition, prolonging the circulatory half-life (Figure. 1.10 and Table. 1.5) (200). This surface charge is designed using different surface coatings or modifications and measured by determining their zeta potential. For example, positively charged NP are coated with amine groups using cationic emulsifiers such as 1,2-Dioleoyl-3-trimethylammoniumpropane (DOTAP), chitosan (CS), CTAB, DMAB), while negatively charged NP are coated with acidic groups such as Polyvinyl alcohol (PVA), poloxamer188 (PF68) or neutral NP charge (near the neutral or slightly negative charged NPs) (251).

Table. 1.5. NPs properties and possible cytotoxic effects (11).

NP properties	Physicochemical dependant cytotoxicity
NP size	• Cellular penetration and crossing tissue barriers • Cellular injury and membrane damage • Escape defence mechanisms and longer retention • Translocation to other organs • Inflammation • Subcellular localization and organelle impairment • DNA damage
NP agglomeration	• Phagocytosis and inflammatory induction • Reduces the uptake
Surface area	• Increased reactivity and toxicity • Increase ROS production
NP shape	• Rod or fibre-like more toxic than rounded shaped NP • Inflammatory induction, membrane or organelle damage
NP charge	• Positive NP: more cellular interaction and cytotoxicity • Negative NP: might increase or decrease cellular uptake, prone to macrophages clearance.
Chemical structure, composition, and purity	• Increased toxicity • Membrane depolarization • ROS generation • Mitochondrial damage • Inflammation and immune modulation • Cellular injury and metabolic impairment • DNA damage • Transporting/adsorbing contaminants and toxins
Poor solubility/ biodurability	• Bioresistant NP induces long term effects as chronic inflammation • Long term effects • Cancer

The NP charge Plays a major role in NP performance and biomolecular interactions. As previously mentioned the cationic NPs are commonly reported to be cytotoxic than the negatively and neutrally charged NP by interacting with cell membrane by different mechanisms (158, 196-199) and higher bimolecular interaction and protein adsorption (23, 74) that makes them suitable for delivery of negatively

charged molecules such as RNAs (23, 97, 102) and different types of macromolecules (3, 23, 25, 74, 101). However, the surface charge and the high adsorption energy and interaction of NPs were involved in the development of protein corona once in contact with a biological medium such as lung fluid and surfactant (139, 252). Protein corona are formed by the adsorption of molecules found in the biological medium at the drug delivery site to NPs surface leading increasing their size and aggregation, masking the surface charge, and opsonizing their surfaces with further enhanced MCC and MC. Protein corona can enhance the NPs efficacy or toxicity (139, 252). There were many studies to evaluate the protein corona *in vitro* and *ex vivo*. *In vitro* is usually assessed via dispersing the designed NPs in the medium used for the cell culture then evaluate their size and charge (size increases, the cationic NPs convert to negative charge) to estimate the NP aggregation and adsorption of protein. Partikel *et. al*, (253) tried to identify and quantify the proteins involved in the protein corona formation from FBS after dispersing *PLGA* NPs (~100 nm and 200 nm, negatively charged), *PLGA*-PEG NPs (*PLGA* 50:50, co-block with 15% PEG 5 KDa) of the same size and charge. The authors found that the amount of protein adsorption was not size dependent as there was almost no big size difference between 100 nm to 200 nm. However, *PLGA* NPs without PEG shielding showed higher amounts of protein adsorption, around 29-39 different types of protein compared *PLGA-PEG* NPs (lower amount of protein adsorption, and 16-23 different types of protein). *PLGA* NPs showed adsorption for proteins with higher MW (29, 66, 118 KDa) but *PLGA-PEG* NPs had adsorption for lower MW and almost no proteins above 118 KDa. Another study investigated the corona formation using *ex vivo* swine lavage lung surfactant was carried by Raesch *et. al.*, (254). Magnetite NPs was functionalized by three different coatings (phosphatidylcholine; (lipophilic NP), PEG5000; Hydrophilic PEG NP), and *PLGA*

coating (*PLGA* NP). The lipid adsorption to NPs was the smallest to PEG NP and the highest to lipid NP. The proteins were more than 300 types identified on the surface of the NPs, with selectivity of SP-A and SP-D adsorption for lipophilic to hydrophilic NPs (254). Hence, shielding the NPs is a mechanism where the NPs are covered with hydrophilic polymers, commonly PEG, to limit the protein adsorption. PEGylated NPs for drug delivery show more stable, longer shelf-life formulations and better therapeutic performance. Hidalgo *et el*., suggested coating NPs by lung fluid surfactants to enhance the their therapeutic performance and limit the corona formation (255).

Mucoadhesive properties (MAP) or mucopenetrating properties (MPP) are being investigated as surface coating modalities for NPs aimed for inhalation delivery to increase the mucosal entrapment and enhance the NP delivery. Schneider *et al*. studied the effect of surface coating with MAP or MPP coatings using polystyrene NPs in *ex vivo* models and *in vivo* mouse models. MAP NPs showed increased entrapment within the mucous layer, aggregations and subsequent clearance, regardless their size. MPP NPs up to a size of 300 nm (after this, entrapment by the mucous mesh networks) showed better uniform lung distribution and enhanced retention. The NPs then were loaded with dexamethasone and studied again *in vivo* concluding the superior effects of the MPP NPs over the MAP NPs and the free drug in reducing acute inflammatory mouse lung model (256).

Nanoparticle morphology: The shape of the NPs is another important factor affecting the membrane vesicle formation, cellular uptake and digestion, circulatory retention and distribution. NP shape can vary from rounded or oval spheres, ellipsoids, wires or rods, cubes, sheets, cylinders and many others (Figure. 1.10 and Table. 1.5). Aspect ratio (AR) is a term to describe non-spherical particles that have a length and a width rather than a diameter. AR is the ratio of length to width (257).

Generally, the spherical NPs are safer and faster to be endocytosed than rod- or fibre-like NPs. Spherical NPs can be deposited in the lung via different mechanism such as impaction, settling or diffusion, but the longer aspect or fibre-like NPs are deposited by interception (132). The fibre-like NPs are accused of causing macrophages frustration with increase the inflammation potentials and carcinogenicity, i.e, asbestos and silica (258).

PLGA-PEG NPs of a needle-shaped showed more cytotoxicity than the spherical particles (similar volume, surface chemistry and negatively charged, prepared by film-stretching from the spherical NPs) when assessed *in vitro* (in HepG2 and Hela cell lines): more cytotoxicity evaluated by MTT, loss of LDH, and DNA fragmentation by (TUNEL assay). The cytotoxicity of needle-shaped *PLGA* NPs were due to damage of the cell membranes and the lysosomal vesicles disruption with upregulating caspase 3/7 and DNA damage and cell apoptosis (257).

Yoo & Mitragotri (259) suggested a shape-switching NP as a mechanism to escape/postpone the phagocytosis. *PLGA* was used to fabricate Rod-like elliptical disks that can switch to spheres upon external stimulation as temperature, pH, and chemical substances. *PLGA* elliptical disks were added to murine macrophages and showed defective phagocytosis, when the stimuli of lowering the pH were applied, the disks underwent spherical shape within time that would enhance their uptake after successful drug release (260).

Nanoparticle chemistry: Generally, NP chemistry is being referred to parent bulk materials of NP core. It usually used to classify NPs such as organic NP, i.e., carbon-based, lipid-based, polymeric, or metallic NPs, i.e., silver, gold, titanium NPs.

However, the exceptional physicochemical properties gained at the nanoscale must be assessed prior to their intended application (Figure. 1.10 and Table. 1.5).

Chemical properties of NPs have an important role in both the pharmaceutical and clinical performances; chemical structure, composition, crystal structure, chirality and isomerism, MW, monomeric ratio, degradability and degradation products, hydrophobicity, drug-loading capacity, drug release kinetics, surface properties or functionalization. Hence, chemistry of NPs provides immense potentials to tune the NPs physicochemical properties to enhance their performance. As aforementioned, versatile nature of biodegradable polymers such as *PLGA* allows for tuning MW, degradation, hydrophobicity, and crystallinity to suit different purposes. For example, tuning *PLGA* (50:50) with different MWs (6, 14.5, 45, 63.6, 85, and 213 KDa) showed effect on the NP size, degradation rate, drug loading, and release. Increasing the MW was accompanied with an increase in the NP size and drug loading, but with slow degradation, and low drug release but continuous and longer (71, 261-263).

Composition of the NP formulation may include remaining solvents, emulsifiers, or excipients or other impurities that could participate in NP toxicity. Grabowski *et al.*, (264) studied the *PLGA* NPs stabilizer free to *PLGA* NPs prepared with different coatings (CS, PF68, PVA) ~ 200 nm size on THP-1 macrophages. *PLGA* NPs stabilized with different coatings showed higher cytotoxicity at high concentrations compared to stabilizer free NPs. LPS contamination is another example that can interfere in evaluating NP inflammatory effects producing false-positive results. It is further compounded by the available commercial assays for LPS detection are subjected to artefacts and NP interferences (265-267).

Nanoparticle aggregation: NP aggregation is another property that depends upon other NPs characteristics and the dispersing media (Figure. 1.10 and Table. 1.5). It needs to be considered to understand the poor correlation between different toxicity studies, i.e. inhalation or instillation or *in vitro* studies. NP aggregation could Play a double effect; it could increase NPs uptake as larger amount of particles in contact with cellular surface (268), or it could reduce their uptake if NP aggregates are bigger than cellular size to permit the uptake (269). *In vivo*, it may play an effective role in reducing their toxicity due to easier macrophages clearance (86). NP aggregates might increase the retention of NPs either in the lung or RES exerting inflammatory potentials (270).

Repeated dose exposure: The repeated lung exposure might happen in chronic lung conditions such as cancer, COPD, CF, and asthma. Here, small doses deposited may accumulate inducing chronic effects. It is well known from lung exposure to environmental and occupational settings, repeated exposure to slow degrading or bioresistant particles are associated with development of serious lung disease. Hence, NPs formulations designed for chronic diseases must be evaluated to ensure the safety and suitability for long term treatments. However, it is difficult to study the chronic exposures *in vitro* and usually preferred to be evaluated *in vivo*. Some studies tried to study chronic exposure by repeated short-term exposures. Attias Cohen *et al.*, (21) formulated *PLGA* NPs (50:50 MW 96KDa, PVA coated) ~ 100 nm coated SP-D as treatment for ARDS in infants to deliver a sustained release drug delivery via the lungs. NPs formulation were tested *in vitro* using A549 cell lines and *in vivo* using C57bl/6 mice after intra-tracheal injection. SP-D *PLGA* NPs showed some cytotoxicity on A549 compared to empty NPs (it was high concentrations used 0.5 and 1 mg/ml). The authors evaluated the structural and functional integrity of SP-D had been preserved within the formulation. *In vivo* acute exposure in mouse model (after 24 hrs postexposure), showed

well tolerated with good release profile of SP-D in BALF and low IL-6 levels, with normal lung histology with several inflammatory infiltrations but were similar to control group exposed only to PBS solution. The chronic study; two weeks and 4 weeks postexposure; BALF should good release profile and low IL-6 levels, normal histological picture of lung tissue with similar number of inflammatory infiltrations to the control.

The dose-dependent toxicity: The mass dose of the NPs alone is not solely responsible for the toxicity in comparison to the conventional parent bulk molecules. However, interpretation of NP physicochemical induced toxicity should be considered. *In vitro* to *in vivo* (*IVIV*) nanotoxicology studies have shown conflicting results regarding the dose-dependent NP toxicity. It is commonly due to high doses used in conducting these studies to obtain detectable signals to uncover the mechanistic interactions under *in vitro* conditions. Therefore, discrimination between test conditions with high doses or within the range of the aimed therapeutic doses should be considered (86).

1.5. Nanotoxicology Assessment Methods:

For nanotoxicological evaluation, NPs biocompatibility must be confirmed by two methods; *in vitro* then progress into the *in vivo* methods prior to clinical trials. There are different methods that are increasingly getting more popular in the research communities, i.e., *ex vivo,* and *in silico* methods and showing promising results (271-273). Prior to their biological interactions, NP physicochemical properties must be thoroughly characterized (274). NP characterization is essential not only to understand and characterize their NP-biological interactions but also to allow for easy comparability and validation, comprehensiveness, wider scientific acceptability, and

understanding of the concluded results for further optimization of nanomedicines (11, 14, 29, 275).

1.5.1. *In vitro* Lung Models:

These are cell-based lung models. They provide simple initial screening, less costly, and non-animal assessment of NP interaction with lung epithelium. These assessments are very desirable both ethically and economically with a better control over the experimental conditions, allowing wide range of concentrations, single or multiple parameters, and many types of NPs to be tested (314, 315).

Types of cells used are either primary or secondary cell lines (Table. 1.6). Secondary cell lines are either cancerous cells or a genetically transformed immortalized cell line, hence called continuous cell line (275). They are more widely used and commercially available from many vendors, i.e., American Tissue Type Culture Collection (ATCC). They provide easier experimental handling and maintenance, faster growth and shorter experiment time (276-278)

Cancerous human cell lines: Calu-3 is one of the commonly used lung cell lines. They are of bronchial epithelial adenocarcinoma origin. They can be cultured under air-liquid interface (ALI) as well as liquid-covered culture (LCC). Calu-3 under ALI develop tight polarized monolayers and more differentiation to airway epithelium (columnar epithelia, ciliated, mucin production). Hence, it is a wide available model for *in vivo* lung (279). A549 alveolar carcinoma cell line is a widely used model for the alveolar epithelium. However, it doesn't form tight polarized monolayers, hence problematic to grow under ALI (280, 281).

Immortalized human cell lines: 16HBE14o-, BEAS-2B are such immortalized bronchial cell lines that are gaining popularity due to their differentiations (mucin

production, ciliated columnar epithelium). Immortalized alveolar cell lines such as NCI-H441, hAELVi, and TT1 cells are very recently developed and showing promising results in forming tight polarized monolayers (276, 277).

Table. 1.6. Examples of *In vitro* human lung cell models (282).

Cell type	Origin	Bronchial	Alveolar	Immune cells
Secondary cells	Cancerous	Calu-3	A549	THP-1* DC*
	Immortalized Genetically transformed	16HBE14o- BEAS-2B CFTE29o– CFBE41o– CuFi-1 NuLi-1	hAELVi NCI-H441 TT1	
Primary cells	Normal lung	NHBE MucilAir; SmallAir EpiAirway	Pneumocyte- II	
*To study immune response as professional immune cells to represent lung exposure				

Primary human cell lines: These are a harvest of a lung tissue during lung biopsies or bronchoscopy available from commercial vendors such as Epithelix (MucilAir) and MatTek (EpiAir). They are provided on special plates with special nutritional media. They are more challenging in isolation, differentiation and phenotyping, maintenance, difficult experimental control, and ethical requirements, and most critically of a short life span. As a result, their use is limited due to very expensive and onerous testing but more closely representative for the *in vivo* counterparts (283).

2D monoculture or co-culture: 2D monoculture of a single type of cells is usually the common and classic model being used. However, it lacks the multiple cells interactions and cross communications of *in vivo* target, it remains the cornerstone widely used model to provide the biomechanistic interactions of NP (282). Co-cultures of different lung cell lines depending upon the aim of the study. For example, co-culturing lung epithelial cells with macrophages are being investigated to provide more resemblance to *in vivo* lung tissue. However, they are very sophisticated with special maintenance requirements, not yet standardized. These are showing promising results so far but yet more need for understanding the complex cross communication between the epithelium, endothelium and the inflammatory cells to reflect a representative model (284).

3D lung models: 3D models have closer representation and are either a single cell type or a co-culture of different cell types within the tissue that provides the cell-cell interaction and communication with enhanced *in vivo* correlated results (285). 3D co-culture models known as spheroids or organoids are grown in a 3D scaffold made of inert materials as collagen, matrigel®, or others, supplemented with stem cells or tissue cell mixtures and stimulated by different stimuli to differentiate the cells into lung structures. ‘’Organ on chip’’ or miniaturized lung, microfluidic systems, 3D bioprinting are alternative 3D co-culture models where the lung organoid is subjected to mechanical and physical factors mimicking the biological environment, i.e., ALI with fluidic flow systems (286). The advantages of these miniaturized lungs models are reliable, more physiologically relevant, and simulating biological environment with the ability to screen many drugs prior to *in vivo* (287). Yet the extreme expensive nature and the complex experimental requirements are major challenges to their widespread use.

Experimental exposure under ALI or LCC: *In vitro* cell lines exposure to NPs is commonly assessed under submerged conditions, i.e., LCC which expose the cells to a liquid NP solution allowing the NPs to sediment/diffuse to cell surfaces. However, ALI exposure systems are being developed and described in many studies to mimic *in vivo* exposure. The difficulty to produce aerosolization mechanisms to generate NPs droplets that can be deposited on the cell layers as well as the expensive nature, and experimental complexity are challenges for their use (322-325).

Cellular endpoints and readouts: Nanotoxicological assays commonly evaluate cellular endpoints such as cellular uptake, internalisation and intercellular transport, membrane potential, mitochondrial potential, effects on the cytokines or chemokines and cell signalling, oxidative stress (ROS or RNS), cell death and apoptosis, gene regulation and toxicity. The goal of these methods is to uncover the mechanism of cell-NP interaction and discriminates between NPs compatibility versus toxicity (172).

These assays commonly employ an enzyme-linked assay with final read-out by fluorometric or spectrometric detectors. Other methods are through special stains or dyes and evaluated under microscopy and flow cytometry. The cells are usually exposed to NP dispersions within a variable range of time (few hours up to days) then processing the cells for the endpoint results (309, 313). For example, a group of tests including the Alamar Blue, Tetrazolium, Neutral Red, Trypan blue-based assays that are used to detect general toxicity of NPs, LDH assays to detect membrane potential, DCF fluorescence assay, lipid peroxidation or Glutathione assay to detect the oxidative stress potential. Inflammatory response can be assessed using ELISA kits or Cytometric Bead Arrays for screening a variety of cytokines and chemokines. Genotoxicity

assessed by using micronucleus, COMET, and chromosomal aberrations tests (316-318).

Recent advances in cell-based assays allow for high throughput screening for toxicity and/or efficacy of NP-biological interactions (Table. 1.7). By assaying numerous material types/functionalization and material concentrations on numerous cell types, all in parallel, complex interactions between materials and cells may be ascertained through complex data analysis that correlates phenotypes with multi-well Plates, cell culture, detection schemes, and recognition schemes (317, 318, 320, 321). This experimental design is practically enabled through the miniaturization and multiplexing of the experimental apparatus and method by utilization of either ultra-small 384-well cell culture plates or nanodrop sample chambers on a chip. The nanodrop assay setup allows for different assays with suitable detection features (e.g., fluorescence, and luminescence) to be performed in a fraction of the volume. Yet the expensive nature limiting its use.

1.5.2. *Ex vivo* lung Models:

These methods employ viable excised animal tissues or organs while their structure maintained under simulated natural conditions (288). *Ex vivo* models provide conditions to mimic *in vivo* response and more control over experimental conditions. They evaluate NP uptake, distribution, and toxicokinetic (Table. 1.7).

Ex vivo animal models such as isolated perfused rat lung (289), precision cut lung slices (290), and porcine lung (291) are being used to test inhaled pharmaceuticals. They require extensive preparation and experimental setup, of short life span (~3 hrs) with interspecies variability.

Ex vivo human single or whole lungs (292), or human resected lung lobes (293), human precision cut lung slices (294) are getting investigated for better representative models to human *in vivo* lung. The major limitations are;

- The heterogenicity of human donor variabilities, i.e., disease, smoking history, other underlying conditions,
- Sampling is possible from alveolar spaces 'odema fluids' and from the venous but it is not possible to sample from the lymphatics or pleural space,
- The absence of multiorgan responses, especially important to study the inflammation,
- The short life span of the model (6-10 hrs),
- Extensive preparation and maintenance nature of these models, the required ethical and skilled expertise made it very demanding task,
- Inability to relate the appropriate dose to the *in vivo* studies remains an un-overcome challenge.

1.5.3. *In vivo* Lung Models:

Inevitably, the *in vivo* studies will follow the *in vitro* experiments to validate a range of realistic NPs doses on animals (Table. 1.7). *In vivo* animal studies provide more consistent clue for uncovering the NP kinetics, and understanding of the biological exposure-response, dose-range, and toxicity to support the subsequent human clinical trials. Some concerns arise when testing the NPs *in vivo*, first, the dose is difficult to translate from *in vitro* doses to the *in vivo* animals where it is not uncommon *in vitro* experiments to have very high toxic dose ranges (295). The main disadvantages, the issues of interspecies variability; where the lung of mice, or rats is

much smaller and less complex compared to human lung, the difficulty in real time bioanalytical assessments of NPs *in vivo* (276)

1.5.4. *In silico* Lung Models:

The use of computer-based programs that use huge piece of available data to predict the NPs toxicity (Table. 1.7). Quantitative structure–activity relationships (QSAR) are rapidly evolving approaches that need developing for the exceptional characteristics of NPs (296). These models aim to provide very accurate models with pre-set standard of parameters to enable predicting and linking NPs based on their physicochemical characteristics and their potential bioactivity, behavior, and toxicity (297). For example, QSAR models have been developed on physicochemical characters (298), or pharmacokinetic models based on *in vitro* and/ or *in vivo* data (25), environmental behavior models (299), e.g. mode of transport and fate. A study by Gupta *et al.*, had successfully predicted the *in vitro* cytotoxicity of five different NPs based on their physicochemical characters (39). *In silico* models are yet to be validated for the NPs models even though they are validated by OECD guidance for conventional chemical testing (288, 300, 301). Successful QSAR models are in need for data availability of accurate and consistent grouping of NPs based on physicochemical characters, mechanisms of action, exposure scenarios, standardized *in vitro* and *in vivo* testing conditions. This is a quite big challenge due to NPs novelty. Furthermore, the availability of these models remains another challenge, as not much is known about how to build up these models and what parameters are needed. Sharing and reporting data have mutual benefit to close the gaps in NP knowledge (1, 275, 302).

Table. 1.7. Advantages and limitations of nanotoxicological assessment methods

	In vitro	*Ex vivo*	*In vivo*	*In silico*
Advantages	• Initial Faster screen • High throughput screen • Easy to perform/ control • Easier dosing • Immortal continuous cell lines • Mechanistic and toxicity studies • Permeability and uptake studies • Non-animal alternative	• Fast screen • Relatively controlled and easy dosing • Better multicellular and organ response for mechanistic and toxicity study	• Whole body exposure • Biodistribution data • Single or repeated exposure • Acute or chronic toxicity • Short term and long-term studies	• Predictive ability for mechanistic and toxicity • No animal cruelty • Computer-based studies
Limitations	• Lack of multicellular interactions • Difficult to translate in-vivo • Short term exposure • Lack of standardizations • Difficult to compare between different studies • Variations between primary and immortalized cell lines	• Lack of biodistribution data • Difficult to maintain and handling • Short term exposure	• Training and handling • Expensive and technically demanding • Animal discomfort and cruelty • Labor demanding • Interspecies variability • Sometimes poor human translation	• The availability of enough information that enables the study • Lack of experiments standardizations makes it difficult to compare different results

.

1.6. Aims of the study:

The aim of the study was to investigate the nanotoxicity of polymeric NPs based on chemistry (*PLGA* vs *PG*A-co-PDL), size (*PGA-co-PDL* & *PLGA* NPs of 200 nm, *PGA-co-PDL* & *PLGA* 500 nm, 800 nm), and the surface charge (Negatively charged vs positively charged) for pulmonary delivery.

This was accomplished through the following chapters:

Chapter. 2: To investigate the effect of physicochemical properties of *PLGA* vs *PGA-co-PDL* NPs on their stability and degradation in different biological media through the following objectives:

1. To formulate and characterize 8 types of NPs based on two polymers (*PGA-co-PDL* vs *PLGA*), 3 sizes (200 nm, 500 nm, and 800 nm), and surface charge (negatively and positively charged),
2. To study the NPs stability, i.e. size and charge, and degradation in different biological media.

Chapter. 3: To investigate and compare *PLGA* vs *PGA-co-PDL* NPs interactions at different concentrations using pulmonary cell lines. This will be achieved using *in vitro* methods through the following objectives:

1. To evaluate the general cytotoxicity using Alamar Blue assays, ROS detection, cell membrane and mitochondrial membrane potentials,
2. To differentiate between the apoptosis and necrosis cell death with evaluating the caspases production,
3. To detect the inflammatory response after THP-1 exposure to NPs by measuring a screen of pro- and anti-inflammatory cytokines,

4. To detect any genotoxicity after NPs exposure by COMET assay.

Chapter. 4: To investigate *PLGA* vs *PGA-co-PDL* NPs internalisation in Calu-3 cell lines through the following objectives:

1. To investigate the NPs effect on the integrity of the epithelial barriers through calculating the apparent permeability coefficient of [^{14}C]-mannitol as a paracellular marker after polarized Calu-3 cell exposure to NPs at different concentrations and time points,
2. To determine the underlying mechanisms for NP uptake using different pharmacological inhibitors,
3. To visually confirm the NPs internalisation and the subcellular co-localization by confocal microscopy.

2. Polymeric Nanoparticles Formulations, and Characterisation

2.1. Introduction:

Aliphatic polyesters such as *PLA, PGA, PLGA* are amongst the commonest synthetic biodegradable polymers widely used in biomedical applications (303). These polyesters can be synthesized through conventional polymerization reaction, which is a group of different chemical reactions that commonly involve either ring-opening polymerization (ROP) and/or polycondensation (62). These methods of polymerization suffer from harsh reaction conditions; using very high temperatures (above 200 ^{o}C), requiring high pressures, being catalysed by hundreds of toxic metallic catalysts, producing multiple by-products, and involving many steps of protection and de-protection of the functional groups (61). The main drawbacks are less control of the polymer chain length, broad molar mass distribution, longer reaction times needed to produce high MW polymers, extensive filtrations and purifications, poor yield, and failure to preserve important functional groups. Alternatively, the use of enzymatic synthesis has provided greener polymerization process (64, 303, 304).

Two decades ago, an enzyme, Lipase, was isolated from Candida antarctica (CA). It catalyses the hydrolysis of lipids and fatty acids and is stable in organic solvents and was successfully used to catalyse polymerization reactions. This enzyme was used to catalyse the synthesis of functional polyesters with pendant hydroxyl groups via ROP (305-307) and polycondensation (308, 309). This was achieved under milder reaction condition and of shorter time, avoiding toxic catalysts, low cost, fewer by-products and easier filtration, and a higher yield of more linear polymers with a narrow molar mass distribution (310). This enzymatic synthesis had characteristic region-selectivity (311) and stereoselectivity (312, 313) protecting functional groups. Various lipases had been explored to catalyse various polymerizations of small or large molecules (304). At LJMU, our group managed to synthesize a novel polyester by

using Novozyme 435 (lipase enzyme (derived from CA) immobilized on microporous resin) to catalyse ROP and polycondensation of three monomers; glycerol, DVA, ω-pentadecalactone to produce *PGA-co-PDL* polyester (in Chapter.1: Figure.1.4) (72). (72, 77, 314). Using equimolar concentrations of these monomers, under very mild reaction conditions (50 ^{o}C), linear polymer chain and high MW, low cost and high yield are advantages of this in-house synthesis of 6 hr (34, 78, 314). This polymer was used to fabricate NPs and MPs using emulsification solvent evaporation methods. It was successfully loaded with a variety of hydrophilic and hydrophobic drugs, macromolecules, vaccines, and gene therapy (23, 25, 34, 72, 74-81, 106, 315-317).

It is very important for novel polymers to show good stability and long shelf life as well as good stability profile for fabricated drug delivery carriers such as NPs. *PGA-co-PDL* polymer showed good storage stability up to 1 year stored at 4 ^{o}C or at room temperature 25 ^{o}C and over drying sieves (0% humidity) in the dark (314). Its degradation was increased by humidity (75%) and high temperature (40 ^{o}C) due to the pendant hydroxyl group (Free OH- per glycerol) which makes it hydrolysable (314). *PGA-co-PDL* biodegradation as a polymeric matrix under physiologic conditions (37 ^{o}C, with continuous agitation) in phosphate buffered saline (PBS) buffer was slower (over 6 weeks) than *PLGA* (50:50), with the later having complete hydrolysis of its matrix in 4 weeks under similar conditions (314, 318). *PGA-co-PDL* hydrolysis is a heterogenous process due to random scission of the polymeric chain. However, MPs fabricated from *PGA-co-PDL* under the same physiologic conditions were completely hydrolysed by 6 weeks duration (314). This demonstrated that the formulated carriers such as MPs showed faster biodegradation profile than the matrix of their parent bulk material. This was due to the increased surface area of MPs compared to polymer matrix of the same mass. Hence, the importance of evaluating the stability and degradation not

only for the bulk polymer but also for the fabricated carriers to reflect on the optimization of nanomedicines. There has been no investigation of how different media could influence the stability and degradation of *PGA-co-PDL* NPs. Hence, this study explored the effect of physicochemical characteristics of *PGA-co-PDL* NPs compared to *PLGA* NPs on their stability and degradation in different biological media.

2.2. Aims:

To investigate the effect of physicochemical properties of *PGA-co-PDL* and *PLGA* NPs on their stability and degradation in different biological media through the following objectives:

1. To formulate and characterize 8 types of NPs based on two polymers (*PGA-co-PDL* vs *PLGA*), 3 sizes (200 nm, 500 nm, and 800 nm), and surface charge (negatively and positively charged),
2. To study the NPs stability, i.e., size and charge, and degradation profile in different biological media.

2.3. General Materials and Methods:

2.3.1. General Materials:

PLGA (50:50) acid terminated with MW of 7000-17000 KDa, Glycerol, ω-pentadecalactone, Nile red (NR) dye, Phosphate buffered saline tablets at pH 7.4 were, Poly (vinyl alcohol) (PVA; MW of 13–23 KDa, 87%–89% hydrolysed) were purchased from Sigma-Aldrich Chemicals, UK. Novozyme 435 (a lipase enzyme derived from CA and immobilized on acrylic macroporous resin) was purchased from Biocatalytics, USA, and was stored over P_2O_5 at 4 °C prior to use. Divinyl adipate (DVA) was obtained from Fluorochem, UK. 1,2-dioleoyl-3-trimethylammonium-propane (chloride

salt) powder (DOTAP) was kindly gifted from Lipoid Company, Germany. Methanol, Tetrahydrofuran (THF), Dimethyl sulfoxide (DMSO), were purchased from Thermofischers, UK. Purified water (DW) from a Millipore Purification System (Billerica, MA, USA) was used.

2.3.2. Methods:

2.3.2.1. Polymer Nanoparticle Formulation and Characterisation:

2.3.2.1.1. *PGA-co-PDL* Synthesis and Characterisation:

PGA-co-PDL polyester was synthesized through ROP and polycondensation catalysed by Novozyme 435 as previously described by Namekawa *et al.* and Thompson *et al.* (72, 315). Briefly, equimolar concentrations of Glycerol, ω-pentadecalactone, Divinyl adipate (0.125 moles) were Placed in three-neck flask 250 mL with 20 mL of THF then immersed in a pre-maintained water bath (50 ^{o}C) and allowed to equilibrate for 20 mins. Overhead mechanical stirrer (Heidolph RZRI type) fitted with a central stirrer paddle, and an open-top condenser (to allow for the acetaldehyde escape) were fitted. Novozyme 435 (1.25 g) was washed down by additional 5 mL THF. Stirring was commenced at a rate of 200 rpm and the reaction was left for 6 hr (typically gives MW ~ 14.5 KDa, increasing the reaction time allows for higher MW production). Then, the reaction was stopped by adding 100 mL DCM followed by filtration through standard Büchner filtration (to remove any residual enzyme resins) and solvent removal by rotary evaporation. To the remaining 20-30 mL pale yellowish viscous fluid, 100-150 mL Methanol was added to precipitate the polymer (removing any unreacted monomers/oligomers) through standard Büchner filtration. The polymer precipitate was left for 48 hr to dry at room temperature then stored in sealed jars under desiccator for further use. Schematic diagram of the chemical

synthesis of *PGA-co-PDL* polymer is represented in Chapter.1: Figure. 1.4. The MW, chemical structure and physiochemical properties were determined as reported by Thompson *et al.* (16).

2.3.2.2. Polymeric Nanoparticles Formulations and Characterisations:

2.3.2.2.1. Formulation of Different Sizes of Polymeric Nanoparticles:

NPs were produced using an emulsion-solvent evaporation method with PVA as an anionic emulsifier and DOTAP as a cationic emulsifier. To achieve three different size groups (~200, 500, 800 nm), three different formulation parameters were adopted from a previous in-house published study (74, 80) (Figure. 2.1. Schematic illustration of NP formulation) with some modifications briefly:

Nanoparticles of size 200 nm group:

NPs were formulated from both polymers, *PLGA* and *PGA*-co-PDL, using oil in water (O/W) single emulsion method. 200 mg of the polymer was dissolved in 2 mL DCM (cationic NPs were prepared with addition of a cationic emulsifier DOTAP as 10% (w/w) to polymer mass prior to adding DCM) and added drop wise to 5 mL of 10% (w/v) PVA under probe sonication (QSonica sonicator, USA) at 65% amplitude for 2 min in an ice bath. The mixture was added drop wise (within 10 min at 600 rpm) to 20 mL of 0.75% (w/v) PVA with continued magnetic stirring (Jeio Tech MS-53M, South Korea) at 500 rpm for 3 hr at room temperature to facilitate evaporation of DCM. NPs (2 mL of the emulsion containing 16 mg) were isolated by centrifugation and washed twice with 5 mL of DW to remove any excess surfactants, at 112,000 xg and 4ºC for 30 min using an Optima L-80 Ultracentrifuge (Beckman Coulter^{TM}, UK) with a 70.1 Ti rotor.

Nanoparticles of size 500 nm group:

NPs were formulated from *PGA-co-PDL* polymer using O/W single emulsion method. 300 mg of the polymer was dissolved in 1.5 mL DCM and added drop wise to (cationic NPs were prepared with addition of a cationic emulsifier DOTAP as 10% (w/w) to polymer mass prior to adding DCM) 2.5 mL of 10% PVA under probe sonication at 65% amplitude for 1 min in an ice bath then continue as above for 3 hr. NPs (1.2 mL containing 16 mg) were isolated as above with ultracentrifugation at 80,000 xg, and 4ºC for 30 min.

Nanoparticles of size 800 nm group:

Double W/O/W emulsion method was used. *PGA-co-PDL*(200 mg) was added to 2 mL DCM (cationic NPs were prepared with addition of a cationic emulsifier DOTAP as 10% (w/w) to polymer mass prior to adding DCM) and upon adding to the internal aqueous phase of 0.5 mL 10% PVA under probe sonication with amplitude 65% in an ice bath for 30 sec. This primary emulsion was then added to external aqueous phase of 25 mL containing 2 % PVA drop wise under probe sonication 45% amplitude for 30 sec and left under magnetic stirring at 500 rpm for 3 hr at room temperature. NPs (2 mL containing 16 mg) were isolated as above with ultracentrifugation at 37,000 xg, and 4ºC for 30 min.

Nile Red Labelled Nanoparticles for Imaging Confocal Microscopy:

NR dye was added to the polymer (2.5% w/w) prior to adding DCM and the process was followed as above to achieve the three sizes of polymeric NPs.

The codes for the different NPs used in the study are represented in Table.2.1.

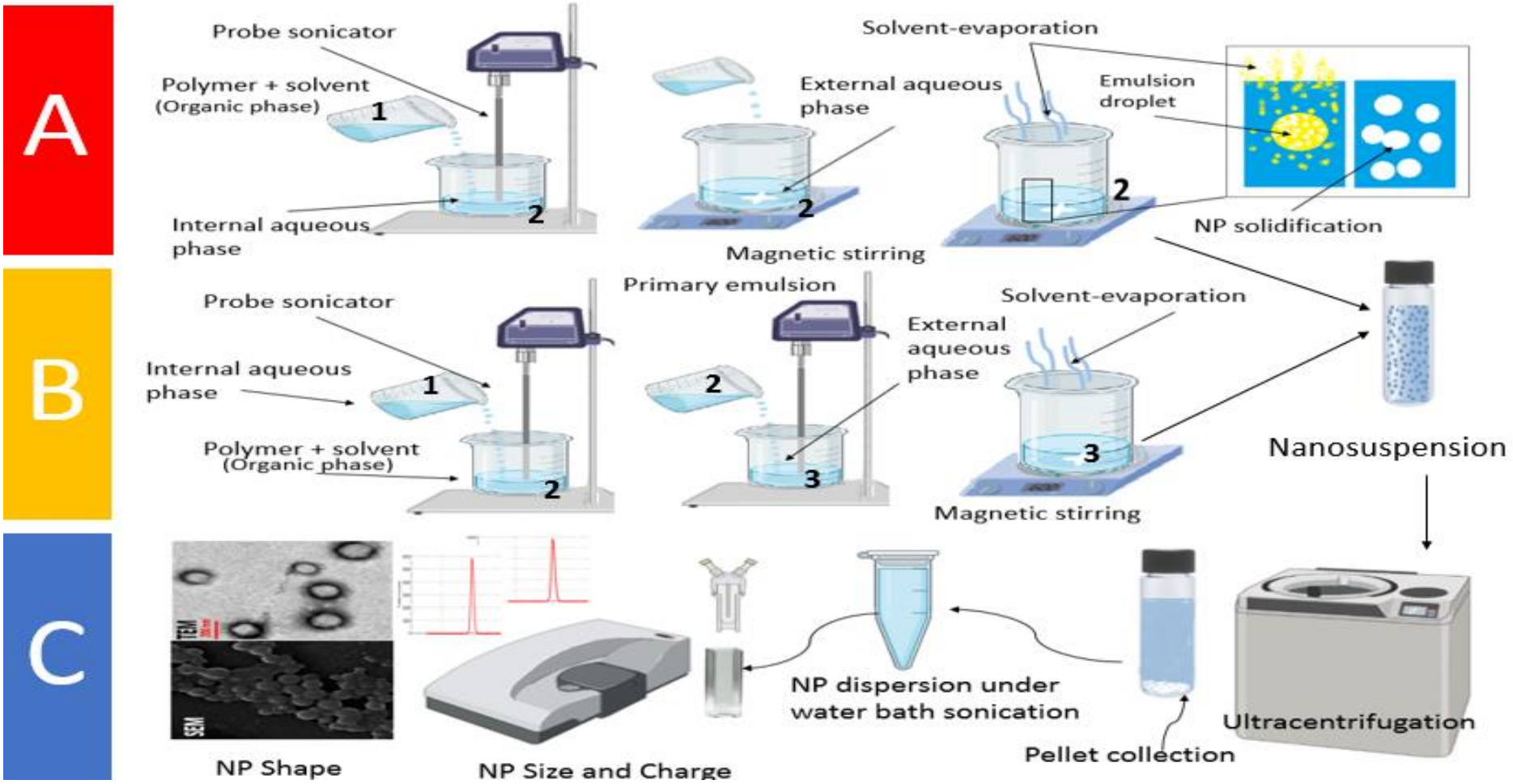

Figure. 2.1. Schematic illustration of NP formulation by emulsification solvent-evaporation methods: (A) Single-emulsion method, (B)Double-emulsion method, and (C) Isolation and Characterisation of NP size, charge and shape.

Table. 2.1. Codes of different NPs used in the study.

Polymer type	Size	Charge	Code used
PLGA	200 nm	Negatively charged/PVA	*PL*-2
PLGA	200 nm	Positively charged/DOTAP	*PL*+2
PGA-co-PDL	200 nm	Negatively charged/PVA	*PG*-2
PGA-co-PDL	200 nm	Positively charged/DOTAP	*PG*+2
PGA-co-PDL	500 nm	Negatively charged/PVA	*PG*-5
PGA-co-PDL	500 nm	Positively charged/DOTAP	*PG*+5
PGA-co-PDL	800 nm	Negatively charged/PVA	*PG*-8
PGA-co-PDL	800 nm	Positively charged/DOTAP	*PG*+8

2.3.2.2.2. Nanoparticle Characterisation:

Particle Size and Zeta Potential:

NPs average size and polydispersity index (PDI) were measured using Dynamic Light Scattering (DLS), and zeta-potential was measured by Zetasizer Nano ZS, Malvern Instruments Ltd, UK. NPs suspension in DW (4 mg/mL) was sonicated using water bath sonicator (Ultrawave, UK) for 10 min to disperse the NPs. A sample of 100 µL of NPs suspension was diluted in 5 mL DW and subsequently placed into cuvettes to measure the size. A sample of 100 µL of NPs suspension was diluted in 2 mL DW and placed into zetasizer cells for measuring the zeta potential. Measurements were taken at 25 ^{o}C ($n=3$).

Scanning Electron Microscopy (SEM):

A drop of the diluted NPs (0.125 mg/mL) sample was mounted on sticky conductive carbon covered aluminium stubs (pin stubs, 13 mm), then air-dried at room temperature prior to coating with palladium (10–15 nm) using a sputter coater (EmiTech K 550X Gold Sputter Coater, 25 mA for 3 min). Then NPs were visualized by SEM (FEI—Inspect S Low VAC Scanning Electron Microscope).

Transmission Electron Microscopy (TEM):

An aliquot of NPs (0.25 mg/mL) was added to an equal volume of a negative stain (1% Uranyl acetate) then a tiny drop was mounted on farmovar-coated cupper grids and air-dried, then visualised using the TEM (FEI Morgagni Transmission Electron Microscope, Philips Electron Optics BV, Netherlands) using acceleration voltage 100.0 kV.

2.3.3. Methods of Nanoparticles Stability and Degradation in Aqueous Media Study:

2.3.3.1. Nanoparticle Size and Charge Stability in Biological Media:

To understand the effect of the dispersing cell culture media such as cell culture media with 10 % FBS (CM) & serum-free media (SFM) on the size and charge of NPs. Polymeric NPs of the three different size groups, negatively and positively charged were formulated using the method described previously in section 2.3.2.2. NPs pellets following centrifugation were resuspended in 4 mL CM or SFM sonicated for 10 min until NPs were completely dispersed. Serial dilution was made to make 0.125 and 0.25 mg/mL NPs suspension. At two-time points; immediately (T0), and after 24 hr incubation at 37 ^{o}C (T24) with gentle shaking, 100 µL of each concentration was dispersed in 4 mL DW and characterized for size and charge using DLS without prior sonication *(n=2)*.

2.3.3.2. Nanoparticle Degradation in Aqueous Media:

The NPs degradation was studied under two conditions; PBS stored at 4 ^{o}C (to simulate *in vitro* storage conditions) and in simulated lung fluid ((SLF), to simulate *in vivo* degradation) prepared by Gamble's solution (pH 7.4) (319) and incubated at 37 ^{o}C

under axial rotation of 15 rpm using Hula Mixer^{TM} Sample Mixer (Life technologies, UK).

Briefly, 10 mg centrifuged pellets were immediately resuspended in 5 mL PBS or SLF and sonicated for 10 min until NPs were completely dispersed. Prior to characterisation (size and charge) and measurement of pH, samples were sonicated for 5 min and analysed at day 0 (D0), D1, D3, D7, D14, D21, and D28. To assess the MW, NPs samples were freeze-dried at D0, D7, D14, D21, and D28. MW measurements were carried out for all the samples at the last daily interval, i.e., D28 using GPC as previously described at section 2.3.2.1.2 *(n=2)*.

2.3.4. Statistical Analysis:

All statistical analysis was performed using GraphPad Prism 7.04 statistical software using One-way analysis of variance (ANOVA) and applying Dunnett's multiple comparison test to compare mean of each formulation with the untreated control and Tukey's multiple comparison to compare the mean of different formulations with each other. All values were expressed as mean ± standard deviation of three independent experiments (*N=3*) unless otherwise specified. The results showed reproducibility. Statistical comparison was done between *PG* and *PL* NPs at 200 nm (*PG*-2 *vs PL*-2, and *PG*+2 vs *PL*+2) to detect the chemistry-induced effect, *PG* NPs of different sizes (NPs 200 nm *vs* 500 nm, NPs 200 nm *vs* 800 nm, NPs 500 nm *vs* 800 nm at the same charge and concentration) to study the size-induced effect, and negatively charged NPs to positively charged counterparts of same size, chemistry, and concentration to study the charge-induced effect. The key symbols used for these comparisons are presented in Table 2.2. The *P* values are expressed as **P*<0.05, ***P*<0.01, ****P*<0.001, *****P*<0.0001 where * could be any key symbol used for the comparison from the Table.2.2.

Table. 2.2. Statistical key symbols used in this study.

Comparison	Symbol
Control, e.g. untreated cells (NC)	•
PG-2 vs *PL*-2 or *PG*+2 vs *PL*+2	#
PG-2 vs *PG*-5 or *PG*+2 vs *PG*+5	**X**
PG-2 vs *PG*-8 or *PG*+2 vs *PG*+8	**Ø**
PG-5 vs *PG*-8 or *PG*+5 vs *PG*+8	**Ö**
PG-2 vs *PG*+2 or *PL*-2 vs *PL*+2, or *PG*-5 vs *PG*+5, or *PG*-8 vs *PG*+8	**+**
Experimental technical difference, e.g. SFM to CM or wash to no wash	**$**

2.4. Results:

2.4.1. Polymer Characterisation:

PGA-co-PDL polymer was synthetized and characterized as previously reported by Thompson *et al.* (72, 75, 76). The polymer was a waxy solid powder with an off-white color and stored at room temperature. The MW of *PGA-co-PDL* polymer was confirmed by the GPC to be 15.7 KDa, and *PLGA* MW was 16.7 KDa. DSC of the synthetized *PGA-co-PDL* confirmed that Tm was ~55 ^{o}C, and Tg was ~39 ^{o}C which was previously published by our group (72, 105, 314). The Tg of *PGA-co-PDL* was similar to *PLGA* (T_g 42-46 °C as reported by the manufacturer) (56, 64, 68).

2.4.2. Nanoparticle Characterisation:

NP Characterisation for size, PDI, and zeta potential were evaluated in DW represented in Table. 2.3. *PL* and *PG* NPs at 200 nm size showed similar size, while the positively charged NPs showed a slight size reduction from their negatively charged counterparts but there was no statistically significant difference. NPs at 200 nm size were statistically smaller from their larger counterparts at 500 nm and 800 nm

(P<0.0001). NPs at 500 nm were were statistically different from their larger counterparts at 800 nm (P<0.0001).

Table. 2.3. Characterisation of polymeric of NPs (*Mean ±SD, n=3*).

NPs Type	**Characterisation**		
	Average diameter (nm)	PDI	Zeta potential (mV)
PG-2	210.11 ± 5.01	0.21 ± 0.02	- 26.80 ± 0.90
PG+2	205.20 ± 7.50	0.23 ± 0.03	+33.30 ± 1.60
PL-2	215.20 ± 3.01	0.20 ± 0.02	-27.70 ± 1.70
PL+2	199.31 ± 5.50	0.20 ± 0.01	+32.40 ± 1.50
PG-5	524.31 ± 6.10	0.32 ± 0.04	-29.30 ± 2.50
PG+5	513.41 ± 4.30	0.30 ± 0.05	+27.50 ± 30
PG-8	825.50 ± 4.50	0.34 ± 0.04	-28.40 ± 1.50
PG+8	810.50 ± 10.50	0.36 ± 0.07	+28.90 ± 3.50

NR-labelled NPs characterisation are represented in Table. 2.4. NPs showed a slight increase of their sizes, and a slight decrease for the recorded zeta potential values. These were not statistically difference to their non-labelled counterparts indicating successful labelling without affecting the original physicochemical properties of the polymeric NPs.

The shape of the polymeric NPs was confirmed by SEM and TEM. *PG*-2 and *PG*+2 are shown in Figure. 2.2. A & B. *PL*-2 and *PL*+2 are shown in Figure. 2.3. A & B. *PG*-5 and *PG*+5 are shown in Figure. 2.4. A & B. Lastly, *PG*-8 and *PG*+8 are shown in Figure. 2.5. A & B. All types of the formulated NPs were found to be spherical in shape with smooth surface. The NPs showed some polydispersity in their size that was more apparent in the larger NPs (500 nm and 800 nm).

Table. 2.4. Characterisation of polymeric of NPs NR labelled NPs for confocal imaging (*Mean ±SD, n=3*).

NPs Type	**Characterisation**		
	Average diameter (nm)	PDI	Zeta potential (mV)
PG-2	234.20 ± 3.50	0.23 ± 0.02	- 23.40 ± 4.30
PG+2	220.10 ± 4.30	0.23 ± 0.03	+21.60 ± 3.40
PL-2	226.31 ± 6.70	0.21 ± 0.03	-19.60 ± 5.40
PL+2	211.20 ± 8.20	0.31 ± 0.01	+24.20 ± 5.30
PG-5	552.40 ± 7.40	0.34 ± 0.04	-22.30 ± 4.40
PG+5	543.50 ± 2.50	0.33 ± 0.05	+23.20 ± 5.90
PG-8	845.30 ± 4.50	0.33 ± 0.03	-25.20 ± 5.40
PG+8	835.30 ± 7.01	0.35 ± 0.05	+26.90 ± 4.20

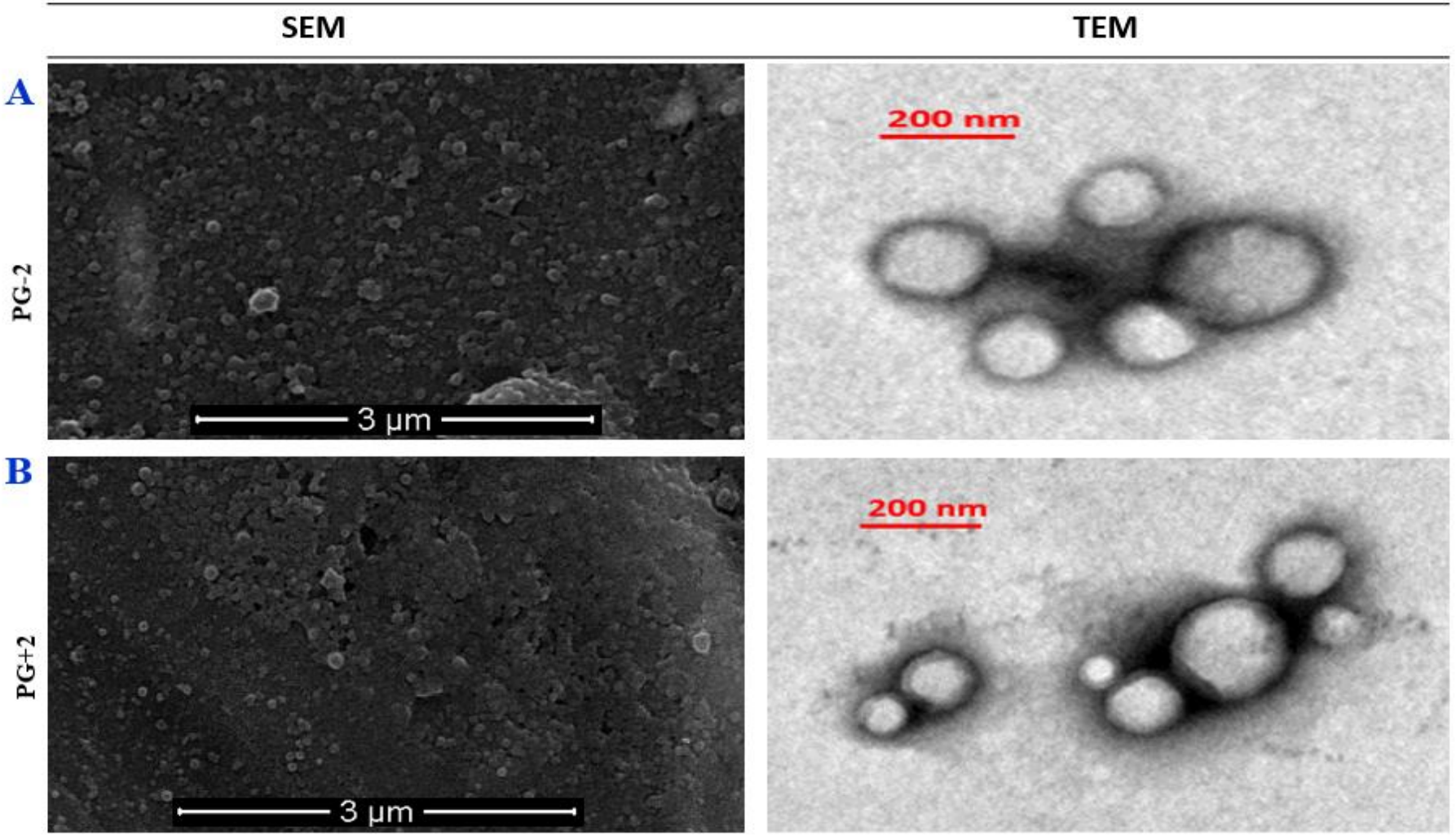

Figure. 2.2. SEM and TEM images of (A) *PG*-2, (B) *PG*+2.

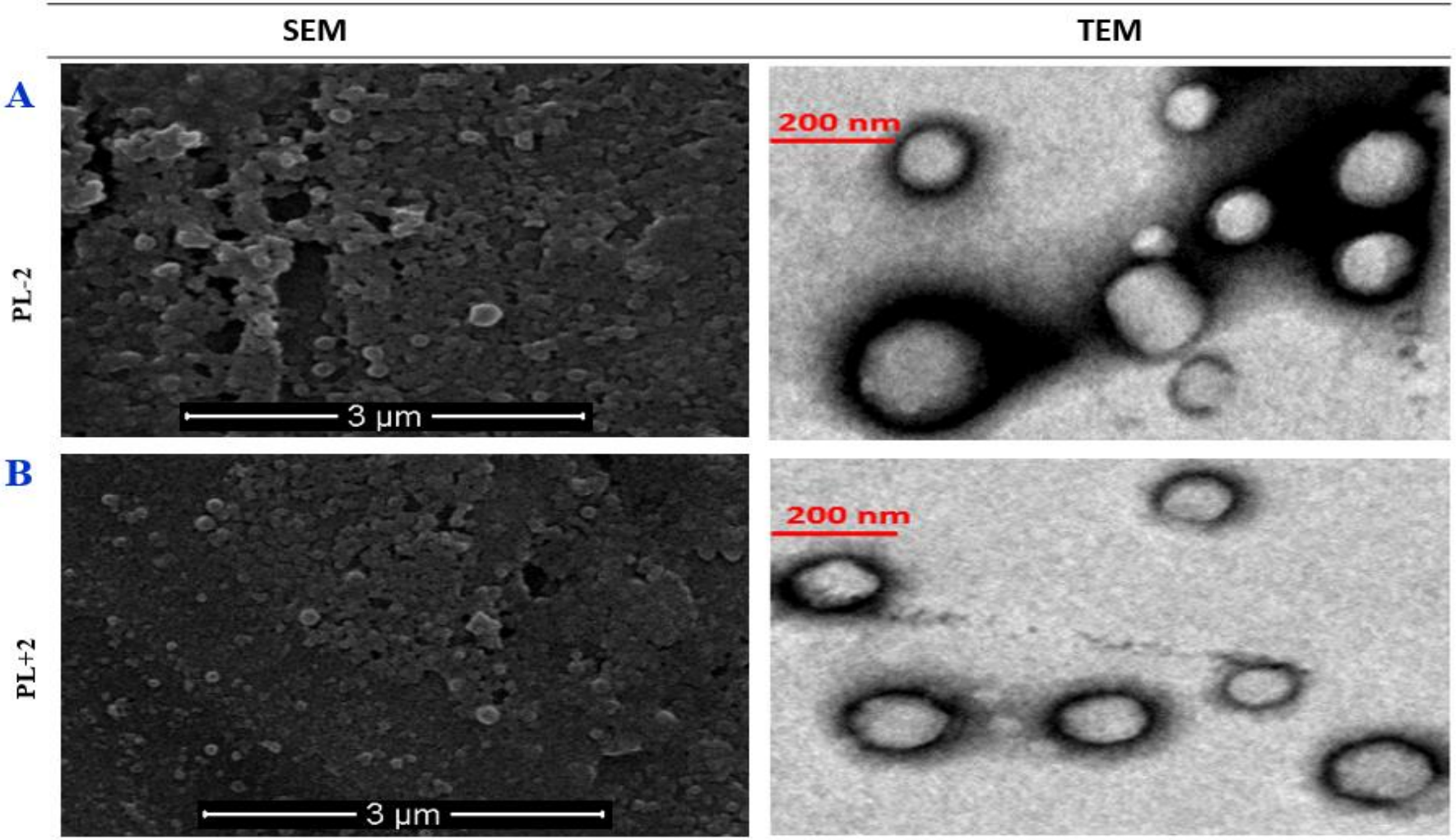

Figure. 2.3. SEM and TEM images of (A) *PL*-2, (B) *PL*+2.

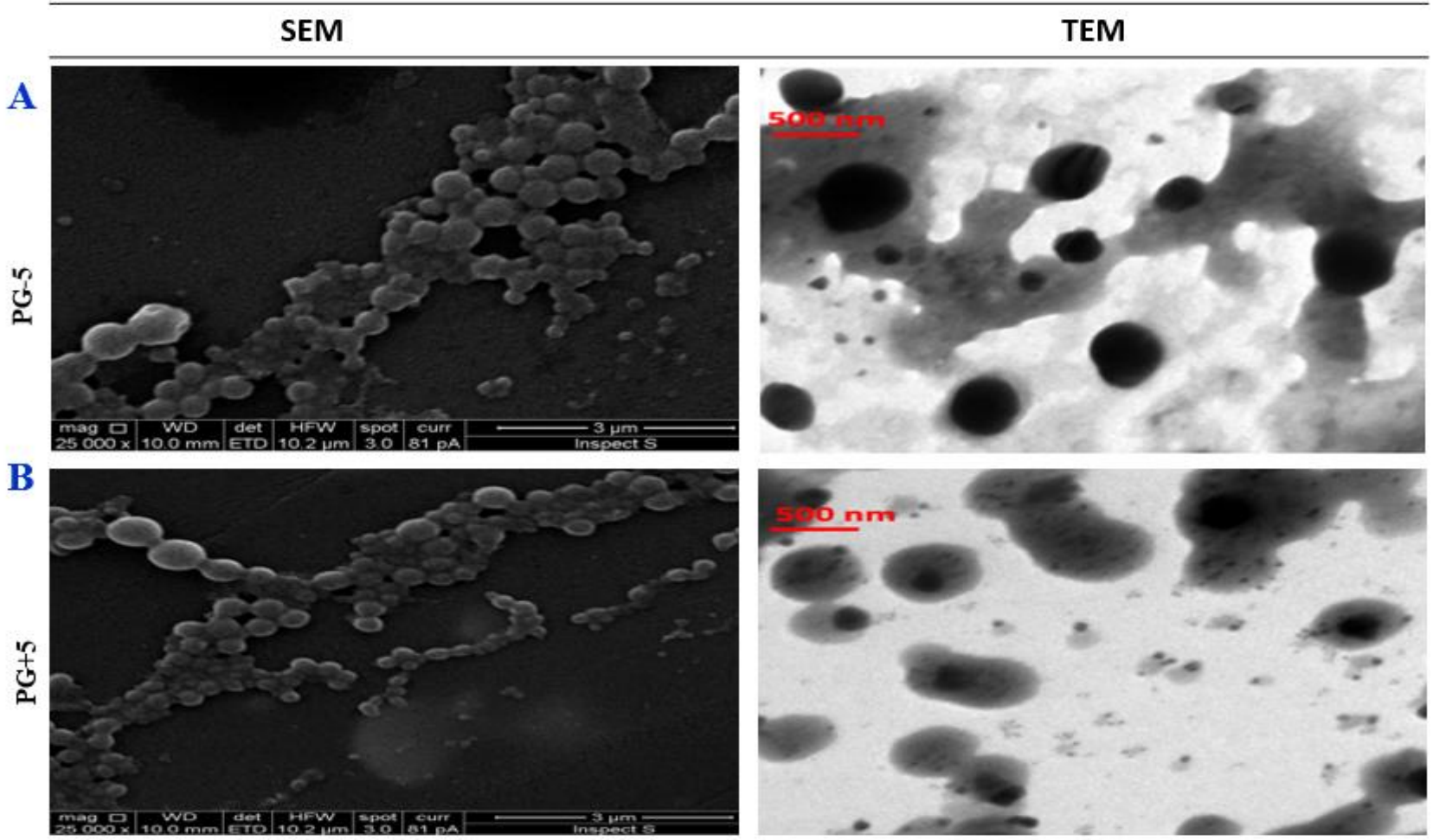

Figure. 2.4. SEM and TEM images of (A) *PG*-5, (B) *PG*+5.

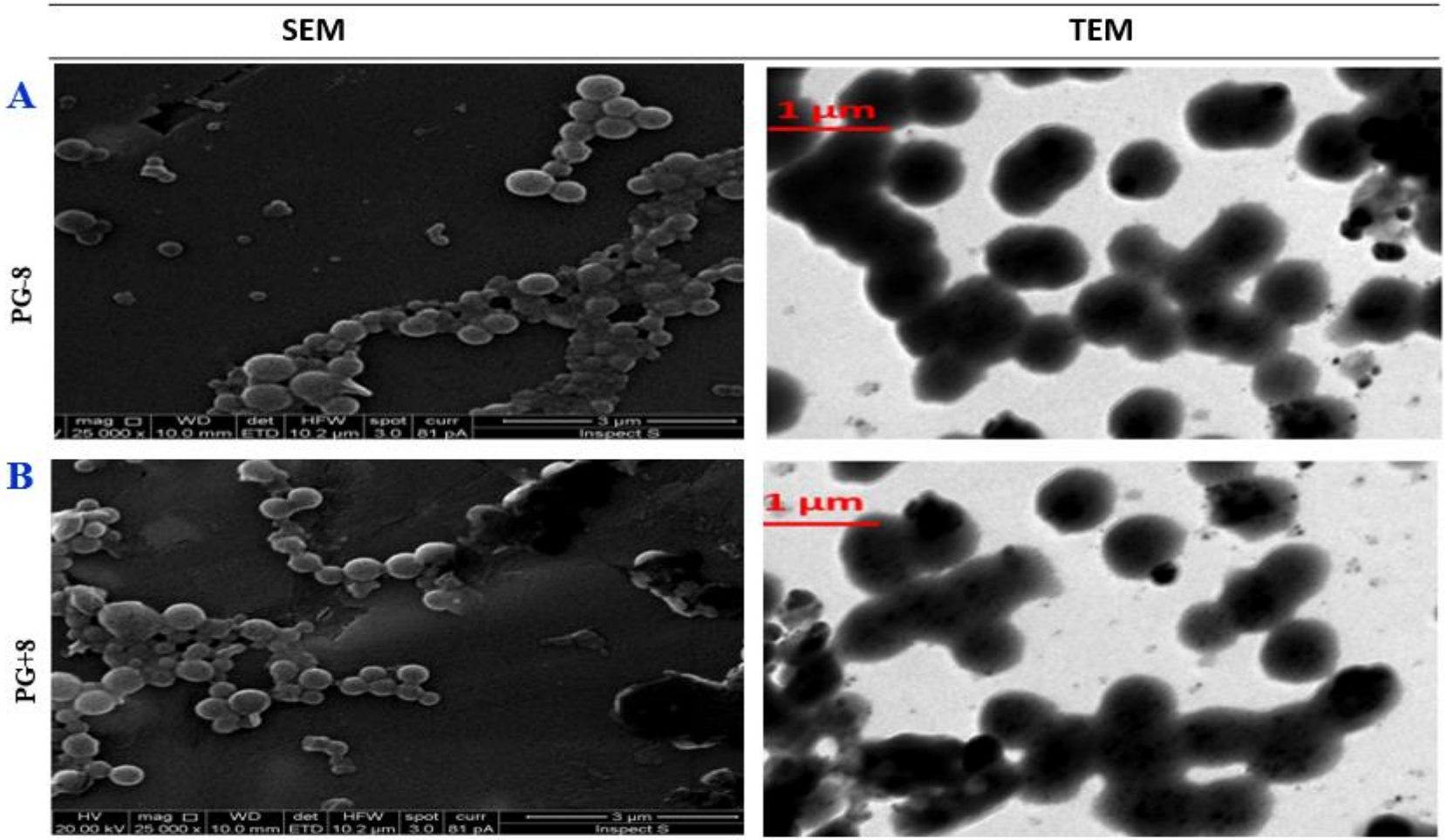

Figure. 2.5. SEM and TEM images of (A) *PG*-8, (B) *PG*+8.

2.4.3. Nanoparticle Stability and Degradation in Different Media:

2.4.3.1. Nanoparticle Size and Zeta Potential Stability in Media:

Figure. 2.6. (A & B) and (C & D) indicate the size characterisation in SFM and CM respectively. While Figure. 2.6. (E & F) and (G & H) indicate the zeta potential characterisation in SFM and CM respectively. The statistical analysis was performed between the following:

(1) Compare NPs size and zeta potential at the same time point between the two conditions: SFM and CM (indicating different experimental conditions/effect of the dispersing media),

(2) Compare NPs size and zeta potential at T0 to T24 under the same condition (indicating the changes due to protein adsorption and/or agglomeration upon dispersion and after 24 hr incubation),

(3) Compare negatively charged NP to positive counterparts under the same condition (indicating the surface chemistry effect),

(4) Compare *PL* NPs to *PG* NPs (indicating any chemistry induced effect).

Size: Upon dispersing the NPs in SFM or CM, there was an increase of their size at T0 and T24. Figure. 2.6 A indicates a size increase with negatively charged NPs; *PG*-2, *PL*-2, *PG*-5, and *PG*-8 in SFM. Size increased with all NPs at T0 and T24 at 37 ^{o}C. There were only significant differences with *PG*-5 and *PG*-8 from their T0 sizes. While positively charged NPs; *PG*+2, *PL*+2, *PG*+5, and *PG*+8 in SFM (Figure. 2.6. B) showed similar trend with slightly higher size increase at T0 and T24 and there was significant difference with *PG*+2, *PL*+2, *PG*+5, and *PG*+8 from their sizes at T0. Only *PG*+5 and *PG*+8 showed a significant size difference to *PG*-5 and *PG*-8 at T0. *PL*-2

and *PG*-2 showed similar size changes that were not significantly different. *PL*+2 was slightly bigger than *PG*+2 but not significantly different.

In CM (Figure. 2.6. C & D), size change of NPs at T0 and T24 showed similar trends to NPs in SFM but with a higher increase of size. It was significantly different to SFM sizes with all NPs except *PG*-8 at T24. NPs of *PG*-2, *PL*-2, *PG*-5, and *PG*+8 showed a significant size increase to their T0 in CM. Negatively charged NPs were slightly smaller in size to their positive counterparts but there were no statistically significant differences at any time points. *PG*-2 NPs were almost similar *PL*-2 at T0, however at T24, *PL*-2 was larger than *PG*-2 but no significant difference. *PL*+2 NPs were slightly larger than *PG*+2 at T0, however, at T24 both NPs were almost of the same size with no significant differences at either time point.

Zeta Potential: Figure. 2.6. (E & F) presents the zeta potential characterisation in SFM. Negatively charged NPs showed their zeta potential slightly lowered from T0 to T24 (more negative at T24), while the positively charged NPs showed conversion of their positive charge to a negative charge. However, there was no significant differences at any time points.

Zeta potential characterisation in CM in Figure. 2.6. (G & H) showed similar trend to SFM with slight lowering of the negative charge from T0 to T24 and conversion of positively charged NPs to negatively charged. There were no significant differences between different NPs at any time point and to their SFM counterparts.

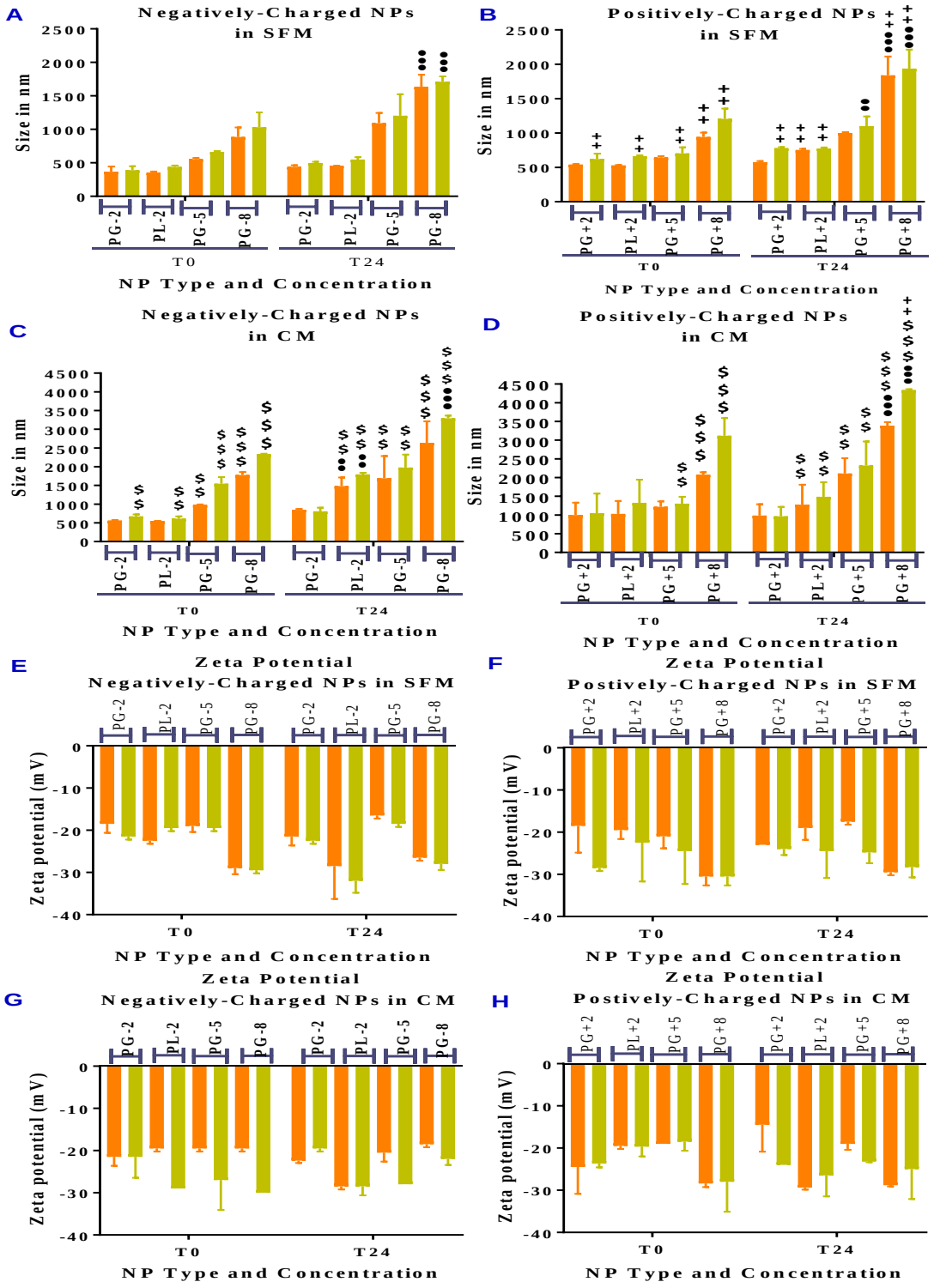

Figure. 2.6. NPs Characterisation: Size 0.125 mg/ml 0.25 mg/ml in SFM (A) Negatively charged NPs, (B) Positively charged NPs, and size in CM (C) Negatively charged NPs, (D) Positively charged NPs, zeta potential in SFM (E) Negatively charged NPs, (F) Positively charged NPs, zeta potential in CM (G) Negatively charged NPs, and (H) Positively charged NPs in CM (Results expressed as Mean ± SD, for statistical symbols and *P*-value please refer to section. 2.3.4).

2.4.3.2. Nanoparticle Degradation in Aqueous Media:

PL-2 and *PG*-2 were studied for degradation under two conditions; suspended in PBS at 4 ^{o}C and suspended in SLF (Gamble's Formula) incubated at 37 ^{o}C under axial rotation of 15 rpm. The changes of NP size, zeta potential, pH, and MW over study interval are presented in Figure. 2.7. (A & B), (C & D), (E & F), and (G & H) respectively.

NP Size: *PG*-2 size changes under both conditions (Figure. 2.7. A) and the NP size was almost stable until D7, then an increase with high SD from D14-D28 that was significantly different from D0 size (pink symbols for SLF, orange symbols for PBS). There was a slightly higher size increase from D14-D28 with SLF than PBS however, no significant difference between the two conditions. Figure. 2.7. B represents *PL*-2 size changes under SLF and PBS with the size almost stable until D7. However, in SLF, the size started to decrease after D7 toward D28, whereas in PBS, the size increased toward D28. There was no significant difference at any time points to D0. However, at D28, *PL*-2 NP size was significantly higher in PBS than SLF. However, there was size differences between *PL*-2 and *PG*-2 from D7-D28 in both conditions, but due to the big error bars with *PG*-2, there was no statistical significance.

Zeta Potential: *PG*-2 zeta potential (Figure. 2.7. C) changes overtime in both conditions. *PG*-2 was negatively charged at D0 with gradual lowering of their negative charge towards D28, however NPs in SLF were less negative to those stored in PBS. There was no significant difference at any time point to their corresponding D0 as well as between SLF and PBS. However, *PL*-2 (Figure. 2.7. D) showed similar trends to *PG*-2 NP at D0-D14 but started to lose their negative charges or approaching the point of neutrality at D14-D28. Moreover, there was less negative charge in PBS than SFL but

almost the same at D21-D28. In addition, there was no significant difference at any time point to their corresponding D0 as well as between SLF and PBS.

pH changes: Figure. 2.7. E shows *PG*-2 NPs had slightly alkaline pH at D0 in both conditions. The pH showed gradual lowering over time denoting acidic changes. However, pH at D28 staggered around neutral pH for both conditions. Statistically significant differences were shown in D7-D28 in PBS from their D0 values. However, the pH in SLF only showed significant differences in D21-D28 to their D0 values. Moreover, there was statistical difference between SLF (less acidic) and PBS in D7-D28. However, for *PL*-2 the pH changes (Figure. 2.7. F) decreased towards acidic pH over time and showed significant acidic pH at D21-D28 to their corresponding D0 in PBS. There were less acidic changes in SFL compared to PBS and was only significant at D28. Comparing *PG*-2 to *PL*-2 there was no significant differences (after normalization to correspondent D0) at the two different conditions except at D28 in SFL which was less acidic in *PG*-2. However, the absolute values of pH with *PL*-2 NPs were significantly more acidic than *PG*-2 at all-time points and both conditions.

MW: MW changes are represented in Figure. 2.7. G & H for *PG*-2 and *PL*-2 respectively. The MW changes showed trend of stability or slightly increased overtime to D21 before returning to levels at D28 comparable to D0. However, there was no significant changes between *PG*-2 and *PL*-2 at any time point or any condition (after normalization to the correspondent D0).

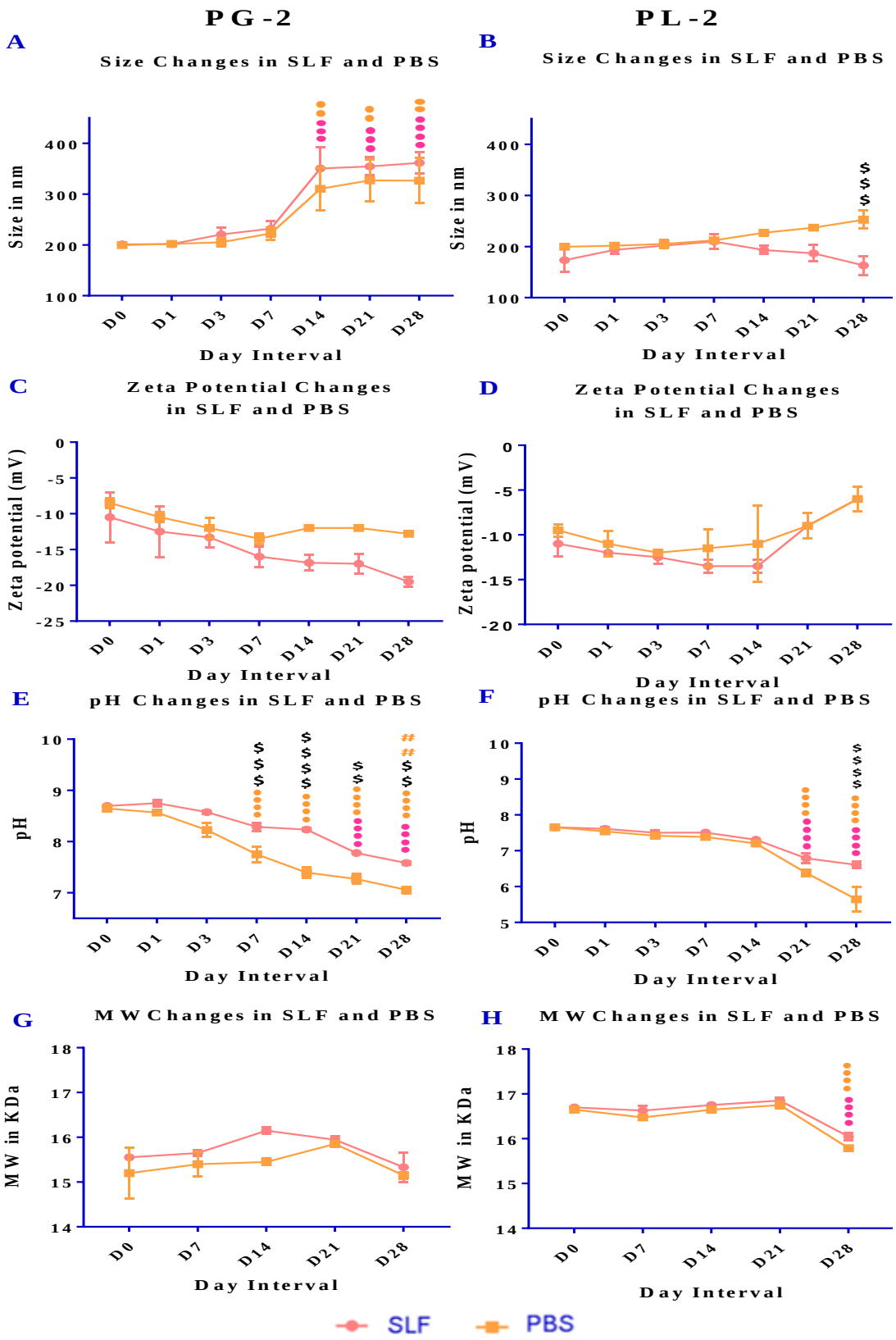

Figure. 2.7. Degradation of *PG*-2 and *PL*-2 NPs in SLF and in PBS: Size changes (A)*PG*-2 and (B) *PL*-2, Zeta potential changes (C) *PG*-2 and (D) *PL*-2, pH changes (E)*PG*-2 and (F) *PL*-2, MW changes (G) *PG*-2 and (H) *PL*-2 (Results expressed as Mean ± SD, for statistical symbols and *P*-value please refer to section. 2.3.4).

2.5. Discussion:

2.5.1. Polymer Synthesis, Nanoparticle Formulation, and Characterisation:

A functional polyester of *PGA-co-PDL* polymer was successfully synthesized and characterized as previously mentioned by Thomson *et al.*, (72). The polymerization reaction was enzymatically catalyzed via Lipase enzyme with ring-opening polycondensation reaction. The chemical structure was confirmed by FT-IR and ^{1}HNMR and was consistent to what was previously reported (23, 72, 77, 81). The monomeric ratio of *PLGA* 50:50 (MW 7-17 KDa) was chosen to be compared to the monomeric ratio of (1:1:1) of *PGA-co-PDL* polymer. MW produced was ~ 15.7 KDa, which was similar to *PLGA* MW (~16.7 KDa characterized via GPC). Both *PL* and *PG* of aliphatic polyester family were of similar MW and monomeric ratio to formulate similar NP size and have a comparable hydrolytic degradation to study the chemistry induced effect of NPs interactions (320).

NPs were successfully formulated from the two polymers using emulsion-solvent evaporation methods (Table. 2.1). The optimization of the different sizes of the *PGA-co-PDL* and *PLGA* NPs used in the study was based on a previously published in-house study of optimizing different NP sizes (74, 80). SE (O/W) method was used to formulate 200 and 500 nm size, while DE (W/O/W) was used to formulate the larger size of 800 nm (321, 322). McCall and Sirianni (321) had extensively studied the use of SE and DE methods with applying many variables such as solvents, emulsifiers, sonication power, and different *PL* polymer mass to tune the NP size in the range of ~150 nm up to 2 μm.

The use of emulsifiers/stabilizers are to improve stability of the emulsion (323) by ensuring the NP surface is covered to allow electrostatic repulsion forces to

deagglomerate and stabilize the produced NPs. PVA is a common anionic emulsifier resulting in a negative charge of NPs (323). However, positively charged NPs were produced by using DOTAP as a cationic emulsifier. DOTAP was previously used to coat polymeric NPs to improve their encapsulation efficiency of negatively-charged macromolecules and potentially increases the cellular uptake and interactions as previously reported (79, 324). The positive charge from DOTAP coating is due to exposure of its cationic moiety of the quaternary amine (325-327). Positively charged NPs were slightly smaller than negatively charged NPs produced by same method but not significantly different. This is due to synergistic effect of both PVA and DOTAP as surfactants. They increased the surface tension required to produce rounded droplets/NPs. This effect reduced the coalescence of droplets and lowered the size. Similar findings were reported in literature (328, 329).

It has been indicated that NP with minimum zeta potential values ± 20 mV are acceptable as stable emulsions (330-332). The reported zeta potential values for the positively charged NPs were in the range of +25 mV or more, while the negative charges NPs were in the range of -25 mV or less confirming the stability of the produced emulsions. Positively charged NPs are commonly fabricated to achieve higher loading for negatively charged molecules such as siRNA (23, 79, 97) or macromolecules (25, 74) and to increase the cellular interactions (333). For example, a study by Mohamed *et al.*, (23) had successfully formulated *PG* NPs positively charged with 15% (w/w) DOTAP that showed higher adsorption to miR146a to target IRAK1 gene expression as therapeutic intervention for COPD. The formulation (~ 240 nm) retained the functional and structural stability with high loading (36.25 µg per 10 mg after 24 hr incubation) with continuous *in vitro* release profile up to 77% after 24 hr. Using A549 cells, the formulation showed a reduced the target gene IRAK1 expression to 40%.

2.5.2. Stability and Degradation of Nanoparticles:

2.5.2.1. Nanoparticle Size and Charge Stability in Culture Media:

Size: Upon dispersing the NPs in SFM or CM (Figure. 2.6. A, B, C, & D), there was an increase of their size at T0 and T24 incubation. The size increase was more manifested with the positively charged NPs under both conditions, with higher increase in CM compared to SFM. The size (T0) change denotes the immediate adsorption to the surrounding molecules of the dispersing media, i.e, proteins in CM, or amino acids and other molecules such as sugars, ions and salts in SFM (334). While the changes over 24 hr /37^{o}C denotes further adsorption of molecules and further agglomeration. There were huge size differences in SFM (smaller size either negative or positive NPs) in comparison to CM at T0 which could be attributed to the high serum proteins contents in CM with high adsorption to surface of NPs (334). At T24 in both conditions, there was an increase with a huge variation in size to T0, but smaller size was observed in SFM than CM indicating more pronounced adsorption and agglomeration in CM. The size increase was due to so called 'protein corona' where the NPs interact with the biological molecules of the dispersing media (334-336) that can be formed within the first 30 seconds and keep increasing with doubling the NP '*apparent'* size to 8 or more folds in less than 10 min resulting in aggravating NP agglomeration with time (337-339). This new NP biological identity dictates *in vivo* pharmacokinetic behaviour as well as influencing cellular uptake with either increasing (such as more prone to phagocytic uptake) or decreasing their internalization and toxicity (340). The nature of proteins, amounts, types are dependent on the NP physicochemical characteristics (such as NP chemistry, size, charge etc.) and the contact site /dispersing medium (341, 342).

Zeta Potential (Figure. 2.6. E, F, G, & H) the negatively charged NPs showed insignificant differences of zeta potential either at T0 or after T24 under both

conditions. This could be related to the repulsion effect between the negatively-charged NPs and the negatively-charged proteins resulting in less protein adsorption (342). However, the conversion of the positively charged NPs to negative charge was indicative of protein adsorption (most of proteins are negatively charged). Although, SFM has 0% FBS, it still contains amino acids (such as glutamine), sugars, and other molecules that are negatively charged and hence can be adsorbed resulting in conversion of NP charge to negative (338, 342, 343).

Similar findings have been reported by Chen *et al*, (344) who developed *PL* NP coated cationic PEI (~ 500 nm) when dispersed in CM (+10% FBS), the size increased up to 1 μm with the positive charge conversion to negative (+45 mV to −25 mV) indicating protein adsorption. Another study by Partikel *et al.*, (345) further investigated protein corona formation around *PL* NPs (~ 200 nm, negatively charged with PVA) when exposed to human serum (HS) and FBS. Incubating *PL* NPs in HS and FBS resulted in a protein corona with almost 60 different types of HS proteins involved while the FBS showed ~ 40 different types in NP corona. Zeta potential of *PL* NPs in DW (−40 mV) had decreased to −34 mV and −21 mV in HS and FBS respectively indicating the abundance of proteins in HS than FBS (total proteins 86.6 mg/mL in HS compared to 47.7 mg/mL in FBS) with adsorption of proteins affecting the zeta potentials by increasing the charge (toward zero). This indicates the importance to evaluate the NP size under the planned experimental procedures to get an estimation of the size changes. Hence, the SFM was chosen as the dispersing media for further experiments as less size changes were encountered and to ensure better correlation of NP physicochemical-dependent cellular interactions that is crucial for the development of safer and more efficient NP based drug delivery systems.

2.5.2.2. Nanoparticle Degradation under Storage or Simulated Physiologic Conditions:

PG-2 and *PL*-2 were investigated under two different conditions to study their degradation: in PBS/4 ^{o}C simulating *in-vitro* storage, and in SLF/37 ^{o}C under axial rotation of 15 rpm simulating the *in-vivo* degradation. *PL* and *PG* NPs of similar size, charge, and MW indicated completely different degradation profiles signifying chemistry induced effect.

Size: (Figure. 2.7. A & B) The NP size was evaluated after sonication for 5 min to disperse NPs. However, *PG* and *PL* NPs had similar sizes but different trends of changes under different conditions. *PG*-2 indicated aggregation after one week with high variations towards D28 which were more pronounced in SFL than PBS. *PL*-2 had shown slight changes in size either increasing (in PBS) or decreasing (SLF) after one week. This implied; firstly, a more stable size for *PL*-2 NPs in the suspension than *PG*-2, and secondly, a degradation trend of *PL*-2 in SLF than in PBS. However, PBS is usually used to represent a body buffer fluid, but it lacks the salt and ionic strength of SLF. It is preferred to study the degradation profile of NPs in a simulated body condition of the target organ for the NPs delivery such as SLF. PBS buffer contains NaCl, KCl, and KH_2PO_4 salts. Whereas, SLF (Gamble's solution) contains 9 different types of salts (such as $MgCl_2$, NaCl, KCl, Na_2HPO_4, Na_2SO_4, $CaCl_2{\cdot}2H_2O$, $C_2H_3O_2Na$, $NaHCO_3$, and $C_6H_5Na_3O_7{\cdot}2H_2O$) that indicated the ionic and salt strength of SLF over PBS (346). Similar findings were reported by Menon *et al*, (347) who formulated NPs from *PL* alone, *PL* coated with CS, and *PL*-co-*PEG* NP (~ 160 nm, 191 nm, 335 nm respectively). The NPs in SLF (Gamble's solution) incubated at 37°C for 5 days showed stability of their size until 5 days, which was consistent with the current study findings for SLF and PBS.

Zeta potential: (Figure. 2.7. C & D) *PG*-2 showed two different trends of a charge increase with time in PBS and SLF that was more manifested in SLF than PBS representing a difference between the two buffers. However, *PL*-2 zeta potential changes in PBS and SLF showed a trend toward zero by the end of the experiment (a slight increase then slight lowering of the negative charge with fluctuations towards zero). This was due to the effect of chelation by ionic and salts contents of the media that were more manifested in SFL than PBS (348).

MW changes: (Figure. 2.7. G & H) MW changes observed for both polymers under PBS and SLF conditions showed modest changes in MW over time with small decrease toward the end of experiment; D28. This indicated MW changes could be slower compared to size, zeta potential and pH changes. This was due to the nature of these polymers of having linear chains of variable lengths giving a wide distribution of MW, with the shorter chains degrading faster (347).

pH changes: (Figure. 2.7. E & F) pH changes are related to the polymeric structure, its functional surface groups and its degradation products. *PL*-2 NPs are based on *PLGA* 50:50 acid terminated polymer (the terminal functional group is capped by carboxyl group) that expressed acidic pH. *PL*-2 showed a decrease in pH after two weeks/ D14; the sharp acidic changes toward the end of the experiments (pH 5.5 in PBS, pH 6.5 in SLF) that denoted the degradation products were of acidic nature and more degradation occurred in PBS than SLF. *PG*-2 NPs were based on *PGA-co-PDL* ester terminated with OH group expressing alkaline pH. *PG*-2 showed gradual decrease of pH with time and towards the end of the experiment was almost a neutral or slightly alkaline pH. This denoted less acidic degradation products and a slower degradation compared to *PL*-2 suggesting better performance of *PG*-2 in the biological media and

of potential importance to lower toxicity and inflammatory effects that would enhance *PG* use for lung delivery.

Both *PL* and *PG* polymers of α-polyester family are known to degrade heterogeneously via bulk erosion by chain random scission through hydrolysing ester linkages, where the rate of hydrolysis and water diffusion into the NP carriers are faster than the release of by-products (348, 349). The hydrolytic degradation rate of *PG* and *PL* NPs are influenced by many parameters such as monomeric ratio, nature of the monomers as well as polymer hydrophobicity and surrounding medium acidity. *PL* with monomeric ratio of 50:50 show faster degradation among all *PL* polymers. The effect of monomeric ratio was examined by Hussein *et al.*, (350) where *PL* NPs (50: 50, MW: 40-75 KDa, ~ 190 nm with negative charge) degraded in PBS/ 37^{o}C with constant shaking completely after 102 days while only 60% of *PL* NPs (85:15, higher lactides, with similar MW, size, and charge) degraded at that time with higher acidic products (320). However, *PG* has equal monomeric ratio of its three monomers that indicated a longer polymeric chain of each molecule, and one of its monomers (ω-pentadecalactone) is composed of a macrolide lactone which is a 15 membered cyclic lactone ring that can be correlated to its slower degradation and hydrophobicity (351).

The acidity of dispersing medium has a role in enhancing the degradation, however both PBS and SLF had a neutral and/or slightly alkaline buffers respectively. The increased acidity over time enhanced the degradation of *PL* NPs by facilitating autocatalytic degradation (349) and was consistent to previously published reports (350, 352). Another study investigated the effect of medium acidity on *PL* degradation rate performed by Swider *et al.*, (353) using *PL* NPs (50:50, MW 7-17 KDa, ~200 nm negatively charges with PVA labelled by fluorescent dyes) incubated in PBS/ 37 °C for 7 days under two different local pH values (7.4 neutral, 5.8 acidic medium). The

authors noted a faster release in acidic pH due to higher buffering capacity present at pH 7.4 to react with *PL* NPs compared to the acidic environment (320). The current study showed that pH changes were of extreme importance as the NPs and its degraded products showed early changes from D1 by lowering the pH while *PG* had maintained alkaline pH and almost reaching neutral pH by the end of the experiment. This could provide potential advantage for lung delivery as well as for pH sensitive drugs. It is important to note the lung interstitial fluid pH are reported from slightly neutral to alkaline (pH 8.5) (354, 355). The normal biological systems are under neutral to slightly alkaline pH where the acidity is found in confined areas and under tight control by body buffering mechanisms (356). Inflammatory conditions are characterized by increased local acidity at the inflammation sites due to releasing lysosomal enzymes for digestion and clean up for invading agents (357). Tumours have acidic local pH compared to normal surrounding tissues impairing basic chemotherapeutics such as epirubicin, doxorubicin, and adriamycin as well as pro-metastatic effect (357). Thus, extracellular induction of alkalinisation/metabolic alkalosis by requiring cancer patient to drink more bicarbonate solutions to enhance the effectiveness of these kind of chemotherapeutics (358-361) are exploited to aid these therapies. The current study postulates this local alkalinisation can be achieved through NPs based on *PG* polymer as there was evidence of raising local pH to alkaline in both buffering conditions as potential strategy for basic chemotherapies (362).

2.6. Conclusion:

Different NPs were successfully formulated into different sizes; 200 nm, 500 nm, 800 nm, and with different charges; negative and positive, from two polymers *PG* and *PL* using emulsification and solvent evaporation methods. The stability in SFM was greater than CM, hence SFM was chosen as the dispersing medium for NPs in

subsequent investigations. The degradation profiles of *PG* and *PL* NPs under storage or simulated body conditions showed different profiles: with *PL* NPs possessing faster degradation rate and more acidic byproducts resulting in acidic environmental pH. However, *PG* NPs showed a degradation with alkaline and slower pH changes denoting its suitability as a promising polymer for lung delivery.

3. *In vitro* Evaluation of Cellular Interactions of Polymeric Nanocarriers with Calu-3 and THP-1 Cells

3.1. Introduction:

Polymeric NPs are gaining interest as drug delivery systems to the lungs via inhalation. However, the safety of polymeric NPs has to be evaluated prior their desired applications. Polymeric NPs interactions with lung cells are usually investigated with a variety of *in vitro* methods prior to *in-vivo* animal testing and clinical trials (11). The *in vitro* methods utilise cell culture models to evaluate a target effect, for example, measuring a variety of metabolic reactions, (i.e., Alamar Blue (AB), ROS assays), or cellular components and their integrity, (i.e., DNA damage, cell or mitochondrial membrane potentials), expression or downregulations of cellular markers or genes, (i.e., caspases increase or cytokines release), or fluorescent cell labelling and direct visualization via electron microscopy (363).

The emergence of NPs has challenged the classic toxicological assays with a completely new set of encounters, which include, the particulate nature of NPs, behaviour in different media, corona formation, their exceptional physicochemical properties, knowledge gap of their potential interactions or interference with the assays that are frequently reported (363-366). Nanotoxicology science drives the research to study, optimize, and understand the different NPs factors that affect their biosafety and methods of their reliable testing prior to their desired applications (59, 367, 368). It is important to optimise experiments when NPs are investigated and use a variety of assays that are dependent on different mechanisms to improve the accuracy and the precision of the concluded results (363, 364). Nevertheless, there's still a long way to go until generalized standard methods are agreed by the wider scientific community and regulatory bodies (368).

PL versatile nature has made it a very attractive candidate for many biomedical applications. *PL* has been used for a variety of applications such as, biodegradable sutures, implants and prosthetic devices, tissue engineering, and in the formulation of many NPs,

microparticles (MP) and other drug carriers. *PL* carriers showed successful loading of different drugs, chemotherapeutics, and macromolecules, with many having been approved by the FDA for clinical use but mostly injectables (68-70). There are no *PL* NP applications approved for inhalation delivery. The main drawbacks of *PL* as a polymer in fabricating NPs are the bulk hydrolytic degradation and accumulation of acidic monomers causing a reduction of local pH at the site of drug action, that affects the stability of pH-sensitive drugs. The accumulation of acidic products after degradation with repeated doses and local acidity may promote an inflammatory response (68) which is a serious side effect (369). In addition, poor loading capacity for drugs, initial burst release, difficulty to scale-up the NPs productions, some cellular toxicities due to the accumulation of degraded products have been previously reported as drawbacks of *PL* (70, 370).

Thus, novel materials are under development to improve upon the physicochemical properties of *PL*. *PG* is such a polymer that has been developed and characterized in LJMU laboratory and under intensive investigations for drug delivery purposes (72). It has successfully been formulated into NPs, MPs, and drug conjugates for lung delivery (34, 72, 74-78). Furthermore, it has successfully encapsulated many small drugs and macromolecules showing very promising results for treating lung diseases and vaccine delivery (23, 25, 34, 38, 74, 77, 79-81). Hence, this current study performed a detailed nanotoxicological screen of *PG* NPs aimed for drug delivery via the lungs. In addition, this was compared to *PL*; as a frequently used polymer in many applications and having FDA approval, at NP size of 200 nm to determine any chemistry-based nanotoxicity.

3.2. Aims:

To investigate the influence of chemistry (*PL* vs *PG*), size (200 nm, 500 nm, and 800 nm), and surface charge (negative vs positive) of polymeric NPs on their potential

cytotoxicity and uncovering the underlying biomechanistic interaction with pulmonary cell lines. This was achieved using *in vitro* methods through the following objectives:

- To evaluate the general cytotoxicity using Alamar Blue assays, ROS detection, cell membrane and mitochondrial membrane potentials,
- To differentiate between the apoptosis and necrosis cell death by evaluating the caspases activation,
- To detect the inflammatory response after THP-1 exposure to NPs by measuring pro- and anti-inflammatory cytokines,
- To detect any genotoxicity after NPs exposure using COMET assay.

3.3. Materials and Methods:

3.3.1. Materials:

Resazurin Sodium salt (for AB) powder, Luperox® TBH70X, *tert*-Butyl hydroperoxide solution (TBHP, 70 wt. % in H_2O), 2′,7′-Dichlorofluorescin diacetate (H2DCFDA) powder, Tween-20, Phosphate buffered saline tablets (pH 7.4), Phorbol 12-myristate 13-acetate (PMA), Lipopolysaccharide (LPS) were purchased from Sigma-Aldrich Chemicals, UK. Methanol, dimethyl sulfoxide (DMSO), TrypLE™ Express and paraformaldehyde were purchased from Thermofischers, UK. Purified water (DW) from a Millipore Purification System (Billerica, MA, USA) was used. Other lab chemicals and solvents were purchased from Sigma unless otherwise specified. Cell culture consumables (including 25 and 75 cm^2 vented-capped flasks, 96 multi-well flat bottom Plates, NUNC Maxisorp® 96 well Plates, micro-tips, disposable serological pipettes, centrifuge tubes, cryo-vials, reservoirs, 8 well-chambers and microscope slides).

Purchased Kits: OxiSelect™ Comet Assay Kit from Cell Biolabs, Inc; Cell Meter™ Multiplexing Caspase 3/7, 8 &9 Activity Assay Kit*Triple Fluorescence Colors* from

AAT Bioquest®; TOX7-*In vitro* Toxicology Assay Kit-Lactate dehydrogenase from Sigma; Cellular Reactive Oxygen Species Detection Assay Kit (Ab186029) (Deep Red Fluorescence), and 7-Aminoactinomycin D (7-AAD): Fluorescent DNA dye (Ex/Em: 540/645 nm) (ab142391) from Abcam; Annexin V Apoptosis Detection Kit, and Human IL-8 ELISA Ready-SET-GO!® from Affymetrix eBioscience®; BD™ Cytometric Bead Array (CBA) Human Th1/Th2/Th17 Cytokine Kit from BD Biosciences.

3.3.2. Methods:

3.3.2.1. Polymeric Nanoparticles Formulations and Characterisations:

As previously mentioned in sections: 2.3, 2.4, and 2.5.

3.3.2.2. Cell Culture Maintenance:

Human bronchial epithelial Calu-3 cell line (HTB-55™; ATCC): Cells were maintained at 37 °C and 5% CO_2 in a humidified atmosphere. Cells were cultured in Dulbecco's modified Eagle's medium (DMEM, Sigma-Aldrich) supplemented with 1% penicillin/streptomycin (Sigma), Fungizone® (Thermofischers) (2.5 µg/mL), L-glutamine (GlutaMax™, Gibco) (2 mM), sodium pyruvate (Sigma) (1 mM), and 10% FBS (FBS, Sigma). The medium was changed every 2 days and cells were passaged at a 1:3 split ratio after detachment by using TrypLE™ Express. Cells with passage numbers from 20-40 were used. Cell confluency were maintained at ~80% in 75 cm^3 flasks prior to splitting or plating. They were seeded at a density of 40 $x10^3$ as 200 µL complete media containing 10% FBS (CM) per well in 96 well plates for 48 hr, the supernatant was removed prior to treating the cells with serial concentrations of NPs prepared in serum-free media (SFM).

THP-1 **monocyte cell line:** The cells were obtained from ATCC. Cells were cultured as suspension in Roswell Park Memorial Institute (RPMI)-1640 Medium (RPMI-1640, Sigma) containing 10 % FBS, L-glutamine (1 mM), 1% penicillin/streptomycin,

Fungizone® (2.5 µg/mL) maintained at 37 °C under 5 % CO_2. Confluency were maintained at $1x10^6$ per mL in 75 cm^3 flasks prior to centrifugation at 200 xg for 2 min, removing the supernatant and adding fresh CM prior to splitting at 1/3 ratio. They were seeded at a density of 40 $x10^3$ cells per well (200 µL) CM in 96 well-plates and differentiated to macrophages upon stimulation with PMA (5 ng/mL) for 48 hr, then culture media were removed prior to adding serial concentrations of NPs prepared in SFM.

3.3.2.3. Cytotoxicity Evaluation by Alamar Blue Assay:

The general cytotoxicity of the NPs was assessed by AB, which determines the cell viability and its metabolic activity by evaluating the reducing intracellular environment through the reduction of a water-soluble resazurin dye (oxidized form, non-fluorescent, blue colour) to resorufin (reduced form, fluorescent, pink colour) through oxidoreductase enzymes-NAD(P)H dependent reactions that occur in the mitochondria and the cytoplasm (371, 372) (Figure. 3.1).

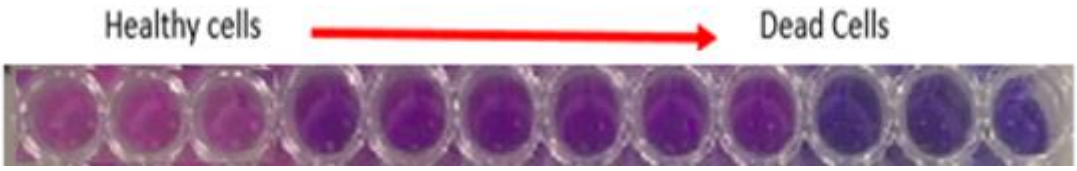

Figure. 3.1. Colour change of AB dye after cellular exposure; pink, light and deep purple, and blue denoting the reduced cell ability to reduce the AB dye.

Calu-3 cells were seeded at a density of 40 $x10^3$ per well (200 µL) in 96 well plates for 48 hr, the supernatant was removed prior to treating the cells with a serial concentration of NPs prepared in SFM (0.125-2 mg/mL, at 200 µL per well, in triplicates) for 24 hr. The supernatant was removed gently without disturbing the monolayers and washed three times (to ensure effective NPs removal with non-significant loss of cells from the monolayers) with warm PBS prior to addition of 100 µL of AB (10 % solution, 44 µM, low cytotoxicity concentration) working solution prepared in PBS. Another set of experiments included cells

after NPs treatments, followed by removing the supernatants from the wells without a wash step to check if there was any technical effect and continued as above. Fluorescence reading was taken every hr up to 3 hr (maximum response that can be reached) incubation (37°C, 5% CO_2) in the dark. Fluorometric evaluation (*Ex/Em* 530/590 nm) using the microplate reader (BMG LABTECH Clariostar plate reader) was measured. The results were expressed as a percent of the negative control (NC) of untreated cells and 10% DMSO was used as a positive (PC) control (*n=3*).

3.3.2.4. Reactive Oxygen Species Detection Assay:

3.3.2.4.1. 2′,7′-Dichlorodihydrofluorescein diacetate (H_2DCFDA) Assay:

ROS production was evaluated by fluorescent labelling of the cells with 2′,7′-dichlorodihydrofluorescein diacetate (H_2DCFDA reagent (Sigma-UK); also known as DCFDA or DCFH-DA). H_2DCFDA is a non-fluorescent cell-permeable probe. Upon cell entry, it was deacetylated by cytoplasmic esterase to a cell impermeable and non-fluorescent 2',7'-dichlorofluorescin (DCFH2) that is very sensitive to hydroxyl and peroxyl radicals, and hydroperoxides and undergoes oxidation to highly green fluorescent 2',7'-dichlorofluorescein (DCF). The fluorescent intensity is directly proportional to the intracellular ROS amount (373, 374).

Calu-3 cells were seeded in a density of 40 $x10^3$ per well (200 µL) in 96 well plates for 48 hr. The supernatant was removed followed by a single wash with warm PBS and the cells were incubated (37°C, 5% CO_2, in the dark) with 100 µL of 10 µM H_2DCFDA solution freshly prepared in PBS (to avoid cleavage by serum esterase) and protected from the light for 30 min. H_2DCFDA solution was then removed and another wash performed prior to treatment with NPs concentrations prepared in SFM as 200 µL per well. After 24 hr incubation in the dark, a wash step was performed with warm PBS, then 100 µL PBS were

added per well prior to measurements of the fluorescence (*Ex/Em:* ~485/535 nm) intensity by the plate reader and the results expressed as a percent of the NC (*n=3*) and using freshly prepared 100µM H_2O_2 in PBS for 30 min as a PC.

3.3.2.4.2. Cellular ROS (Deep Red) Assay (ab186029):

This assay uses a ROS sensitive sensor (its chemical structure and the reaction is not declared by the manufacturer) that is a cell-permeable probe that reacts with the intracellular ROS especially superoxide anion (O_2^-) and hydroxyl radicals generating a deep red fluorescence that can be measured by a plate reader (375). Calu-3 cells were seeded at a density of 40 x10^3 per well (200 µL) in 96 well plates for 48 hr. Media was removed and a wash with PBS was performed prior to treatment with serial NP concentrations prepared in SFM at 200 µL per well for further 24 hr (using freshly prepared 100µM H_2O_2 in PBS for 30 min as a PC). This was followed with removal of supernatant and a three-wash step with warm PBS, or removal of supernatants without wash steps (no wash) prior to treatment with 100µL of ROS Deep Red dye working solution (per the protocol instruction) for 1 hr (37°C, 5% CO_2, in the dark). Fluorometric evaluation was determined using plate reader (*Ex/Em*: 650/675 nm). The results were expressed as a percent of the NC (*n=3*).

3.3.2.5. Mitochondrial Membrane Potential (JC-1):

Mitochondrial membrane potential ($\Delta\Psi m$) was detected by staining with a cell-permeable cationic JC-1 dye (5,5,6,6'-tetrachloro-1,1',3,3' tetraethylbenzimi-dazoylcarbocyanine iodide). JC-1 dye is very selective to the mitochondrial membrane and gives a characteristic change of fluorescence colour from red to green as the mitochondrial membrane is depolarizing. In healthy mitochondria, the JC-1 dye forms highly red fluorescent J-aggregates whereas in unhealthy mitochondria, the dye remains as green fluorescent monomers (376).

Calu-3 cells were seeded at a density of 40 x10^3 per well (200 µL) in 96 well plates for 48 hr, followed by removal of media. Cells were washed with PBS prior to treatment with 2 µM JC-1 dye solution prepared in PBS for 30 min at 37˚C in the dark. Treatment incorporated serial concentrations of NPs for 24 hr (using 10 % DMSO as a PC) prior to fluorescence measurement using a plate reader (*Ex/Em* 485/545, *Ex/Em* 485/595 with a cut off 530 nm). The ratio of measurements at 595 nm/545 nm (red/green ratio) was used as the measurement of the changes of $\Delta\Psi m$ in Calu-3 cells. The results were expressed as a percent of the NC (*n=3*).

3.3.2.6. Cell Membrane Integrity:

Cell membrane integrity was evaluated by the Lactate dehydrogenase (LDH) which is an intracellular enzyme that can be released to the extracellular media upon cell membrane damage. This can be detected by adding the enzyme substrate mixture with a colorimetric indicator (lactate substrate conversion to pyruvate with NADH+ production, the diaphorase mediates tetrazolium salt conversion using NADH oxidation forming formazan dye) absorbance at ~490 nm that can be correlated to the amount of LDH released.

Calu-3 cells were seeded in a density of 40 x10^3 per well (200 µL) in 96 well plates for 48 hr, followed by removal of media from the 96 well plate. Treatment incorporated serial concentrations of NPs at 200 µL per well for 24 hr. Triton X-100 (2% w/v, in PBS) was used as a PC for 30 min (377, 378). TOX7- *in vitro* Toxicology Assay Kit, (Sigma) was used to assess the LDH release, the kit offers two methods of assessing LDH; by LDH Total or Release methods that were used per published protocol (374, 379-381).

LDH Release: In this assay, the LDH released in the medium after NPs exposure was evaluated. This indicated the membrane integrity and the cell viability. After 24 hr exposure to NPs, Calu-3 treated 96 well plates were centrifuged at 400 xg for 4 min to pellet the cells. Then aliquots of 50 µL of the supernatant were transferred to clean Plates. Freshly

prepared LDH assay mixture was added to each well as 100 µL and left at room temperature for 30 min in the dark. The reaction was terminated by adding 15 µL of 1 N HCL to each well then proceed to measurement. The results were expressed as a percent of the NC (*n=3*).

LDH Total: In this assay, the total amount of LDH was evaluated. This evaluation would give an indication for the cell viability (378, 382). It was performed with another set of Calu-3 treated 96 well Plates, where the lysis buffer was added to each well as 20 µL and left at room temperature for 45 min in the dark and proceeded as the release assay. The absorbance of converted dye was measured at a wavelength of 490 nm with subtraction of the background noise at a wavelength of 690 nm. The results were expressed as a percent of the NC (*n=3*).

3.3.2.7. Apoptosis and Necrosis Assay:

Cell death was assessed by staining with annexin-V-FITC and 7-AAD using flow cytometry (374, 383, 384). One of the early signs of apoptosis is the flip of the inner cell membrane phosphatidylserine molecules to the outside. Annexin V is a high binding protein to these molecules in Ca^{++} rich environment. While, 7-AAD is a cell impermeable dye that in late apoptosis/necrosis cross through damaged cell membrane and attaches to DNA by intercalating to GC rich regions (243).

Calu-3 cells were seeded at a density of 40 $x10^3$ per well (200 µL) in a 96 well plate for 48 hr, then media was removed followed by treatment of serial concentrations of NPs for 4, 12, and 24 hr. Thereafter, cells were washed three times by warm PBS, detached by 100 µL TrypLE™ for 10-15 mins, and aliquots of 100 µL CM (containing 10% FBS) were added to each well to deactivate/neutralize TrypLE™, and then transferred to Eppendorf's tubes. The samples were centrifuged at 400 xg for 2 mins. The supernatant was removed without disturbing the cell pellets prior to staining by a mixture containing 2/3 of its CM volume, 1/3 containing Ca^{++} rich binding buffer of 1 µL per sample of annexin-V solution

(the concentration is not disclosed by the manufacturer), and 1 µL per mL (7-AAD final concentration: 50 µg/mL) of 7-AAD for 15 min in the dark at room temperature and analysed immediately using a flow cytometer (BD Accouri). The results were expressed in comparison to the NC (*n=3*).

Flow Cytometry Settings and Gating Strategy:

For each experiment, the BD Accuri C6 flow cytometry (FC) was set to fast flow rate (66 µL/min), and 3 blue-1 red lasers. Density-plot (Dot-plot) showing the forward scatter characteristics (FSC-A) and side scatter characteristics (SSC-A) was used to gate around the morphologically viable and apoptotic cell population and exclude the cellular debris and acellular particles (Figure. 3.2. A: P1 gate). FSC-Area plotted against FSC-Height (FSC-A vs FSC-H) was used to gate around the singlet cells (Figure. 3.2. B: P2 gate).

The acquisition limits based on the previous gating were set to 5000 events in the singlets P2 gate with 50 µL sample volume as a secondary limit. Non-labelled negative controls (untreated cells) and labelled negative controls stained with fluorescent probes (separately or both) were used to set the gates, exclude any debris, and determine the positive population gates. NPs samples were labelled with each dye separately, and both dyes were used to exclude the NPs interferences. The PC of cells exposed to heat shock of 60 ^{o}C for 5 min then stained with the staining mixture was used to select the positive median fluorescence intensities (MFI) (385). MFI were collected in FL-1 (M1 for Annexin-V-FITC: *Ex/Em*: 488/525 nm on green channel) and FL-3 (M2 for 7-AAD: *Ex/Em*: 488/647 nm on red channel) (Figure. 3.2. C & D).

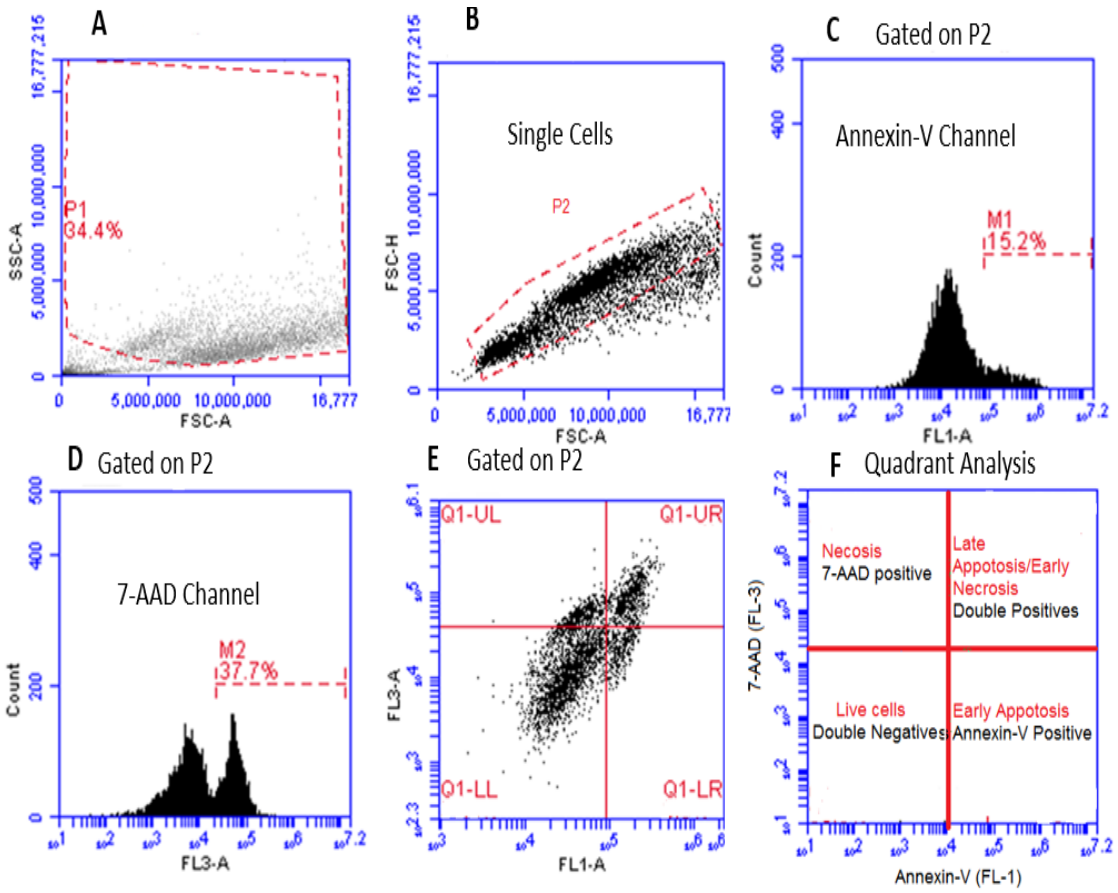

Figure. 3.2. Flow cytometry gating strategy and analysis, (A) SSC-A vs FSC-A Dot-plot, (B) FSC-A vs FSC-H Dot-plot, (C) FL-1 or Annexin-v histogram, (D) FL-3 or 7-AAD histogram, (E) Quadrant analysis Dot-plot, (F) Schematic diagram of quadrant analysis.

Single parameter histograms (FL-1 or FL-3), or two parameters dot-plot (FL-1 vs FL-3) (Figure. 3.2. E & F) using the quadrant analysis were used to determine the positive cell populations as follows; where live cells were double negatives for annexin-V and 7-AAD, early apoptotic cells were only annexin-V positive, late apoptotic cells were double positives for annexin-V and 7-AAD, and the necrotic cells were only 7-AAD positive (Figure. 3.2. E & F) (*n=3*).

3.3.2.8. Caspases Quantification Assay:

Caspases 3/7, 8 and 9 were evaluated by Cell Meter™ Multiplexing Caspase 3/7, 8 and 9 Activity Assay Kit, Triple Fluorescence Colours (AATBioquest®, USA) (242, 374, 386). As per published protocol, after 24 hr of treatment with NPs, a triple wash with warm

PBS was performed. The reagents were prepared fresh by adding 50 µL of each solution in 10 mL assay buffer prior to adding 100 µL per well. The 96-well plate was left at room temperature in the dark for 1 hr prior to fluorescence measurements using a plate reader (Caspase 3/7: red (*Ex/Em*: 535 nm/620 nm), Caspase 8: green (*Ex/Em*: 490 nm/525 nm), Caspase 9: blue (*Ex/Em*: 370 nm/450 nm). The results were expressed as a percent of the NC (*n=3*) and 10% DMSO was used as a PC.

3.3.2.9. Inflammatory Response:

3.3.2.9.1. IL-8 Detection ELISA Kit:

IL-8 (previously known as neutrophil activating protein 1 (NAP-1), granulocyte chemotactic protein 1 (GCP-1), monocyte-derived neutrophil-activating peptide (MONAP) and protein 3-10C) is a pro-inflammatory chemokine (strong chemoattractant for immune cells especially T-cells, neutrophils and basophils) that is secreted by a variety of endothelial cells and monocytes. IL-8 ELISA assay is a quantitative solid-phase sandwich ELISA that measures the IL-8 by a sandwich bound of two antibodies (374, 387). The NUNC Maxisorp® plates were coated by IL-8 specific monoclonal antibody (immobilized capture antibody). The samples, standards, and control were added to the wells where any IL-8 would bind to the capture antibody. A sandwich or second antibody (detector antibody and linked to an enzyme) was added to the wells to bind to the IL-8 bound immobilized antibody. A substrate solution was added to each well that reacted with the sandwich linked enzyme and produced IL-8 concentration dependent measurable absorbance at 450 nm and subtracting the background noise at 570 nm by plate reader.

Calu-3 cells were seeded at a density of 40 $x10^3$ per well (200 µL) in 96 well-plates for 48 hr, then culture media were removed prior to adding serial concentrations of NPs prepared in SFM. THP-1 cells were seeded at a density of 40 $x10^3$ per well (200 µL) in 96

well-plates and differentiated to macrophages upon stimulation with PMA (5 ng/mL) for 48 hr. The culture media was removed prior to adding serial concentrations of NPs prepared in SFM. After 24 hr exposure, the supernatants were processed per the published protocol of Human IL-8 ELISA Ready-SET-GO!® kit from Affymetrix eBioscience®. Cells treated with LPS at 15 µg/mL concentration were used as a PC. The results were expressed as a percent of the NC (*n=2*).

3.3.2.9.2. Cytokines Beads Array (CBA):

Further inflammatory potentials were measured by BD™ CBA Human Th1/Th2/Th17 Cytokine Kit (BD biosciences). BD CBA kit measures IL-2, IL-4. IL-6, IL-10, IL-17A, Tumour Necrosis Factor (TNF-α), and Interferon-γ (IFN-ɣ). The principle of BD CBA kit is similar to the sandwich detection of IL-8 (387) (capture antibody attached to bead + cytokine/analyte + detection antibody linked to a fluorescent reporter dye) where this assay uses the bead array technology to allow for multiple simultaneous measurements of seven cytokines using easy and fast flow cytometry (374, 388, 389). Each bead is coated with a specific antibody against one of these cytokines and characterized with a distinct fluorescence signal when bound to the target cytokines and with the addition of the detector antibody phycoerythrin (PE)–conjugated (fluorescent reporter dye), both produce characteristic fluorescence of the bead and the detector dye that can be resolved in a red channel (i.e., FL3 or FL4).

THP-1 cells were seeded at a density of 40 $x10^3$ per well (200 µL) in 96 well plates and differentiated to macrophages upon stimulation with PMA (5 ng/mL) for 48 hr. The culture media was removed prior to adding NPs concentrations (0.125, 0.5, 2 mg/mL) 200 µL per well prepared in SFM. After 24 hr, supernatants were collected and stored at -20 for the day of analysis. The samples thawed and processed as the published protocol and

analysed by a flow cytometer (BD Accouri). Briefly, standards (20-5000 *PG*/mL) dilutions and supernatant samples (without dilutions) were incubated with a solution of capture beads (2 µL of each bead per sample and toped up to 50 µL per sample of assay diluent) at room temperature in the dark for 1 hr. Then each sample was mixed with 50 µL of the detection reagent (10 µL of PE-detection antibody per sample+40 µL assay diluent per sample) and kept for further 2 hr. Thereafter, centrifuged at 200 xg for 5 min using Eppendorf centrifuge, and supernatants were removed, and samples were resuspended in 50 µL wash buffer. Cells treated with LPS at 15 µg/mL concentration were used as a PC. Cytokine beads were collected in FL2/FL4. The results were expressed as a percent of the NC (*n=2*).

Flow Cytometry Settings and Gating Strategy:

For each experiment, BD Accuri C6 FC was set to medium flow rate (33 µL/min), and 2 blue-2 red lasers. The SSC-A vs FSC-A dot-plot was used to gate around the population of beads exclude the debris and particles (Figure. 3.3. A: R1 gate) and the acquisition limits were set to collect 2100 events in R1.

The beads were excited by the red laser and detected by FL-4 channel (Figure. 3.3. B), while the PE reporter was excited by the blue laser and detected in FL-2 single channel or in FL-2 vs FL-4 dot-plot (Figure. 3.3. C). MFI of FL-2 was used for the analysis.

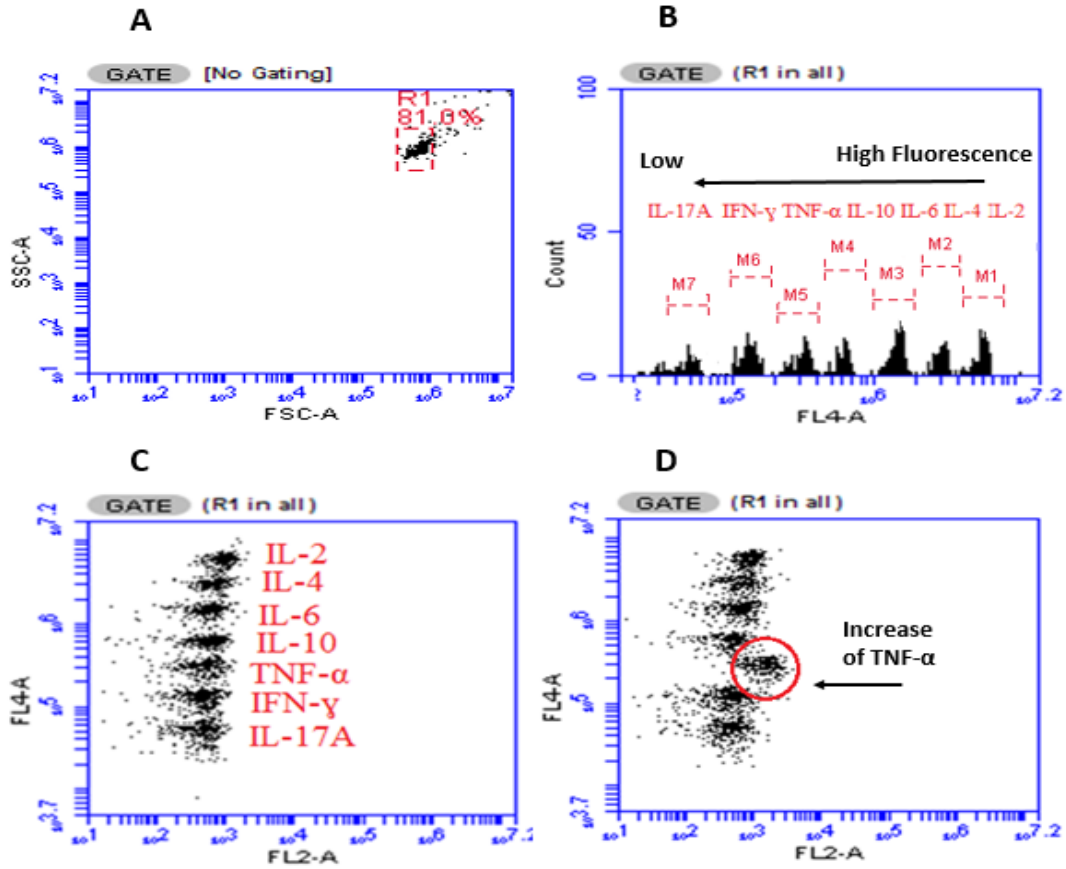

Figure. 3.3. Flow cytometry gating strategy and analysis, (A) SSC-A vs FSC-A Dot-plot, (B) FL-4 histogram showing the beads, (C) FL-2 vs FL-4 dot-plot, (D) Example of one analyte bead; TNF-α showing an increase in its MFI.

3.3.2.10. Comet Assay:

DNA damage was evaluated by OxiSelect^{TM} Comet Assay Kit (Cell Biolabs, Inc) and evaluated in Calu-3 cells (390-392) by conducting single cell alkaline electrophoresis to detect any single strand or double strand DNA breaks and alkali-labile sites. According to the manufacturer protocol, briefly, Calu-3 cells were seeded at a density of 40 x10^3 per well (200 µL) in 96 well plates for 48 hr, then culture media was removed prior to adding two concentrations of NPs prepared in SFM (0.125 and 2 mg/mL) in duplicates. After 24 hr exposure, cells were harvested in Eppendorf's tubes, counted by a haemocytometer, then centrifuged at 400 xg for 2 min followed by removal of supernatant and cell wash by warm PBS. This was followed by another cycle of centrifugation and removal of the supernatant

prior to preparing cell suspension of 10 x10^4 cells/mL in PBS (to avoid cell and comets overlapping) mixed with low gelling temperature molten comet agarose at 1:9 v/v dilution. 100 µL of this mixture was added to the precoated comet slides with agarose. The slides were submerged in a lysis buffer (2.5 M NaCl, 10 mM Tris base, 100 mM Na2EDTA, 1 % Triton X-100, pH 10) for 45 min at 4°C in the dark. Thereafter, replaced with prechilled alkaline buffer (1 mM Na2EDTA, 300 mM NaOH, pH 13, to unzip the double strands) and kept for 30 min at 4°C in the dark. The slides were kept under alkaline conditions during the electrophoresis (25 V, 300 mA, 1.04 V/cm) for further 30 min at room temperature. The slides were washed with cold water and then fixed by 70% chilled ethanol and air-dried prior to staining with working solution of Vista Green DNA dye (1/10^4 dilution) at 100 µL per well at room temperature for further 15 min. The slides were visualized with Leica Fluorescence Microscopy using FITC filter where 50 cells or more per well were photographed. Image analysis was performed using TriTek CometScore Pro ver. 2.0.0.0. commercial software measuring the fluorescence intensity and the length of the head and of the tail of comets.

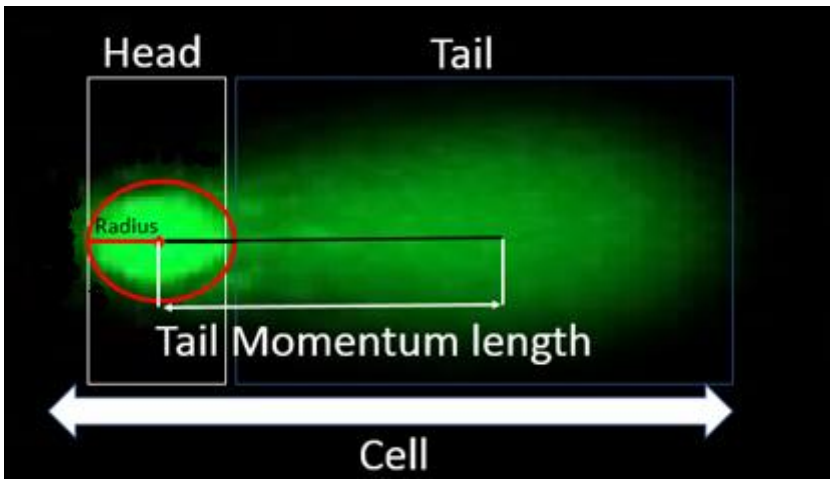

Figure. 3.4. Comet shape and the calculations used to determine the DNA damage.

DNA damage was quantified by calculating Head DNA%, Tail DNA % (100 – head DNA %), and Olive Tail Moment (Tail Moment Length*tail DNA %)/100) (393) (Figure.

3.4). Cells were treated by 100 µM H_2O_2 for 30 mins as a PC. The results were expressed in comparison to the NC (*n=2*).

3.3.2.11. Statistical Analysis:

as previously mentioned in section 2.3.4.

3.4. Results:

3.4.1. Polymeric Nanoparticles formulations and Characterizations:

As previously mentioned in section 2.3, 2.4, and 2.5.

3.4.2. Alamar Blue Assay:

Cell viability after the exposure to different NPs was assessed by AB (Figure. 3.5., 3.6, & 3.7 for readings after 1 hr (T1), 2 hr (T2), and 3 hr (T3) respectively). All NPs showed a trend of concentration-dependent decrease of the cell viability.

For T1, Figure. 3.5. (A & B) showed the cell viability after 1 hr incubation with AB reagent. Negatively charged NPs (Figure. 3.5. A) showed significant statistical difference from NC at *PG*-2/1-2 mg/mL, *PL*-2/0.25-2 mg/mL, *PG*-5/1-2 mg/mL, and *PG*-8/1-2 mg/mL. There was no significant difference between *PG*-2 and *PL*-2. However, *PG*-2 showed slightly lower viability than *PG*-5 and *PG*-8 and was statistically different from *PG*-5/2 mg/mL.

Positively charged (Figure. 3.5. B) NPs showed similar trend and were statistically different from NC at 1-2 mg/mL of *PG*+2 and *PL*+2, and 2 mg/mL of *PG*+5 and *PG*+8. *PG*+2 showed higher cell viability compared to *PL*+2 at all concentrations but was not significant. However, *PG*+2 showed lower viability from *PG*+5 and *PG*+8 with statistical difference at 0.25 mg/mL from *PG*+5 and *PG*+8. *PG*-2 NPs showed lower viability compared *PG*+2 but was non-significant. *PL*-2 showed higher viability to *PL*+2 and was

statistically different at 0.125 mg/mL. *PG*-5 and *PG*-8 showed lower viability to *PG*+5 and *PG*+8 and was statistically different at 2 mg/mL for *PG*-5 and *PG*-8, and at 0.25 mg/mL for *PG*-8.

No wash/T1, in Figure. 3.5. C & D represented Calu-3 cell viability after exposure to all NPs for 24 hr, followed by removing supernatants without a wash step (NPs were still covering the surface of monolayers) and further incubation for 1 hr with AB reagent. All NPs demonstrated a similar trend of decreasing the cell viability with increasing NP concentration. The results indicate lower cell viability compared to applying wash step and were statistically different at *PG*-2/2mg/mL, *PG*-8/2mg/mL, *PG*+2/1-2 mg/mL, *PG*+5/1-2 mg/mL, *PG*+8/2mg/mL. However, control samples of NPs mixed with the AB reagent only, were similar to blank wells (media only), but within the presence of cellular/ biological media, NPs interference and/or inefficient removal were possibilities explaining the lower viability reported when no wash of NPs was applied.

For T2, Figure. 3.6. (A & B) showed the cell viability after 2 hr to investigate the ability of the cell to recover. All NPs showed a concentration-dependent decrease of the cell viability, but the cell viability showed an increase from T1. Negatively charged NPs (Figure. 3.6. A) showed reduced viability with statistical differences from NC for *PG*-2 at 0.5-2 mg/mL, *PL*-2 at 0.25-2 mg/mL, *PG*-5 at 1-2 mg/mL, and *PG*-8 at 1-2 mg/mL. Furthermore, *PG*-2 showed a non-significant decrease in cell viability to *PL*-2 except at 1-2 mg/mL. Moreover, *PG*-2 showed a higher viability than *PG*-5 and *PG*-8 with statistical difference from *PG*-5 at 2 mg/mL. Positively charged NPs (Figure. 3.6. B) NPs showed similar trend with statistical difference from NC with *PG*+2 at 1-2 mg/mL, *PL*+2 at 2 mg/mL, *PG*+5 at 1-2 mg/mL, and *PG*+8 at 0.25, 1-2 mg/mL. *PG*+2 showed significantly lower viability from *PL*+2 at 1-2 mg/mL. *PG*+2 showed lower viability than *PG*+5 and *PG*+8 but no statistical difference at all concentrations. *PG*-2 and *PL*-2 NPs indicated lower

cell viability to *PG*+2 and *PL*+2 but was not statistically different. *PG*-5 indicated a slight decrease in cell viability compared to *PG*+5 and was statistically different at 2mg/mL.

No wash/T2, Figure. 3.6. (C & D), comparing the no-wash experiments to the 3-steps wash, indicated a decrease in cell viability that was only significant at 2 mg/mL of *PG*-2 and *PG*+2. There were some variations in the cellular ability for the recovery denoted by large error bars showing the standard deviations that affected the statistical analysis comparison.

For T3, Figure. 3.7. (A & B), showed the cell viability after 3 hr. All NPs showed a concentration-dependent decrease of the cell viability that was higher viability compared to T1 and T2 for each concentration. NPs showed similar trend as previously mentioned while the lower concentrations (0.125-0.5 mg/mL) showed similar or higher viability than the NC at T3. A higher viability from the NC was seen at *PG*-2/ 0.125 mg/mL (no statistical difference), *PG*-5/ 0.125 mg/mL (statistically different), *PG*-8/ 0.125-0.25 mg/mL (statistical different at 0.25 mg/mL), *PG*+2/ 0.125-0.25 mg/mL (no statistical difference), *PL*+2/ 0.125-1 mg/mL (no statistical difference), *PG*+5/ 0.125-0.25 mg/mL (statistically different), and *PG*+8/ 0.125-0.25 mg/mL (statistically different at 0.125 mg/mL). However, a reduced cell viability was statistically different from NC at *PG*-2/ 1-2 mg/mL, *PG*-5/ 0.5-2 mg/mL, *PG*-8/ 1-2 mg/mL, *PG*+2/ 1-2 mg/mL, and *PG*+5 and *PG*+8 at both 1-2 mg/mL. In addition, *PG*-2 showed a decrease in cell viability that was statistical different to *PL*-2/ 1-2 mg/mL. *PG*-2 showed a higher viability than *PG*-5 and *PG*-8 and was statistically different at 2mg/mL. *PG*+2 showed significant less viability than *PL*+2/ 2 mg/mL.

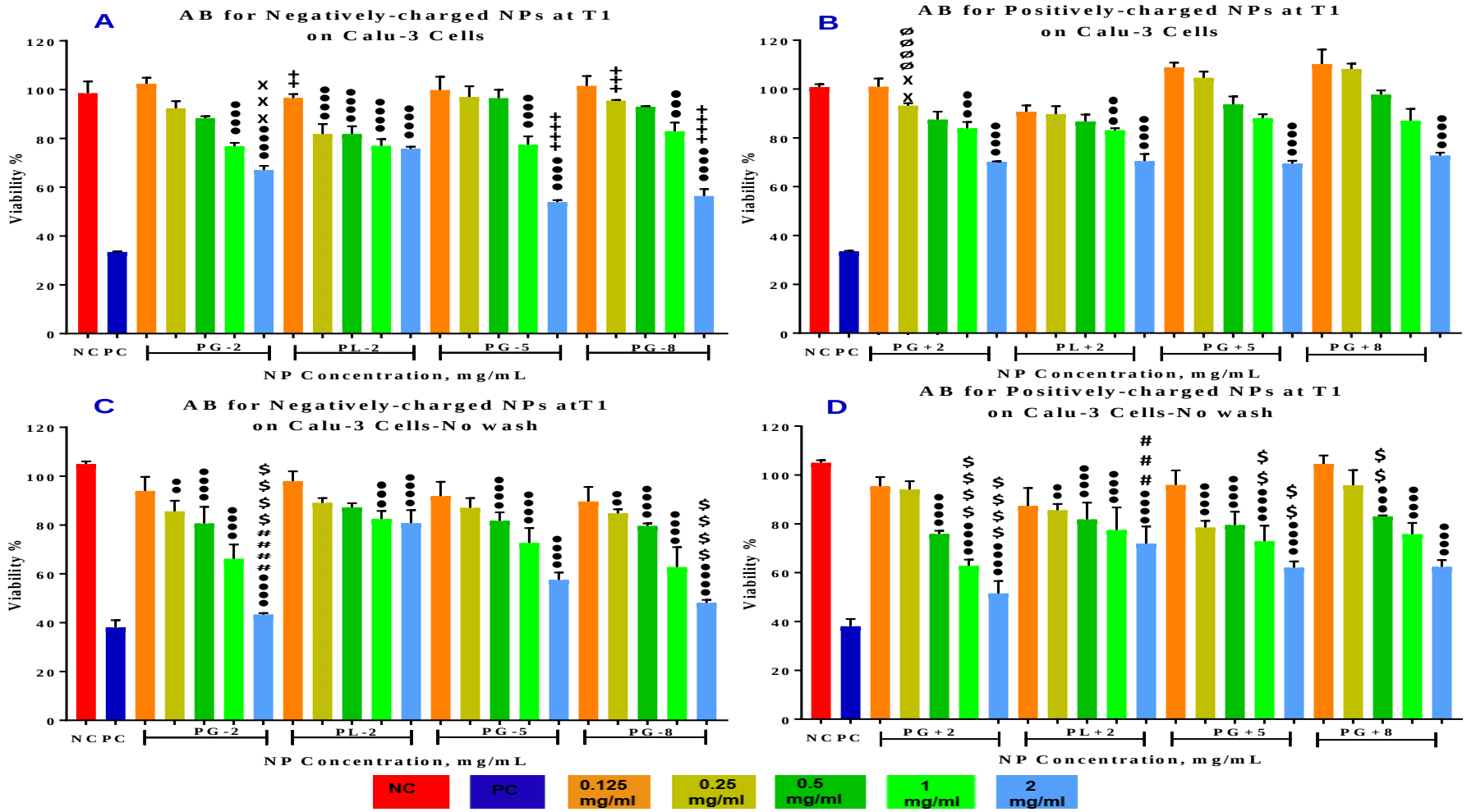

Figure. 3.5. AB at T1. (A) negatively charged NPs, (B) positively charged NPs with optimized wash step. (C) negatively charged NPs and (D) positively charged NPs without wash step (Results expressed as Mean ± SD, for statistical symbols and *P*-value please refer to section. 2.3.4).

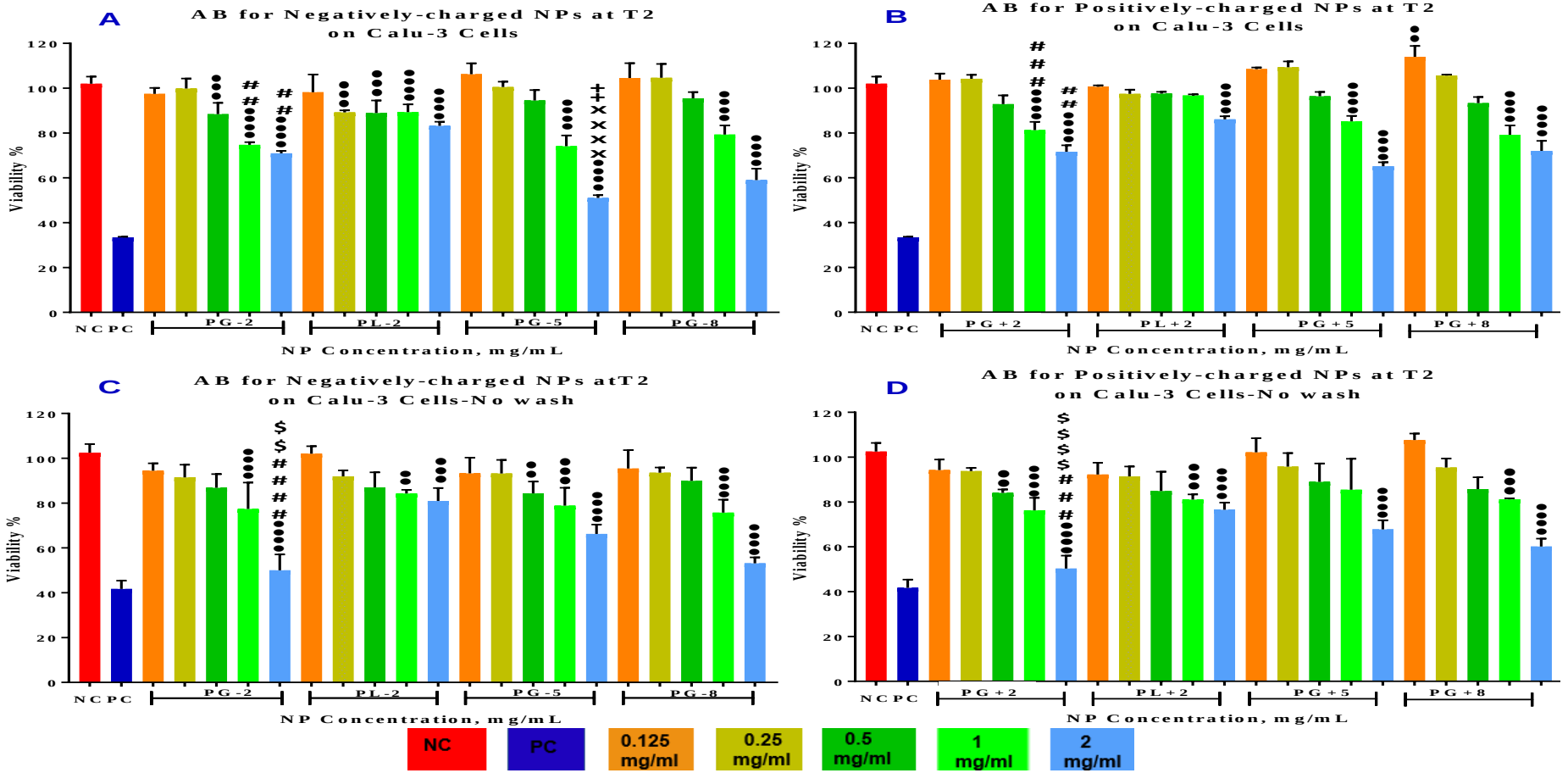

Figure. 3.6. AB at T2: (A) negatively charged NPs, (B) positively charged NPs with optimized wash step. (C) negatively charged NPs and (D) positively charged NPs without wash step (Results expressed as Mean ± SD, for statistical symbols and *P*-value please refer to section. 2.3.4).

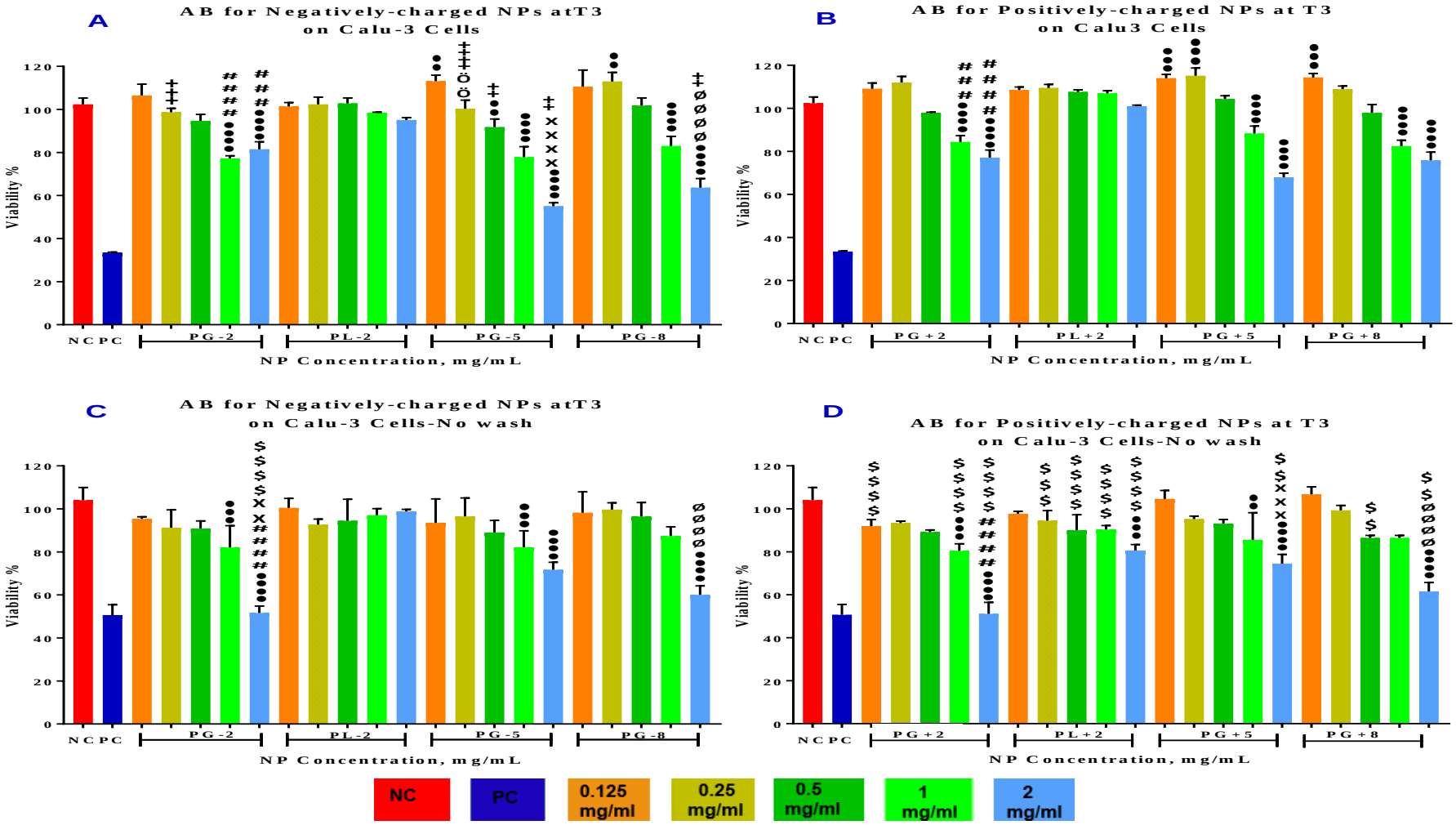

Figure. 3.7. AB at T3: (A) negatively charged NPs, (B) positively charged NPs with optimized wash step. (C) negatively charged NPs and (D) positively charged NPs without wash step (Results expressed as Mean ± SD, for statistical symbols and *P*-value please refer to section. 2.3.4).

No wash/T3, Figure. 3.7. (C & D), comparing the no-wash experiments to the 3-steps wash, showed a decrease in cell viability that was statistically different at *PG*-2/ 1-2 mg/mL, *PG*+2/ 1-2 mg/mL, *PG*-5/1-2 mg/mL, *PG*+5/1-2 mg/mL, *PG*-8/2 mg/mL, *PG*+8/ 2mg/mL, *PL*+2/ 2 mg/mL. The lower cell viability and statistical differences in many NPs concentrations indicated the importance of removing the NPs prior to incubation with the reagent. However, the trend was not affected but better cell recovery, less NP interference and narrower error bars were obtained in the experiments involving removing the supernatant containing the NPs and performing 3-wash steps prior to adding the reagents.

3.4.3. Reactive Oxygen Species (ROS) Detection Assay:

2′,7′-Dichlorodihydrofluorescein diacetate (H_2DCFDA) Assay:

ROS detected after 24 hr exposure of Calu-3 cells to NPs was evaluated via H_2DCFDA reagent and represented in Figure. 3.8.

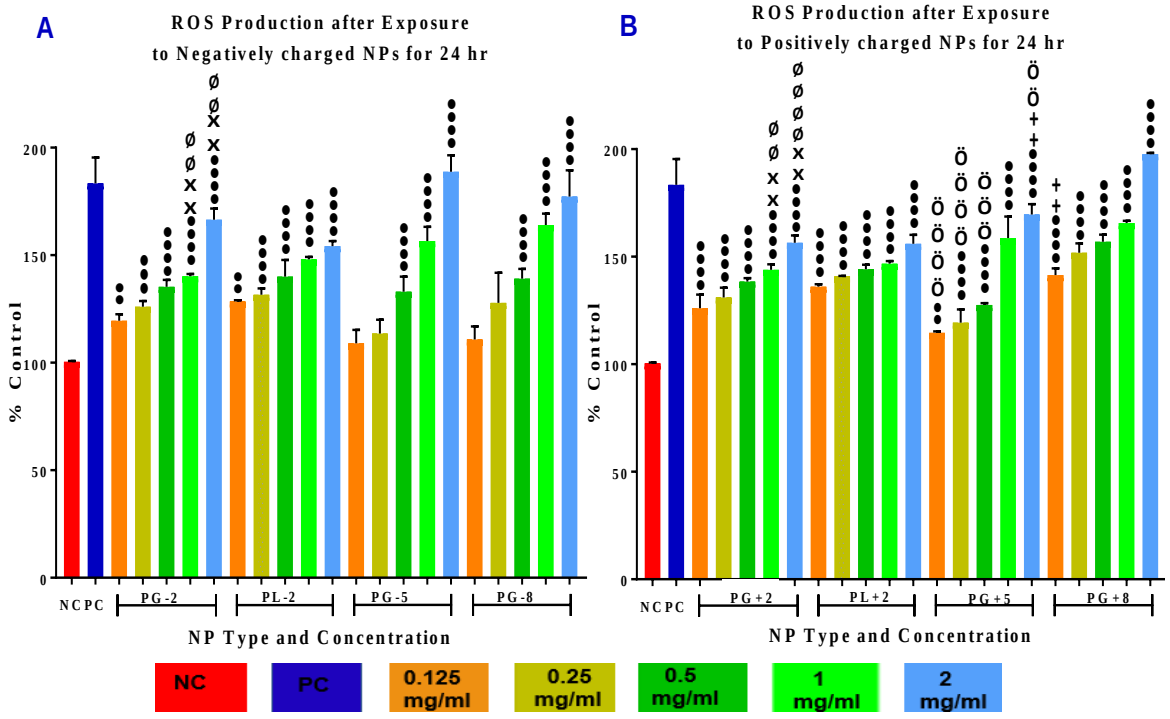

Figure. 3.8. A and B: ROS detection by H_2DCFDA in Calu-3 cells after 24 hr exposure to NPs: (A) Negatively charged NPs, (B) Positively charged NPs (Results expressed as Mean ± SD, for statistical symbols and *P*-value please refer to section. 2.3.4).

All NPs showed a trend of increasing the ROS production with increasing NP concentration compared to NC. Negatively charged NPs are shown in Figure. 3.8. A. *PG*-2 and *PL*-2 showed a significant rise in ROS production but no statistical difference between both types at all concentrations. *PG*-5 showed non-significant ROS production at low concentrations (0.125, 0.25 mg/mL) but a significant increase at higher concentrations (0.5-2 mg/mL). *PG*-8 showed a significant increase in ROS production above 0.5 mg/mL concentration. *PG*-2 showed a significant ROS production to *PG*-5/ 1- 2 mg/mL, and to *PG*-8/ 1-2 mg/mL.

Positively charged NPs are shown in Figure. 3.8. B. All NPs showed a similar trend of a concentration-dependent increase of ROS production. All positively charged NPs showed significant ROS production compared to the NC. *PG*+2 and *PL*+2 showed no statistical difference. However, *PG*+2 showed higher ROS production to *PG*+5/ 0.125-0.5 mg/mL, but with significantly lower ROS production at 1-2 mg/mL. Furthermore, *PG*+2 showed significantly lower ROS production to *PG*+8/ 1-2 mg/mL. *PG*+8 showed a significant increase in ROS production to *PG*+5 at correspondent concentrations of 0.125, 0.25, 0.5 and 2 mg/mL. There was only statistical difference between *PG*-5 from *PG*+5/ 2mg/mL.

ROS detected after 24 hr exposure of Calu-3 cells to NPs evaluated via H_2DCFDA confirmed a significant involvement of ROS induction in the cellular cytotoxicity after NPs exposure. *PG* and *PL* NPs showed no significant differences in a concentration-dependent ROS production. However, *PG*-5 and *PG*-8 showed no ROS production at low concentrations (0.125 – 0.25 mg/mL) denoting limited uptake of these larger sized NPs. *PG*-5, *PG*+5, *PG*-8, *PG*+8 showed a significant higher ROS production at 1-2 mg/mL compared to *PG*-2, and *PG*+2 that can be correlated to their higher cytotoxicity. The effect of the charge and chemistry was negligible compared to the NP size.

Cellular ROS (Deep Red) Assay (ab186029): Deep Red assay was used to evaluate the ROS production mainly $O_2^{\bullet-}$ and $OH^{\bullet-}$ radicals after Calu-3 cells exposure to NPs for 24 hr and represented in Figure. 3.9. where (A & B) presents the results of the assay after removal of NPs and applying 3 wash steps, and (C & D) presents the results after removal of supernatant containing NP without efficient removal by washing (No wash step).

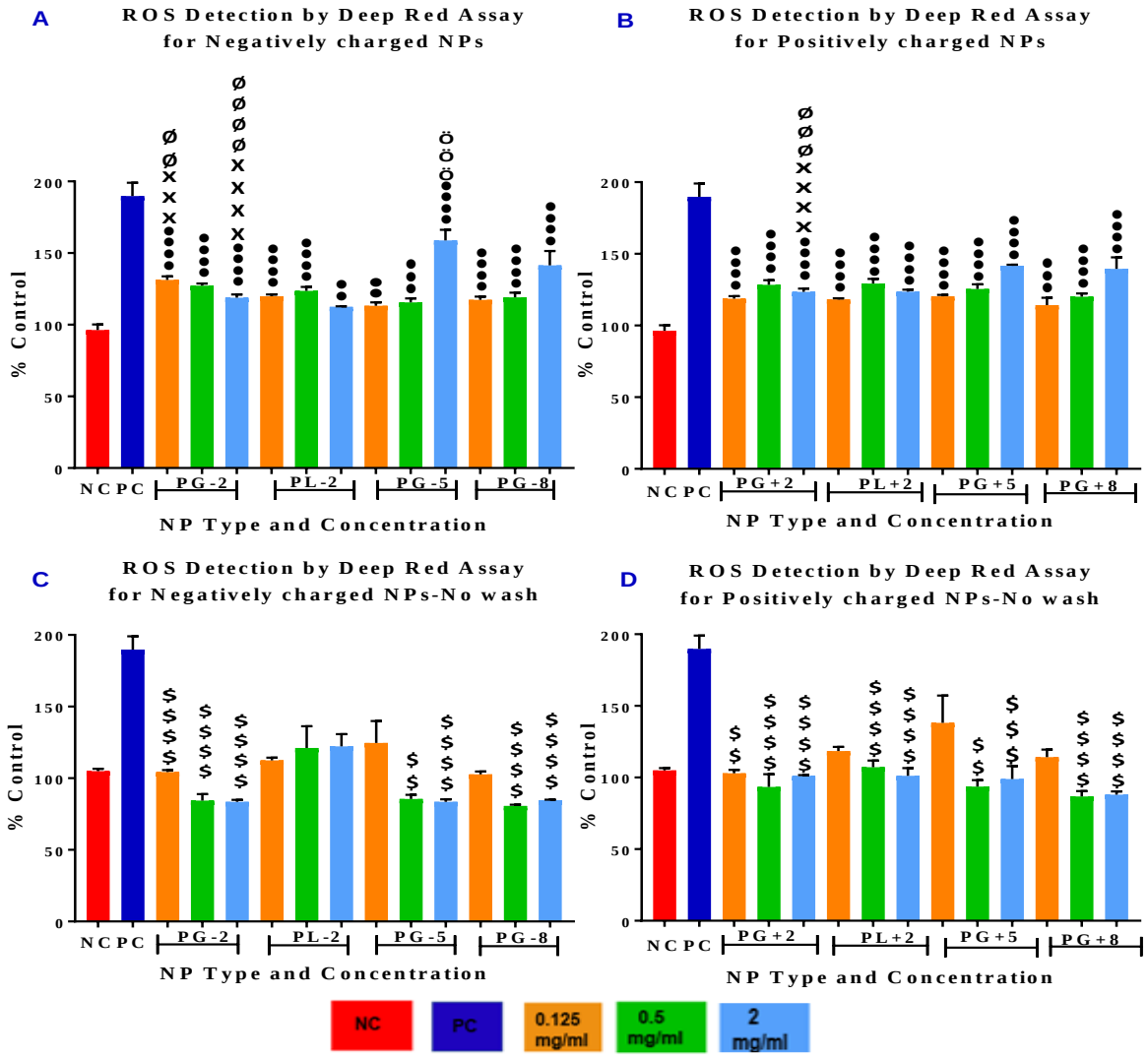

Figure. 3.9. ROS detection by Deep Red Assay in Calu-3 cells after 24 hr exposure to NPs: (A) Negatively charged NPs and (B) Positively charged NPs response after wash step, while (C) Negatively charged NPs and (D) Positively charged NPs with no wash step (Results expressed as Mean ± SD, for statistical symbols and *P*-value please refer to section. 2.3.4).

There was significant high production of ROS at all concentrations (0.125, 0.5, and 2 mg/mL only used) compared to NC using the Deep Red assay (Figure. 3.9. A & B). However, only *PG*-5 and *PG*-8 at 2mg/mL showed the highest production of ROS. There was no statistical difference between the different types of NPs except *PG*-2 which showed a statistical difference to *PG*-5 and *PG*-8 at 0.125 mg/mL (higher ROS) and 2 mg/mL (lower ROS). *PG*-5/ 2 mg/mL showed statistical difference to *PG*-8 (higher ROS), and *PG*+2/ 2mg/mL showed statistical difference from *PG*+5 and *PG*+8 (lower ROS).

Comparing the Deep Red assay (3 wash steps) to H_2DCFDA assay demonstrated lower values and almost a concentration independent for the low concentrations of all NPs, except at 2mg/ mL of *PG*-5, *PG*+5, *PG*-8, and *PG*+8.

No wash experiment presented in Figure. 3.9. C & D. There were significant differences between the two experimental procedures where the ROS production showed lower values compared to the experiment with applying 3-washes. The measured values were lower than what was evaluated using 3 washes step procedure. The lower values were statistically different to *PG*-2 (at all concentrations), *PG*-5 (at 0.5 and 2 mg/mL), *PG*-8 (at 0.5 and 2 mg/mL), *PG*+2 (at all concentrations), *PL*+2 (at 0.5 and 2 mg/mL), *PG*+5 (at 0.5 and 2 mg/mL), and *PG*+8 (at 0.5 and 2 mg/mL). This denoted a strong possibility of NPs interference with this assay (394).

3.4.4. Mitochondrial Membrane Potential (JC-1):

ΔΨm of Calu-3 cells after 24 hr exposure to NPs was evaluated by JC1 dye using the red/green ratio (Figure. 3.10. A and B). All NPs showed similar trend of a concentration-dependent reduction of ΔΨm compared to NC and was statistically significant at all concentrations, indicating loss of mitochondrial polarized healthy state, which is a sign of cytotoxicity and apoptosis.

Negatively charged NPs (Figure. 3.10. A) showed a trend of decreasing ΔΨm with increasing NP concentration. *PG*-2 showed a less impaired ratio to *PL*-2 and was statistically different at concentrations 0.125-1 mg/mL. Furthermore, *PG*-2 showed a less impaired ratio from *PG*-5 and *PG*-8 at concentrations 0.125 and 0.25 mg/mL. Moreover, *PG*-5 and *PG*-8 were almost similar in values of ΔΨm with no statistical difference between them.

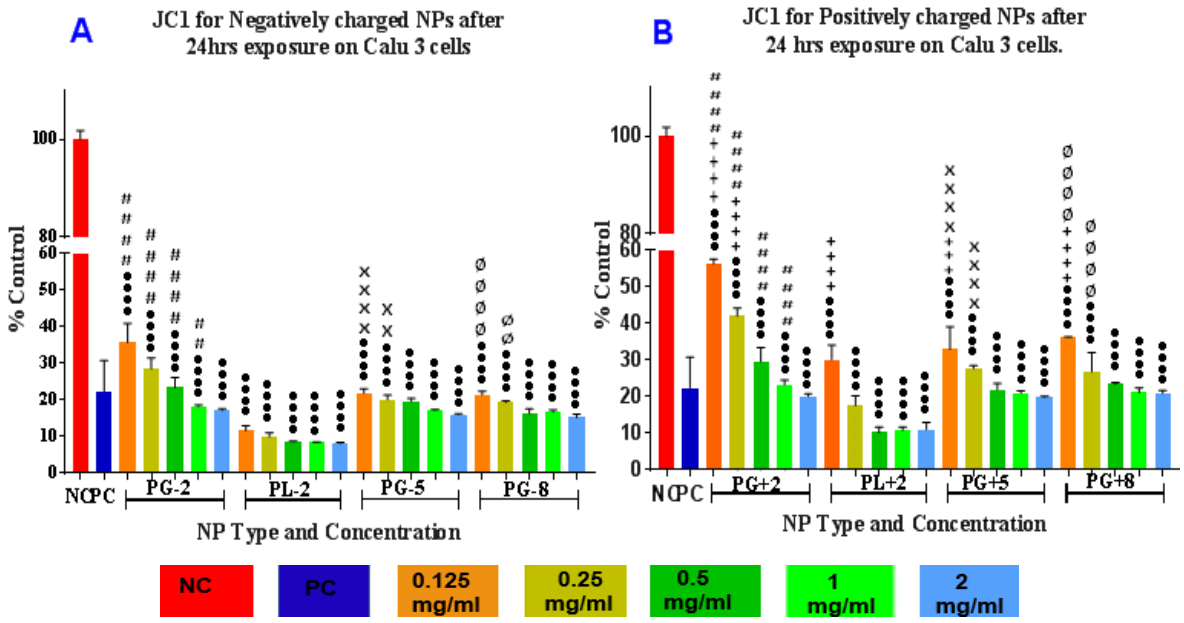

Figure. 3.10. MMP by JC-1 dye: (A) Negatively charged NPs, (B) Positively charged NPs (Results expressed as Mean ± SD, for statistical symbols and *P*-value please refer to section. 2.3.4).

Positively charged NPs (Figure. 3.10. B) showed similar trend. *PG*+2 showed a significantly less impaired ratio to *PL*+2 (at 0.125-1 mg/mL). *PG*+2 showed a significantly less impaired ratio to *PG*+5 (at 0.125 and 0.25 mg/mL) and *PG*+8 (at 0.125 and 0.25 mg/mL). However, *PG*+2, *PL*+2, *PG*+5, and *PG*+8 showed a less impaired ratio that was significant compared to their negative counterparts at *PG*+2 (0.125 and 0.25 mg/mL), *PL*+2 (0.125 mg/mL), *PG*+5 (0.125 mg/mL), and *PG*+8 (0.125 mg/mL).

3.4.5. Cell Membrane Integrity (LDH):

Cell membrane integrity was evaluated by LDH Total (with the use of total cell lysis) or release (spontaneous release in the supernatant without cell lysis step) assays after Calu-3 cells exposure to NPs for 24 hr (Figure. 3.11).

LDH Total; All NPs showed a similar trend of a concentration dependent decrease of LDH Total compared to NC. For negatively charged NPs **(**Figure. 3.11. A), *PG*-2 showed a statistical difference to NC at 1-2 mg/mL. *PL*-2 showed no statistical difference at all concentrations to NC. *PG*-5 showed statistical difference to NC at 0.25-2 mg/mL, and *PG*-8 showed statistical difference to NC at 0.25-2 mg/mL. *PG*-2 showed a significant low LDH Total compared to *PL*-2 (at 1-2 mg/mL). Furthermore, *PG*-2 showed a significantly high LDH Total compared to *PG*-5 (at 0.5-2 mg/mL) and to *PG*-8 (at 0.25-2 mg/mL). *PG*-5 was significantly lower than *PG*-8 (at 0.5-2 mg/mL). Positively charged NPs (Figure. 3.11. B) showed similar trend with all NPs statistically different than NC at 1-2 mg/mL. However, there was no statistical differences between the different positively charged NPs. *PG*+2 showed significant higher LDH Total to *PG*-2 at 1-2 mg/mL. This was also seen with *PG*+5 which showed a significant higher LDH Total content compared to *PG*-5 (at 0.5-2 mg/mL). *PG*+8 showed a significant higher LDH Total content compared to *PG*-8 (at 0.25-2 mg/mL).

LDH Release: All NPs showed a similar trend of a concentration dependent increase of LDH Release from the NC. However, all the released amounts were significantly lower than the NC at all concentrations of all NPs. For negatively charged NPs (Figure. 3.11. C), *PG*-2 was significantly lower than *PL*-2 at all concentrations. Positively charged NPs (Figure. 3.11. D) showed similar trend and were significantly lower than the NC at all concentrations of all NPs. *PG*+2 showed slightly higher LDH release compared to *PL*+2, but was slightly lower than *PG*+5, and *PG*+8. However, statistical difference was only observed at *PG*+8 (0.125 and 0.25 mg/mL). *PG*+2 showed higher LDH release to *PG*-2 and was

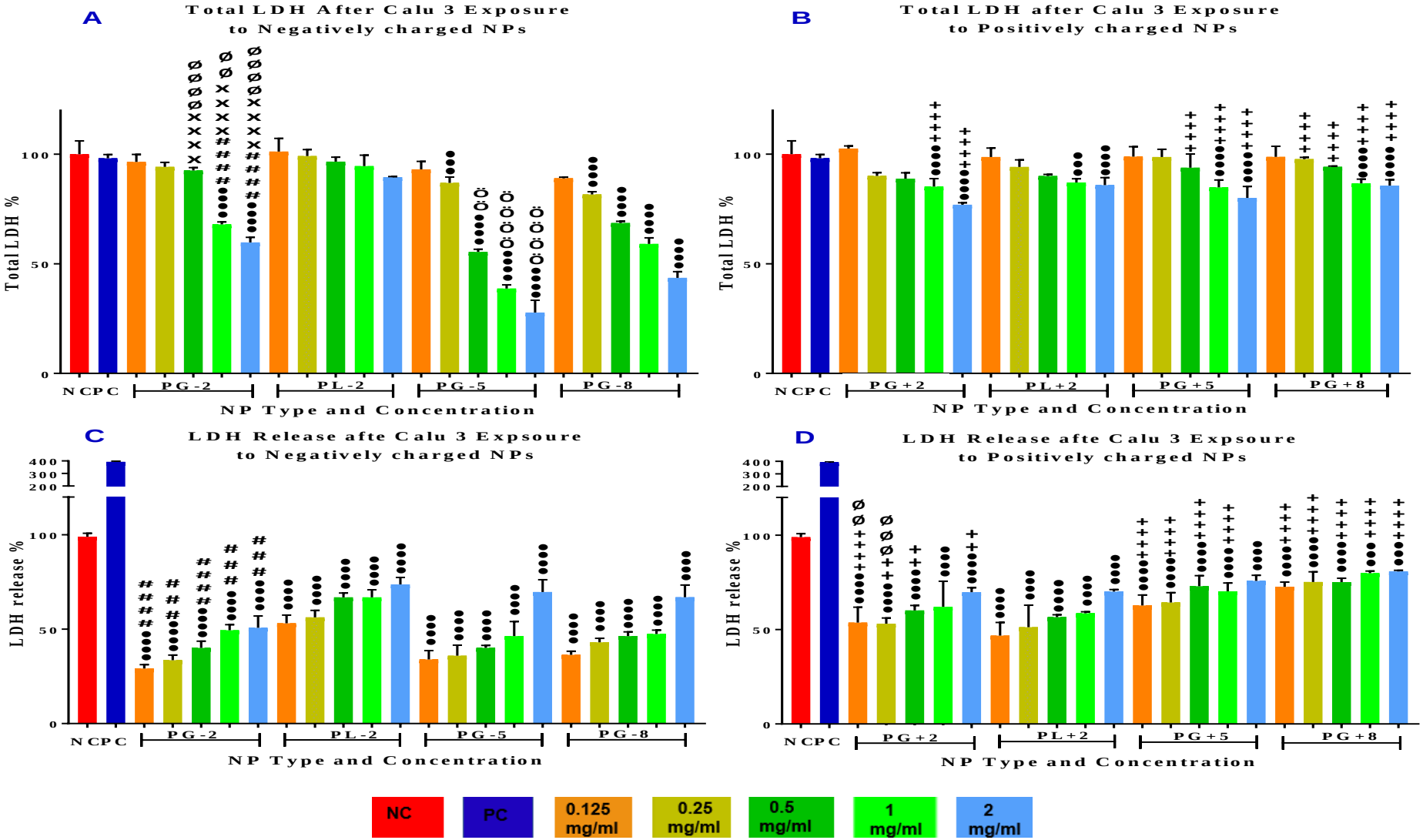

Figure. 3.11. LDH after NPs exposure for 24 hr, (A & B) are LDH Total, and (C & D) LDH Release.

statistically different at 0.125, 0.25, 0.5, and 2 mg/mL. *PG*+5 showed higher LDH release to *PG*-5 and was statistically different at 0.125-1 mg/mL. *PG*+8 showed higher LDH release to *PG*-8 and was statistically different at all concentrations.

Comparing the two methods; All NPs showed a decrease of the LDH Release compared to corresponding NPs concentrations that showed a significant decrease of their LDH Total by the LDH Total method. For example, *PG*-2 at 1-2 mg/mL is showing a significant decrease of LDH Total that is not reflected with an increase in LDH Release with the correspondent concentrations. This represents a strong evidence of the ability of NPs to adsorb LDH released in the medium. Hence, this could lead to false negative results if the LDH Release assay was applied alone to assess the cell membrane potential.

3.4.6. Apoptosis and Necrosis Assay:

Based on the quadrant analysis results (% Live cells, % Annexin V positive cells (early apoptotic), % Double positives (Annexin V and 7-AAD; late apoptotic), and % 7-AAD positive cells (necrotic)), the double positives and 7-AAD positives showed time-course linked changes that were chosen to plot bar graphs between the different concentrations and time points and statistically analysed. Double positive graphs are represented in Figure. 3.12. A & B, C & D, and E & F for T4, T12, and T24 respectively. 7-AAD positive graphs are represented in Figure. 3.13. A & B, C & D, and E & F for T4, T12, and T24 respectively.

Double positive/late apoptosis percentage: At T4, (Figure. 3.12. A & B) all NPs showed a trend of increasing the NP concentration was associated with increasing the late apoptotic percentage. Only *PG*-2 and *PG*+2 showed a statistical difference to NC at 2 mg/mL, and *PG*+8 showed a statistical difference to NC at 1 mg/mL.

At T12, (Figure. 3.12. C & D) all NPs showed a trend of increasing the NP concentration was associated with increasing the late apoptotic percentage except *PG*+8 which showed a decreasing trend. There were no statistical differences to NC or between the NPs. However, there were huge variations as indicated by the large error bars that resulted in non-significant differences from the NC for all NPs.

At T24, (Figure. 3.12. E & F) all NPs showed a non-significant decreasing trend with the small sized NPs; *PG*-2, *PL*-2, *PG*+2, and *PL*+2 from the NC. However, the large sized NPs; *PG*-5, *PG*+5, *PL*-8, and *PG*+8 showed an increasing trend that was significant at *PG*-8/ 2 mg/mL, *PG*+5/ 0.25 mg/mL, and *PG*+8/ 0.5-2mg/mL. There were no other statistical differences between the NPs and to NC.

7-AAD positive/necrotic percentage: **At T4** (Figure. 3.13. A & B), all NPs showed an increasing trend of necrotic percentage with *PG*-2, *PL*-2, *PG*-5, *PG*-8, *PG*+2, *PL*+2, *PG*+5, and *PG*+8 increasing concentration. There were statistical differences from NC at *PL*-2/ 2 mg/mL, *PG*-8/ 2 mg/mL, and *PL*+2/ 2 mg/mL. *PG*-2 was lower and statistically different to *PG*-8/ 2 mg/mL. *PG*+8 was lower and statistically different to *PG*-8/ 2 mg/mL.

At T12 (Figure. 3.13. C & D), all NPs showed an increasing trend of necrotic percentage and was statistically different from the NC at all concentrations of *PG*-5, *PG*-8, *PG*+5 and *PG*+8. *PG*-2 was lower and statistically different to *PG*-5 (0.125 and 0.5 mg/mL) and *PG*-8/ 0.125 mg/mL. *PG*+2 showed significant difference from *PG*+8/2 mg/mL.

At T24 (Figure. 3.13. E & F), all NPs showed similar trend of increasing the necrotic percentage with increasing the concentration. However, there was a drop in the percentage of the necrotic percentage with *PG*-5/ 0.125-1 mg/mL, *PG*-8 at 0.125, 0.25,

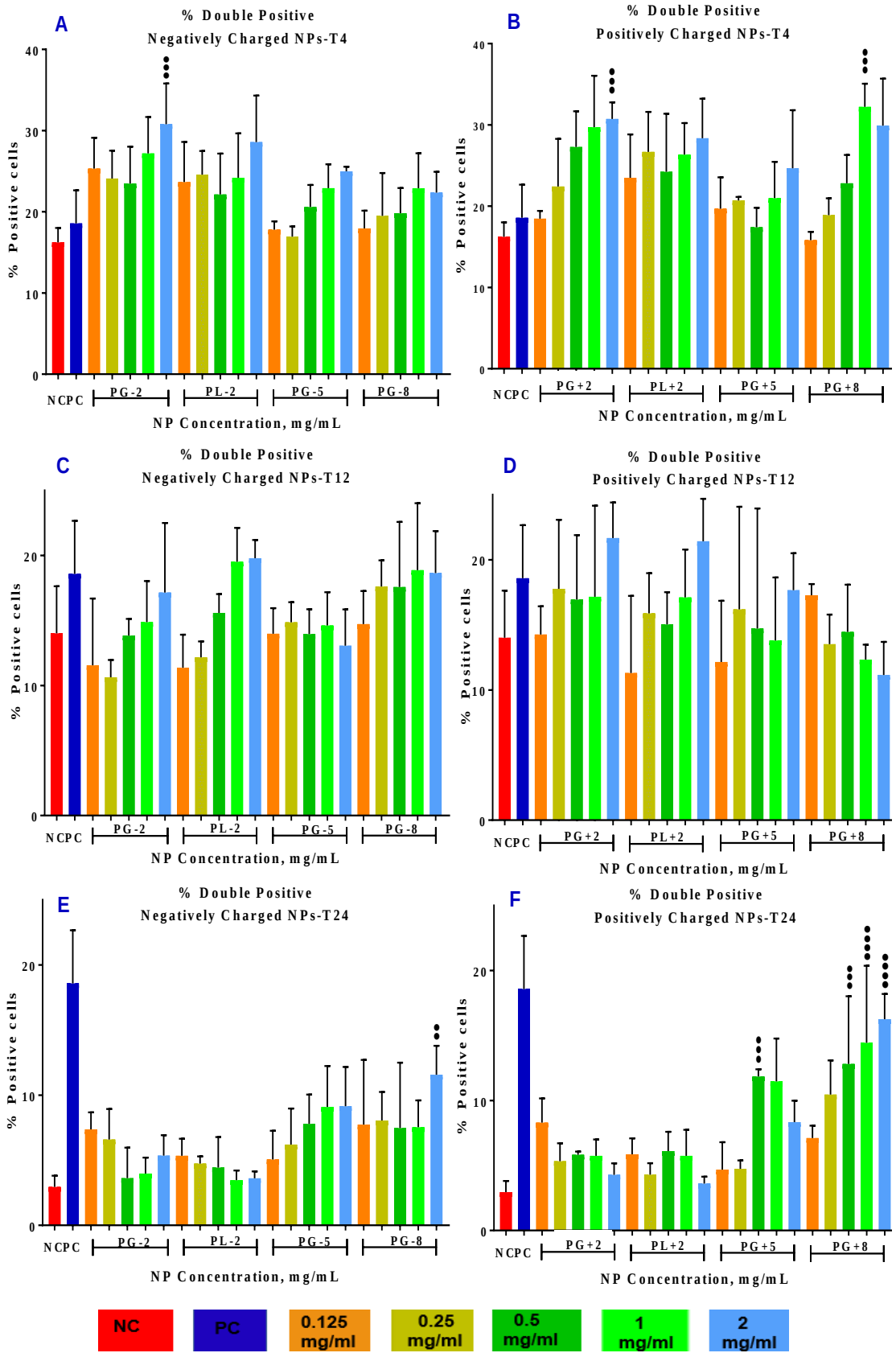

Figure. 3.12. Double positive cells for Annexin V and 7-AAD: (A & B) At T4, (B & C) at T12, and (E & F) at T24 (Results expressed as Mean ± SD, for statistical symbols and *P*-value please refer to section. 2.3.4).

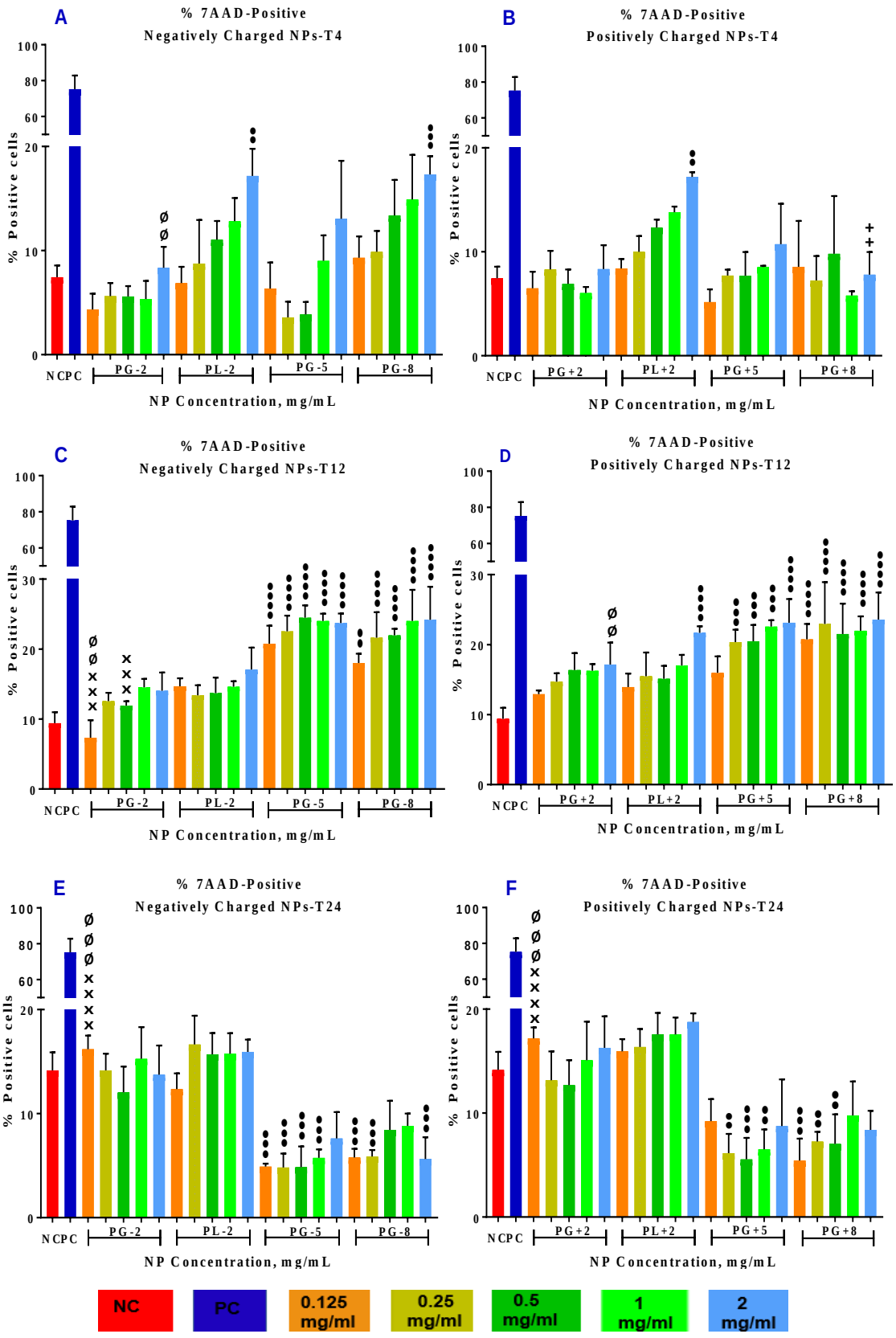

Figure. 3.13. 7-AAD positive cells: (A & B) at T1, (C & D) at T12, and (E & F) at T24 (Results expressed as Mean ± SD, for statistical symbols and *P*-value please refer to section. 2.3.4).

and 2 mg/mL, *PG*+5/ 0.25-1 mg/mL, *PG*+8 at 0.125-0.5 mg/mL. *PG*-2 showed a significant difference from *PG*-5 and *PG*-8 at 0.125 mg/mL. *PG*+2 showed a significant difference from *PG*+5 and *PG*+8 at 0.125 mg/mL. There were no statistical differences between the other NPs and to their NC.

3.4.7. Caspases Quantification Assay:

Caspases 3/7, 8 and 9 quantification was evaluated in Calu-3 cells after 24 hr exposure to NPs (0.125, 0.5, and 2mg/mL) (Figure. 3.14). Caspase 8 (Figure. 3.14. C & D) was the highest induced caspase followed by caspase 3/7 (Figure. 3.14. A & B) and then caspase 9 (Figure. 3.14. E & F).

Caspase 3/7: All NPs (Figure. 3.14. A & B) showed a biphasic trend of caspases 3/7 induction: At low concentrations (0.125 and 0.5 mg/mL) a trend of increasing the concentration was associated with increasing caspases 3/7 induction, while the highest concertation 2mg/mL showed a decrease. Negatively charged NPs (Figure. 3.14. A) showed statistical differences from the NC at *PG*-2/ 0.5 mg/mL, *PL*-2/ 0.5 mg/mL, *PG*-5/ 0.125 and 0.5 mg/mL, and *PG*-8/ 0.125 and 0.5 mg/mL. *PG*-2 was similar to *PL*-2 with no statistical difference. *PG*-2 was lower than *PG*-5 and *PG*-8 at all concentrations. *PG*-5/ 2 mg/mL was significantly lower than *PG*-8.

Positively charged NPs (Figure. 3.14. B) showed statistical differences from NC at *PG*+2/ 0.5 mg/mL, *PL*+2/ 0.5 mg/mL, *PG*+5/ 0.125-2 mg/mL), and *PG*+8/ 0.125-0.5 mg/mL). *PG*+2 was similar to *PL*+2 with no statistical difference. *PG*+2 was significantly lower than *PG*+5 at all concentrations and *PG*+8/ 0.125 mg/mL. *PG*+5 was significantly lower than *PG*+8/ 0.5-2 mg/mL. *PG*+2, *PL*+2, *PG*+5, and *PG*+8 was significantly higher from *PG*-2, *PL*-2, *PG*-5, and *PG*-8 at 2mg/mL.

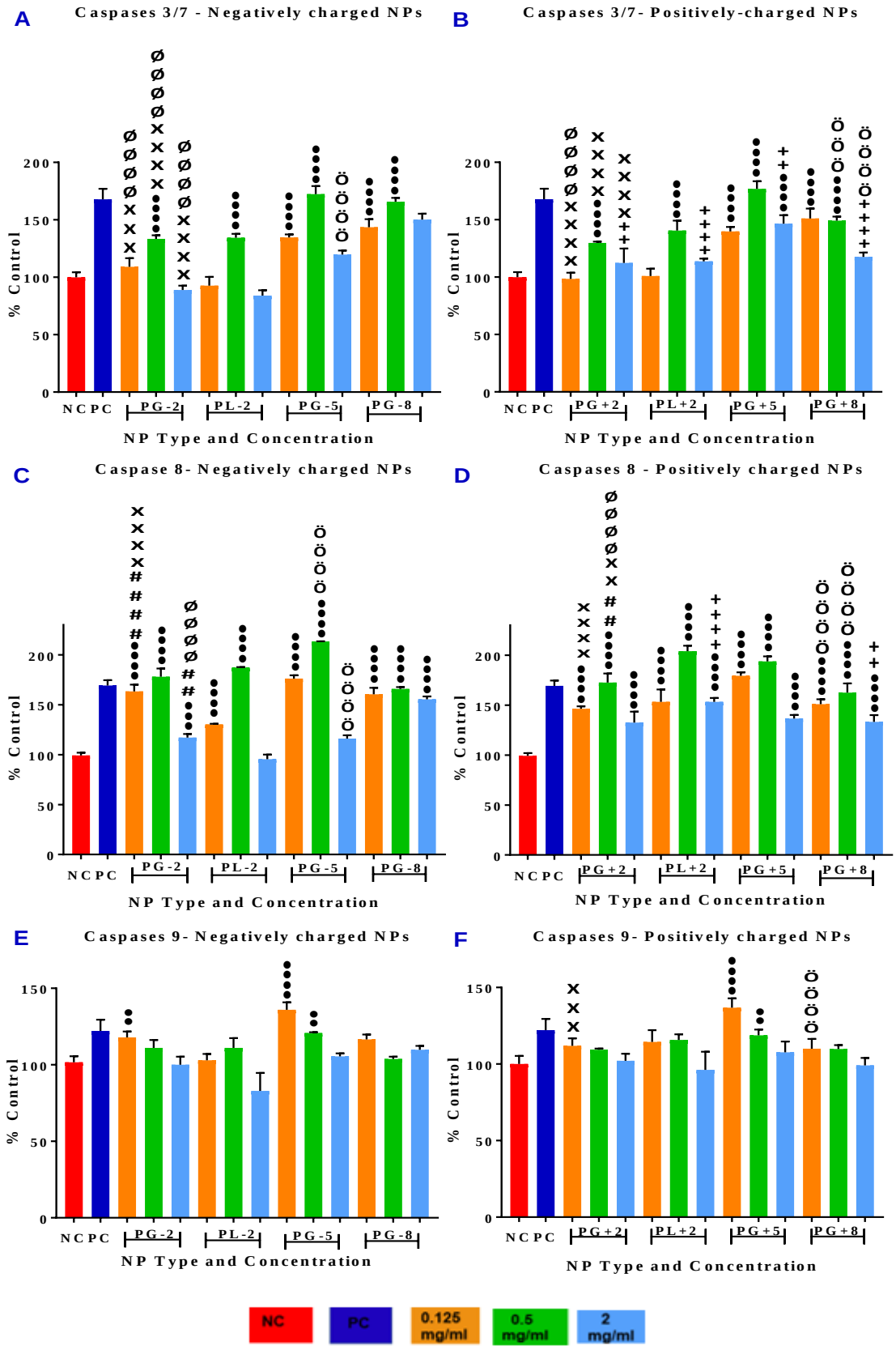

Figure. 3.14. Caspases quantification: (A & B) Caspases 3/7, (C & D) Caspase 8, (E & F) Caspase 9 (Results expressed as Mean ± SD, for statistical symbols and *P*-value please refer to section. 2.3.4).

Caspase 8: All NPs (Figure. 3.14. C & D) showed a similar trend of a biphasic response. Negatively charged NPs (Figure. 3.14. C) showed statistical differences from the NC at *PG*-2 at all concentrations, *PL*-2/ 0.125-0.5 mg/mL, *PG*-5/ 0.125-0.5 mg/mL, and *PG*-8 at all concentrations. *PG*-2 showed a significant higher caspase 8 induction compared to *PL*-2 at 0.125 and 2 mg/mL. *PG*-2 showed a significant less caspase 8 induction compared to *PG*-5/ 0.125 mg/mL, and to *PG*-8/ 2 mg/mL. *PG*-5 had a significantly higher caspase 8 induction compared to *PG*-8 at 0.5 mg/mL with lower significant induction at 2 mg/mL.

While positively charged NPs (Figure. 3.14. D) showed similar trend and were statistically different from NC for all NPs at all concentrations. *PG*+2 showed a significant lower caspase 8 induction compared to *PL*+2/ 0.5 mg/mL, and to *PG*+5/ 0.125-0.5 mg/mL. *PG*+2 showed a significantly higher caspase 8 induction compared to *PG*+8/ 0.5 mg/mL. *PG*+5 showed a significantly higher caspase 8 induction compared to *PG*+8/ 0.5-1 mg/mL. *PL*+2 showed a significantly higher caspase 8 induction compared to *PL*-2/ 2 mg/mL. *PG*+8 showed a significant lower caspase 8 induction compared to *PG*-8/ 2 mg/mL.

Caspase 9: All NPs (Figure. 3.14. E & F) showed a concentration-dependent decrease that was significant from the NC at *PG*-2, *PG*-5, and *PG*+5, all at 0.125 mg/mL. *PG*+2 showed a significant less caspase 9 induction compared to *PG*+5/ 0.125 mg/mL. *PG*+5 showed a significant higher caspase 9 induction compared to *PG*+8/ 0.125 mg/mL. The reduction of the caspases productions at high concentration could be correlated to the cytotoxicity.

3.4.8. Inflammatory Response:

3.4.8.1. IL-8 Detection ELISA Kit:

All NPs (0.125-2 mg/mL) did not cause any significant rise of IL-8 after Calu-3 cells exposure for 24 hr (Figure. 3.15. A & B). All *PG* NPs showed similar results to *PL* NPs with no statistical differences. To exclude any bacterial contamination to NPs that might be causing a rise in IL-8 production for THP-1 cell line exposure, NPs at concentrations 0.125 and 0.25 mg/mL were centrifuged and the supernatant (NPs free) used as treatments for THP-1 using the same protocol (Figure. 3.15. C), and non-significant rise in IL-8 was observed.

Upon THP-1 exposure to NPs, (Figure. 3.16. A & B) NPs showed a size, charge, and chemistry dependent differences. *PL*-2 showed a significant rise at 0.125-0.25 mg/mL, followed by a non-significant decrease of IL-8 production. *PG*-5 and *PG*-8 showed a highly significant rise of IL-8 compared to the NC with a concentration-dependent decrease. However, *PG*+2 showed a non-significant rise of IL-8 followed by a decrease. *PL*+2 showed a significant rise at 0.125-0.25 mg/mL, followed by a non-significant decrease of IL-8 production. *PG*+5 and *PG*+8 showed a highly significant rise of IL-8 compared to the NC with a concentration-dependent decrease. The negatively charged NPs didn't show any significant difference to their positive counterparts at the same correspondent concentrations. *PG*-5, *PG*+5, *PG*-8, and *PG*+8 showed a significantly higher IL-8 rise compared to *PG*-2 and *PG*+2 respectively.

To investigate if the IL-8 decrease with increasing the NP concentration was due to cell reduction or a possible adsorption to NPs surface, a viability assay by AB was performed (Figure. 3.16. C & D). This indicated that *PL*-2 and *PL*+2 had the highest viability, followed by *PG*-2, *PG*-5, and *PG*-8. *PG*+2, *PG*+5, and *PG*+8 showed the

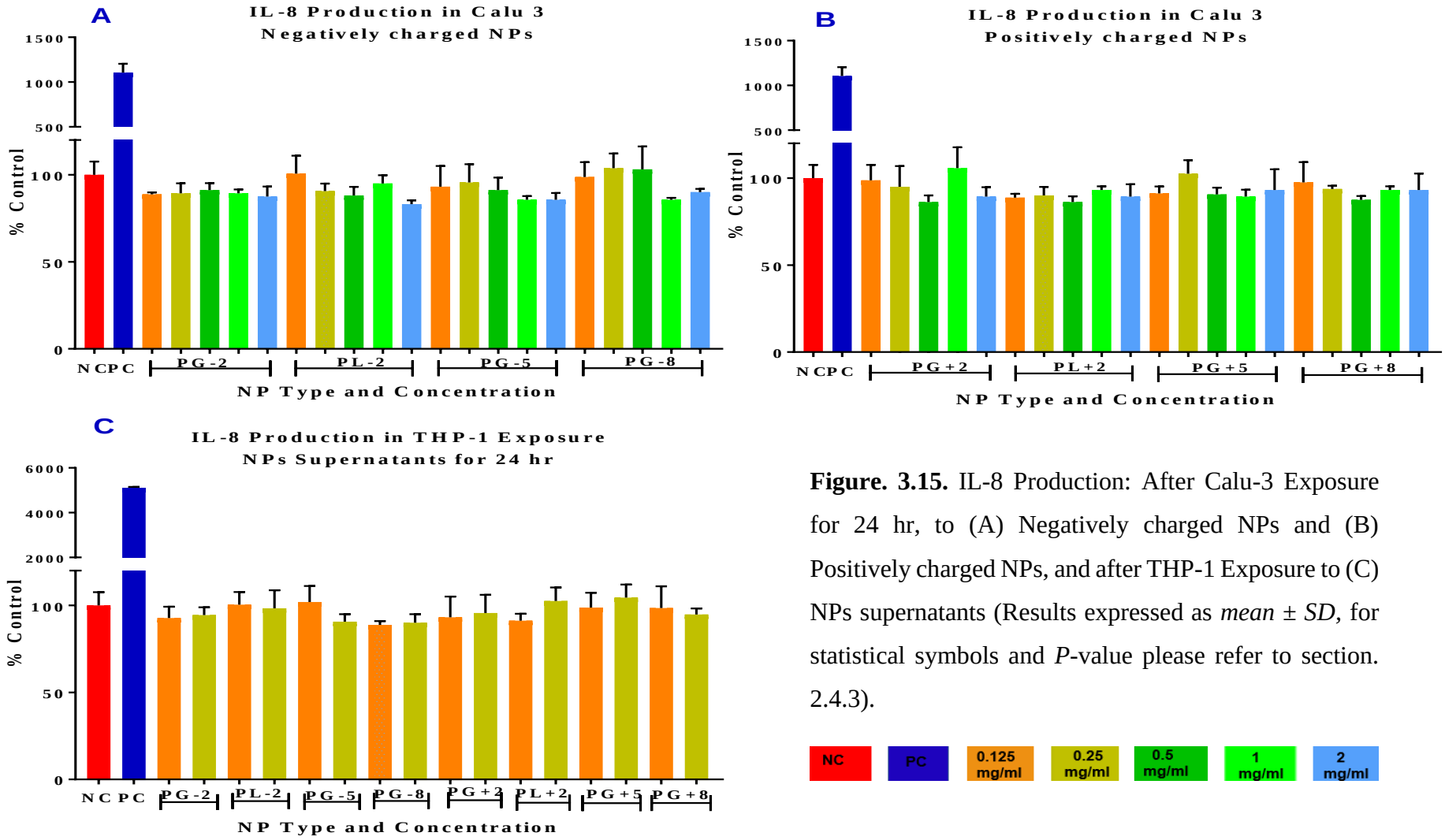

Figure. 3.15. IL-8 Production: After Calu-3 Exposure for 24 hr, to (A) Negatively charged NPs and (B) Positively charged NPs, and after THP-1 Exposure to (C) NPs supernatants (Results expressed as *mean* ± *SD*, for statistical symbols and *P*-value please refer to section. 2.4.3).

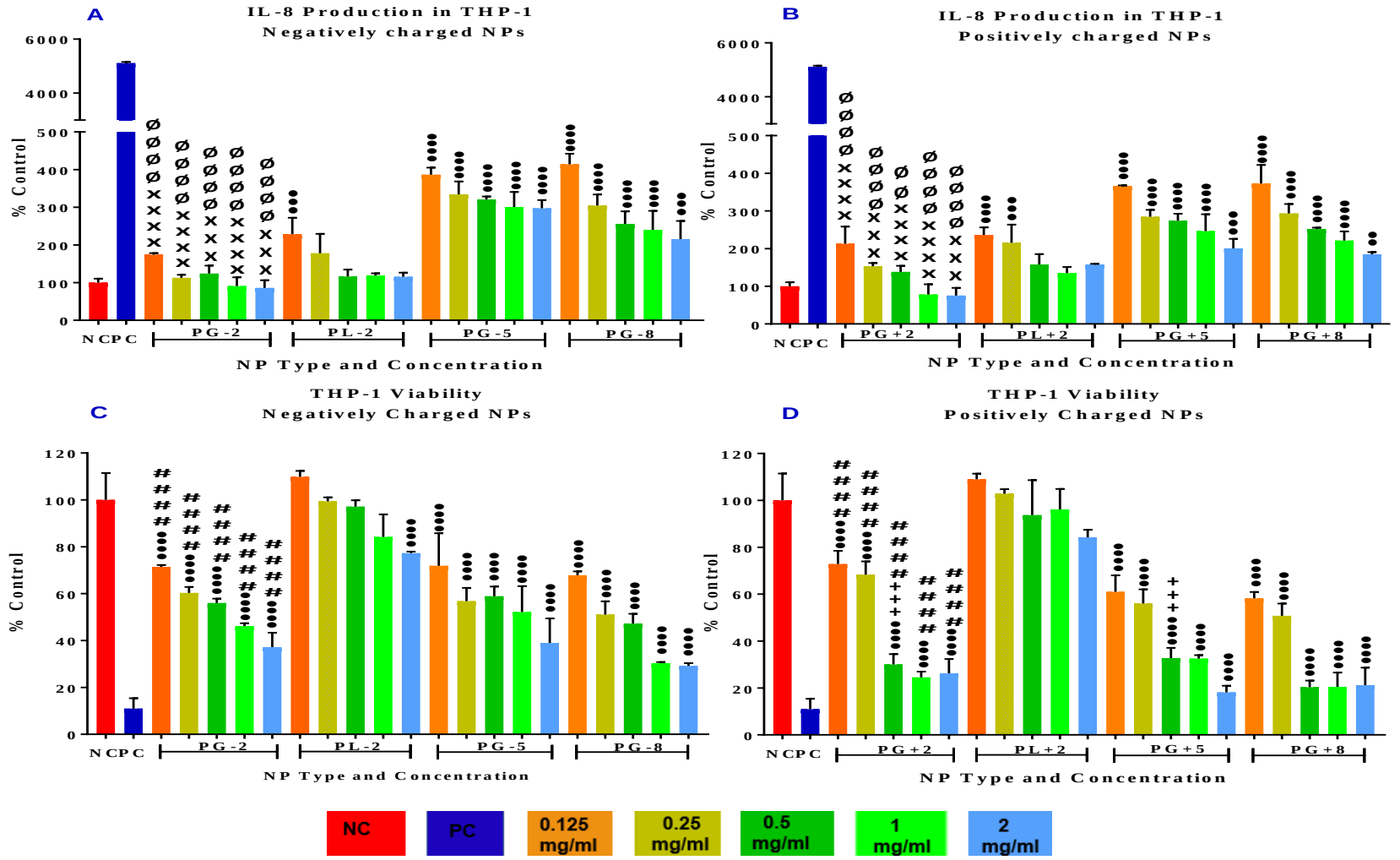

Figure. 3.16. IL-8 Release after THP-1 Exposure for 24 hr, to (A) Negatively charged and (B) Positively charged NPs, (C, D) Corresponding Viability of THP-1 estimated by Alamar Blue assay(Results expressed as Mean ± SD, for statistical symbols and *P*-value please refer to section. 2.3.4).

highest viability at the lowest concentrations of 0.125 mg/mL (denoting their higher toxicity to differentiated THP-1 macrophages). Hence, this concentration (0.125 mg/mL) was selected to further investigate the inflammatory response using CBA kit.

3.4.8.2. Cytokines Beads Array (CBA):

To further investigate the cytokines release, CBA was used to screen multiple cytokines in the same sample. NPs at concentration of 0.125 mg/mL was evaluated as the highest viability of THP-1 cells was achieved at this concentration after 24 hr exposure. The cytokines screened were IL-2, IL-4, IL-6, IL-10, TNF-α, IFN-ɣ, and IL-17a. Only IL-6, IL-10, TNF-α, IFN-ɣ (Figure. 3.17. A, B, C, D respectively) increased to significant levels compared to the NC.

IL-6 (Figure. 3.17. A) showed a significant rise to NC for *PG*+2, *PL*+2, *PG*-5, *PG*-8, *PG*+5, and *PG*+8 NPs. *PL*+2 was statistically higher than *PL*-2. There were no statistical differences between the other NPs.

IL-10 (Figure. 3.17. B) showed a significant rise to NC only for smallest NPs; *PG*-2, *PL*-2, *PG*+2, and *PL*+2 NPs. *PG*-2 was higher and statistically different to *PG*-5 and *PG*-8. *PL*+2 was higher and statistically different to *PL*-2. *PG*+8 was higher and statistically different to *PG*-8. There were no statistical differences between the other NPs.

TNF-α (Figure. 3.17. C) showed a highly significant rise to NC for larger NP; *PG*-5, *PG*-8, *PG*+5, and *PG*+8 NPs. *PG*-2 was lower and statistically different to *PG*-5 and *PG*-8. *PG*+2 was lower and statistically different to *PG*-8. There were no statistical differences between the other NPs.

IFN-ɣ (Figure. 3.17. D) showed a significant rise to NC for small NPs; *PG*-2, *PL*-2, *PG*+2, and *PL*+2 NPs and a significant downregulation to NC for larger NPs;

PG-5, *PG*-8, *PG*+5, *PG*+8. *PG*-2 was higher and statistically different to *PG*-5 and *PG*-8. *PG*+2 was higher and statistically different to *PG*+5 and *PG*+8. There were no statistical differences between the other NPs.

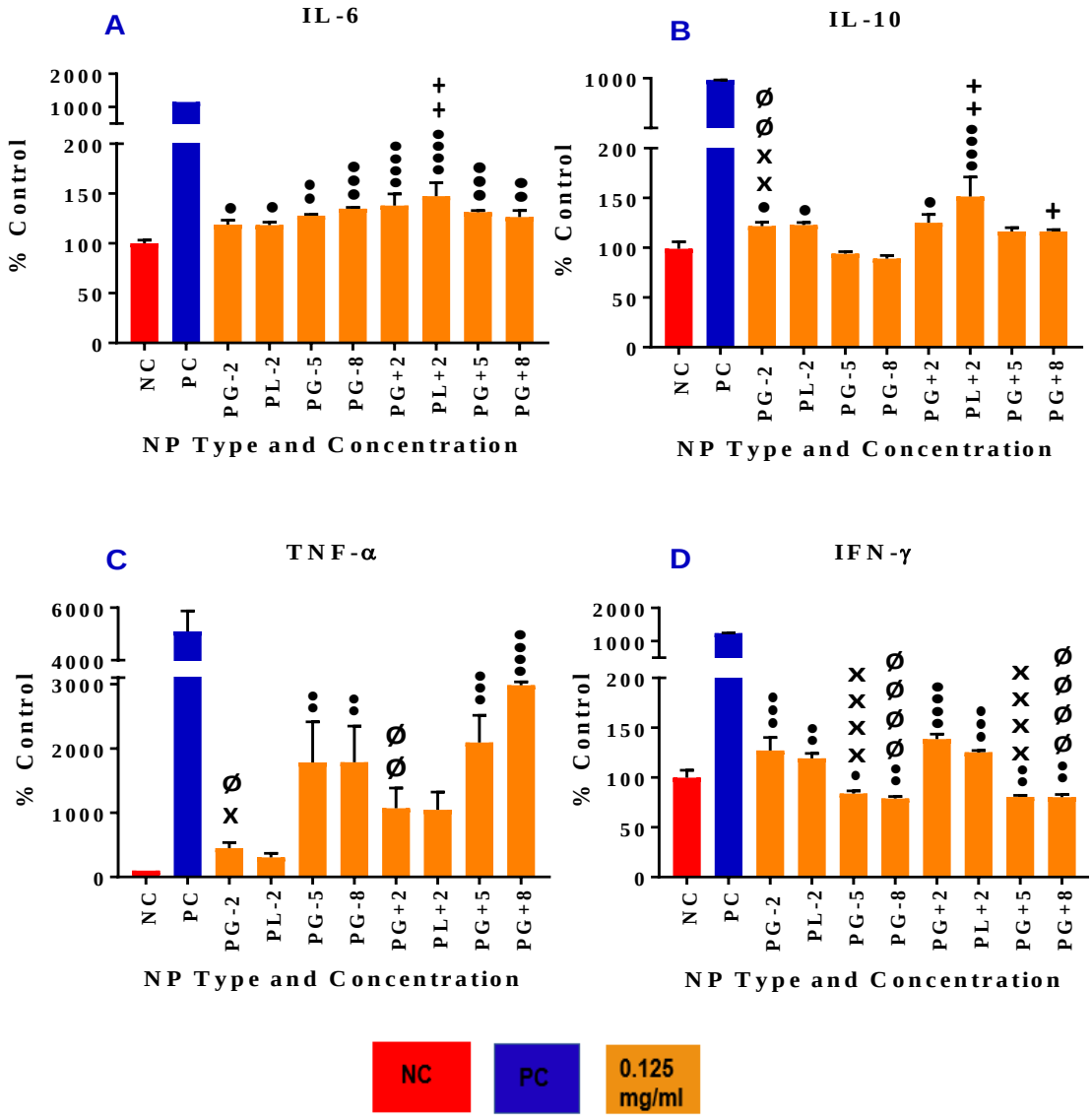

Figure. 3.17. Cytokines release after THP-1 Exposure to NPs (0.125 mg/mL) for 24 hr, (A) IL-6, (B) IL-10, (C) TNF-α, and (D) INF-ɣ (Results expressed as Mean ± SD, for statistical symbols and *P*-value please refer to section. 2.3.4).

3.4.9. Comet Assay:

Comet assay results are shown in Figure. 3.18. (A & B) representing head DNA %, (C & D) representing Tail DNA %, and (E & F) representing Olive Tail Momentum.

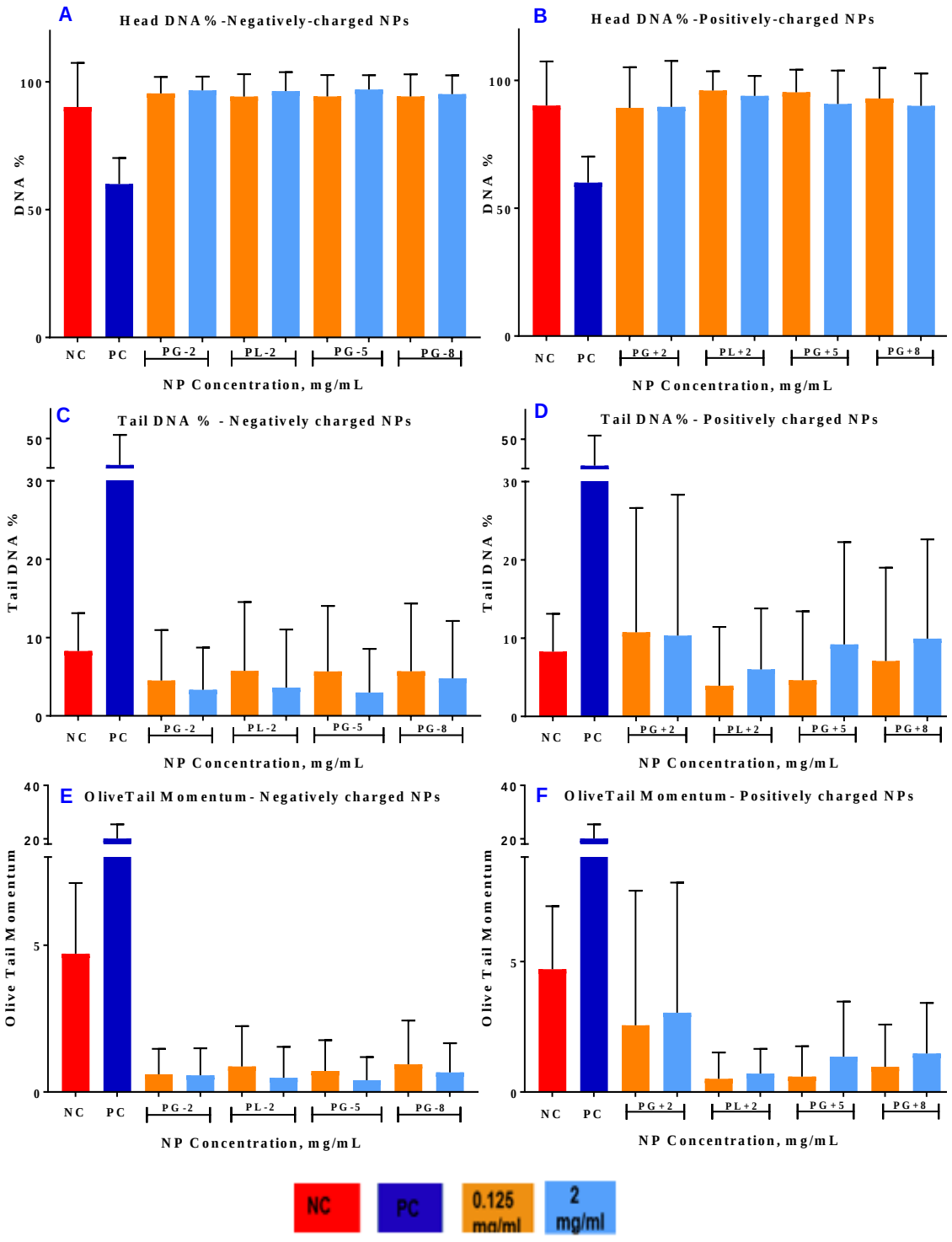

Figure. 3.18. Comet assay: DNA%:(A) Negatively charged NPs, and (B) Positively charged NPs, Tail DNA%:(C) Negatively charged NPs, and (D) Positively charged, Olive Tail Momentum:(E) Negatively charged NPs, and (F) Positively charge (Results expressed as Mean ± SD, for statistical symbols and *P*-value please refer to section. 2.3.4).

All different NPs exposure for 24 hr treatments didn't show any significant DNA damage compared to the NC (the bigger the DNA tail area, the longer the tail, the smaller the DNA head area, the more significant is the DNA damage). Hence there was no genotoxicity such as single or double strands break when evaluated by Comet assay alkaline gel electrophoresis. Significant DNA damage was only observed in PC (100 µM H_2O_2 for 30 mins).

3.5. Discussion:

3.5.1. Alamar Blue Assay:

Cell cytotoxicity was assessed by AB viability assay. AB is a redox indicator of the general metabolic cellular function and is widely used for evaluating cellular viability after NPs exposure (395). Cell viability after NP exposure was evaluated at T1 after discontinuing the NP exposure (application of 3 washes or No wash) to evaluate the metabolic state immediately after NPs removal, while the viability was evaluated at T2 and T3 to indicate the ability of cell recovery. The outcomes can be noted in the following:

The effect of chemistry: *PL* and *PG* NPs of the same size and surface charge had shown differences in their cytotoxicity and recovery. At low concentrations (< 0.5 mg/mL), both NPs showed no statistical difference of the cellular viability denoting their biocompatibility at these low concentrations over time. While high concentrations (1-2 mg/mL), showed more cytotoxicity of *PG* compared to *PL* NPs over time. This indicated the cellular tolerability of the low concentrations with slightly better biocompatibility of *PL* NPs at higher concentrations. This could be due to faster *PL* NPs degradation compared to *PG* NPs as concluded from Chapter.2 results. The ability of the cellular recovery (back to NC), the *PL* NPs showed almost 90-100% similarity

to NC after 3 hr at all concentrations while *PG* NPs at low concentrations were similar to *PL* NPs but at high concentrations staggered around 75-80% of NC. This represented either slower recovery at high *PL* NP concentrations or irreversible cellular insult with a loss of cellular function compared to NC.

The effect of size: *PG* NPs of 200 nm of the same surface charge showed lower cell viability to their larger size NPs of 500 and 800 nm at lower concentrations, while at high concentrations they showed higher viability. This can be explained by the size, surface area, mass, and NPs number relationship. For the same mass, decreasing the NP size is associated with increasing the surface area (more reactivity), and the number of NPs (396). Hence, for the same concentration of the 200 nm size NPs, there is larger surface area and higher number of NPs available for cellular interaction than 500 nm and 800 nm. Consequently, this indicated lower NP number was delivered to the cells in case of *PG*-5, *PG*+5, *PG*-8, and *PG*+8 compared to *PG*-2 and *PG*+2. In addition, at high concentration, higher cytotoxicity with the larger NPs can be explained by higher mass delivered per NP which induced higher toxicity and slower degradation for the larger size. In addition, as concluded from Chapter.2 experiment of size changes in culture media, the agglomeration and size changes were slight with *PG*-2 and *PG*+2 in comparison to the larger sizes NPs, which can result in better uptake for the smaller size (397). The ability of the cellular recovery showed the larger sized NPs, at the lower concentrations had higher viability than the smaller size and even higher than the NC at T3 indicated their limited uptake. While the high concentrations (of all *PG* NPs) staggered between 50-80% of the NC that denoted irreversible cellular injury.

The effect of surface charge: The negatively charged NPs (with PVA, more hydrophilic) showed higher cytotoxicity to their positively charged (with DOTAP, more hydrophobic) counterparts. Based on Chapter.2 experiment of size changes in

culture media, size and zeta potentials changes of positively charged NPs showed a huge size increase and charge conversion to negativity after dispersion in media compared to their negative counterparts. This implied larger size for the positively charged NPs that denoted their lower uptake.

However, many studies have indicated conflicting results regarding the effect of NP charge on cellular interactions. Cationic NPs show more electrostatic interaction with the negatively charged cell membranes hence more cytotoxicity while the anionic NPs show repulsion from the negatively charged membranes (398). However, there are many examples showing more cytotoxicity with anionic NPs compared to cationic NPs (251, 344, 399). That's due to the interplay of the different surface coatings with different hydrophobicity and agglomeration behaviour rendering each NPs with unique physicochemical properties affecting their cellular interactions outcomes (251, 344, 399).

The trend over time and cellular recovery. All NPs concentrations showed improved viability over time (up to T3). At the lowest concentrations (0.125-0.25 mg/mL), cell viability had resumed to 100% or more from the NC, indicating the ability of the cells to recover and the cellular injuries were reversable. The increase above the 100% of NC is associated with the hyperactive state of the cells that were under stress compared to untreated cells (400). At high concentrations, small NPs of *PG* and *PL* were recovered to 80-100% while the larger sized NPs staggered at 50-75% denoting a serious and irreversible cellular injury. This was similar to what was previously reported for cellular haemostasis in response to different cell injuries (400); where mild to moderate cell injury, the cell survives by upregulating protective mechanisms to maintain its survival. However, in severe cell injury, the cells activate stress signalling

pathways trying to survive but failure to handle the stress, drives the cell into cell death either through apoptosis or necrosis (401).

The experimental technical difference (3 washes and no wash): The application of 3 wash steps to remove the NPs prior to adding the reagent provided better results with smaller error bars, better viability and recovery. This was due to the efficient removal of NPs from the media, and avoidance of NPs interference with the AB reagent ensuring the measured endpoint was due to genuine NPs effects on the cells. However, the no wash experiments showed a decreasing viability trend with increasing NP concentrations, but the viability percentages were always lower than the experiments with 3 washes, denoting a false higher cytotoxicity. This indicated the importance of optimizing the *in vitro* experiments when it comes to NPs testing.

The current findings are in a good agreement with has been previously published in the literature for *PG* and *PL* NPs. A study by Kunda *et al.,* (38) investigated *PG* NPs (~200 nm size, negatively charged with PVA) and their viability after 4 hr NP exposure in JAWS II DCs to concentrations up to 1.25 mg/mL evaluated by MTT assay (2 hr). There was a decreasing trend of viability with increasing the NPs concentration reaching ~ 55% at 1.25 mg/mL. However, this could denote a higher cytotoxicity at the high concentration and of shorter duration of NP exposure compared to the current study findings. Kunda *et al.* demonstrated the use of MTT assay with addition of the reagent onto the cells without prior removal of the content or applying any washes, as well as the different cell line; DCs. This can be compared to the no-wash experiments at T2 where a higher cytotoxicity encountered due to inefficient removal of NPs from the extracellular environment and possible NP interactions.

Another study by Mohamed *et al.,* (79) investigated *PG* NPs of ~245 nm size, negatively and positively charged (PVA or DOTAP (15% w/w)) and their viability after 18 hr NP exposure in A549 lung cell line to concentrations up to 1.25 mg/mL evaluated by MTT assay (2 hr). There was a decreasing trend of viability with increasing NPs concentration reaching ~ 65% for positively charged *PG* NPs (more cytotoxic) while it was ~ 80% for negatively charged *PG* NPs at 1.25 mg/mL. That was contradictory to the current study findings which could be due to the use of A549 cell lines rather than Calu-3 and the higher concentration of DOTAP used by Mohamed *et al.,* (15% w/w) compared to 10% (w/w) was used in this current study that increased their cytotoxicity.

There are many reports that showed the negatively charged NPs had higher cytotoxicity compared to the positively charged NPs. Mura *et al.,* (251) showed *PL*/PVA, *PL*/CS, *PL*/PF68 (~230 nm) viability on Calu-3 cell lines, with concentrations up to 5 mg/mL after 4, 24, and 72 hr exposure, and showed well tolerated cell compatibility. However, the negatively charged *PL*/PVA and *PL*/PF68 demonstrated higher cytotoxicity to *PL*/CS that was similar to current findings where the negatively charged NPs were more cytotoxic (251). The authors reported quantifying the internalisation of NPs to confirm the *PL*/PF68 had higher internalization to the other NPs. Similar findings were reported in two studies by Grabowski *et al.,* (264, 384) who investigated *PL* NPs ~230 nm up to 3.5 mg/mL concentration and negatively-charged with pluronic® F68 (*PL*/PF68) had shown more cytotoxicity than the neutral *PL*/PVA NPs and positively charged *PL* coated with chitosan (*PL*/CS) after 48 hrs exposure using MTT assay (2 hr) in A549 and THP-1 cell lines, which was in agreement to the study findings. However, the viability percentages were higher than the correspondent T2 interval which could be due to the use of MTT assay, CM and difference in cell lines.

There have been many studies reported in literature which explored larger sized NPs for *PL* for comparison to *PG* NPs of 500 nm and 800 nm size. A study by Xiong *et al.*, (397) investigated cytotoxicity of *PL* NPs of different sizes (60, 100, and 200 nm, concentrations: 10 to 100 μg/ml) on RAW264.7 and BEAS-2B after 24 hr exposure. The results indicated the smaller the size of NP the higher the cytotoxicity. This was due to increasing the surface area, NPs number, and reactivity with lowering the NPs size, which is of relevance to findings in this study (396).

Similar findings were reported for *PG* NPs by Kunda *et al.*, (81) who evaluated *PG* NPs (~ 235 nm and positively charged with cationic surfactant didodecyl dimethyl ammonium bromide (DMAB)) cytotoxicity in A549 by MTT assay after 24 hr exposure up to 0.32 mg/mL. There was increasing cytotoxicity with higher concentration reaching 50% with 0.156 mg/mL for *PG* NPs of 200 size evaluated after 2 hr incubation with MTT. *PG* NPs viability can be correlated to T2 with no wash and was showing higher cytotoxicity compared to *PG*+2 that can be due to the use of DMAB coating rather than DOTAP for *PG*+2 NPs (396).

Another study of *PL* NPs of different sizes was reported by Roces *et al*., (402) (~200 nm, 450 nm, 1 μm sizes) prepared from different monomeric ratio of *PL* polymer (50:50, 75:25, 85:15) loaded with a model antigen (H56 TB vaccine) and the viability analysed by CellTitre Blue® assay on THP-1, RAW264.7, and MH-S (alveolar macrophages) cell lines at concentrations of 0.1-0.2 mg/mL for 24 hr exposure. This can be compared to *PG* NPs of 200 nm, 500 nm, and 800 nm where at these very low concentrations the larger NPs and MPs showed slightly higher viability than the smaller NPs. A study by Gratton et al., (403) investigated the internalisation of different sizes (~ 100 nm up to 10 μm) of NPs and MPs of non-spherical shape and their uptake into Caco-2 cells. NPs showed a 2.5 folds higher internalisation than 1μm and 6 folds higher

than 10 μm size. Hence this demonstrated smaller particles have higher uptake and hence show higher cytotoxicity.

3.5.2. Reactive Oxygen Species (ROS) Detection Assay:

H_2DCFDA Assay: ROS detected after 24 hr exposure of Calu-3 cells to NPs was evaluated via H_2DCFDA. There was direct correlation of ROS production with increasing NPs concentration. At low concentrations (< 0.5 mg/mL), ROS production was not associated with low viability (as detected by AB) indicating the cellular ability to combat oxidative stress by effective antioxidants (404, 405). However, at high concentrations (1-2 mg/mL), ROS production was associated with cytotoxicity which indicated the induction of oxidative stress had a significant involvement of cytotoxicity and cell death after NPs exposure (406). This agreed with previously reported literature for the cellular haemostasis after excessive ROS production (405, 406). In addition, mild to moderate ROS production can be tolerated with efficient antioxidant mechanisms or cell death via apoptosis. However, high ROS production inhibits the apoptosis and cell death via necrosis (243, 407, 408).

This assay is indicative for ROS production but doesn't indicate the cause or the sources of increased intracellular ROS (409). ROS are produced by many intracellular sources due to their immense roles in cellular signalling and regulatory pathways (405) such as membranous ROS (produced by (NADPH) oxidases (NOXes)), mitochondrial ROS (produced via aerobic respiration and electron chain), cytosolic ROS (produced via xanthine oxidases), peroxisomes and endoplasmic ROS (via to their oxidases, primarily H_2O_2) (404, 405, 407). Mitochondria are the main producers of ROS due to their involvement in aerobic oxidation and electron chain with primarily $O_2^{\bullet-}$ radicals that are dismutated by SOD dismutase to H_2O_2 that are further decomposed to O_2 and H_2O via antioxidants such GSH (410, 411). Thus, increasing ROS production could be

due to NPs intracellular hydrolytic degradation leading to further oxidation of the degraded products by Krebs cycle (more mitochondrial ROS production) (64, 65), or increased molecular interactions, or decreasing the antioxidant mechanisms or all together (222, 407, 412).

The effect of chemistry; *PG vs PL* NPs where all NPs showed similar increase in ROS production denoting similarity in their intracellular metabolic pathways that would generate ROS.

The effect of size; smaller NPs (*PG*-2 and *PG*+2) showed higher ROS production at low concentrations (< 0.5 mg/mL) than larger sized NPs. This implied the limited uptake of these large size NPs. However, at high concentrations (1-2 mg/mL), larger sized NPs showed higher ROS production than the smaller sized NPs. This symbolised larger doses being delivered intracellularly (413), and the larger NPs showed enhanced toxicity that could be related to their slower degradation. Similarly, *PG*-5 and *PG*+5 showed lower ROS production to *PG*-8 and *PG*+8.

The effect of surface charge; all negatively charged NPs showed similar ROS production levels to their positively charged NPs. However, there are limited reports evaluating polymeric NPs ability of ROS production or evaluating it at very low concentrations that rarely induce any significant high ROS levels.

A study by Singh and Ramarao, (414) investigated eight different polyester based NPs which were negatively charged by PVA; (i) *PL* NPs of different underlying monomeric ratio (50:50, 65:35, 75:25, 85:15) with a size range of ~ 234 - 295 nm, (ii) DL-*PL*A (~ 288 nm), (iii) poly-ε-caprolactone (PCL, ~ 360 nm), (iv) poly(lactide-co-caprolactone (*PL*CL, of different monomeric ratio; 25:75 and 80:20 and size range ~ 228 - 241 nm). NPs (suspended in CM) were tested for ROS induction by DCFDA for

24 hr exposure in RAW 246.7 cells to concentrations up to 1 mg/mL. Increasing the concentrations (0.1-0.3 mg/mL) showed an increase of ROS production that was highly significant at 0.3 mg/mL at ~ 1.5 – 2.5 folds greater than NC. This can be related to 0.125 and 0.25 mg/mL for the small NPs (~ 200 nm) in the current study findings. However, Singh and Ramarao reported the increase of concentration to 1 mg/mL showed less ROS production which was explained by a quenching effect at this high concentration, that was contradictory to our findings. The procedure used by Singh and Ramarao was after 24 hr exposure of macrophages to different NPs, this was followed by 5 washes of PBS prior to incubating the cells with DCFDA reagent (50 μM) for 30 min.

Singh and Ramarao had stated the corresponding viability of cells at the high concentrations; ~80% at 0.3 mg/mL while it was ~50-60% at 1 mg/mL. Their procedure might induce an artefact by losing cells at high concentration with ~ 50% viability, where the cells were damaged and liable to detach easily. This indicated lower number of viable cells were able to uptake the DCFDA dye and produce any signals, and the 30 min dye incubation, could be of a very short duration for these cells to uptake enough dye. However, treating the cells with DCFDA dye prior incubating them with NPs, ensured enough dye delivered, equal uptake, and equal cell viability. The cell (RAW 246.7), and cellular density ($1x\ 10^5$) reported in their study was different to our study where Calu-3 used at a higher density (4×10^4).

A study by Stevanović *et al.*, (412) *PL* NPs (~270 nm, negatively charged with PVA) was reported not to generate ROS at very low concentrations up to 66.5 μg/mL in He*PG*2 cell lines for 5 hr (412) which indicated the very low concentration didn't induce any ROS. The concentrations were very low to induce any ROS or cell death. The ROS production after NPs exposure could be considered as a toxic effect as well

as employed for therapeutic purposes. The ROS produced can be enhanced as synergistic ROS inducer as a cytotoxicity mechanism for cancer therapeutics (222, 415-417). However, to exclude any toxic effect for lung drug delivery, these experimental doses are very high compared to realistic dose distribution over the large surface area of lungs (~ 80-140 m^2 surface area) that denoted a very low induction of ROS. The ROS reported in this current study were after 24 hr exposure to high doses of NPs which are not expected to be seen in a realistic lung exposure denoting their safety.

Cellular ROS (Deep Red) Assay (ab186029): Deep Red assay was used to evaluate ROS production ($O_2^{\bullet-}$and $OH^{\bullet-}$ radicals) after Calu-3 cells exposure to NPs for 24 hr, and showed non-significant differences between all different types of NPs and almost a concentration-independent response. ROS detected was similar at low concentrations (< 0.5 mg/mL) while the viability was near NC, however, at highest concentration, where viability was reduced, ROS showed similar levels to the low concentrations. That was contradictory to what was seen with H_2DCFDA assay.

The experimental technical difference (3 washes and no wash): In the no-wash experiments, there was a significant concentration dependent decrease of ROS production, and with statistically significant lower values to 3 washes-experimental procedures denoting a strong possibility of NPs interference with this assay. Therefore, precautions are needed to exclude any NP interference with the assays. It is recommended when it comes to NPs testing, to choose multiple assays to ensure the accuracy of the measured endpoints (11, 166, 418, 419)

Comparing the Deep Red (3 wash steps) to H_2DCFDA assay results showed that there were lower values and almost a concentration independent for all NPs, except at 2 mg/ mL of larger size NPs: *PG*-5, *PG*+5, *PG*-8, and *PG*+8, which had a higher

ROS induction. This might be due to the sensor of Deep Red assays measuring mainly $O_2^{\bullet-}$and $OH^{\bullet-}$ radicals, whereas the H_2DCFDA assay is a more general indicator for reactive species including both oxygen and nitrogen species (420-422). Moreover, $O_2^{\bullet-}$ is known to be rapidly reduced to H_2O_2 by superoxide dismutase (SOD)(400, 405, 416) which may explain the cellular ability of $O_2^{\bullet-}$ clean-up in the low concentrations and all small NPs compared to impaired clean-up and accumulation at the highest concentration of larger sized NPs. To the best of our knowledge, there was no study for polymeric NPs that had used Deep Red assay.

3.5.3. Mitochondrial Membrane Potential (JC-1):

ΔΨm of Calu-3 cells after 24 hr exposure to NPs was evaluated by JC1 dye, which is a cationic fluorescent probe of ΔΨm. This ratiometric dye indicates lowering/ loss of ΔΨm by a decrease in the red/green ratio (J-aggregates/monomers ratio; healthy/non healthy ratio) due to the spectral shift of fluorescence that is potential-sensitive (423). Lowering ΔΨm implied impairment of the mitochondrial membrane polarized state and permeability that might adversely affect the cellular haemostasis and is considered as a sign of apoptosis (408, 424).

JC1 dye is a slow cationic potentiometric/ratiometric dye (600 Da) that gives an indication of the ΔΨm (423, 425). The dye resides in the mitochondria in the intermembranous space and respond to changes in ΔΨm and membrane permeability in a slow manner that allows it to track slow or steady changes in ΔΨm and hence, render it unsuitable to measure fast changes. Other examples are rhodamine 123, safranin O, JC-9, and $DiOC_6$. Consequently, in this study the cells were incubated with the JC1 dye prior to NPs treatments for 24 hr.

ΔΨm is an electrical potential of mitochondrial membranes generated by the electron transfer chain complexes that generate a proton gradient of hydrogen ions by the charge separation (chemiosmosis: electrons trapped inside mitochondrial matrix and protons pumped outside the inner mitochondrial membrane generating negative ΔΨm and alkaline pH) (426, 427). ΔΨm is essential for energy production via oxidative phosphorylation to produce ATP (ATP synthase) and maintenance of mitochondrial haemostasis (importing and exporting essential molecules and ions required for normal function as well as mitochondrial regeneration) (426, 428). Besides the proton pumps, ΔΨm is maintained by tight control of the mitochondrial membrane permeability via highly regulated pores most importantly, mitochondrial permeability transition pore (mPTP) (429-431). Hence, lowering ΔΨm (depolarized state) is due to the loss of control on mitochondrial membrane permeability and opening mPTPs (404, 408, 432).

mPTPs are large channel proteins at the inner mitochondrial membrane that are stimulated to increase the membrane permeability to molecules with MW ~ 1.5 KDa and a size ~3 nm (427, 428). Consequently, the mitochondrial membranes lose the ability to maintain the proton gradient with a drop in ΔΨm and failure to produce ATP. This further leads to a loss of metabolic gradients with molecules and ions released into the cytoplasm (a release of Ca^{2+}, mitochondrial key proteins such as proapoptotic proteins, i.e., cytochrome c, Smac/ Diablo, and HtrA2/Omi) resulting in osmotic swelling, rupture, and ultimately cell death ensues either through apoptosis or necrosis. Circumstances that have been shown to induce mPTPs openings include Ca^{2+} ions overload, elevated ROS, ATP depletion, inorganic phosphates, cellular acidosis (233, 426-428).

All NPs showed a significant decrease of ΔΨm that could be mirrored with the increased ROS production (H_2DCFDA assay) and decreased viability (T1 with 3

washes; was measured after 1 hr from discontinuing the NPs exposure following 24 hr incubation) and can be noted as following:

The effect of chemistry; *PG vs PL* NPs where *PG* NPs showed higher ΔΨm than *PL* NPs denoting that *PG* NPs were less impairing ΔΨm than *PL* NPs. *PL* NPs showed higher viability and similar ROS production but a higher mitochondrial impairment in comparison to *PG* NPs. This can be correlated to the faster degradation and acidic pH changes encountered with *PL* NPs than the slowly degrading *PG* NPs and their alkaline pH changes (as concluded from Chapter.2 results).

The effect of size; smaller NPs (*PG*-2 and *PG*+2) showed less impaired ΔΨm at low concentrations (< 0.5 mg/mL) than larger sized NPs. While at high concentrations, they were similar with low ΔΨm. This indicated less impaired ΔΨm for the smaller NPs than their larger sized NPs which could be due to their faster degradation (349, 433).

The effect of surface charge; positively charged NPs showed less impaired ratio to their negative counterparts at low concentrations (mostly at 0.125 mg/mL). This could be associated to the higher viability encountered with the positively charged NPs than negatively charged NPs by AB assay. Furthermore, this can be correlated to the large size differences as well as the neutralization or conversion to negative charge after dispersion in the medium leading to limited cell uptake (as concluded from Chapter.2 results) (332).

Many therapeutic approaches have been reported for *PL* NPs based on the ability to interact and co-localise with the mitochondria. For example, *PL* NPs (~ 200 nm and negatively charged) ability to localise in mitochondria (visual confirmation by microscopy) and successful delivery of cyclosporine A as a cardioprotective agent

against reperfusion injury in cardiomyocytes as a model of myocardial infarction and as inhibitor of mPTP (oxidative stress induced by H_2O_2) *in vitro* (433-435). In addition, *PL* NPs have been used for NP mediated therapies for mitochondrial knockout approach as anticancer therapies (436-439) or reducing the oxidative stress for many aging and mitochondrial based diseases (437, 440). However, in the study by Singh and Ramarao (414), the authors reported ΔΨm assessed by rhodamine 123 and safranin O uptake assays. The authors investigated a very low concentration (0.3 mg/mL) of the eight NPs after 24 hr exposure in RAW 264.7 cell lines. The assay was performed post-exposure to NPs and after 30 min incubation with the reagents. The rhodamine assay showed no effect on ΔΨm compared to the NC, while safranin O showed a significant low ΔΨm with two NPs only (*PL*CL 25:75 and *PL*CL 80:20). This indicated the difference and sensitivity of the assays had a major impact on the results. In the current study, ΔΨm was evaluated with the use of JC1 assay that was reported to be a very sensitive assay to evaluate ΔΨm and cells were treated with JC1 dye prior to NPs exposure (376, 441). As previously mentioned, rhodamine 123, safranin O, and JC1 are slow cationic dye not be suitable for fast change measurements of ΔΨm that can give underestimated measurements (423).

The time course of AB assay indicated the low concentrations (< 0.5 mg/mL) were reversable after discontinuation of NP exposure while the high concentrations (1-2 mg/mL) were associated with irreversible reduction of viability. This denoted similar effects on ΔΨm would be expected where reversible changes allow the mitochondria to regenerate and resume its functions. A study by Fan *et al.*, (442), demonstrated *in vitro* induction of ROS and oxidative stress in C_2C_{12} mouse myocytes (rich in mitochondria) with increasing concentrations of H_2O_2 (250, 1000, 2000 μM H_2O_2) for 5 hr followed by 24 and 48 hr recovery. Post-exposure, ΔΨm showed a reduction of 40% from its

NC, with low cytotoxicity for 250 μM H_2O_2. In addition, CLSM imaging showed a significant mitochondrial impairment manifested by increased fragmentation with all treatments after 5 hr, that was mainly reversable to a more healthier network morphology after 24 and 48 hr with only 250 μM H_2O_2.

3.5.4. Cell Membrane Integrity (LDH):

LDH is an intracellular enzyme found in the cytoplasm and mitochondria and catalysing anaerobic glycolysis (pyruvate oxidation to lactate that is more favoured in cancer cell lines even in presence of oxygen; 'Warburg effect'). LDH release is indicative for cytotoxicity, loss of membrane integrity, and cell death via necrosis.

LDH Total: LDH Total is the total content of LDH in all cells. So, an increase or a decrease of viable cell number would have a huge effect on the measurements and reading (443). Hence, this assay can be correlated to the AB viability assay. There was a concentration dependent decrease of the total LDH content that was dependent on NPs physicochemical characters as following:

The effect of chemistry: *PG vs PL* NPs. *PG*-2 NP were similar to *PL*-2 at low concentrations while at high concentration *PG*-2 NPs were showing lower content of LDH Total. However, *PG*+2 was slightly less than *PL*+2 but non significantly different. This can be due to the faster degradation of *PL* NPs than *PG* NPs. This can be correlated to their viability assessed by AB and showing similar effects.

The effect of size: at low concentration, *PG*-2 showed a higher content of LDH compared to *PG*-5 and *PG*-8. While the *PG*+2 showed similar LDH Total to the larger NPs. This confirmed the positively charged NPs behaved in a similar way due to their larger size encountered after dispersion as concluded from Chapter.2 results.

The effect of surface charge: there was a clear difference in LDH Total based on NPs charge that was mainly apparent at higher concentrations. Here, negatively charged NPs showed decrease of LDH Total compared to the positively charged counterparts. This can be explained due to the positively charged NPs showing a stronger adsorption to extracellular proteins that limited their uptake while the electrostatic repulsion between the negatively charged NPs and the negatively polarized cell membrane induced cell membrane damage (330, 344, 444, 445). This was similar to the AB viability where the positively charged NPs showed higher underlying viability to the negatively charged NPs.

LDH Release: using LDH Release method, the assay indicated the loss of membrane integrity with the leakage of key cytosolic markers (443). The results were different to those obtained with LDH Total. All NPs exposures showed a concentration dependent increase in LDH Release in supernatants that was significantly very low to NC spontaneous LDH Release. The increase of the LDH Release was associated with the decrease of the Total LDH that correlated with the cytotoxicity at higher concentration as evaluated with AB viability.

Regarding the NPs physicochemical characters dependency, noted as following:

The effect of chemistry: *PG vs PL* NPs. There was more association of LDH Release to the surface charge than the chemistry. *PG*-2 NPs was less than *PL*-2 NPs however, the *PG*+2 showed more release compared to *PL*+2 NPs. This can be correlated to their underlying viability.

The effect of size: the larger sized NPs showed a higher release of LDH than the smaller NPs indicating their higher cytotoxicity was associated with membrane damage.

The effect of surface charge: the positively charged NPs showed higher release than their negatively charged NPs. This can be correlated to the higher LDH content that indicated a higher underlaying viability as assessed by LDH Total and AB assays respectively.

Comparing LDH Total to LDH Release: the LDH Release showed lower amounts in comparisons to the highly significant LDH Total decrease at the same concentrations denoting:

(i) a strong possibility of NPs adsorption effect: Here the LDH Total decrease signified a high underlying cytotoxicity that was expected to increase the membrane leakage of LDH. However, the LDH release was not amounting to the NC that indicated a NP interference. The LDH as a cellular protein can be subject to adsorption to the surface of the NPs (as the measurements evaluated the supernatants where the NPs were located) that limits its detection.

In a study where *PL* NPs of ~ 60 nm, 100 nm, 200 nm were incubated with BSA protein as a model protein to uncover the adsorption properties, the NPs showed an increase in the protein adsorption with the smaller larger surface area NPs (397). As *PG* NPs belong to the same α-polyester family, it is feasible this can happen too. Another study where *PL*/PVA, *PL*/CS, *PL*/PF68 had shown LDH Release that was low compared to the NC on A549 cells after 24 hr exposure to concentrations up to 4 mg/mL (384). These results are similar to the current study of LDH Release assay that indicated a possibility of NPs interference.

(ii) and /or the underlying cytotoxicity with down expression/inhibition of the cellular activity and certain cellular proteins is associated with a decrease of total LDH and is a sign of late apoptosis (secondary necrotic cell death) (401).

This agreed with previous findings in which the reduced Total LDH was associated with cells undergoing apoptosis, and the increase of the ROS production, increase mitochondrial membrane permeability (Ca^{2+} release, cytochrome c release (subsequent activation of caspase-9 then caspase-3)), with a decrease of the $\Delta\Psi m$ (446).

LDH release cannot differentiate between a primary necrosis (acute accidental cell death) and secondary necrosis (late apoptotic/necroptotic) (447). Hence it is important to differentiate between apoptosis and necrosis, preferably in a time coarse manner as well as quantification of caspases. These were evaluated in the subsequent experiments. Experimental designs that neglect the possibility of NPs adsorption, might perceive similar LDH Release results as no effect on the cell membrane integrity had been caused, and was possibly masked by the adsorption to NPs surface. Based on these results, the ability of measuring cellular markers released in the supernatant containing NPs should carefully exclude the adsorption to NPs surface by evaluating the response of different methods prior to draw a conclusion.

When mirroring the results obtained by LDH Total (as a cytotoxicity assay) to AB viability (immediately after 24 hrs exposure: T1 with 3 washes), the ability of AB to measure the cellular recovery was advantageous. The AB uses a redox indicator that can be applied after removal of NPs from the surrounding medium and measuring cellular recovery. However, this recovery effect cannot be evaluated with the LDH Total where cell lysis step is used. Moreover, the evaluation of LDH either Total or Release had to be done from cell supernatants (where NPs were existing) that might increase NP interference.

LDH measurements had shown many cases of NPs interference that was previously reported, .e.g. by adsorption to CNTs when mixed with LDH standard (448), metallic NPs as Ag and Cu NPs (449) were proved to have dissolution and ions shedding deactivating the LDH, in the same study using a rat lung epithelial Type-I cell line R3/1, however, TiO2 NPs showed adsorption deactivation for LDH. Other reports of Au NPs (450) and platinum NPs (451) can independently oxidize the NADH causing false positive LDH release. Thus, NPs can show various protein interactions via adsorption or inactivation and its likely to be nonspecific and requires extra caution to interpret and validate assays using protein measurements (449, 452, 453). For this experiment, the kit lacks the LDH standard to perform a control experiment, however, using a controlled amount of cell lysate as a NC and as a standard to be mixed with serial concentrations of NPs to prove or exclude the adsorption effect can be done in future directives.

3.5.5. Apoptosis and Necrosis Assay:

Necrosis is unprogrammed passive cell death, which is initiated by sudden severe cellular insults such as heat stress, hypoxia, and extremely high concentrations of drugs. It is characterized by loss of membrane integrity, cell haemostasis and eventually osmotic swelling and cell lysis (454).

A time coarse study of apoptosis and necrosis was performed after 4 hr, 12 hr and 24 hr of Calu-3 exposure to NPs. Annexin-V/7-AAD staining assays are frequently employed using FACS analysis (455-458). FACS allows for cellular segregation based on their staining that facilitates the quadrant analysis of different cell populations in the same sample. However, live (double negative) and early apoptotic (Annexin-V positive only) quadrants were not shown as their trends and percentages of these cell populations were almost negligible over time. In contrast to the other quadrants, late apoptotic

(double positives) and necrotic (7-AAD positive only) indicated time related changes and can be noted as following:

Firstly, the trends over time: At T4: the late apoptotic populations were higher among smaller NPs than larger NPs and ranging from 20-35% of the total cell population, whereas the necrotic populations were mainly seen at higher concentrations and ranging from 10-20% of the total cell population.

At T12: there was a general decrease of the percentages of both quadrants, while late apoptotic population ranged between 10-20% of the total cell population that was similar to all NPs. The necrotic population showed an increase with larger NPs with population percentage ranging between 15-30% of the total cell population especially at the high concentrations.

At T24: there was further decrease of the percentages of both quadrants, while late apoptotic population ranged between 10-15% of the total cell population that was higher in larger than the smaller NPs. Although the necrotic population showed a similar or slight decrease in population percentage of smaller NPs ranging ~ 15% of the total cell population. The larger NPs showed a decrease of necrotic population percentage even less than the NC and ranging ~5%.

Secondly, the effects of physicochemical properties of NPs: There was a difference based mainly on the size of NPs rather than the chemistry and charge. This can be explained by the following reasons:

(i) FACS sample preparation required the removal of free NPs found in the supernatants, 3 washes, trypsinization, centrifugation, and decanting the supernatant prior to addition of staining mixture. While FACS analysis provides great technical advantages such as multiparametric analysis, its use

for NPs assays showed some problems such as interfering with the gating. In such assays requiring collecting, adding dye or dead cells detached in the supernatants, with washes to remove NPs, will inevitably result in a loss of these cells (459, 460).

(ii) FACS analysis had shown large error bars which resulted in non-significant statistical differences between all types of NPs. The issue with the FACS Sampling and detectors is the dependability on the gating strategy (or cell population selection) for subsequent analysis. This meant the gate had to be the same with each sample of cells, however cells are responding to different NPs concentrations and have different characteristics that makes the planned gate unsuitable for each individual sample and need to be adjusted accordingly that creates some variations (385).

(iii) Differences between *PL* and *PG* NPs were minimal indicating the size was a very critical factor for the cytotoxicity response. While all smaller NPs demonstrated earlier and higher peak of late apoptotic response at T4, the larger NPs showed a slow and sustained high late apoptotic response over the three time points. A higher induction of necrotic response detected at T12 with a drop at T24 indicated a huge loss of cell number after 12 hr of NPs exposure. This indicated the smaller NPs were taken up earlier and within 4 hr intervals they exerted cellular response, and within the next 12-24 hrs were decreasing to NC levels. However, larger size NPs were slowly up taken and exerting their maximum response in 12 hr interval, which dropped in the next 12 hr. This can be clearly seen with low concentrations.

(iv) The results of T24, when compared to AB viability and LDH Total and Release, the cytotoxicity seen was mainly due to apoptosis due to the high late

apoptotic populations in comparison to the necrotic population. This was confirmed with subsequent caspases quantification.

Thirdly, comparing these findings to the literature; Most of the available studies measured only one time point, commonly 24 hr, and either presenting their results in different ways such as presenting the quadrant graphs of FACS, or presenting one or more of the quadrants analysis as bar or line graphs depending on the study interest. However, some studies were suitable for comparison with the current study findings.

In a study by Grabowski *et al.,* (264) who investigated the effect of surface coating on apoptosis and necrosis induction (via FACS Annexin-V/7-AAD) by *PL* NPs on THP-1 cell lines. *PL* NPs of similar size and different surface charge *PL*/PF68, *PL*/PVA NPs, *PL*/CS as well as *PL* NPs-stabilizer free without any surfactants were used at 0.1 or 1 mg/mL concentrations for 24 hr. The authors' findings indicated the NPs with surface coating were all involved in inducing a necrotic response that was slightly higher than stabilizer free *PL* NPs and non-significant differences between the different NPs due to the large error bars. The differences here are related to use the NPs in CM rather than use of SFM that was proven in earlier chapter.2 to have an impact on the size of NPs, as well as THP-1 is a professional macrophage that can employ more phagocytic uptake than the epithelial Calu-3 cell lines. The authors had not detailed the FACS gating strategy used with referring to merely apoptosis and necrosis without clarifying what were the subpopulations.

Grabowski *et al.,* (399) further investigated the uptake and apoptosis and necrosis of the previous NPs (0.1 mg/mL for 24 hr) using FACS and an in-house developed coculture of A549 and THP-1 cell lines (CD14-PE labeling where A549

were negative while THP-1 were positive). The uptake of NPs was higher for THP-1 than A549 cells. There was more induction of necrosis (7-AAD positive only) in case of THP-1 than A549 cells, and more necrosis of *PL* NP stabilizer free than stabilized NPs.

However, the two studies showed ~ 10% necrotic population with very low apoptotic populations. Possible artefacts in the procedure followed by Grabowski *et al.*, (264, 399), (i) one wash step was employed, however a very low NPs concentration was used but the NPs require efficient removal from surface of monolayers with many washes required, (ii) staining of the cells prior to their trypsinization, that might induce loss of staining, especially Annexin-V, where it was surface attached and with trypsinization, erosion and loss of surface molecules on the outer membrane layer, are frequently reported (460-462). This might explain the persistent of 7-AAD (retained inside the cell) while lowering the Annexin-V staining (463, 464), and (iii) very late time point, 24 hr, in which usually the cells would show higher necrosis and earlier time points are recommended (465).

3.5.6. Caspases Quantification Assay:

Caspases are a group of enzymes that regulate cell survival. There are two subsets; initiators and executors (242). The initiators are caspase 8, 9, and 10 and they stimulate the activation of the executor caspases. The executors are caspase 3, 6, and 7 and they initiate cellular reactions to process the biochemical and morphological pathway of apoptosis such as vacuolation, DNA fragmentation and loss of cytoskeleton (401).

Apoptosis is a programmed cell death, and it is initiated either through extrinsic or intrinsic pathways (Figure. 3.19) (466). The extrinsic pathway initiated by external

stimuli mediated through cell membrane death receptors (DRs), and caspases dependent. The major signalling cascades are: (i) DRs signalling followed by activation of caspase 8 then executor caspases 3/7. According to Redza-Dutordoir & Averill-Bates, (467) "These receptors include Death receptor 1 (DR1) (also known as TNF-R1, CD120a, p55), DR2 (Fas, CD95 or Apo-1), DR3 (Apo-3, TRAMP, LARD or TNFRSF25 (TNF receptor superfamily 25)), DR4 (TNF related apoptosis-inducing ligand (TRAIL)-R1 or Apo-2), DR5 (TRAILR2 or TRICK2) and DR6 (TNF receptor superfamily member 21(TNFRSF21))". These receptors can be stimulated by TNF-α, ROS production, and FasL (454, 467).

(ii) DRs signalling and activation of caspase 8, followed by activation of domain death agonist (BID), impairment of mitochondrial outer membrane permeability (MOMP including mPTPs), then activation of caspases 9 and then executor caspases 3/7.

The intrinsic pathway initiated by internal stimuli such as ROS production, genotoxicity, and many metabolic disturbances that will affect the mitochondria (Figure. 3.19). This was mediated by Bcl-2, Bax and Bak proteins (468-470). MOMP is affected with the release of cytochrome c (a hallmark of mitochondrial mediated apoptosis) triggering activation of APAF-1 apoptosome that activates caspase 9 that will activate executor caspases 3/7 and apoptosis ensues.

From our results, induction of caspases was caspase 8 > caspases 3/7 > caspase 9. This denotes that extrinsic apoptosis pathway was mainly activated, and later followed by intrinsic pathway activation following the cellular exposure to NPs. NPs cytotoxicity was proved to be associated with high ROS production (as previously confirmed in section 3.5.2), that can provide the link for induction of extrinsic and

intrinsic of apoptosis pathways. However, other stimuli include TNF-α (was evaluated in subsequent inflammatory section 3.5.7), or over expression of Fas and FasL (can be evaluated in future directive studies) (243).

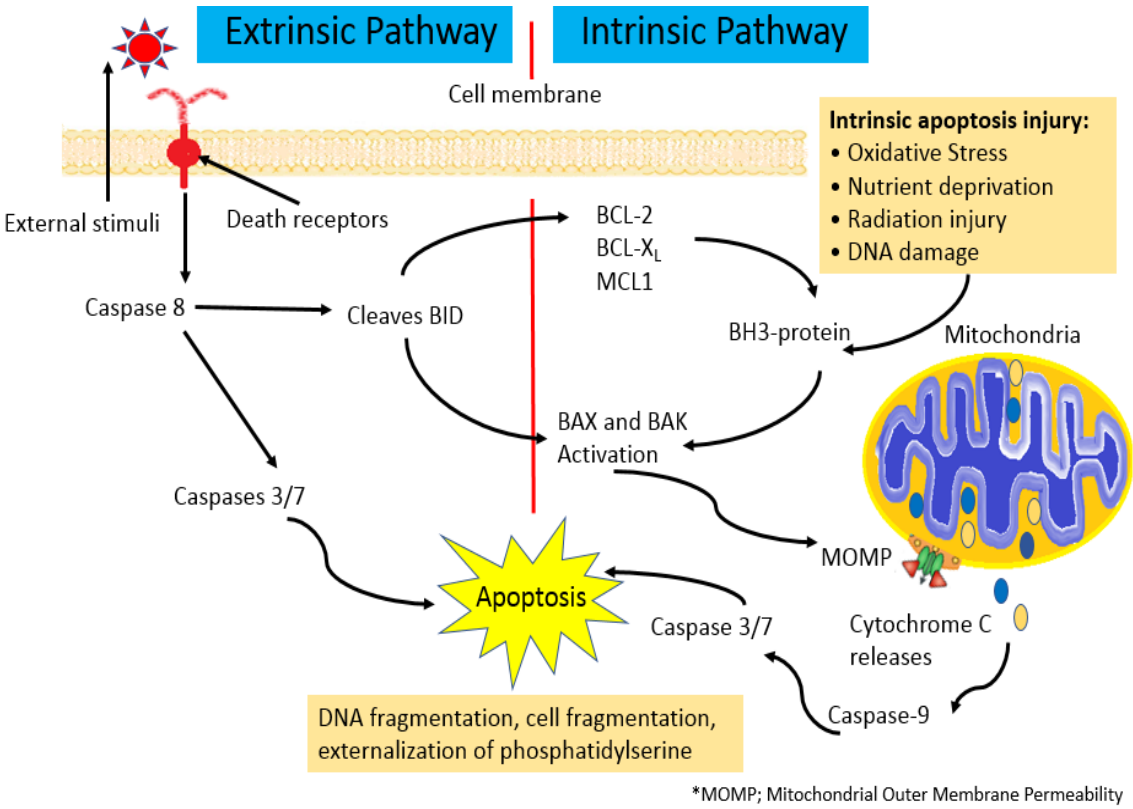

Figure. 3.19. Apoptosis signalling pathways.

The effect of chemistry: *PG vs PL* NPs. All NPs induced similar trends that can be related to their ROS production. **The effect of size:** Larger sized NPs induced higher caspases than smaller NPs. When correlated to their viability, the larger NPs showed higher viability at low concentrations that denoted limited uptake. However, at high concentrations there was higher cytotoxicity with higher ROS production. **The effect of surface charge:** The positively charged NPs showed a higher induction of caspases at all concentration compared to their negative counterparts NPs. This can be correlated to their high viability and ROS production.

The biphasic trend: The trend was increasing at low concentrations (0.125 and 0.5 mg/mL) and decreased at the highest concentrations (2 mg/mL). Such a decrease can be explained by:

(i) The correspondent high underlying cytotoxicity at the highest concentrations seen by AB, and associated with high ROS production and low ΔΨm

(ii) The decrease of caspases at highest concentrations could be correlated to the decrease of LDH Total and the increase of LDH release; indicative of late apoptosis or secondary necrotic cell death involvement (400).

(iii) Several lines of evidence confirming ROS role in regulating the caspases (404): Where mild to moderate ROS, can activate the apoptosis and caspases increase, while the very high ROS inhibit the caspases (471). In addition, ROS were reported to regulate FasL expression and subsequent activation of extrinsic pathway (472).

Caspases evaluation showed completely novel insights of induction of caspases and apoptosis pathways by *PG* NPs as well as *PL* NPs in Calu-3 cell lines. Most of studies in literature (as previously mentioned in the previous section) they evaluated the cell death either apoptosis or necrosis after exposure to drug free *PL* NPs, without further investigations of caspases involvement. This was usually due to the expensive nature of these assays that commonly employed for drug loaded NPs.

3.5.7. Inflammatory Response:

Calu-3 cells response: All NPs (0.125-2 mg/mL) did not induce IL-8 after Calu-3 cells exposure for 24 hr. This was similar to the findings of Mura et al. (251) where the study used *PL* NPs of ~200 nm size coated with PVA and Chitosan (CS) didn't induce any IL-8 or other cytokines (IL-6, TNF-α) up to 0.2 mg/mL for 24 hr

exposure on Calu-3 cell lines. All *PG* NPs of different sizes showed similar results to *PL* NPs and this is a novel observation. Calu-3 as a human *in vitro* model derived from lung adenocarcinoma can produce inflammatory mediators upon exposure to particulate matter to stimulate the inflammatory cells. It has been used in different studies to assess the airway epithelial inflammatory response (251, 473, 474) (475).

There are many studies reporting NPs adsorption to protein and cellular molecules with many examples of polymeric polyester NPs such as *PL* NPs that increased with decreasing the size and increasing surface area (334, 335, 337, 344, 397). IL-8 cytokines were released in the supernatants that contained the NPs where possibility of interaction and adsorption exist. However, the adsorption ability of these NPs to the IL-8 was not investigated in the current study and future investigation would be recommended.

The possibility of NPs contamination by LPS was excluded by investigating the supernatants of NPs and no IL-8 was induced. However, this method has been criticized by some researchers as the supernatants might be free from contamination while the NPs might be adsorbing the LPS into their surfaces (367). It is better to exclude the bacterial contamination by some commercial assays (Limulus Amebocyte Lysate (LAL) assay) or quantify the LPS contamination so it can be excluded. However, artefacts had been reported due to NPs interference with these assays (266, 267). Other suggestions of incubating the NPs with LPS inhibitor such as polymyxin B might reduce the LPS contamination but the risk of altering the NPs surface might interfere with the results (476). However, almost all glassware, reusable consumables, and lab equipment (as possible) were decontaminated with 70% ethanol prior to autoclave. The water was used from Milli Q dispenser and all cell culture consumables were

industrially sterilized and endotoxin free. These efforts kept the risk of contamination to the lowest possible.

THP-1 **Response: IL-8 and CBA:** CBA was chosen over ELISA for measuring the released cytokines (374, 381). ELISA allows one cytokine to be measured at a time, implementing higher cost for each cytokines, extensive Sampling and time-consuming procedures, requiring more sample volume to screen multiple cytokines that might limit its uses when multiple cytokines are needed (387, 389). CBA techniques facilitate the multiple detections of different cytokines in the same sample, requiring smaller volumes, using the flow cytometry analysis that facilitate faster, sensitive, and more efficient detections (389).

THP-1 macrophages are more professional inflammatory cell lines compared to Calu-3 cells. It gives vital insights for which cytokines of interest that can be secreted following an exposure and helps to determine them prior to screening upon *in-vivo* response (239). For the lungs, inflammatory responses are implicated in development of serious diseases as COPD, asthma, CF, and cancer (235). The tested concentration is far higher than the actual exposure *in-vivo* where these experimental doses are distributed over a large surface area over adult lungs (~70-140 m^2).

There are many other cytokines regulated and secreted by T cells. However, the study screened a representative group of cytokines. TNF-α is proinflammatory cytokine that increases the phagocytosis, has a well-known role in endotoxic shock (induction of fever, muscle fatigue, loss of appetite, increase C- reactive protein), Plays a role in programmed cell death, and metabolic disturbances in cancer cells (477). IL-6 is an important mediator of innate response; increases the acute phase inflammatory cytokines and stimulate B-lymphocytes. IL-10 has anti-inflammatory effect on B-cells

and macrophages and controlling the regulatory T cells that involved in controlling the inflammatory response and the tolerance reaction (478, 479). IL-2 and IL-4 induce proliferation and activation of both B and T cells (480). IFN-γ increases the macrophages activation (480). IL-17A has proinflammatory effect and neutrophil recruitment (481).

However, THP-1 exposure to NPs (0.125mg/mL) for 24 hr showed stimulation of IL-8 (earlier evaluated by ELISA Kit), IL-6, TNF-α, IFN-γ, and IL-10 while no effect on IL-17A, IL-2, and IL-4 that denoted a generation of proinflammatory reaction was dependent on NPs physicochemical properties as following:

The effect of chemistry: *PG vs PL* NPs: Both NPs induced similar inflammatory response of inducing IL-8, IL-6, IL-10, TNF-α, and IFN-ɣ. This indicated the size had more potent effect than the chemistry.

The effect of size: Larger NPs showed a higher induction of IL-8 and TNF-α, a lower induction of IL-10 and IFN-ɣ, and almost similar induction of IL-6 than smaller NPs. Similar findings were reported where ~400 nm *PL* NPs coated with PVA on murine macrophages induced significant high levels of TNF-α (477) after 4 hr incubation. This explained that the bigger the size of NPs are, the more the macrophages recognize and phagocytose the NPs (482).

The effect of surface charge: The positively charged NPs didn't show any difference in IL-8 induction to the negatively charged NPs, but showed slightly higher production in IL-6, IL-10, TNF-α, and IFN-ɣ. This denoted more interactions of the positively charged NPs with the THP-1 as noted from its AB results; the positively charged NPs were more cytotoxic on the macrophages than their negatively charged counterparts. Similar findings were reported by Grabowski *et al*., (264) for ~200 nm

PL/ PVA, *PL*/ PF68, *PL*/ CS, *PL*-stabilizer free using THP-1 cell lines that showed induction of IL-8, IL-6, TNF-α, but was at a high concentration (1 mg/mL). However, the authors used similar THP-1 cell density, but the procedure involved using 12 well plates and using 2 mL of NPs suspended in CM. The current study used 96 well plates with 200 µl volume of NPs suspended in SFM which meant the concentration of 0.125 mg/mL was a concentrated microenvironment compared to 12 well plates with lower number of NPs (less surface area for adsorption). Hence, the inflammatory induction emerged with IL-6, IL-8 and TNF-α at a lower concentration. Another study by Xiong *et al*., (397) where ~200 nm *PL*/PVA NPs showed non-significant increase of TNF-α release up to 0.3 mg/mL on murine macrophages RAW264.7 cell lines that was similar to the small NPs (*PG* and *PL*) findings of the current study. Furthermore, Guedj *et al.*, (483) investigated *PL*/ PVA NPs coated with and without BSA (~ 200 nm size) and showed no inflammatory induction using *ex-vivo* human neutrophil apoptosis assay. Moreover, they followed up the studies *in-vivo* murine air pouch acute inflammatory model where 0.1 mg/mL didn't induce any significant leucocytes lung infiltrations. Using the above studies as examples to prove the inflammatory response evaluation vary between different experimentation models according to the type of cell lines or models used and the cytokines measured. The *PG* NPs results here in comparison to *PL* NPs of the current study or previously published studies exhibited similar responses.

3.5.8. Comet Assay:

Genotoxicity assays can evaluate different mutagenicity or carcinogenicity endpoints, i.e., SD or DS DNA damage, mutations, micronuclei, chromosomal aberration, cell repair mechanism and cell cycle checkpoints. Many assays are available for *in vitro* as well as *in vivo* assessment of NP such as comet assay, micronucleus assay, chromosomal aberration, Ames test etc (367).

Genotoxicity potentials of NPs was evaluated by Comet assay alkaline gel electrophoresis. Comet assay is a reliable tool to detect genotoxicity of NPs as previously reported (230, 390, 392, 484). Comet assay can detect SS or DS DNA damage or oxidative lesions that could be repairable or irreversible. All different NPs exposure (two concentrations: 0.125 mg/mL (minimal toxicity effect) and 2 mg/mL (maximum toxicity observed)) for 24 hr didn't induce any genotoxicity in Calu-3 cells when evaluated by Comet assay alkaline gel electrophoresis.

The current findings for *PL* NPs are in agreement with the literature where *PL* NPs of different sizes, coated with different coatings, and tested in different cell lines (231, 232, 485) showed no genotoxicity potential evaluated by comet or micronucleus assays. However, there has not been any previous genotoxicity studies published for *PG* and *PL* NPs on Calu-3 and limited genotoxicity studies for *PL* NPs on other cell lines were reported.

PG NPs of different sizes showed no genotoxicity and were similar to *PL* NPs. A study by Tulinska *et al.,* (231) investigated two *PL* NPs functionalized with polyethylene oxide (size ~ 140 and 180 nm, a negatively charged) and showed no genotoxicity when evaluated in human blood cell model. There was no genotoxicity reported with no SS or DS or oxidative DNA lesions by comet assay as well as no increase of the micronucleated-binucleated cells by micronucleus assay after 24 hr exposure up to doses 3 $\mu g/cm^2$.

Another study where *PL* NPs of similar sizes (~ 80 nm) and different surface charges (negatively charged/ bare *PL*, neutrally charged/ PEG, and positively charged/ CTAB) were studied in three cell lines (16HBE14o-, mouse lymphoma L5178Y, and TK6 human B-lymphoblastoid cells) for their genotoxicity. All NPs didn't show any

genotoxicity by comet or micronucleus assay in these two cell lines: L5178Y and TK6 cells (24 hr exposure, up to 75 μg/cm^2). However, *PL* NPs functionalized with CTAB showed genotoxicity only on 16HBE14o- cells (increase the number of micronucleated cells) (230). All *PL* NPs had induced concentration dependent cytotoxicity associated with higher ROS production. This confirmed that not only the physicochemical properties of NPs Play a role in their NP-cellular interactions but also the cell lines show an effect on the outcomes of this interaction (231, 232). In addition, cancer cells are expected to be more susceptible to genotoxicity potentials of NPs due to their frequent divisions, impaired DNA repair mechanisms and with being more prone to accumulate DNA damage over time (486).

NPs are reported to cause DNA damage, but in a physicochemical dependent manner. For example, smaller NPs of ~10 nm can directly cross through the nuclear pores to the DNA while NPs size > 15 nm can bind to the DNA during the cell division where the nuclear envelop is dissolute (367, 487). These NPs cause DNA damage via strong adsorption to DNA bases or stands or via impairing the repair enzymes. For example, TiO_2 NPs (~ 20 nm) were reported to induce genotoxicity in lung cell lines (BEAS-2B and A549 cells) due to the impairment of DNA repair process. While larger sized NPs can cause DNA damage indirectly via other mechanisms such as oxidative stress, inflammation, and organelles damages. ROS are commonly encountered with genotoxicity of metallic NPs such as silver NPs (488) or gold NPs (489), and ZnO NPs (490). However, the exact mechanisms are yet under investigations.

3.6. Conclusion:

There is a fast-growing application and use of NPs in various scientific and non-scientific fields of life and the growing use of these NPs for medical purposes due to

their exceptional properties. The safety evaluation of these NPs remains as a corner stone for their faster widespread applications, however, it's a quite challenging and demanding. Given the exceptional physicochemical properties of NPs, the adoption of the classical/standard chemical safety assays can confound the nanotoxicological profiles of these NPs that has been proved with the current study requiring researchers to practise extra caution in validating and concluding the experimentation results. NPs had shown a size-dependent property interfering with the established *in vitro* assays. This requires a full characterization of NPs in the physiological media, and within the experimental environment with subsequent validation of the results by proper controls or the use of different methods to uncover toxicity endpoints by different mechanisms. An urgent need is to find a common ground for NPs testing standards agreed nationally and internationally between the scientific and industrial communities. Technological growth in developments of less NP-interference labile assays remains a must for the future.

4. *In vitro* Evaluation of Polymeric Nanoparticle Uptake and Intracellular Co-localisation using Calu-3 Cells

4.1. Introduction:

Due to the particulate nature and high MW, NPs uptake is most likely to be through endocytosis (173, 491-493). Endocytosis are different cellular uptake mechanisms with underlying variable molecular and structural basis, i.e., phagocytosis, micropinocytosis, and several receptor-mediated mechanisms (clathrin-dependent, caveolin-dependent, caveolin and clathrin-independent). All these mechanisms have a common feature of vesicular uptake with subcellular endolysosomal destination (169). However, non-vesicular or free cytosolic NPs have also been reported due to endolysosomal escape or other uncharacterized/non vesicular transport mechanisms that are yet to be explored (178, 494). Numerous studies have emphasized that the NPs characteristics, i.e., size (491, 495-498), shape (499-501), surface charge, chemistry and lipophilicity (502, 503), all play a critical role in the cellular uptake, subcellular interaction and trafficking from the site of entry to the distribution and localisation in target diseased cells (504). Understanding how these NPs are internalized is critical for subsequent modification of the physicochemical properties to optimize their drug delivery capabilities (494).

To determine and understand the mechanism of NPs internalisation, pharmacological inhibitors are used for certain processes using *in vitro* cell lines (159, 505). NPs are usually tagged with certain labels, i.e. fluorescent dyes, either chemically bound or physically loaded. Initially, internalisation is probed under cold temperature (4 ^{o}C) to exclude any passive transcytosis transport (159, 506). Then the internalisation is probed under physiologic temperature (37 ^{o} C) to exploit the active mechanisms requiring ATP (507). The experimental principal compares cell exposure under no inhibition to exposures under selective inhibitors to explore the affected/inhibited pathway (169, 506). This can be achieved by using different techniques, such as

fluorescence labelling of NPs that can be evaluated by spectrofluorimetric plate readers, flow cytometry or fluorescent microscopy (508, 509).

Fluorescence labelling is one of the commonly used strategies to study NPs uptake and internalisation. The NPs are labelled with certain fluorescent dyes (such as Nile Red, FITC, and BODIPY-FL) that allows to trace the NP cellular interaction and their intracellular fate by fluorescence detectors in microscopes, plate reader or flow cytometry (510). This strategy provides many advantages such as sensitivity, specificity, cost effective, feasibility and simplicity allowing the scanning of many NPs in a short time, as well as allowing multiple fluorophores labelling for evaluating multiple signals such as in co-localisation studies (511). This can be studied *in vitro* using multiwall plates to evaluate the transcellular transport (transcytosis transport including endocytosis, active transport, or passive diffusion), or re-structuring the epithelial barrier over Transwell permeable inserts to evaluate both; transcellular transport and paracellular passive transport, as well as evaluating the integrity of the barrier upon NP exposure (512). Paracellular passive transport describes the transport of molecules through the intercellular spaces where the rate of NPs permeability is controlled by the tight junctions (TJs).

TJs are complex groups of integral transmembrane proteins including claudins, occludins, and junctional adhesion molecules that attach with the corresponding proteins from the neighbouring cells on their lateral surfaces. These proteins are connected to peripheral membrane proteins such as zonula occludins (ZO-1, ZO-2, and ZO-3), which link transmembrane proteins to regulatory cytoskeleton proteins. TJs are at the apical part of the intercellular contact and regulate the paracellular permeability and the integrity of the epithelial barrier (513). TJs are highly selective and allow for water and solutes, such as Na^+ and Cl^- ions, exchange in the extracellular spaces (514).

Air-to-blood lung epithelium is the main rate-limiting factor for the transport of drugs and NPs, and its integrity is vital for successful inhalation delivery (276). Thus, restructuring the TJs in polarized monolayers provides invaluable information to study lung barrier integrity after NP exposure (276-278). Calu-3 cells is such an *in vitro* model of human lung bronchial adenocarcinoma derived to study lung barrier permeability (515). Calu-3 cells can develop polarized monolayers with strong TJs. To mimic *in vivo* lung epithelium, Calu-3 are grown on Transwell permeable inserts to confluence over two to three weeks under air-liquid interface (ALI) with basolateral cell feeding while the apical surface is exposed to air (276). Calu-3 under ALI showed differentiation to mimic primary airway epithelium (516).

Barrier integrity and tightness are evaluated by measuring the electrical resistance and/or determining the paracellular permeability of paracellular markers. Transepithelial electrical resistance (TEER) are usually measured by epithelial voltohmmeter to ensure the confluent monolayers developed tight polarized monolayers and post exposure to ensure the integrity of the barrier was maintained after NP exposure (517). Furthermore, the paracellular permeability can be determined by calculating the apparent permeability coefficient (P*app*) of paracellular markers or tracers to ensure the integrity was preserved throughout the duration of the experimental NP exposure (276, 278, 281, 518). Paracellular markers such as [^{14}C]-mannitol or sodium fluorescein, lucifer Yellow, are passively transported across TJs. These molecules are of small MW, hydrophilic, small size (514, 519) where TJs are impermeable to molecules with a diameter larger than 22-30 Å (Å or Angstrom is 0.1 nm) which effectively excludes all NPs above 1 nm size (512, 519, 520).

4.2. Aims:

To investigate *PGA-co-PDL* and *PLGA* NPs internalisation and mechanism of uptake in Calu-3 cell lines through the following objectives:

- To investigate the NPs effect on the integrity of the epithelial barriers through calculating the apparent permeability coefficient of [^{14}C]-mannitol as a paracellular marker after polarized Calu-3 cell exposure to NPs at different concentrations and time points,
- To determine the underlying mechanisms for NP uptake using different pharmacological inhibitors,
- To visually confirm the NPs internalisation and the subcellular co-localisation by confocal microscopy.

4.3. Materials and Methods:

4.3.1. Materials:

- Genistein, Chlorpromazine hydrochloride, Nocodazole, Dynasore hydrate, Methyl-β-cyclodextrin, 5-(N-Ethyl-N-isopropyl) amiloride (EIPA), Cytochalasin D, 4',6-diamidino-2-phenylindole dilactate (DAPI), Nile red (NR) dye, Phosphate buffered saline tablets (pH 7.4), Fluoromount™ Mounting media were purchased from Sigma-Aldrich Chemicals, UK. Methanol, dimethyl sulfoxide (DMSO), TrypLE™ Express, MitoTracker™ Green FM, paraformaldehyde, and Nunc™ Lab-Tek™ II Chamber Slide™ System and chambered cover glass 8-wells were purchased from Thermofischers, UK. Purified water (DW) from a Millipore Purification System (Billerica, MA, USA) was used. LysoTracker® Green DND-26 and Alexa Flour® 488-Phalloidin were purchased from Cell Signalling Technology, UK. CoStar Corning 12-well plates;

12 mm Transwell® with 0.4 µm Pore Polycarbonate Membrane Insert from Corning Lab, UK. Radioactive D-[2-^{14}C]-Mannitol, 50µCi, (MW: 182 Da, selective reactivity of 57.0 mCi/mmol), liquid scintillation cocktails, and vials were purchased from PerkinElmer, USA. Other lab chemicals and solvents were purchased from Sigma unless otherwise specified. Cell culture consumables were supplied (including 25 and 75 cm^2 vented-capped flasks, 96 multi-well flat bottom Plates, micro-tips, disposable serological pipettes, centrifuge tubes, cryo-vials, reservoirs).

4.3.2. Methods:

4.3.2.1. Polymeric Nanoparticles Formulations and Characterisations:

As previously mentioned in sections; 2.3, 2.4, and 2.5.

4.3.2.2. Cell Culture Maintenance:

As previously mentioned in section 3.3.2.2

4.3.2.3. The Apparent Permeability Coefficient (P_{app}):

Culturing the tight polarized monolayers: Calu-3 cells were cultured as previously described by Ehrhardt et al, (521) with modifications. Briefly**,** Calu-3 cells (80-90% confluent) were trypsinized using TrypLE™ Express. Transwells were pre-conditioned with 0.25 mL CM supplied with 10% FBS in apical and 0.5 mL in basolateral chambers and kept in an incubator (humified air with 5% CO_2 at 37 ^oC) for 30 min. Calu-3 cell suspension (0.5 mL) were seeded at a density of 5×10^5 cells/mL on Transwell apical chambers (1.12 cm^2 surface area, 0.4 µm pore, 12 well plate, CoStar Corning, UK), and CM (1 mL) was added to the basolateral chamber prior to incubation. Schematic diagram of the method is presented in Figure. 4.1.

After one day, the medium was removed from both apical and basal compartments and only replaced in the basal compartment with fresh 1 mL to produce ALI. Every other day, renewing the basal compartment media was completed by adding fresh 1 mL prewarmed medium and the apical layer was gently washed with 0.5 mL medium. After 3-4 days, TEER values were measured by chopstick electrodes of an epithelial voltohmmeter (World Precision instruments, precalibrated by standard resistances and tared to zero prior to the measurements) every other day. The chopsticks were initially sterilized by submerging into 70% ethanol for 15 mins then left to air dry. Prior to TEER measurements, submerged culture conditions were resumed by adding prewarmed media (0.5 mL) to the apical compartment and (1 mL) to the basolateral compartment and left to equilibrate for 30 minutes in the incubator (humified air with 5% CO_2 at 37 ^oC). Following TEER measurements, apical medium was removed to retain the ALI. After an additional 10 days, the cell layers were expected to reach maximum confluency of ~100% on Transwell inserts and TEER values had increased to a minimum value of 800 Ω cm^2 under the conditions described earlier. This denoted the formation of tight polarized epithelial layers that can be used to study the NPs effect on integrity of the epithelial barrier.

Permeability experimental procedure: The apical layers were washed three times with warm PBS. Prewarmed SFM was used to replenish basal compartment then left to equilibrate for 30 min in the incubator (humified air with 5% CO_2 at 37 ^oC) (Figure. 4.1). NPs solutions (Concentrations used: 0.125, 0.5, 2 mg/mL) were added as 300 µL SFM containing (2 µM, 0.1 µCi per mL) radiolabeled mannitol to the apical layers. A control for monolayer integrity was performed using radiolabeled mannitol at 300 µL SFM containing (0.1 µCi per mL) radiolabelled mannitol and added to the

apical chamber for untreated cells as a negative control and cell-free Transwell inserts serving as blank.

Within 1 min, a sample of 10 μL of the solution was removed from each donor chambers to establish the initial donor concentration (C_0), and a sample of 100 μL from each basal compartment was collected to establish initial recipient concentration at T0 that was replaced with fresh 100 μL SFM. The inserts were maintained in the incubators (humified air with 5% CO_2 at 37 ^oC), and samples (100 μL) were taken from the basal compartment at 1, 2, 3, 4, 5, and 24 hr intervals with the replacement of sampled solution with fresh 100 μL SFM. At 5 and 24 hr, another 10 μL samples from the apical chambers were taken to determine the final donor concentrations. Samples were collected in scintillation vials and 5 mL of scintillation cocktails were added per sample prior to being analysed by liquid scintillation counter (Beckman Tri-Carb).

The apparent permeability coefficients (P_{app}) for each type of NPs was calculated according to the following equation:

$$\boldsymbol{P_{app} = (dQ/dt)/CS.}$$

Where **dQ/dt**: change rate of radiolabeled mannitol concentration in the basal chamber (mol/sec); $\mathbf{C_0}$: was radiolabeled mannitol concentration in the donor chamber (mol/mL) at time T0; **S**: was the surface area of the PET membrane of the Transwell chamber (1.12 cm^2), and P*app* is the apparent permeation rate (cm sec^{-1}). The data is presented as Mean ± SD, for three independent experiments ($n=3$).

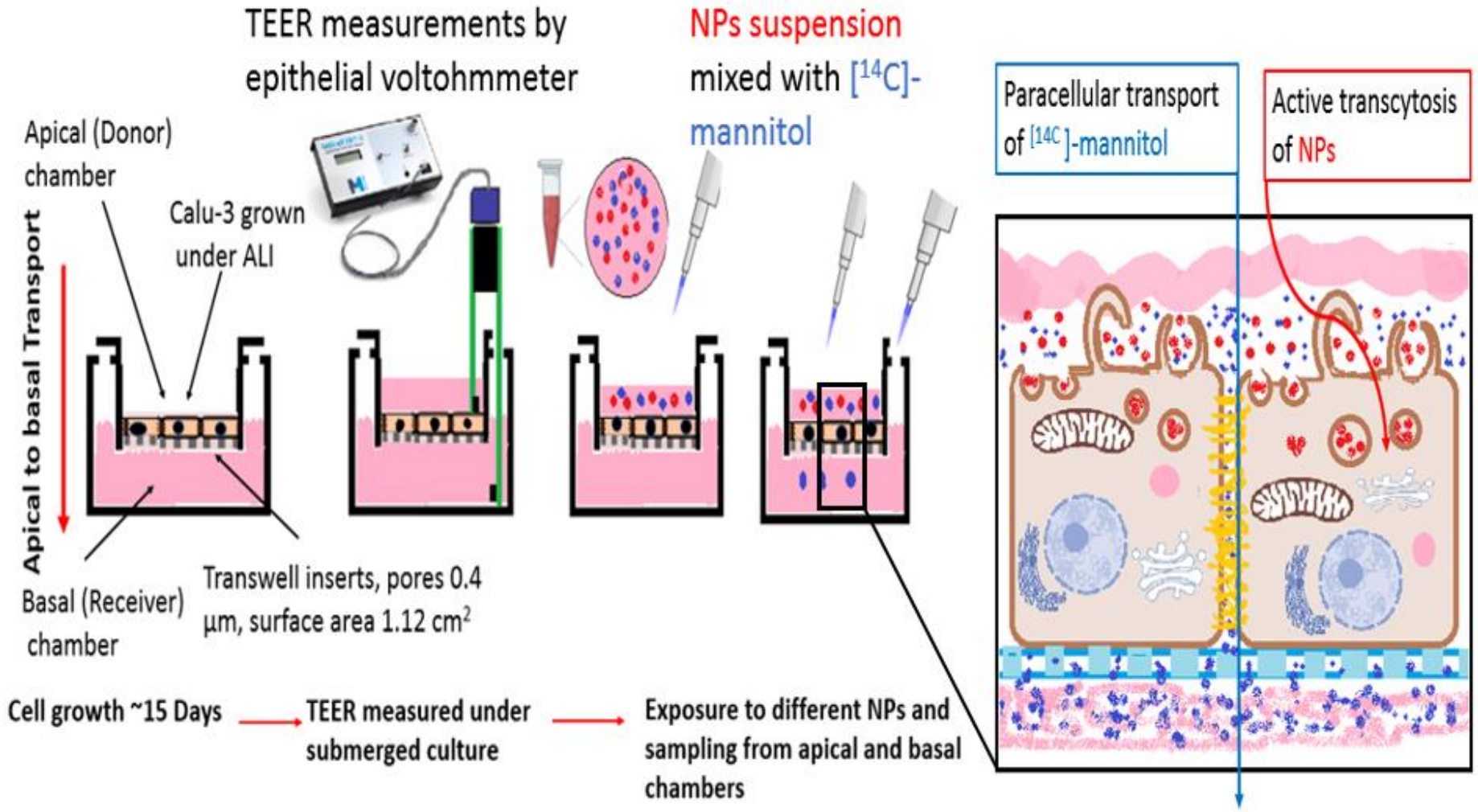

Figure. 4.1. Schematic diagram of the apparent permeability method used.

4.3.2.4. Investigation of Nanoparticle Internalisation Mechanisms:

To confirm NPs internalisation; Calu-3 cells were treated with NP-NRs concentrations (0.5 mg/mL) for 1 hr. Briefly, Calu-3 cells were seeded at a density of 40 x10^3 per well (200 µL) in 96 well plates and incubated (37 ^oC and 5% CO_2) for 48 hr, then supernatant was removed. NR-NPs were added (200 µL per well, in triplicates) and cells incubated (37 ^oC and 5% CO_2) for 1 hr and supernatants were removed followed by washing of the monolayers with ice-cold PBS containing (5%) trypan blue (cell impermeable) to quench the effect of free and surface-bound NPs (522, 523). After trypsinization by TrypLE™ Express (200 uL for 20 min), cells were collected in Eppendorf's and centrifuged for 2 minutes at 4°C (400 xg). Cell pellets were resuspended in 50 µL of fresh warm CM prior to analysis by flow cytometry. MFI of cells internalising NP-NRs was quantified and used as control (NP treated cells) for the subsequent experiment for NP internalisation inhibition by pharmacological inhibitors. NR dye release was excluded by preparing NR-NP suspension (0.5 mg/mL) in SFM and incubated for 1 hr prior to centrifuging and filtering through 0.2 µm filter and measuring any fluorescence by plate reader (*Ex/Em*: 550/647 nm).

Determination of the mechanism of NP transport: A group of inhibitors was selected to block passive, active, and endocytic pathways of transport (Table. 4.1). Initially, a pre-optimization experiment was done via AB viability assay (as previously mentioned in Chapter.3, section 3.3.2.3) to determine the suitable concentration of each of the pharmacological inhibitors (tested concentrations: 50, 25, 12.5, 6.25, 3 µM, for 2 hr exposure) to block the transport without inducing overt toxicity (< 20% cell death) on Calu-3 cell lines.

At 4 ^oC experiment to block the active transport (505); briefly, Calu-3 cells were seeded at a density of 40 x10^3 per well (200 µL) in 96 well plates for 48 hr, then the

supernatant was removed. SFM was added to wells prior to their storage at 4 ºC for 30 mins. After 30 mins, supernatants were removed and NP-NRs solutions (0.5 mg/mL) were added to the wells then further stored at 4 ºC for 1 hr prior to sample processing as above.

At 37 ºC, Calu-3 cells were seeded (40 x10^3 per well (200 µL)) in 96 well plates incubated (humified air with 5% CO_2 at 37 ºC) for 48 hr, then supernatant was removed. Pharmacological inhibitors were added (as 100 µL per well) and incubated for 30 mins. Supernatants were removed and a solution of NP-NRs (0.5 mg/mL, as 200 µL per well) containing the same concentration of the inhibitors were added to the wells and further incubated for 1 hr prior to sample processing as above.

Flow Cytometry Settings and Gating Strategy: BD Accuri C6 FC was set to fast flow rate (66 µl/min), and 3 blue-1 red lasers. Dot-plot FSC-A vs SSC-A was used to gate around the cell population and exclude the debris and particles (Figure. 4.2. A, P1 gate). Dot-plot FSC-A vs FSC-H was used to gate around the singlet cells (Figure. 4.2. B, P2 gate). The acquisition limits were set based on the gating to 5000 events/P2 in the singlets gate with 50 µL sample volume as a secondary limit. MFI was collected in FL-3 (M1 for NR, 550/647 nm on red channel) (Figure. 4.2. C). The results were expressed as a percentage of NP treated cells under no inhibition at 37 ºC.

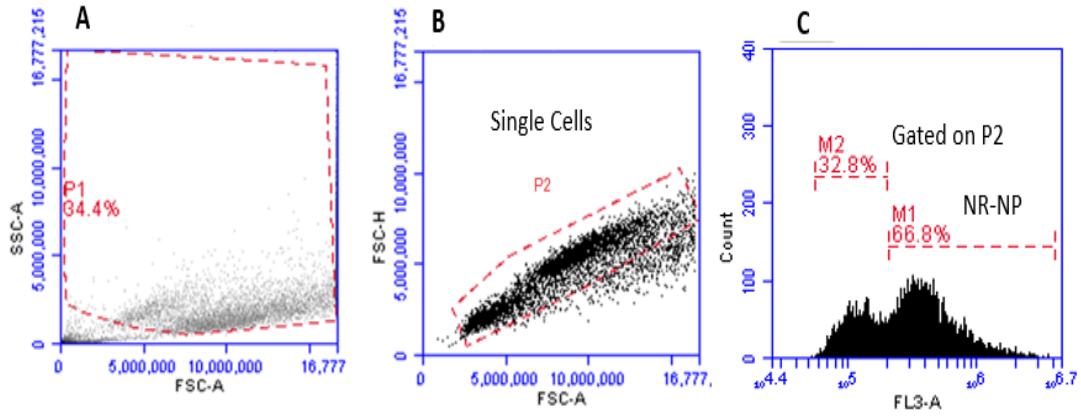

Figure. 4.2. Flow cytometry gating strategy: (A) FCS-A vs SCC-A: gating around the cells/P1 gate, (B)FSC-A vs FSC-H: gating around single cells/P2 gate, and (C) FL-3 histogram: gating around the negative (M2) and positive (M1) populations.

4.3.2.5. Visual Confirmation of Nanoparticle Internalisation and Intracellular Trafficking by Confocal Microscopy:

NP internalisation was visually confirmed by confocal laser scanning microscopy (CLSM; Carl Zeiss LSM 710, UK). NPs were fluorescently labelled/ physically loaded with NR (*Ex/Em*: 550/647 nm, red fluorescence, Sigma-UK) as described in section 2.3.2. The cells were visualized while outlining cell membranes with green fluorescence using Alexa Flour®488-Phalloidin ((AF488), *Ex/Em*: 495/518, Cell Signalling Technology, UK) that binds to F-actin filaments of the cytoskeleton, and the nuclei counterstained with blue fluorescence using 4',6-diamidino-2-phenylindole (strong binding to Adenine-Thymine DNA regions, DAPI, *Ex/Em*: 358⁄461 nm, Sigma-UK).

Table. 4.1. Pharmacological inhibitors (their key labels) and their mechanism of actions and doses used (159, 493, 505).

Pharmacological Inhibitor	Mechanism of Action	Dose used
Dynasore Hydrate (Inh1)	Dynamin-dependent endocytosis: GTPase inhibitor for dynamin1 and 2.	Stock solution (10 mM) prepared in DMSO and final concentration of 12 µM in SFM was used.
Genistein (Inh2)	Caveolin-mediated endocytosis inhibitor (Tyrosine Kinase inhibitor; caveolin formation requires phosphorylation and dependent on kinase): Inhibits epidermal growth factor receptor kinase.	Stock solution (10 mM) prepared in DMSO and final concentration of 25 µM in SFM was used.
Cytochalasin-D (Inh3)	Cytoskeleton inhibitor: disturbs the polymerization of Actin filaments	Stock solution (10 mM) prepared in DMSO and final concentration of 25 µM in SFM was used.
Nocodazole (Inh4)	Cytoskeleton inhibitor: disturbs the polymerization of microtubules	Stock solution (10 mM) prepared in DMSO and final concentration of 25 µM in SFM was used.
EIPA (Inh5)	Macropinocytosis: inhibits the NA^{+}/H^{+} exchange/Ca^{++}channel blocker, lowers cytoplasmic pH	Stock solution (10 mM) prepared in DMSO and final concentration of 12 µM in SFM was used.
Methyl-β-cyclodextrin (Inh6)	Caveolin-mediated endocytosis inhibitor: cholesterol depletion and inhibition of lipid raft formation	Stock solution (10 mM) prepared in H_2O and final concentration of 50 µM in SFM was used.
Chlorpromazine (Inh7)	Clathrin-mediated endocytosis inhibitor: inhibit the Clathrin pits assembly	Stock solution (10 mM) prepared in H_2O and final concentration of 12 µM in SFM was used.

Briefly, Calu-3 cells (5×10^4 cells per well, 0.5 mL) were seeded in an 8-well chambered cover glass slides (Nunc Lab-Tek, Thermo Scientific, UK) and incubated (humified air with 5% CO_2 at 37 ^oC) for 48 hr. The supernatant was removed, and cells were treated with 0.5 mg/mL NR-NPs freshly prepared in SFM and further incubated for 1 hr. Cells were then washed with PBS three times followed by staining the nucleus with DAPI (100 µL per well of 100 nM DAPI solution prepared in PBS) for 15 mins, followed by three PBS washes (5 mins soaking each wash). Cells were fixed with 4% paraformaldehyde for 10 mins followed by three PBS washes (5 mins soaking each wash). AF488 staining was prepared in methanol (as 6.6 µM, 20X solution) and diluted to 0.33 µM working solution in PBS and added as 100 µL per well for 15 mins followed by three PBS washes (5 mins soaking each wash). The chambers were removed, and coverslips were mounted on the slides using Fluoromount^{TM} mounting media (Sigma, UK). The slides were visualized under CLSM using a plan-Apochromat 63× objective lens (numerical aperture 1.40, oil immersion), and pinhole diameter was set near ~1 AU. Lasers used were a diode laser 405 nm to excite DAPI, an argon laser 488 nm to excite AF488, and a helium neon (HeNe) laser 543 nm to excite NP-NR. Band pass filters were set to collect the emitted fluorescence 410-480 nm for the blue channel, 490-550 nm for the green channel, and 590-690 nm for the red channel (to avoid channel crosstalk). Autofluorescence from untreated Calu-3 cells was negligible under the acquisition settings and did not interfere with the fluorescently labelled NPs. Images were processed by Fiji software.

NP intracellular co-localisation: NPs trafficking to the cytoplasm and co-localisation with cell organelles were investigated. Calu-3 cells (5×10^4 cells per well, 0.5 mL) were seeded in 8-well chambers (Nunc Lab-Tek, Thermo Scientific, UK) and incubated (humified air with 5% CO_2 at 37 ^oC) for 48 hr. The supernatant was removed,

and cells were treated with 0.5 mg/mL NR-NPs freshly prepared in SFM and further incubated for 1 hr. Cells were then washed with PBS three times followed by staining the nucleus with 100 µL per well of 100 nM DAPI solution for 15 mins, followed by three PBS washes (5 mins soaking each wash). Cells were stained with either LysoTracker® Green DND-26 ((LT-26), *Ex/Em*: 495/518 nm, Cell Signalling Technology, UK) as 100 µL per well of 50 nM prepared in CM to counterstain the lysosomes or with MitoTracker™ Green ((MT), *Ex/Em*: 490/516 nm, Thermofischers) as 100 µL per well of 100 nM prepared in PBS to counterstain the mitochondria. Cells were washed three times with warm PBS (5 mins soaking each wash) and CM were added (200 µL per well) prior to visualizing under live conditions. The chambers were visualized under CLSM using a plan-Apochromat 63× objective lens (numerical aperture 1.40, oil immersion), and pinhole diameter was set near ~1 AU. Lasers used were a diode laser 405 nm to excite DAPI, an argon laser 488 nm to excite LT-26 or MT, and a helium neon (HeNe) laser 543 nm to excite NP-NR. Band pass filters were set to collect the emitted fluorescence 410-480 nm for the blue channel, 490-550 nm for the green channel, and 590-690 nm for the red channel. Images were processed by Fiji software.

4.3.2.6. Statistical Analysis: As previously mentioned in section 2.3.4.

4.4. Results:

4.4.1. Polymeric Nanoparticles Formulations and Characterisations:

As previously mentioned, and discussed in previous sections 2.3.2., 2.4.2, 2.5.1

4.4.2. The Apparent Permeability Coefficient (P_{app}):

TEER values recorded over 15 days of Calu-3 growth under ALI over Transwell permeable inserts are shown in Figure. 4.3. The graph shows an increasing trend of the

epithelial electrical resistance over time. TEER values reached a maximum of ~1000 ohms.cm^2 at day 15. This denoted the successful development of polarized monolayers and tight junctions and was similar to previously reported work (281, 513, 521, 524).

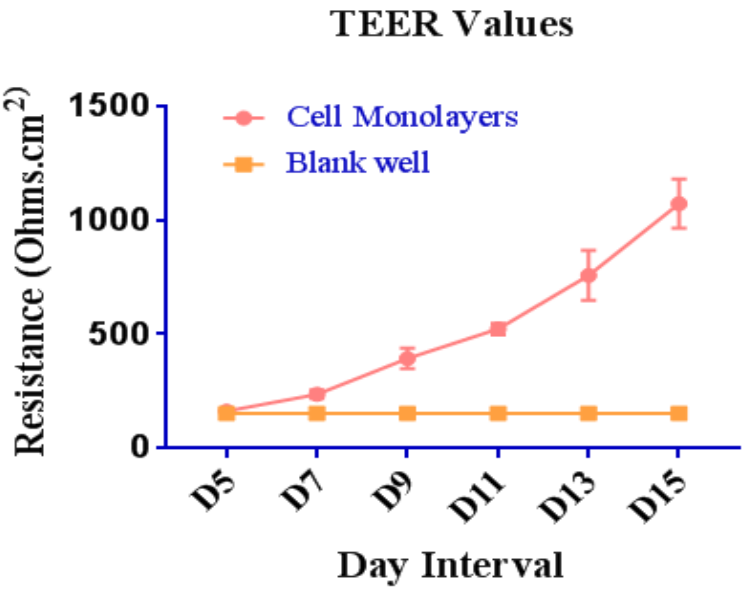

Figure. 4.3. TEER values measured over time for Calu-3 cell lines grown under ALI (*Mean± SD, n=3*).

The permeability coefficient (P*app*) of the radioisotope [^{14}C]-mannitol as a paracellular marker was used to confirm the barrier integrity after exposure to NPs at three concentrations (0.125, 0.5, and 2 mg/mL) over time (1, 2, 3, 4, 5, 24 hr). P*app* values were presented as line graphs for each NPs to show the differences between the three concentrations over time (Figure. 4.4) and as bar graphs to compare between the different types of NPs at the same concentration and time point (Figure. 4.5. & 4.6).

In Figure. 4.4; all NPs concentrations had followed the same trend. P*app* of [^{14}C]-mannitol had initial high values (~ 4 x 10^{-7} cm sec^{-1}) at T1 that was the maximum with a subsequent slow decline of P*app* rate over time until T24 hr (~ 1.5-2 x 10^{-7} cm sec^{-1}). All concentrations showed the same trend with the highest concentration (2 mg/mL; Orange lines) showed the highest P*app* values compared to lower

concentrations (0.5 mg/mL (dark green lines) and 0.125 (light green lines)). These changes followed the same trend of the untreated cells (NC, Pink lines). However, the P*app* values were slightly higher than NC. *PG*-2 and *PG*+2 (Figure. 4.4. A & B), *PL*-2 and *PL*+2 (Figure. 4.4. C & D), *PG*-5 and *PG*+5 (Figure. 4.4. E & F), and *PG*-8 and *PG*+8 (Figure. 4.4. G & H) showed similar P*app* behaviour and pattern where the highest concentration showed the highest level of P*app* values, followed with 0.5 mg/mL, then the lowest 0.125 mg/mL.

To compare the different types of NPs on the epithelial integrity at the same concentrations and time point:

In T1; Figure. 4.5 (A & B) NPs of *PG*-2 and *PL*-2 had similar trend of increasing the P*app* values with increasing NPs concentration but no statistical differences to NC. Their positive counterparts showed the same trend with no statistical differences between them, or to their negative counterparts. However, *PG*-5 NPs showed slightly higher P*app* values compared to *PG*-2 and *PG*-8. *PG*+5 was similar to the *PG*-5 and slightly higher than *PG*+8 but no statistical differences. The highest P*app* values reached were (~ 4×10^{-7} cm sec^{-1}) for the 2mg/mL concentrations for all different NPs.

In T2; Figure. 4.5 (C & D) showed all NPs had universal drop of the P*app* values after 2 hr with all NPs and NC (with a concentration dependent differences in P*app* values preserved as previously mentioned). The highest concentrations (2mg/mL) showed the highest P*app* values with all types of NPs (~ 3×10^{-7}cm sec^{-1}) and were statistically significant from the NC with *PG*-2, *PG*-5, *PG*+2, *PL*+2, *PG*+8, while the *PL*-2, *PG*-8, *PG*+5 were not statistical different to the NC.

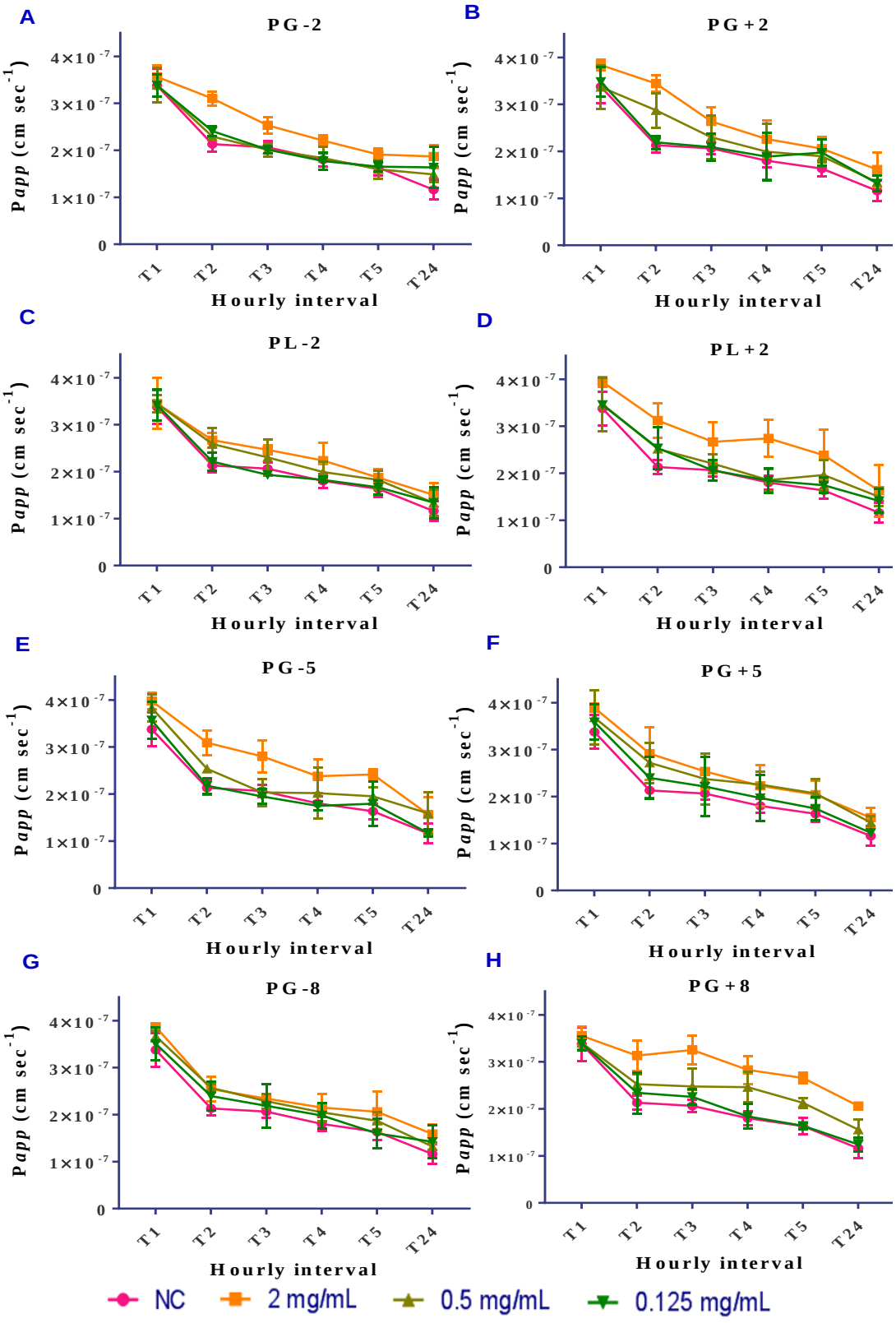

Figure. 4.4. P*app* of [^{14}C]-mannitol measured under different NPs exposures over time: (A) *PG*-2, (B) *PG*+2, (C) *PL*-2, (D) *PL*+2, (E) *PG*-5, (F) *PG*+5, (G) *PG*-8, and (H) *PG*+8 (Results expressed as *Mean* ± *SD*, for statistical symbols and *P*-value please refer to section. 2.3.4).

In T3; Figure. 4.5 (E & F) showed all NPs concentration of (0.125 and 0.5 mg/mL, orange and green bars respectively) had a decline of P*app* rates that was almost in line with NC, whereas the highest concentrations of (2mg/mL, blue bar) staggered slightly less than its values at T2 (~2.5 - 3 x 10^{-7}cm sec^{-1}). These trends of a concentration-dependent increase of P*app* were similar at all negative and positive NPs and didn't show any statistical differences except *PG*+8/2mg/mL.

In T4; Figure. 4.6 (A & B) showed all NPs concentration had a further decline of concentration-dependent increase of P*app* values that was similar to NC. However, the highest concentrations staggered slightly less than its values at T3 (~ 2.5 - 3 x 10^{-7} cm sec^{-1}). These were similar to all negative and positive counterparts and didn't show any statistical differences except *PG*+8/2 mg/mL was still high and significantly different from the NC.

In T5; Figure. 4.6 (C & D) showed a consistent decline P*app* values where the highest two concentrations (0.5 and 2mg/mL) were near (~ 1.7 – 2.5 x 10^{-7} cm sec^{-1}) values. There were slight differences between the different types of NPs but no statistical difference. Only *PG*-5/ 2mg/mL, and *PG*+8/ 2mg/mL were the highest values and were statistically significant different from the NC at T5.

In T24; Figure. 4.6 (E & F) showed a consistent decline P*app* values where the highest two concentrations (0.5 and 2mg/mL) were near ~ 1.5 – 2 x 10^{-7} cm sec^{-1} values. There were slight differences between the different types of NPs but no statistical difference. Only *PG*+8/ 2mg/mL was the highest and statistically significantly different from NC at T24.

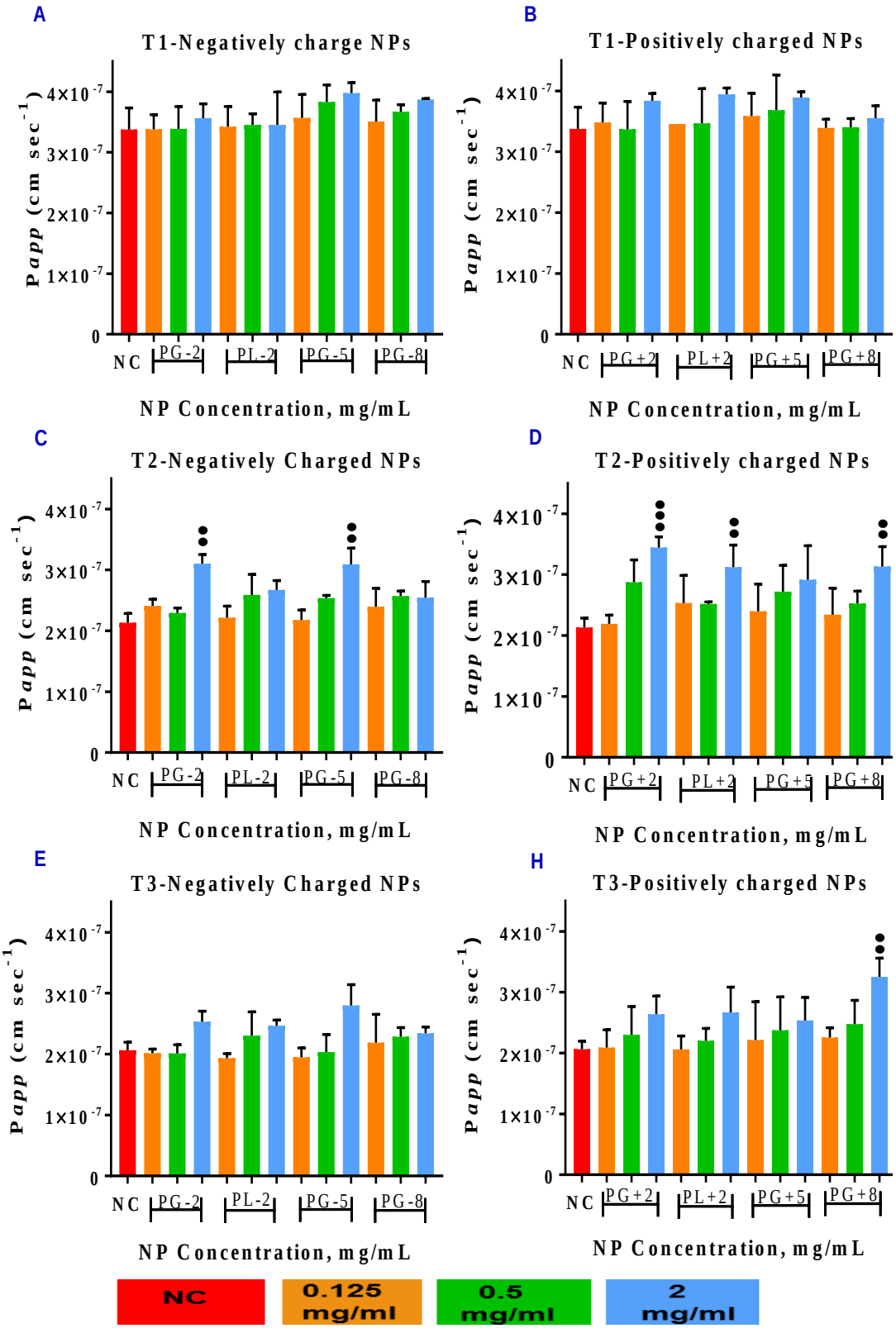

Figure. 4.5. Comparisons of P*app* of [^{14}C]-mannitol measured under different NPs at the same time point; (A & B) all NPs at T1, (C & D) at T2, (E & F) at T3 (Results expressed as Mean ± SD, for statistical symbols and *P*-value please refer to section. 2.3.4).

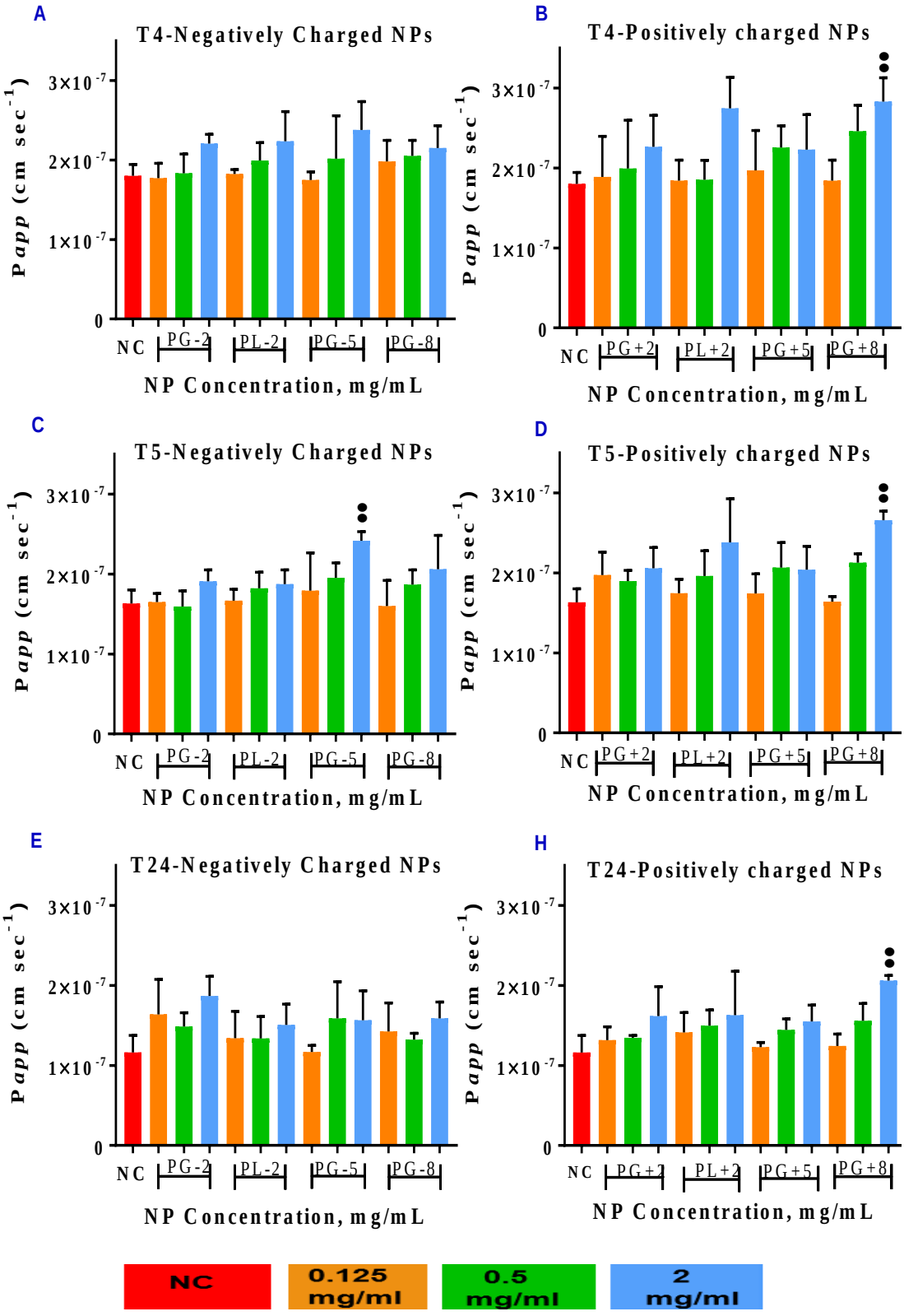

Figure. 4.6. Comparisons of P*app* of [^{14}C]-mannitol measured under different NPs at the same time point; (A & B) all NPs at T4, (C & D) at T5, (E & F) at T24 (Results expressed as Mean ± SD, for statistical symbols and *P*-value please refer to section. 2.3.4).

4.4.3. Transport Mechanisms:

The confirmation of NPs uptake and elucidation of the endocytosis mechanism following 1 hr exposure was carried by flow cytometry and shown in Figure. 4.7. All NPs were internalised to Calu-3 cells (NP treated, blue bars) and was almost 100 times more than the untreated cells (grey bar). All NPs transport showed a significant inhibition at 4 ^{o}C indicating the energy dependent transport.

In Figure. 4.7. A, *PG*-2 internalisation was statistically significantly inhibited by Inh1 ((~40% reduction of NP treated), Dynasore: Dynamin 1 and 2 inhibitor, green bar), Inh2 ((~40% reduction of NP treated), Genistein: tyrosine kinase inhibitor for caveolin endocytosis, light blue bar), Inh4 ((~50% reduction of NP treated), Nocodazole: Cytoskeleton inhibitor (disturbs the polymerization of microtubules, pink bar), and Inh6 (~40% reduction of NP treated), Methyl-β-cyclodextrin: cholesterol and lipid depletion for caveolin-inhibition, red bar). While there was slight but no statistical significant reduction of Inh5 (EIPA, Na+/H+ ionic channel exchange for micropinocytosis inhibition, light brown) and no effect for inh3 (Cytochalasin-D: Cytoskeleton inhibitor: disturbs the polymerization of actin filaments, purple bar) and Inh7 (Chlorpromazine: Clathrin pits assembly inhibitor, black bar).

In Figure. 4.7. B, *PG*+2 internalisation was inhibited by ~ 50% reduction with Inh1, Inh2, Inh3, and Inh4. There was slight reduction of the internalisation by Inh5 and Inh6 but was not statistically significant difference, and Inh7 had no effect on the uptake.

In Figure. 4.7. C, *PL*-2 internalisation was inhibited by ~25% by Inh1, ~ 30% by Inh2, and ~ 25% Inh7. There were reductions of the internalisation by Inh3, Inh4,

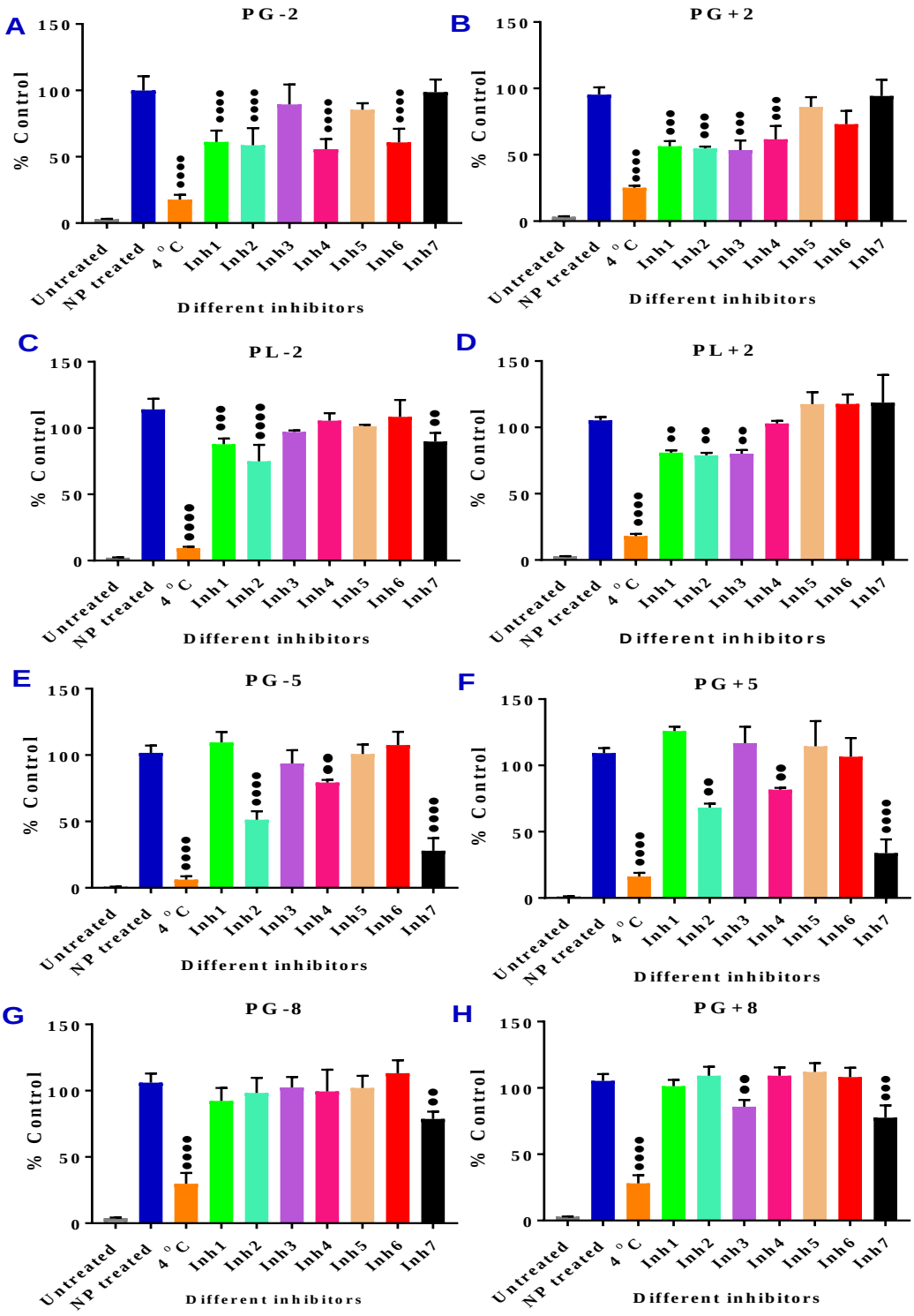

Figure. 4.7. NPs internalisation and the effects of different inhibitors on the internalisation of (A) *PG*-2, (B) *PG*+2, (C) *PL*-2, (D) *PL*+2, (E) *PG*-5, (F) *PG*+5, (G) *PG*-8, (H) *PG*+8; where Inh1: Dynasore, Inh2: Genistein, Inh3: Cytochalasin D, Inh4: Nocodazole, Inh5: EIPA, Inh6: Methyl-β-cyclodextrin, Inh7: Chlorpromazine (Results expressed as *Mean* ± *SD*, for statistical symbols and *P*-value please refer to section. 2.3.4).

and Inh5 but were not statistically significant difference, and Inh6 had no effect on the uptake.

In Figure. 4.7. D, *PL*+2 internalisation was inhibited by ~ 20% reduction with Inh1, Inh2, and Inh3. There were reductions of the internalisation by Inh3, Inh4, and Inh5 but were not statistically significant, and Inh6 had no effect on the uptake. There was no effect of Inh4 but there was an increase of the uptake with Inh5, Inh6, and Inh7 but was not statistically significant.

In Figure. 4.7. E, *PG*-5 internalisation was inhibited by ~50% by Inh2, ~20% by Inh4, ~78% by Inh7. There was an increase of the internalisation by Inh1 and Inh6 but was not statistically significant. There was no effect of Inh5 on the uptake.

In Figure. 4.7. F, *PG*-5 internalisation was inhibited by ~30% reduction with Inh2, ~20% by Inh4, ~70% by Inh7. There was an increase of the internalisation by Inh1, Inh3, and Inh5 but was no statistically significant difference. There was no effect of Inh6 on the uptake.

In Figure. 4.7. G, *PG*-5 internalisation was inhibited by ~25% by Inh7. There was no effect of Inh1, Inh2, Inh3, Inh4, and Inh5 on the uptake. There was an increase with Inh6 but was no statistically significant difference.

In Figure. 4.7. H, *PG*+8 internalisation was inhibited by ~15% by Inh3, and ~ 20% by Inh7. There was an increase of uptake with Inh2, Inh4, Inh5, Inh6 but was no statistically significant difference. There was no effect of Inh1 on the uptake.

4.4.4. Visual Confirmation of NP Internalisation and Co-localisation:

Visual confirmation of NPs internalisation by CLM is shown in Figure. 4.8: (A) *PG*-2 and (B) *PG*+2, Figure. 4.9: (A) *PL*-2 and (B) *PL*+2, Figure. 4.10: (A) *PG*-5 (A)

and (B) *PG*+5, and Figure. 4.11: (A) for *PG*-8 and (B) *PG*+8. Nuclei of Calu-3 cells were stained by DAPI (blue channel) whereas the cell membranes were stained by AF488 (green channel), and NP-NR shown in red channel. The three channels were merged in overlay images. All types of NPs were internalised into the cell cytoplasm. NPs could be observed in the space between the nuclei and the outer cell membranes indicating internalisation and successful cytoplasmic delivery.

NP co-localisation with lysosomes shown in Figure. 4.12: (A) *PG*-2 and (B) *PG*+2, Figure. 4.13: (A) *PL*-2 and (B) *PL*+2, Figure. 4.14: (A) *PG*-5 and (B) *PG*+5, and Figure. 4.15: (A) *PG*-8 and (B) *PG*+8. The lysosomes were counterstained by LT-26 (green channel), and NP-NR in red channel. Co-localisation of lysosomes and NP-NRs are shown by green and red channel overlay giving an orange to golden-yellow colour denoting the co-localisation). The three channels were merged in overlay images to show signals from NPs superimposed/co-localised with lysosomes and the relation to nucleus.

NP co-localisation with mitochondria shown in Figure. 4.16: (A) *PG*-2 and (B) *PG*+2, Figure. 4.17: (A) *PL*-2 and (B) *PL*+2, Figure. 4.18: (A) *PG*-5 and (B) *PG*+5, and Figure. 4.19: (A) *PG*-8 and (B). The mitochondria were counterstained by MG (green channel), and NP-NR in red channel. Co-localisation of mitochondria and NP-NRs are shown by green and red channel merge giving an orange to golden-yellow colour denoting the co-localisation. The three channels were merged in overlay images to show signals from NPs superimposed/co-localised with mitochondria and the relation to nucleus.

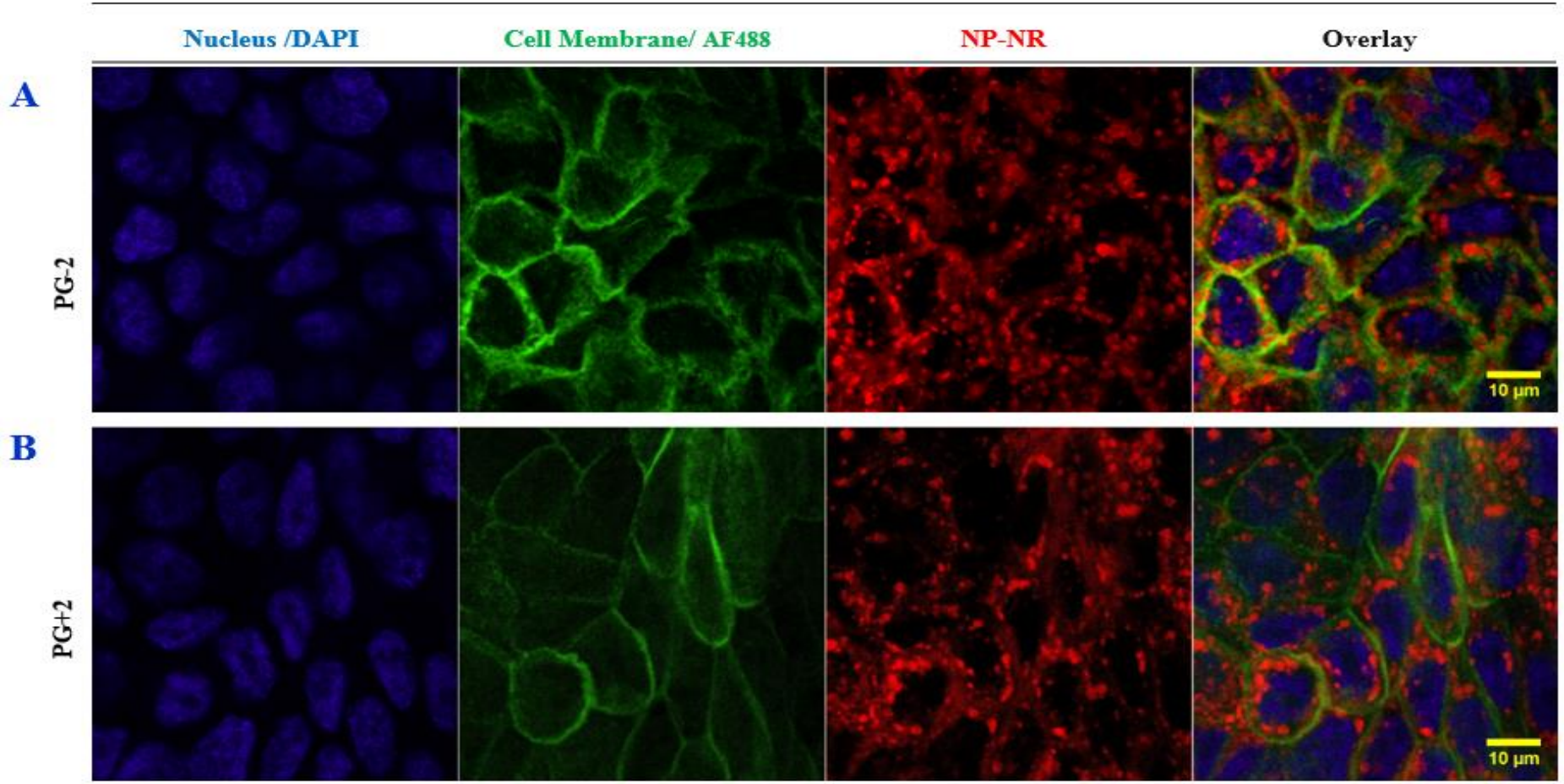

Figure. 4.8. Confocal microscopy study of Calu-3 internalisation of NPs where nuclei labelled by DAPI and cell membranes labelled by AF488 after incubation for 1 hour with (0.5 mg/mL) NP-NRs (A) *PG*-2, (B) *PG*+2.

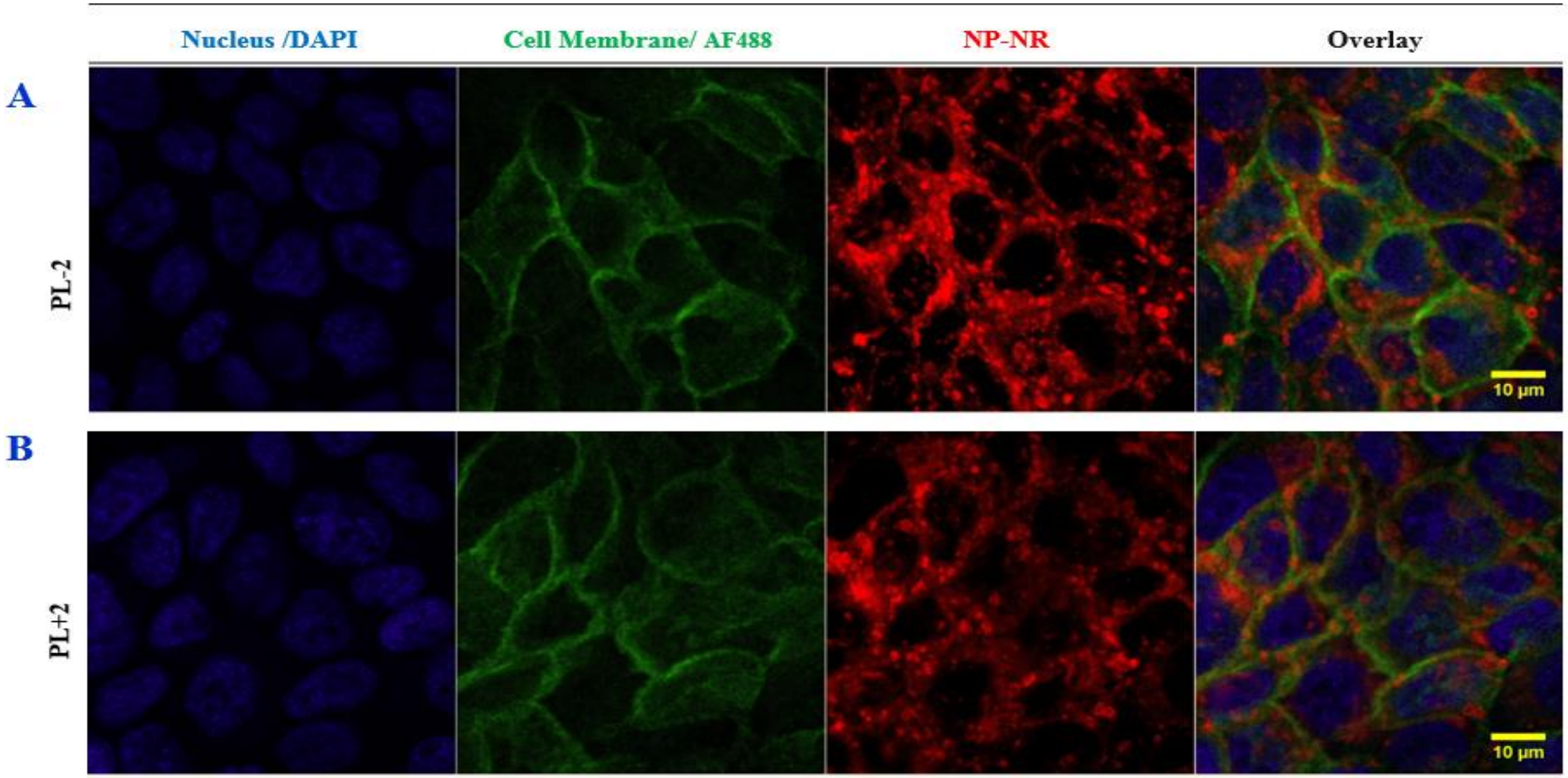

Figure. 4.9. Confocal microscopy study of Calu-3 internalisation of NPs where nuclei labelled by DAPI and cell membranes labelled by AF488 after incubation for 1 hour with (0.5 mg/mL) NP-NRs (A) *PL*-2, (B) *PL*+2.

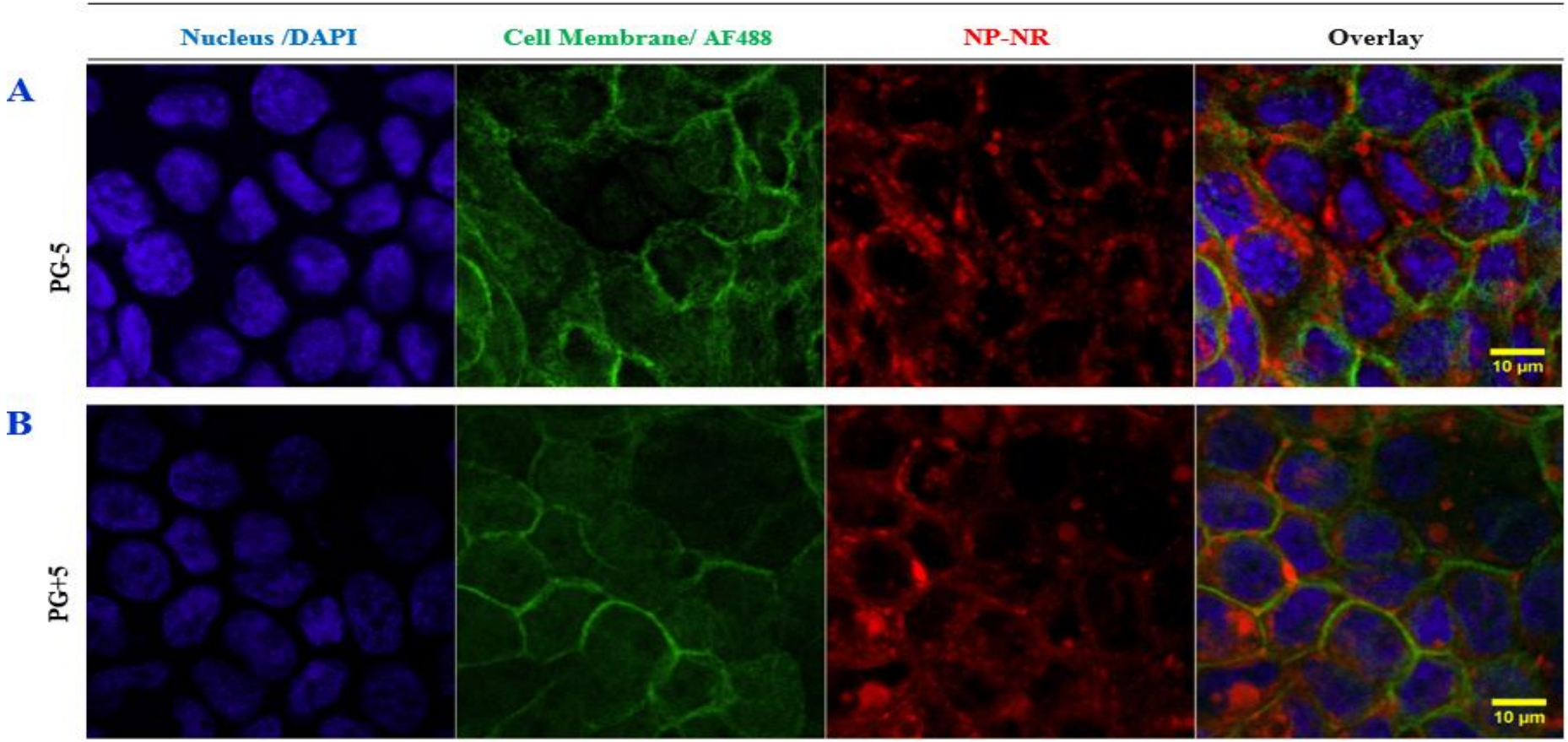

Figure. 4.10. Confocal microscopy study of Calu-3 internalisation of NPs where nuclei labelled by DAPI and cell membranes labelled by AF488 after incubation for 1 hour with (0.5 mg/mL) NP-NRs (A) *PG*-5, (B) *PG*+5.

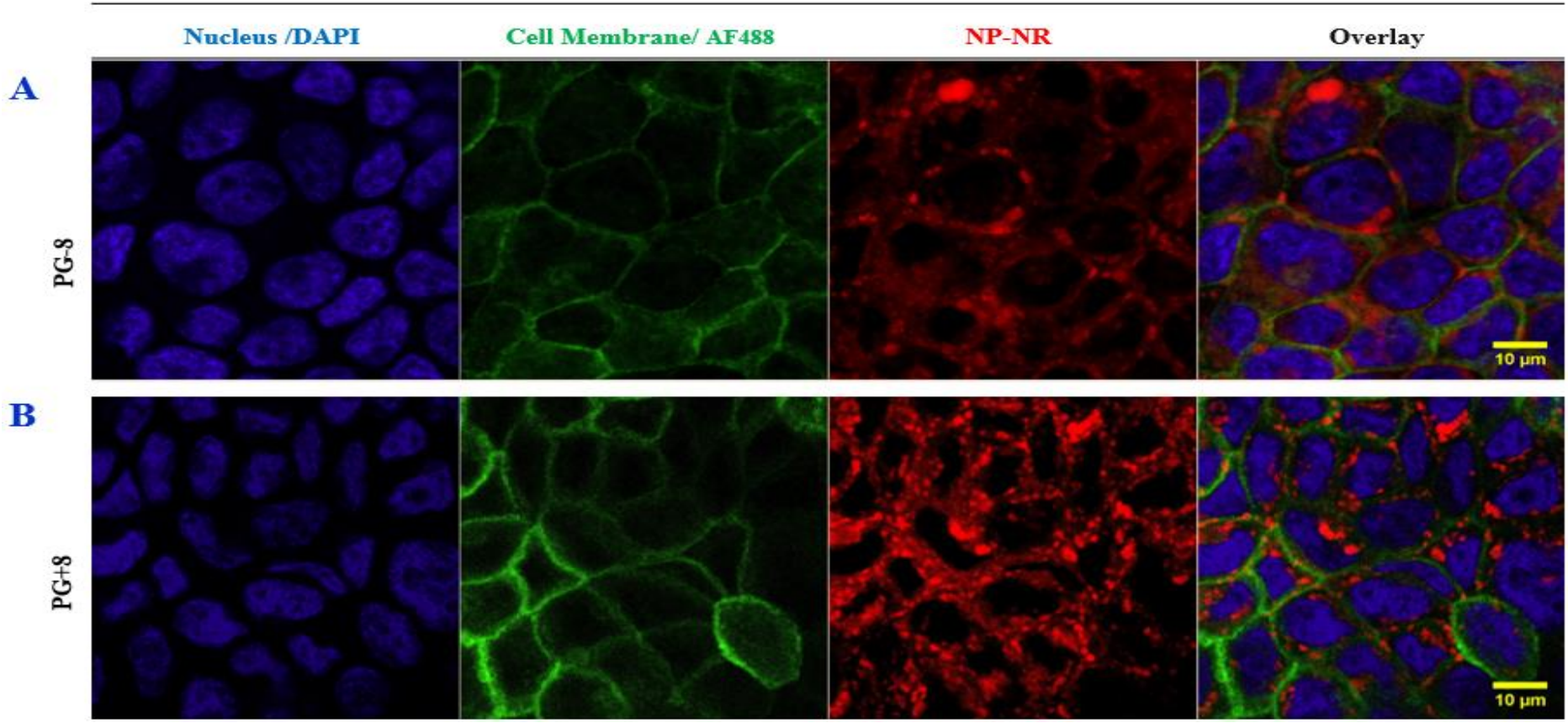

Figure. 4.11. Confocal microscopy study of Calu-3 internalisation of NPs where nuclei labelled by DAPI and cell membranes labelled by AF488 after incubation for 1 hour with (0.5 mg/mL) NP-NRs (A) *PG*-8, (B) *PG*+8.

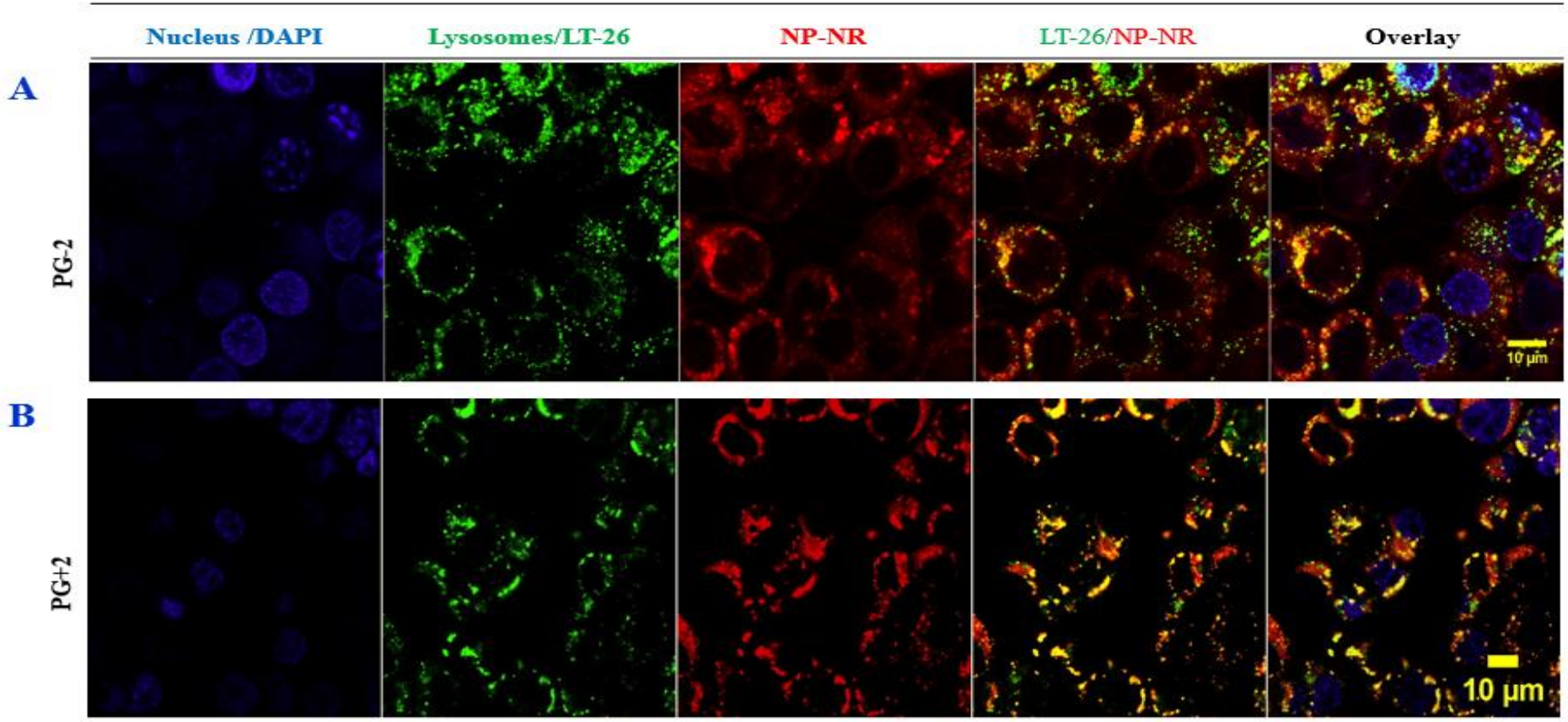

Figure. 4.12. Confocal microscopy study of NPs co-localisation with lysosomes in Calu-3 cells where nuclei labelled by DAPI and lysosomes labelled by LT-26 after incubation for 1 hour with (0.5 mg/mL) NP-NRs (A) *PG*-2, (B) *PG*+2.

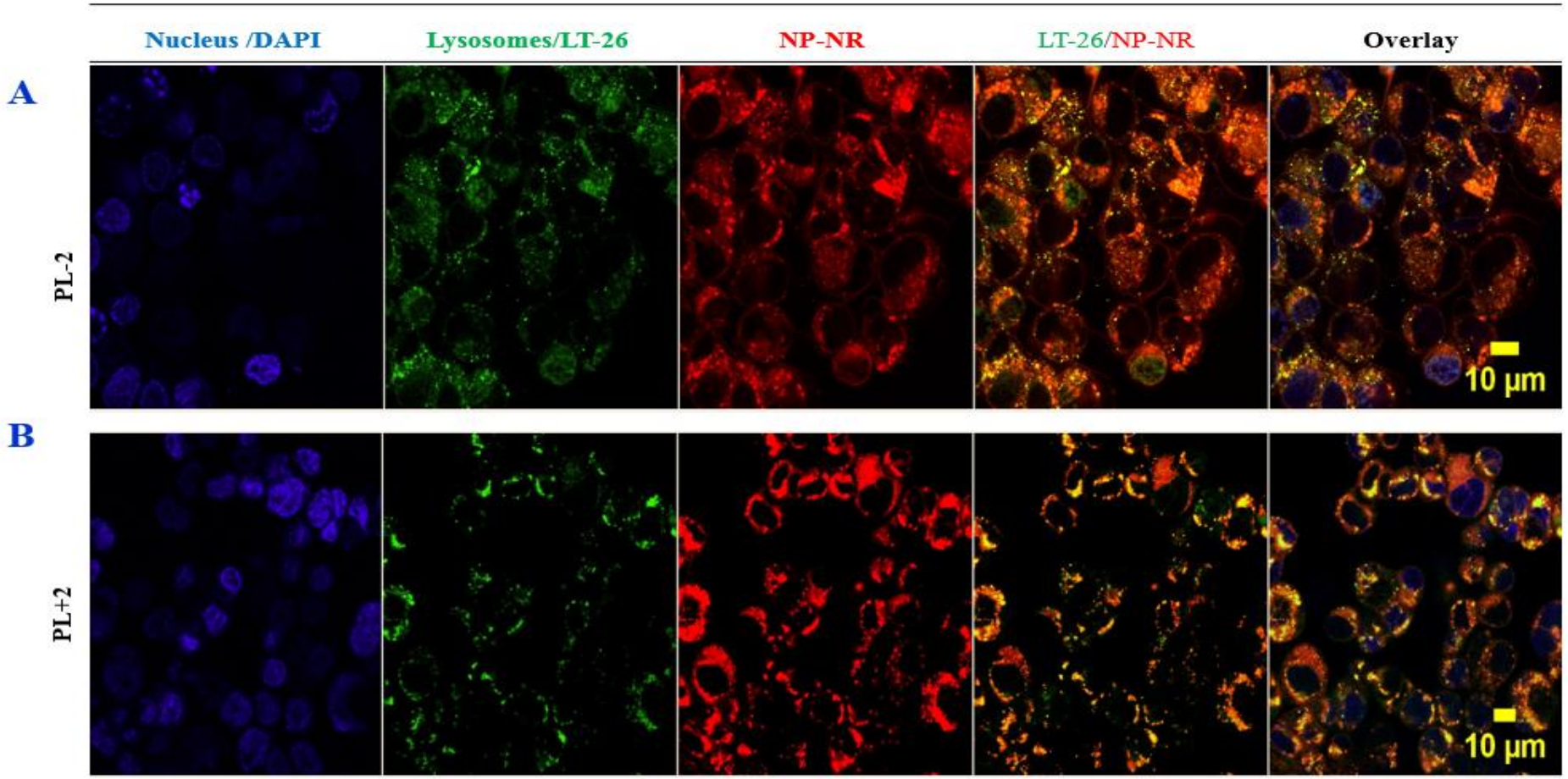

Figure. 4.13. Confocal microscopy study of NPs co-localisation with lysosomes in Calu-3 cells where nuclei labelled by DAPI and lysosomes labelled by LT-26 after incubation for 1 hour with (0.5 mg/mL) NP-NRs (A) *PL*-2, (B) *PL*+2.

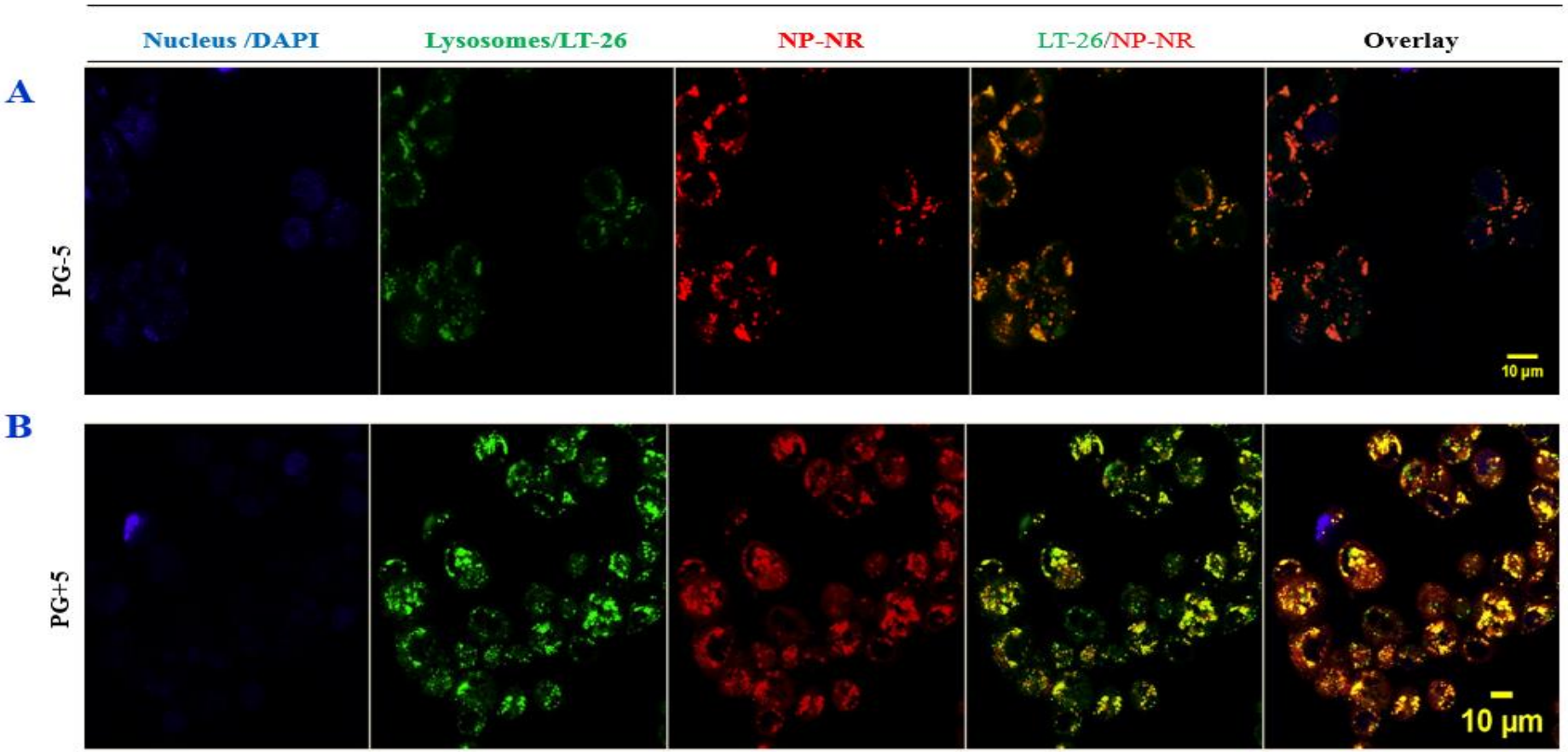

Figure. 4.14. Confocal microscopy study of NPs co-localisation with lysosomes in Calu-3 cells where nuclei labelled by DAPI and lysosomes labelled by LT-26 after incubation for 1 hour with (0.5 mg/mL) NP-NRs (A) *PG*-5, (B) *PG*+5.

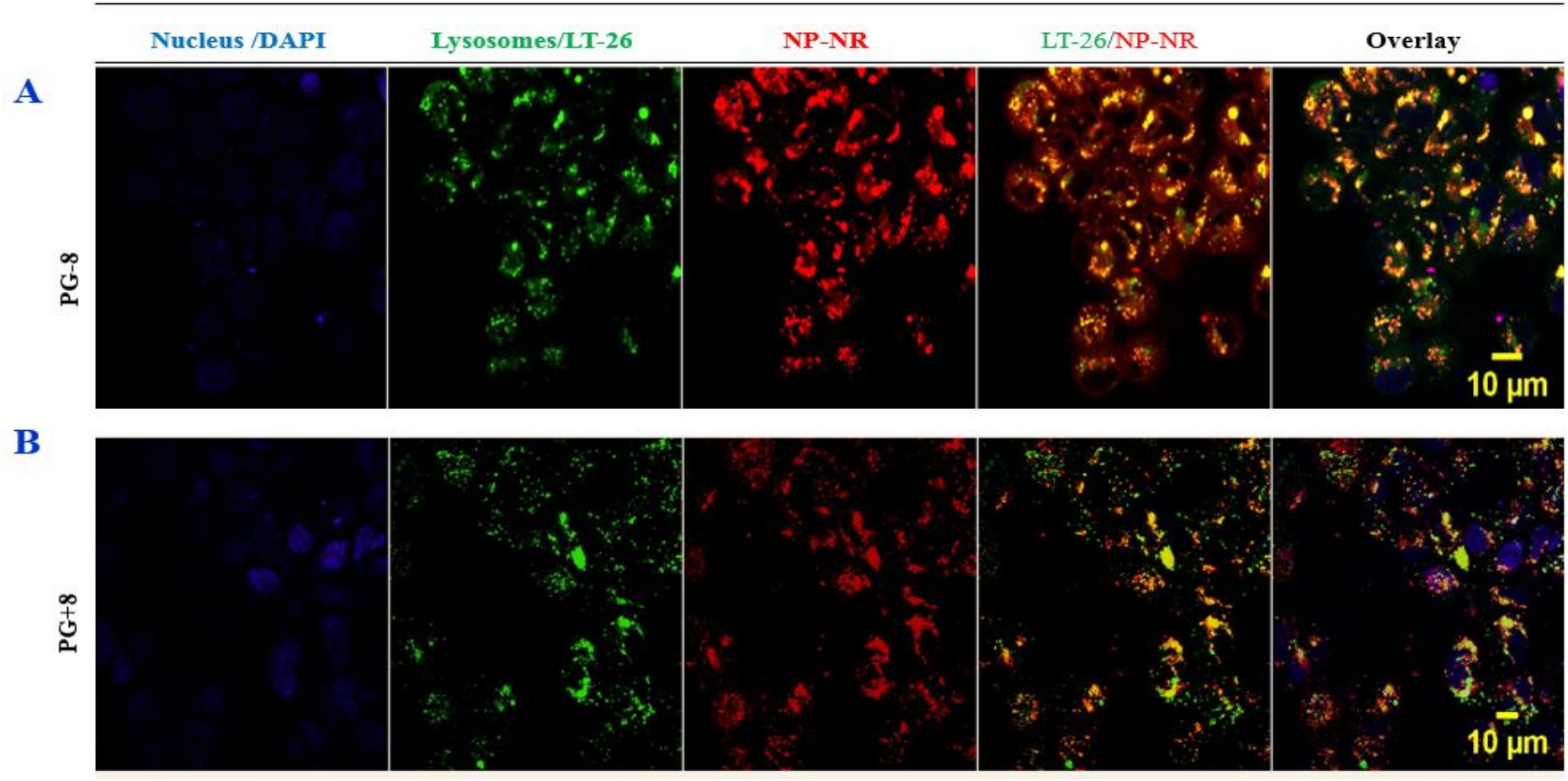

Figure. 4.15. Confocal microscopy study of NPs co-localisation with lysosomes in Calu-3 cells where nuclei labelled by DAPI and lysosomes labelled by LT-26 after incubation for 1 hour with (0.5 mg/mL) NP-NRs (A) *PG*-8, (B) *PG*+8.

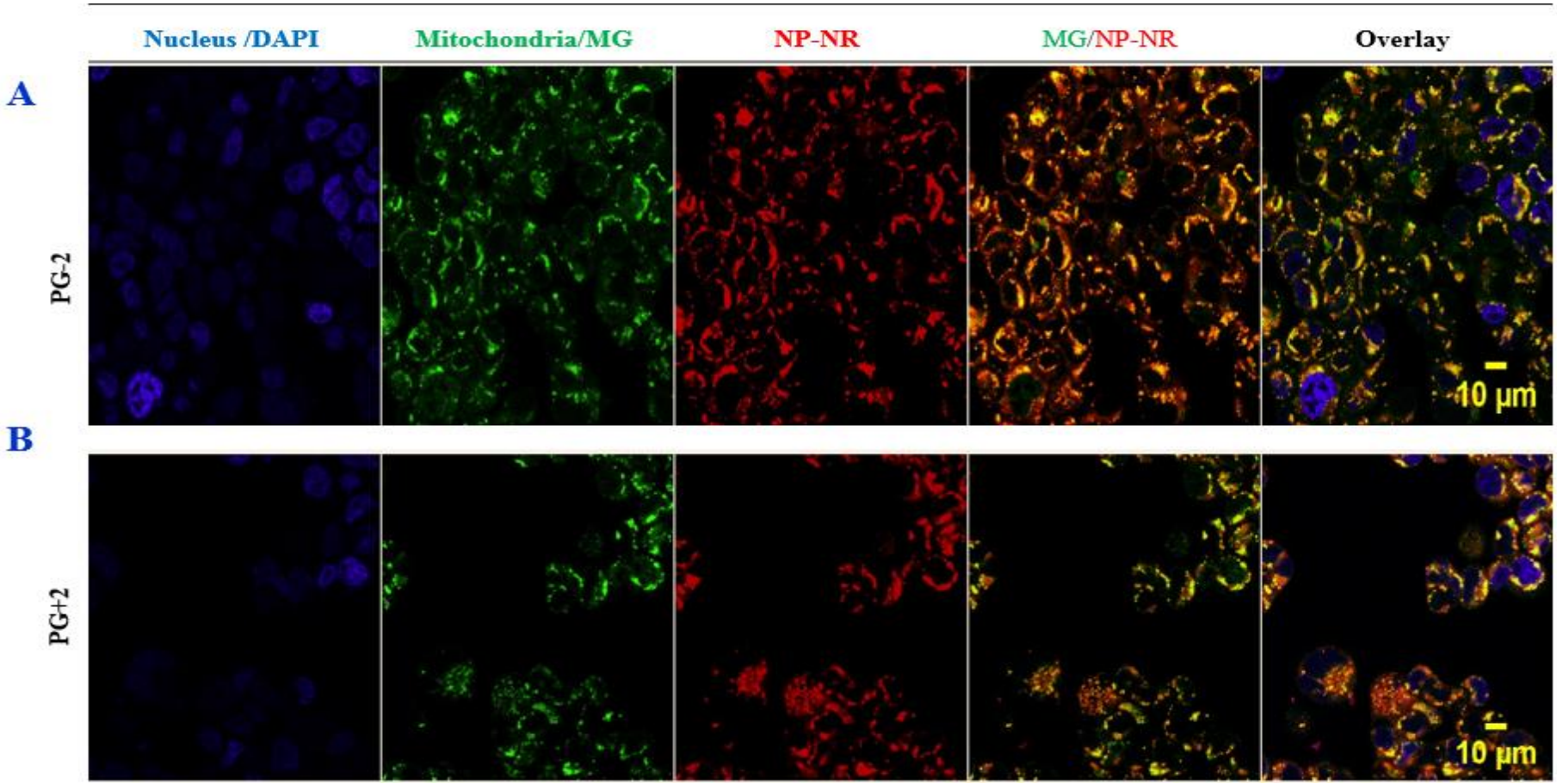

Figure. 4.16. Confocal microscopy study of NPs co-localisation with mitochondria in Calu-3 cells where nuclei labelled by DAPI and mitochondria labelled by MG after incubation for 1 hour with (0.5 mg/mL) NP-NRs (A) *PG*-2, (B) *PG*+2.

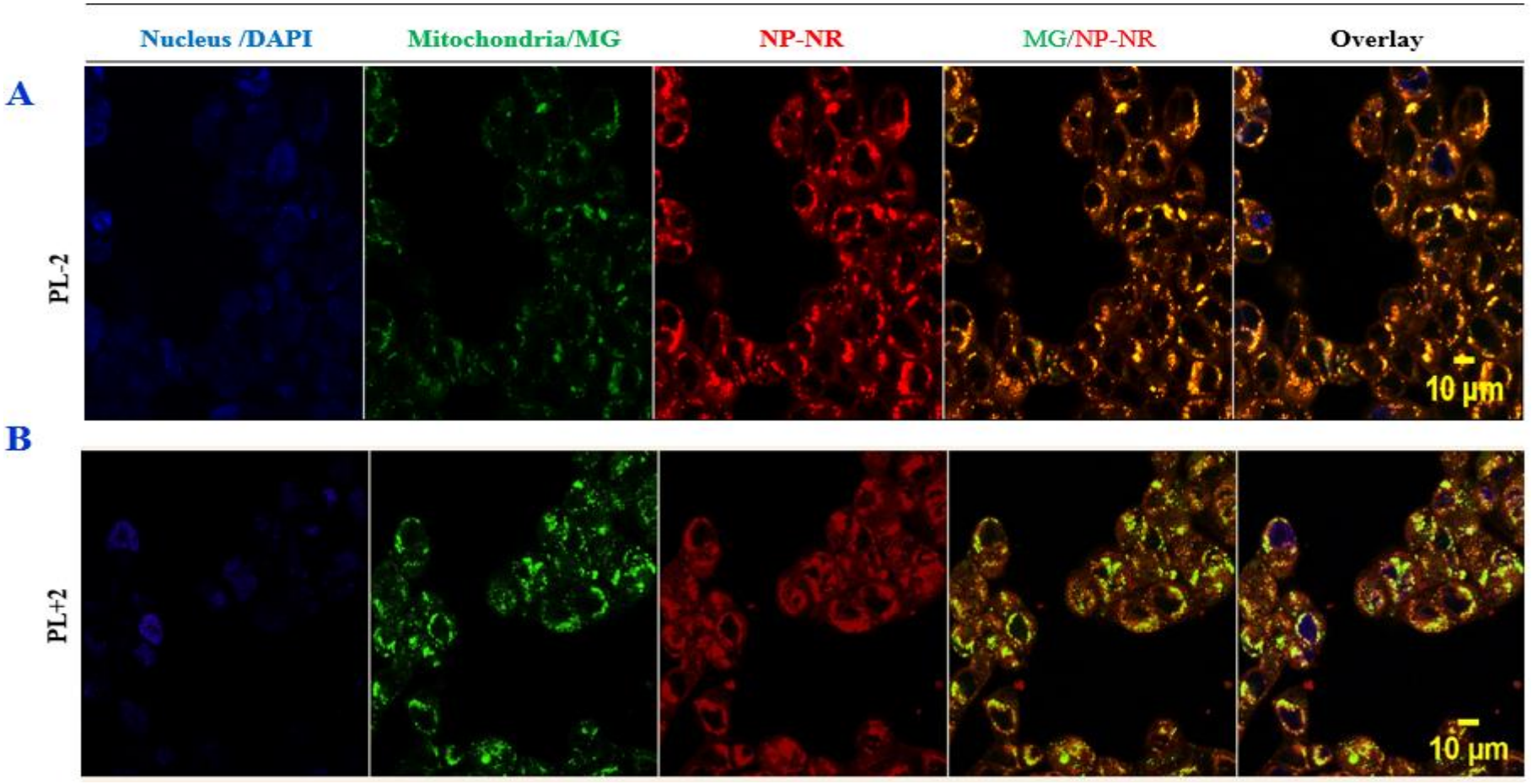

Figure. 4.17. Confocal microscopy study of NPs co-localisation with mitochondria in Calu-3 cells where nuclei labelled by DAPI and mitochondria labelled by MG after incubation for 1 hour with (0.5 mg/mL) NP-NRs (A) *PL*-2, (B) *PL*+2.

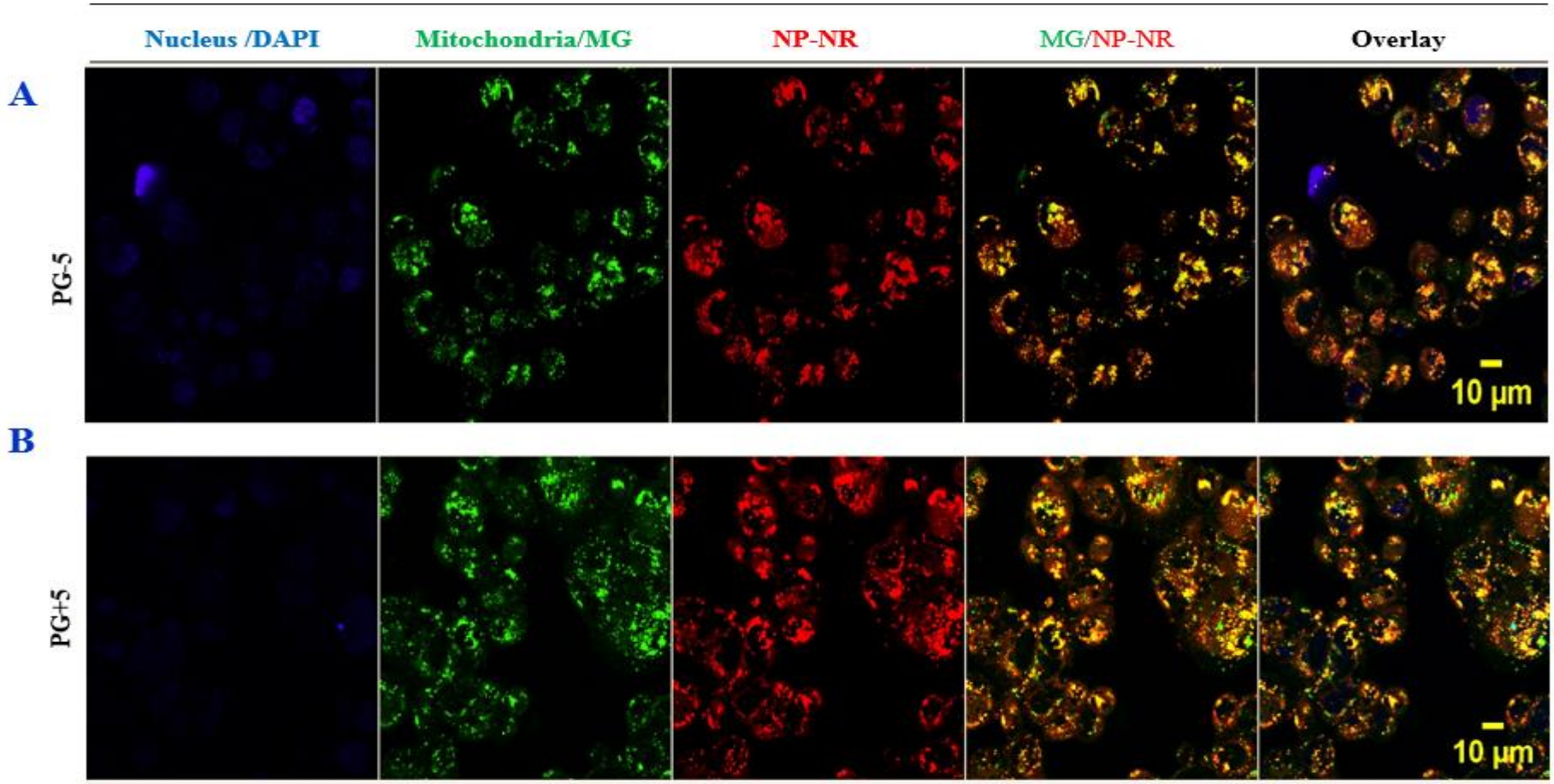

Figure. 4.18. Confocal microscopy study of NPs co-localisation with mitochondria in Calu-3 cells where nuclei labelled by DAPI and mitochondria labelled by MG after incubation for 1 hour with (0.5 mg/mL) NP-NRs (A) *PG*-5, (B) *PG*+5.

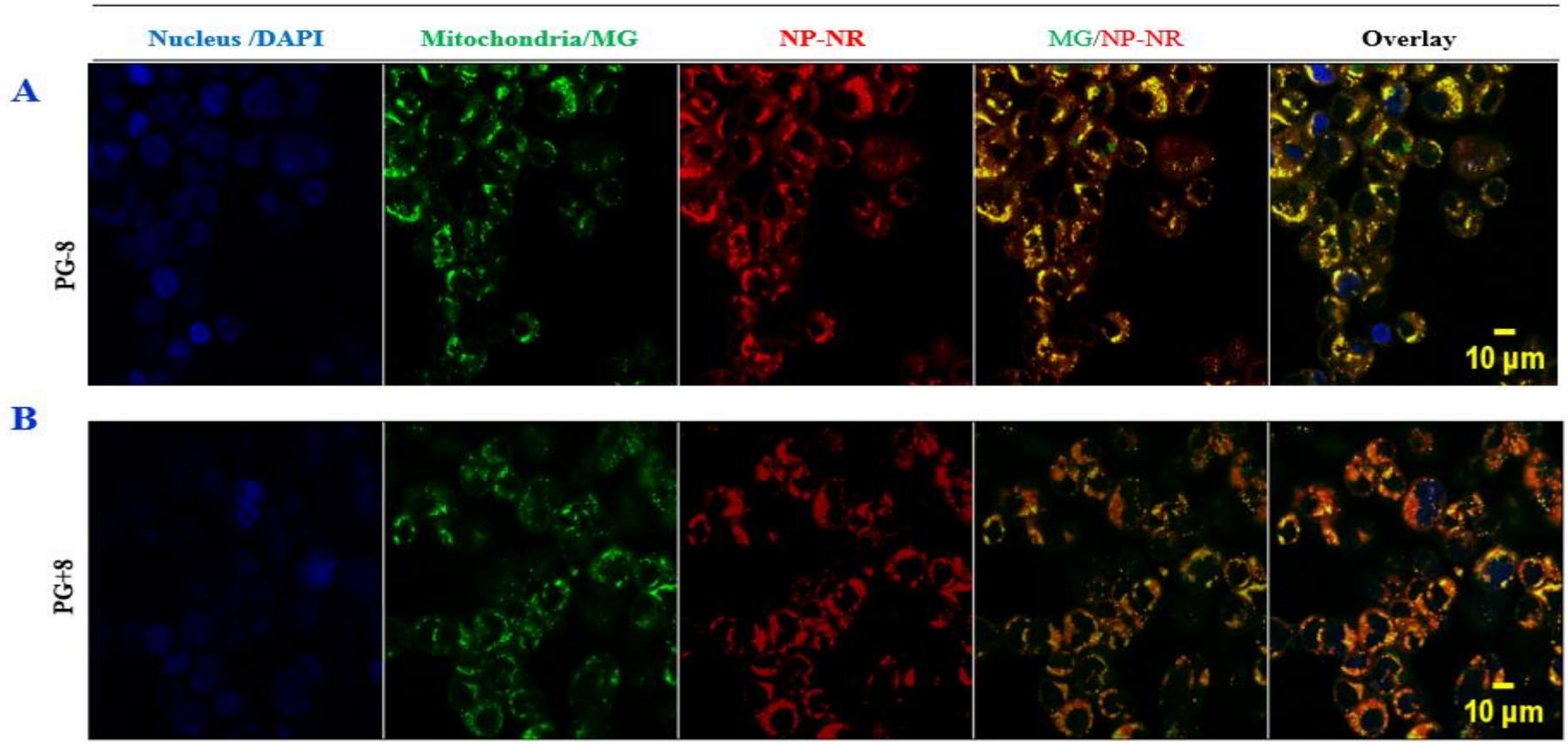

Figure. 4.19. Confocal microscopy study of NPs co-localisation with mitochondria in Calu-3 cells where nuclei labelled by DAPI and mitochondria labelled by MG after incubation for 1 hour with (0.5 mg/mL) NP-NRs (A) *PG*-8, (B) *PG*+8.

4.5. Discussion:

4.5.1. TEER and The Apparent Permeability Coefficient (P_{app}):

Calu-3 under ALI showed formation of tight polarized monolayers that have been reported to have strong resemblance to lung cells *in vivo* (277), improved reproducibility and more differentiation (single columnar epithelium with apical cilia, mucous secretion, and tight junctions) (518, 524) to the airway epithelium than other lung cell lines such as primary (human bronchial epithelial cells, HBEC), or continuous (BEAS) bronchial epithelial cell (525). Moreover, Calu-3 under ALI have been reported to secrete mucous (rich in mucin) more than the liquid-covered culture LCC (281, 526). In addition, Calu-3 shows airways functional properties such as transferrin transporter, metabolizing enzymes; cytochrome P450, and express cystic fibrosis transmembrane conductance regulator (CFTR) genes (527). Hence, they have been reported to show good *IVIVC* correlation for predicting the *in vivo* lung drug absorption (278, 513, 527). Furthermore, Calu-3 tight monolayers showed consistent TEER values that represent the measured electrical resistances developed by the monolayers for the passage of the electric current through the epithelium (518). Hence, Calu-3 under ALI represent a powerful *in vitro* model to study the *in vivo* lung barrier.

TEER values measured over time (Figure. 4.3) showed increasing TEER values until the experimental day (Day 15) for NP exposure. TEER values recorded and accepted for the experiment were > 800 ohms.cm^2, which denoted successful development of TJs and polarized monolayers mimicking *in vivo* conditions (518). TEER values reported in literature for Calu-3 polarized models varies from 500-1200 ohms.cm^2 (276, 278) depending on the condition of growth, time and passage number (526). In this current study, Calu-3 with passage numbers [20-30] grown under ALI for

15 days produced TEER values of ~800-1200 ohms.cm^2. These results were similar to what was previously reported for Calu-3 under ALI, with TEER values peaking above 500 Ohms.cm^2 deemed as confluent monolayers with tight TJs (281, 518, 521, 526, 528).

Apparent permeability coefficient (P_{app}): The integrity of the epithelial barrier, using P*app* coefficient of [^{14}C]-mannitol as a paracellular marker, was investigated on Calu-3 polarized monolayers grown under ALI (Figure. 4.4, 4.5, & 4.6.). Radiolabelled [^{14}C]-mannitol is one of many paracellular markers (e.g. Na fluorescein, Inulin, and lucifer yellow (276)) available to study the paracellular transport across polarized monolayer. It has small MW (182 Da), hydrophilic molecule that is passively transported across the monolayers and has been used in many studies (276, 518, 527). The experimental NPs exposures used 8 different types of NPs based on their physicochemical characters under different concentrations and time intervals. The outcomes from this experiment can be noted at the following:

Firstly, there were no statistically significant differences between the different types of NPs under the tested concentrations (0.125, 0.5, & 2 mg/mL) over the study interval (1, 2, 3, 4, 5, & 24 hr). In addition, there were no statistical differences between the different sizes of NPs: 200 nm, 500 nm, 800 nm, or charge: negative or positive, or chemistry (*PG* vs *PL* NPs). Most of the P*app* values under these exposure conditions were similar to the control and not significantly different. This denoted the strength and well preserved integrity of the Calu-3 polarized monolayers over the study interval and confirmed the barrier ability to filter a wide range of NPs with variable underlying physiochemical properties (281, 518, 521). That's similar to what is seen with the natural lung barrier being able to act as a defence barrier against various inhaled particles, dust, bacteria and viruses (246).

Secondly, the P*app* coefficient of [^{14}C]-mannitol were sustained under what was previously reported in literature as acceptable range of paracellular or passive absorption rates across Calu-3 monolayers. This range varies from 1- 4 x 10^{-7} cm sec^{-1} for the integrity of Calu-3 polarized monolayers under ALI (276, 281, 513, 518, 524, 527). This range was reported for other types of polarized monolayers for different epithelial cells, such as NCI-H441 (529), hAELVi cells (530), MucilAir (527), 16HBE14o- (531, 532), and non-lung epithelia such as Caco-2 (533, 534), MDCK (527) and many other cell lines (534).

Thirdly, the trend of the P*app* coefficient of [^{14}C]-mannitol with increasing the NPs concentrations; P*app* coefficient of [^{14}C]-mannitol showed a concentration dependent increase, with the highest concentrations (2 mg/mL) responsible for the highest P*app* values. This meant the barrier integrity was negatively influenced at these high concentrations and was manifested by increasing the P*app* values/permeability. However, the paracellular P*app* values were in the acceptable range of paracellular marker permeability reported by different studies (516, 518, 521, 535). If paracellular P*app* values showed levels above the maximum of the acceptable range (P*app* values > 4 x 10^{-7} cm sec^{-1} denoting cellular injury and serious damage to TJs), it meant the barrier integrity or TJs had been damaged. For example, if the tested compounds damaged the TJs or caused cellular toxicity, this deterioration to the barrier integrity would result in an increase of the paracellular P*app* values. However, all NPs and their concentrations showed P*app* values that were maintained within the acceptable range of paracellular permeability denoting no adverse effects on TJs.

It must be emphasised these are experimental doses that are rarely or not going to be achieved on therapeutic inhalation doses due to the high surface area of the lungs. To explain more, a schematic illustration of the dose distribution over the surface area

of different *in vitro* and *in vivo* exposures is shown in Figure. 4.20. This illustration shows the dose dilution by the surface area under different exposures, for example in 96 wells plate or 12 Transwells plate used for *in vitro* experiments in comparison to an inhalation dose in adult lungs *in vivo*. The lowest concentration (0.125 mg/mL) is the nearest to a therapeutic dose range and showed almost similar or even overlapping trend to the NC. This confirmed the lung barrier safety at such exposure to very low doses of NPs investigated in this study.

The highest concentration used (2 mg/mL) had shown cytotoxicity effects on Calu-3 cell lines after 24 hr exposure as previously reported in Chapter.3 such as reducing the viability by AB, producing ROS etc. Hence, it was expected to see some cytotoxicity on the barrier manifested by increasing barrier permeability with P*app* values > 4×10^{-7} cm sec^{-1}. However, there was no indication of cytotoxicity or impairing the barrier integrity. This was due to Calu-3 under ALI being tightly packed monolayers with well-developed TJs over the Transwells in comparison to 2 days interval of Calu-3 growth (~ 80% confluency) in case of 96 well plates experiments. The dose delivered per surface area (as explained above in Figure. 4.20) of Transwells was lower than the 96 well plates and hence showed no toxic effects manifested by impairing the barrier integrity. In addition, Calu-3 under ALI were reported to be well differentiated and express mucus production (281, 518, 524), which has been shown to reduce or inhibit the molecules mobility across the epithelium (247).

This inhibitory effect correlates with the MW and lipophilicity that may hinder the permeability of the NPs. In addition, mucus has high mucin content of high viscosity and mucus mesh pores size. The size filtering pores are reported to be in the range of 100 nm up to few micrometres in diameter and effectively can entrap various sizes of NPs (246, 247). Taking into consideration, the agglomeration and size increase with

increasing the concentrations, and more pronounced with positively charged NPs (as shown from chapter.2 results), the big agglomerates are filtered earlier on the initial mucosal layers, leaving only smaller NPs to migrate deeper tightening the mucosal mesh. This could possibly explain the lack of toxicity associated at the highest concentrations.

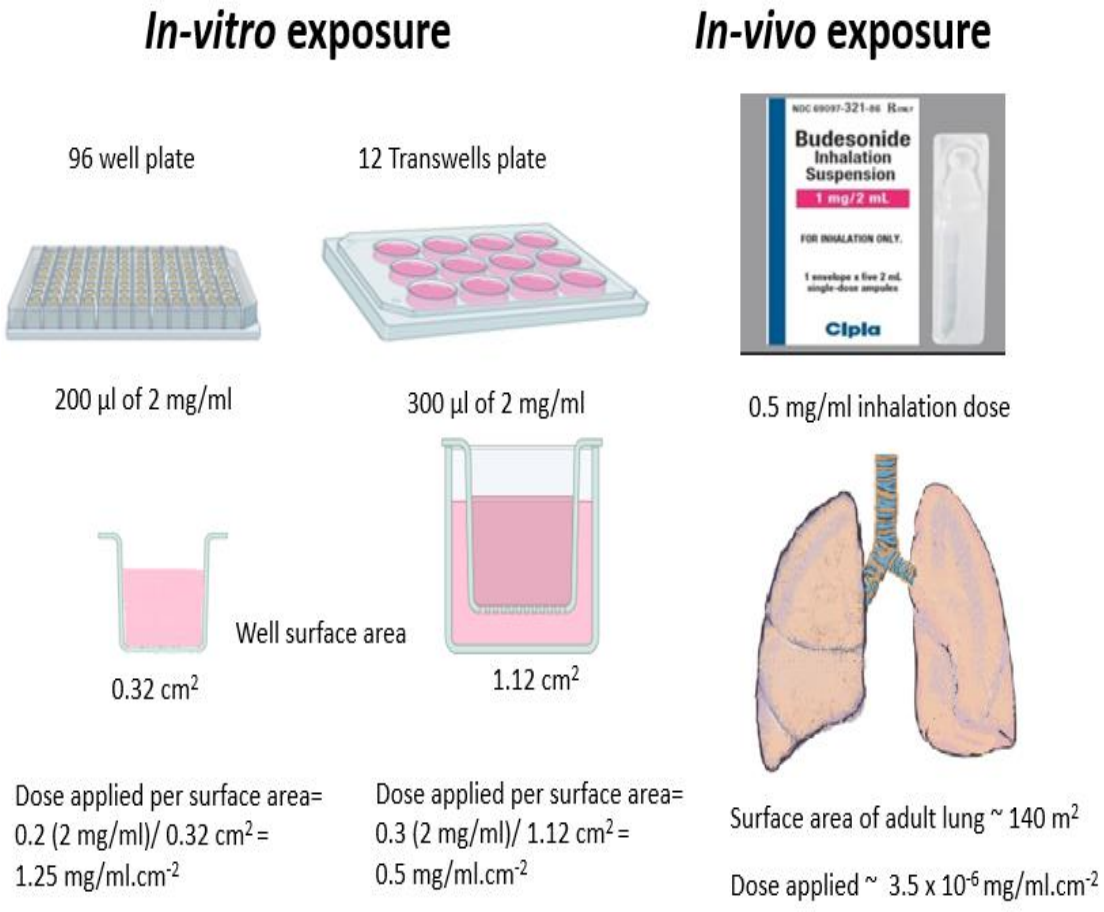

Figure. 4.20. Schematic representation for the dosing between *in vitro* exposure: 96 well plates and 12 wells Transwell permeable inserts, and *in vivo* exposure.

A study by Mura *et al.*, (474) investigated the surface charge effect of three *PL* NPs (size: 100-200 nm, functionalized by three different surface charges; neutral/ PVA, negative/ PF68, and positive/ CS) on Calu-3 monolayers integrity under ALI. This was investigated by evaluating the TEER values over time and quantifying the fluorescent labelled NPs permeability. Neutral and negatively charged *PL* NPs didn't induce any

TEER value changes over time (up to 24 hr). However, *PL*/CS NP had induced a transient lowering of the TEER values with increase in NPs permeability that recovered to normal after 3 hr. This was due to the ability of CS to interact with the negatively charged mucus. This was documented for CS as a mucosal absorption enhancer (536) that interacts with the mucus with high mucoadhesive/ penetrative properties and opens TJs (537). Moreover, Mura *et al*., studied the NPs permeation through mucus by staining with a fluorescent label (AlexaFluor-488-labeled wheat germ agglutinin) by confocal microscopy. *PL*/PF68 (highest hydrophilicity) had crossed the barrier earlier than *PL*/PVA and *PL*/CS and was internalised faster. However, the later NPs showed a slow and sustained crossing over the mucus. The cellular uptake evaluated by quantifying the fluorescent labelled (Rhodamine dye) showed *PL*/ PF68 (negatively charged) were better internalised than *PL*/CS and *PL*/PVA, which showed similar amounts. When evaluating the mucus gene expression (via MUC5AC mRNA expression or MUC5AC protein levels), none of the NPs induced any change in the mucus production. This indicated the ability of tuning the NPs physicochemical properties as well as the safety of *PL* NPs on the lung barrier.

Another study used three different *PL* polymers (*PL* 50:50 ester terminated (R1), *PL* 50:50 acid terminated (R2), *PL*-PEG diblock (50:50 ester terminated and 10% PEG) (R3)) to formulate 12 NPs with median size differences 100-600 nm and negatively charged with PVA. Blank NPs and drug-loaded with a model drug showed well preserved epithelial integrity of Caco-2 cell lines and a better P*app* profile for R1 NPs confirming the chemistry had an effect on the internalisation and permeability of NPs (538). However, the authors' focus was to improve the permeability of the model drug, their results confirmed the versatile ability of tuning the NPs physicochemical characters to control NP residence time and drug release profile when meeting the tight

polarized monolayers. These NPs successfully delivered fenretinide as a model drug with lowering its toxicity on the epithelial barrier whilst preserving the TJs integrity. That was similar to the observed results of *PL* NPs in the current study where the epithelial integrity was preserved. These are just examples for *PL* NPs, while all *PG* NPs have acted similarly to *PL* NPs denoting their well tolerability and safety interactions with the epithelial barrier.

Fourthly, the trend of the P*app* coefficient of [^{14}C]-mannitol over time. The highest values of P*app* were reported at T1 with a subsequent slow decline over time until T24. While under all different NPs exposures, the P*app* values were higher at all study time intervals (apart from the lowest concentrations almost mirrored NC) than NC but followed similar decreasing trend as the NC. This indicated the decline was related to the barrier where the barrier was developing more restrictive properties (less permeable) over time. From T1 to T2, the barrier or cells developed some cellular machinery to restrict the TJs for the next study intervals. During the interval of 2-5 hr, the barrier showed a very slow decline with slight changes to the permeability. This suggests that these intervals are more suitable times to measure the P*app* for drug loaded NPs. P*app* studies of many NPs and other drugs across the polarized monolayers use the P*app* of paracellular marker or evaluating TEER values postexposure or both as probes of the barrier integrity after NPs exposure. However, postexposure assessment of TEER values after the experiment were not recorded to avoid radioactive contamination to the electrodes. The paracellular P*app* values were reported showing a decreasing trend over time in many studies such as Bol *et al.*, (535), Ehrhardt *et al.*, (521) Foster *et al.*, (524), Bharatwaj *et al.*,(528), Stentebjerg-Andersen *et al.*, (518) and Grainger *et al.*, (281). These studies had evaluated TJs proteins; ZO-1 occludens during the experimental exposure to show the TJs proteins expression was increasing over

time, with surrounding TJs as belts that can restrict the paracellular flow of solutes and molecules (535).

4.5.2. Transport Mechanisms:

All NPs had been internalized mainly via transcellular active endocytosis processes. However, quantifying NPs uptake to uncover which NPs were better internalised was not feasible (due to the unequal NR dye loading capacities). The current study investigated NPs internalisation process by using a group of pharmacological endocytosis inhibitors covering many mechanisms as indicated in Table. 4.1 (505, 506, 522, 523). The study of the internalisation and its mechanisms by inhibitors was limited for one-hour exposure (491). It is commonly recommended to study the internalisation under these inhibitors for short periods of exposures preferably for one hour (539). The long periods of exposure to these inhibitors allows the cell to activate alternative pathways of internalisation (159, 493, 505, 506, 523). The toxicity under these inhibitors as well as the NR dye released during the exposure were excluded. However, the concentrations for these inhibitors used were similar to what was reported in literature for Calu-3 and other cell lines (173, 491, 522, 523, 540). The NR dye is reported to be released within culture media containing high amounts of serum proteins (541-544). Here, the current study used SFM with all cellular exposures to NPs due to the reduced size and charge variation compared to CM containing 10% FBS as concluded from Chapter.2 experiments; section 2.4.3. The NP-NRs were used from freshly prepared emulsions and there was no degradation risk. However, the uptake of any released NR to the surrounding medium was found to be very low and slow process requiring more than 3 hr to achieve 25% NR uptake compared to NR internalized via NPs (poly(n-butyl cyanoacrylate) PBCA based NPs) per cell (541,

543). Furthermore, another study by Raudszus *et al.,* (545) had reported a release of < 0.1 % Lumogen® Red dye from *PL*A NPs in media containing 10% FBS up to 24 hr.

The possibility of NP-NRs being attached to the cell membranes rather than being intracellularly internalized were excluded by the following experimental procedures;

- The cell monolayers were washed three times with ice-cold PBS containing 5 % trypan blue. This step immediately stopped the active internalisation at this time point by cold temperature (159, 178). Moreover, the trypan blue is a cell impermeable dye that quenches the fluorescence from free NPs in solution and NPs attached to the outer cell membranes (522, 523).
- Trypsinization step was to detach the cell monolayers from the plate. In the process, the cell membranes were gently eroded and detached from one-another, the underlying well-surface, and from NPs on their outer surfaces (463, 464).
- The samples were collected in Eppendorf's and centrifuged. The speed used was enough to collect the cells and leaving any free NPs in the solution to be decanted and discarded. However, this was investigated by a study (543) and proved three washes with PBS and after one centrifugation had greatly diminished the attached NP-NR from the surface of the monolayers.
- Flow cytometry techniques are highly advanced with high precision. They enable the differentiation between the cellular component of the sample and the non-cellular debris and particles that can be excluded by the gating strategy (508, 544, 546).

Thus, the fluorescent signals measured were solely originated from intracellular internalised NP-NRs. However, the low MFI recorded at 4 °C can be attributed to

passive NR dye entry via diffusion into the cells from the NPs attached to cell membrane as previously reported (353, 547). A summary of the results is shown in Table 4.2. All different types of NPs internalisation were active/energy dependent processes where a large inhibition of the uptake under 4 ^{o}C was encountered with all NPs. This was similar to what was reported for different polymeric and non-polymeric NP due to their large size and MW that limits their passive diffusion (499, 505).

PG-2 NPs internalisation was dependent on GTPase-dynamin, tyrosine kinase-caveolin, microtubules, and cholesterol rafts and not dependent on actin polymerization, Na+/H+ ionic channels of micropinocytosis, and Clathrin. *PG*-2 NPs showed ~ 20% internalisation under passive uptake (4 ^{o}C). **The uptake was mostly by caveolin and macropinocytosis.** While its positive counterpart, *PG*+2 NPs internalisation was dependent on GTPase-dynamin, tyrosine kinase-caveolin, actin polymerization and microtubules, and not dependent Na+/H+ ionic channels of micropinocytosis, cholesterol depletion, and clathrin. *PG*+2 NPs showed ~ 25% internalisation under passive uptake (4 ^{o}C). **It is uptake mostly by caveolin endocytosis.**

PL-2 NPs internalisation was dependent on GTPase-dynamin, tyrosine kinase-caveolin, and clathrin pits assembly. It was not dependent on actin polymerization, microtubules, and Na+/H+ ionic channels of micropinocytosis. It showed more inhibition under caveolin than clathrin, so its uptake mostly **caveolin and clathrin mediated endocytosis**. *PL*-2 NPs showed ~ 10% internalisation under passive uptake (4 ^{o}C). While its positive counterparts, *PL*+2 NPs internalisation was dependent on GTPase-dynamin, tyrosine kinase-caveolin, actin polymerization. *PL*+2 NPs showed ~ 20% internalisation under passive uptake (4 ^{o}C). *PL*+2 NPs uptake mostly facilitated by **caveolin endocytosis**. *PG*-5 and *PG*+5 NPs internalisations were dependent on

clathrin (70% reduction, Inh7), caveolin (50% reduction, Inh2), and to lower extent microtubules and macropinocytosis (20%, Inh4). They are mostly facilitated by **clathrin and caveolin endocytosis**. *PG*+5 showed more passive uptake (~ 15% internalisation under passive uptake (4 ^{o}C) than *PG*-5 (~ 5% internalisation under passive uptake (4 ^{o}C).

PG-8 internalisation was dependent on **clathrin** while *PG*+8 was dependent on clathrin and actin polymerization. Their uptake was facilitated by **clathrin endocytosis**. Their passive uptake amounted to ~ 30% internalisation under passive uptake (4 ^{o}C).

Comparing the current study findings to the literature, there were many studies supporting the physicochemical properties of NPs generated a unique identity for each NPs, with dependence on the cell type, showed internalisation by different mechanisms (159, 493). To the best of our knowledge, the current study represents a novel evaluation of both *PL* and *PG* NPs internalisation mechanisms in Calu-3 cell lines. However, *PL* NPs internalisation mechanism had been evaluated in many cell lines. The physicochemical properties of the NPs and the cell type Play a major role in the internalisation mechanism.

PL NP ~ 100 nm size negatively charged showed internalisation by different mechanisms; clathrin, caveolin, and lipid raft endocytosis in MDCK cell line (548). While the same authors reported in another study (549) that *PL* NPs ~ 80 nm size negatively charged showed internalisation by the same mechanisms with addition of macropinocytosis in Caco-2 cell line. *PL* NPs of ~ 160 nm size and negatively charged was preferentially internalised by monocyte derived DCs via macropinocytosis while the cationic CS coated *PL* NPs of ~180 nm size were internalised via clathrin endocytosis (550). Another study by Vasir *et al.,* (551) investigated *PL* NPs (290 nm

and negatively charged NP, and 310 nm coated with cationic poly(L-lysine) with negative charge in neutral pH and turns positive in acidic pH in human breast carcinoma cell line MCF-7 to show both NPs were preferentially internalised by clathrin endocytosis. In addition, another study by Sahin *et al.*, (552) investigated the internalisation mechanism of two *PL* NPs of different sizes (230 nm, 160 nm, negatively charged) in HEK293 cell line and both NPs were internalized by different mechanisms via caveolin, clathrin, and macropinocytosis with higher uptake compared to smaller NP. The current results are favourably similar to what was previously reported by literature where NPs of size 150-200 nm are internalized by either caveolin or clathrin endocytosis for the small NPs of 200 nm; *PG*-2, *PG*+2, *PL*-2, and *PL*+2. However, the larger sizes NPs (*PG*-5, *PG*+5, *PG*-8, and *PG*+8) indicate internalisation via clathrin and caveolin that are commonly reported for smaller NPs ~ 200 nm. This could be due to the dispersity of NPs with the smaller particles were more effectively internalised than the larger NPs (552).

Visual confirmation by CLSM showed all NPs had been internalised. The NPs were trafficked intracellularly and showed some co-localisation with the lysosomes denoting and confirming their vesicular transport. NPs showed some co-localisation with mitochondria denoting their ability to interact with subcellular targets that can be used for therapeutic purposes and designing less-toxic carriers.

Table. 4.2. Summary of the endocytosis transport inhibitors results.

Mechanism Inhibited	*PG*-2	*PG*+2	*PL*-2	*PL*+2	*PG*-5	*PG*+5	*PG*-8	*PG*+8
Energy/active process (4 ^{o}C)	+ + + +	+ + + +	+ + + +	+ + + +	+ + + +	+ + + +	+ + + +	+ + + +
GTPase-dynamin (Inh1)	+ + + +	+ + +	+ + +	+ +	-	-	-	-
Tyrosine Kinase-Caveolin assembly (Inh2)	+ + + +	+ + +	+ + + +	+ +	+ + + +	+ +	-	-
Actin polymerization (Inh3)	-	+ + +	-	+ +	-	-	-	+ +
Microtubules arrangement (Inh4)	+ + + +	+ + +	-	-	+ +	+ +	-	-
NA^{+}/H^{+} exchange marcopinocyctosis (Inh5)	-	-	-	-	-	-	-	-
Cholesterol de*PL*etion-Caveolin (Inh6)	+ + + +	-	-	-	-	-	-	-
Clathrin pits assembly (Inh7)	-	-	+ +	-	+ + + +	+ + + +	+ +	+ + +

Endocytosis Mechanism	Caveolin and macropinocytosis	Caveolin and macropinocytosis	Caveolin and Clathrin	Caveolin and macropinocytosis	Caveolin and Clathrin and	Clathrin and caveolin	Clathrin	Clathrin and macropinocytosis

4.6. Conclusion:

Understanding the NPs interaction at the cellular and molecular levels provides immense abilities to tune the NP physicochemical characters to enhance nano based medicines. There are many available methods to quantify and confirm the NPs internalisation. The current methods faced with many challenges not only because of NP novelty but also for the complex nature of their cellular and subcellular interactions that require careful monitoring of possible NP interference and to minimize it as possible. For reliable NPs determination of NPs internalisation, it is recommended to combine different approaches, e.g., flow cytometry and visual microscopy.

5. General Discussion, Conclusion, and Future Directives

5.1. General Overview:

NPs Are Promising Vehicles for Pulmonary Drug Delivery:

At nano scale, i.e., 1-1000 nm, NPs develop exceptional physicochemical properties rendering them very attractive to pharmaceutical and clinical applications. NPs are renovating new class of medicines known as *Nanomedicines* that have enhanced properties to cross biological barriers (32), encapsulate a variety of active agents (553), allow for active targeting and control of drug release (554), and allow for combinational therapy (50). Consequently, NPs enabled drug delivery enhances the clinical outcomes, e.g., lowering off-target side-effects, lowering dose frequency, improving the therapeutic efficacy, and increasing patient compliance.

Recently, biodegradable polymers appeared very attractive for NPs formulations, fuelling the development of drug delivery systems due to their biocompatibility, biodegradability, diversity and versatility of physicochemical properties, and ease of fabrication and functionalization (10, 55-58). *PL* is an aliphatic polyester polymer and widely used for many biomedical applications approved by FDA for clinical use (68-70). The main drawbacks of *PL* as a polymer in fabricating NPs are the bulk hydrolytic degradation, accumulation of acidic monomers causing a reduction of local pH at the site of drug action. This affects the stability of pH-sensitive drugs and the long degradation with repeated doses and local acidity promoting an inflammatory response (68). Thus, *PG* is such an alternative polymer that has been developed and characterized in-house in LJMU laboratory to improve upon the physicochemical properties of *PL*. It has successfully encapsulated many small drugs and macromolecules, i.e., ibuprofen, dexamethasone phosphate, bovine serum albumin, pneumococcal protein, gene delivery, and vaccine; showing very promising results for treating lung diseases and vaccine delivery (23, 25, 34, 38, 74, 77, 79-81).

There is burgeoning interest in NP drug delivery to the lungs via aerosols. NP aerosols can localize the drug topically in the lungs with enhanced pharmacokinetic properties in terms of retention and direct local action in the treatment and management of lung diseases, compared to other routes of administration. This limits the systemic off-target side effects. Moreover, lung delivery can be used as a systemic portal for drug delivery with better patient compliance and enhanced therapeutic efficiency (32, 86, 87)

The aims of the project were to evaluate the nanotoxicological effects of NPs formulated from *PL* and *PG* polymers stem from their chemistry, size, and surface charge using pulmonary cell lines.

5.2. NP Formulation and Characterisation, NP Stability and Degradation:

Eight different NPs were formulated from *PG* and *PL* polymers using emulsification-solvent evaporation methods and characterised for their size, charge, and shape.

NPs stability after dispersion in culture media, e.g. in SFM or CM was investigated immediately (T0) and after 24 hr (T24) incubation (37 ^{o}C) for any changes in NP size and surface charge (Figure. 2.6.). All NPs showed an increase in their size at T0 and further increase at T24. All negatively charged NPs indicated lowering their charge, while the positively charged exhibited conversion to negatively charge. The positively charged NPs showed higher size increase than their negative counterparts. The changes were more manifested in CM than SFM. These findings were similar to literature findings where protein rich media showed more adsorption to the surface of NPs and to a greater extent to the positively charged NPs than the negatively charged

NPs (97, 253, 345). Hence, NPs dispersion in SFM were more stable than in CM, thus SFM was chosen as the dispersing medium for NPs in subsequent investigations.

The degradation profiles of *PG* and *PL* NPs (200 nm) was studied under two conditions; PBS stored at 4 ^{o}C (to simulate *in vitro* storage conditions) and in SLF, to simulate *in vivo* degradation) for 0, 1, 3, 7, 14, 28 days. *PG* and *PL* NPs size, charge, MW, and pH changes were evaluated.

Size: *PG* and *PL* NPs had similar sizes but different trends of changes under different conditions (Figure. 2.7. A & B). *PG*-2 indicated aggregation after one week with high variations towards D28 which were more pronounced in SFL than PBS. *PL*-2 had shown slight changes in size either increasing (in PBS) or decreasing (SLF) after one week. This implied; firstly, a more stable size for *PL*-2 NPs in the suspension than *PG*-2, and secondly, a degradation trend of *PL*-2 in SLF than in PBS that indicated the ionic and salt strength of SLF over PBS (346).

Zeta potential: *PG*-2 showed two different trends of a charge increase with time in PBS and SLF that was more manifested in SLF than PBS representing a difference between the two buffers (Figure. 2.7. C & D). However, *PL*-2 zeta potential changes in PBS and SLF showed a trend toward zero by the end of the experiment. This was due to the effect of chelation by ionic and salts contents of the media that were more manifested in SFL than PBS (348).

MW changes: MW changes observed for both polymers under PBS and SLF conditions showed modest changes in MW over time with small decrease toward the end of experiment; D28 (Figure. 2.7. G & H). This indicated MW changes could be slower compared to size, zeta potential and pH changes. This was due to the nature of

these polymers of having linear chains of variable lengths giving a wide distribution of MW, with the shorter chains degrading faster (347).

pH changes: pH changes are related to the polymeric structure, its functional surface groups and its degradation products (Figure. 2.7. E & F). *PL*-2 NPs are based on *PLGA* 50:50 acid terminated polymer (the terminal functional group is capped by carboxyl group) that expressed acidic pH. *PL*-2 showed a decrease in pH after two weeks/ D14; the sharp acidic changes toward the end of the experiments (pH 5.5 in PBS, pH 6.5 in SLF) that denoted the degradation products were of acidic nature and more degradation occurred in PBS than SLF. *PG*-2 NPs were based on *PGA-co-PDL* ester terminated with OH group expressing alkaline pH. *PG*-2 showed gradual decrease of pH with time and towards the end of the experiment was almost a neutral or slightly alkaline pH. This denoted less acidic degradation products (adipic acid of less acidic nature) and a slower degradation compared to *PL*-2 suggesting better performance of *PG*-2 in the biological media and of potential importance to lower toxicity and inflammatory effects that would enhance *PG* use for lung delivery.

Both *PL* and *PG* polymers of α-polyester family are known to degrade heterogeneously via bulk erosion by chain random scission through hydrolysing ester linkages, where the rate of hydrolysis and water diffusion into the NP carriers are faster than the release of by-products (348, 349). The hydrolytic degradation rate of *PG* and *PL* NPs are influenced by many parameters such as monomeric ratio, nature of the monomers as well as polymer hydrophobicity and surrounding medium acidity. *PL* with monomeric ratio of 50:50 show faster degradation among all *PL* polymers. However, *PG* has equal monomeric ratio of its three monomers that indicated a longer polymeric chain of each molecule, and one of its monomers (ω-pentadecalactone) is composed of a macrolide lactone which is a 15 membered cyclic lactone ring that can be correlated

to its slower degradation and hydrophobicity (351). The increased acidity over time enhanced the degradation of *PL* NPs by facilitating autocatalytic degradation (349) and was consistent to previously published reports (350, 352).

5.3. Toxicological Assessment of Polymeric NPs Using *In vitro* Methods:

5.3.1. Pulmonary Cell Lines:

Calu-3 Cell Line: Calu-3 is one of the commonly used human lung cell lines. They are of bronchial epithelial adenocarcinoma origin. They can be cultured under ALI as well as LCC. Calu-3 under ALI develop tight polarized monolayers and more differentiation to airway epithelium (columnar epithelia, ciliated, mucin production). Hence, it is a widely available *in vitro* model mimicking *in vivo* lung (279).

THP-1 **Cell Line**: THP-1 is a human monocytic cell line and a commonly used model to represent immune response. THP-1 undergo differentiation to adherent non-proliferative macrophages by activation of PKC pathway by PMA (399, 478). THP-1 macrophages retain their inflammatory characteristics, i.e., they express differentiation markers (CD14, CD36) that respond to LPS. They are reported to produce a variety of inflammatory mediators such as TNF-α and IL-1ß, denoting intact TL4R, activation of NF-κß and MAPK pathways (555). Hence, THP-1 was chose to represent an inflammatory lung model (381, 556).

5.3.2. Toxicological Screen:

General Viability: Cell viability after NP exposure was evaluated at T1 after discontinuing the NP exposure (application of 3 washes or No wash) to evaluate the metabolic state immediately after NPs removal, while the viability evaluated at T2 and T3 was to indicate the ability of cell recovery (Figure. 3.5., 3.6, & 3.7). All NPs showed

a trend of concentration-dependent decrease of the cell viability. Cell recovery: At the lowest concentrations (0.125-0.25 mg/mL), cell viability had resumed to 100% or more from the NC, indicating the ability of the cells to recover and the cellular injuries were reversable. At high concentrations, small NPs of *PG* and *PL* were recovered to 80-100% while the larger sized NPs staggered at 50-75% denoting a serious and irreversible cellular injury. This was similar to what was previously reported for cellular haemostasis in response to different cell injuries (A summary of results are showed in Table. 5.1) (400).

ROS: ROS detected after 24 hr exposure of Calu-3 cells to NPs evaluated via H_2DCFDA confirmed a significant involvement of ROS induction in the cellular cytotoxicity after NPs exposure (Figure. 3.8.). All NPs showed a trend of increasing the ROS production with increasing NP concentration compared to NC (Table. 5.2).

Mitochondrial Membrane Potential: All NPs showed a significant decrease of $\Delta\Psi m$ that could be mirrored with the increased ROS production (H_2DCFDA assay) and decreased viability (T1 with 3 washes) after 24 hr NPs exposure (Figure. 3.10.). Lowering $\Delta\Psi m$ (depolarized state) was due to the loss of control on mitochondrial membrane permeability and opening mPTPs (404, 408, 432) that might adversely affect the cellular haemostasis and is considered as a sign of apoptosis (Table. 5.3) (408, 424).

Cell Membrane Integrity: Cell membrane integrity was evaluated by LDH Total (with the use of total cell lysis) or LDH Release (spontaneous release in the supernatant without cell lysis step) assays after Calu-3 cells exposure to NPs for 24 hr (Figure. 3.11). All NPs showed a similar trend of a concentration dependent decrease of LDH Total compared to NC, whereas, NPs showed a similar trend of a concentration dependent increase of LDH Release from the NC. However, all the released amounts

were significantly lower than the NC at all concentrations of all NPs that denoted a possibility of NP interference and or underlaying cytotoxicity (Table. 5.4).

Apoptosis and Necrosis: A time coarse study of apoptosis and necrosis was performed after 4 hr, 12 hr and 24 hr of Calu-3 exposure to NPs. Two quadrants: Late apoptotic (double positives, Figure. 3.12.) and necrotic (7-AAD positive only, Figure. 3.13.) indicated time related changes. **At T4:** the late apoptotic populations were higher among smaller NPs than larger NPs and ranging from 20-35% of the total cell population, whereas the necrotic populations were mainly seen at higher concentrations and ranging from 10-20% of the total cell population. **At T12:** there was a general decrease of the percentages of both quadrants, while late apoptotic population ranged between 10-20% of the total cell population that was similar to all NPs. The necrotic population showed an increase with larger NPs with population percentage ranging between 15-30% of the total cell population especially at the high concentrations. **At T24:** there was further decrease of the percentages of both quadrants, while late apoptotic population ranged between 10-15% of the total cell population that was higher in larger than the smaller NPs. Although the necrotic population showed a similar or slight decrease in population percentage of smaller NPs ranging ~ 15% of the total cell population. The larger NPs showed a decrease of necrotic population percentage even less than the NC and ranging ~5% (Table. 5.5).

Caspases: Activation of caspases was caspase 8 > caspases 3/7 > caspase 9 (Figure. 3.14). This denotes that extrinsic apoptosis pathway was mainly activated, and later followed by intrinsic pathway activation following the cellular exposure to NPs. NPs cytotoxicity was associated with high ROS production (as previously confirmed in section 3.5.2), that can provide the link for induction of extrinsic and intrinsic of apoptosis pathways. However, other stimuli include TNF-α (that showed an increase

after NPs exposure), or over expression of Fas and FasL (can be evaluated in future directive studies) (Table. 5.6) (243).

Inflammatory: Calu-3 cells response: All NPs (0.125-2 mg/mL) did not induce IL-8 after Calu-3 cells exposure for 24 hr (Figure. 3.15. A & B). THP-1 **Response:** THP-1 exposure to NPs (0.125mg/mL) for 24 hr showed stimulation of IL-8 (earlier evaluated by ELISA Kit), IL-6, TNF-α, IFN-γ, and IL-10 while no effect on IL-17A, IL-2, and IL-4 that denoted a generation of proinflammatory reaction (Figure. 3.16 and Figure. 3.17) (Table. 5.7).

Genotoxicity: Genotoxicity potentials of NPs was evaluated by Comet assay alkaline gel electrophoresis (Figure. 3.18) (230, 390, 392, 484). All different NPs exposure (two concentrations: 0.125 mg/mL (minimal toxicity effect) and 2 mg/mL (maximum toxicity observed)) for 24 hr didn't induce any genotoxicity in Calu-3 cells when evaluated by Comet assay alkaline gel electrophoresis (Table. 5.8).

Table. 5.9. Summary of physicochemical dependent cytotoxicity concluded in this project.

Investigation	Chemistry	Size	Charge
Higher viability	*PL* > *PG*	*PG* 800 > *PG* 500 > *PG* 200	Positive NPs > negative NPs
Higher ROS production	*PG* = *PL*	At low concentrations: *PG* 200 > *PG* 500 > *PG* 800, while at high concentrations, larger sized produced more ROS than smaller	Negative = Positive NPs
Lowering ΔΨm	*PL* > *PG*	*PG* 800 > *PG* 500 > *PG* 200	Negative NPs > Positive NPs
LDH Total	*PL* > *PG*	*PG*-2 > *PG*-5 and *PG*-8 but *PG*+2 almost the same as *PG*+5 and *PG*+8	Positive NPs > Negative NPs
LDH Release	*PL*-2 > *PG*-2 *PG*+2 > *PL*+2	*PG* 800 > *PG* 500 > *PG* 200	Positive NPs > Negative NPs
Apoptosis or Necrosis	*PG* = *PL* Apoptosis induction	Smaller NPs showed earlier apoptosis than larger size NPs, Larger size NPs showed higher necrosis in later interval (T12)	Positive NPs = Negative NPs
Caspases	*PG* = *PL*	Larger sized NPs induced higher caspases than smaller NPs.	Positive NPs > Negative NPs
Inflammatory inducer	*PG* = *PL*	Larger sized NPs induced higher IL-8 and TNF-α than smaller NPs, lower induction of IL-10 and IFN-ɣ, similar induction of IL-6	Positive NPs > Negative NPs
Genotoxicity	No genotoxicity potential was detected with any of these NPs		

5.4. NP Uptake and Internalisation in Calu-3 Cell lines:

5.4.1. Calu-3 Epithelial Integrity:

Calu-3 under ALI showed the formation of tight polarized monolayers with a strong resemblance to lung cells *in vivo* (277), improved reproducibility and more differentiation (single columnar epithelium with apical cilia, mucous secretion, and tight junctions) (518, 524) to the airway epithelium.

TEER values measured over time (Figure. 4.3) showed increasing TEER values until the experimental day (Day 15) for NP exposure. TEER values recorded and accepted for the experiment were > 800 ohms.cm^2, which denoted successful development of TJs and polarized monolayers mimicking *in vivo* conditions (518).

Apparent permeability coefficient (P_{app}): The integrity of the epithelial barrier, using P*app* coefficient of [^{14}C]-mannitol as a paracellular marker, was investigated on Calu-3 polarized monolayers grown under ALI (Figure. 4.4, 4.5, & 4.6.) overtime (1, 2, 3, 4, 5, and 24 hr following NPs exposure). Radiolabelled [^{14}C]-mannitol is one of many paracellular markers (e.g. Na fluorescein, Inulin, and lucifer yellow (276)) available to study the paracellular transport across polarized monolayer.

All NPs concentrations showed a decreasing trend and was similar to NC. P*app* of [^{14}C]-mannitol had initial high values (~ 4 x 10^{-7} cm sec^{-1}) at T1 that was the maximum with a subsequent slow decline of P*app* rate over time until T24 hr (~ 1.5-2 x 10^{-7} cm sec^{-1}). The highest concentration (2 mg/mL) showed the highest P*app* values compared to lower concentrations (0.5 and 0.125 mg/mL). The P*app* coefficient of [^{14}C]-mannitol were sustained under what was previously reported in literature as acceptable range of paracellular or passive absorption rates across Calu-3 monolayers.

This range varies from 1- 4 x 10^{-7} cm sec^{-1} and indicated the integrity of Calu-3 polarized monolayers under ALI are preserved (276, 281, 513, 518, 524, 527).

Most of the P*app* values under these exposure conditions were similar to the control and not significantly different. This denoted the strength and well preserved integrity of the Calu-3 polarized monolayers over the study interval and confirmed the barrier ability to filter a wide range of NPs with variable underlying physiochemical properties (281, 518, 521). That's similar to what is seen with the natural lung barrier being able to act as a defence barrier against various inhaled particles, dust, bacteria and viruses (246). The paracellular P*app* values were reported showing a decreasing trend over time in many studies such as Bol *et al.,* (535), Ehrhardt *et al.,* (521) Foster *et al.,* (524), Bharatwaj *et al.,*(528), Stentebjerg-Andersen *et al.,* (518) and Grainger *et al.,* (281). These studies had evaluated TJs proteins; ZO-1 occludens during the experimental exposure to show the TJs proteins expression was increasing over time, with surrounding TJs as belts that can restrict the paracellular flow of solutes and molecules (535).

5.4.2. NP Uptake and Internalisation Mechanisms, and Subcellular Co-localisation:

The current study investigated NPs internalisation process by using a group of pharmacological endocytosis inhibitors covering many mechanisms as indicated in Table. 4.1 (505, 506, 522, 523). All NPs had been internalized mainly via transcellular active endocytosis processes that were mainly caveolin, clathrin, and macropinocytosis (a summary was shown in Table. 4.2)

Visual confirmation by CLSM showed all NPs had been internalised. The NPs were trafficked intracellularly and showed some co-localisation with the lysosomes

denoting and confirming their vesicular transport. NPs showed some co-localisation with mitochondria denoting their ability to interact with subcellular targets that can be used for therapeutic purposes and designing less-toxic carriers.

5.5. Future Directives:

- Further confirmation and validation of the obtained results in multicellular co-culture, primary lung epithelial models and microfluidic systems.
- Further investigation of NPs interactions with the mucous layer, NPs adsorption with LDH or inflammatory cytokines, and NPs adsorption to serum proteins,
- Further investigation of these NPs in in vivo models: to evaluate a whole systemic body response for acute and chronic studies, with a focus on exploring the inflammatory response, histological picture of the lung after exposure, NPs deposition, lung retention, distribution, metabolism, and elimination,
- Visual confirmation of the mechanism of internalisation of NPs under live imaging with labelling with certain markers that specific for certain endocytosis mechanisms, confirmation of intracellular NPs fate after internalisation and subcellular interaction, and cellular recovery after removal of NPs using highly advanced microscopy, for example, super-resolution microscopy (STORM) technique, particle tracking technologies , and imaging flow cytometry,
- Evaluation of residual surfactant of DOTAP and PVA in each NPs,
- Further investigation of *in vitro* degradation of larger sized NPs,
- Investigating functionalisation of *PG* polymer by covalent chemical fluorescent labelling to facilitate accurate quantification of NPs internalisation, and minimize risk of dye release,
- Further investigation of scalability of *PG* NPs using newer methods of fabrications such as microfluidic systems,

5.6. General Conclusion:

Nano-enabled drug delivery offers many promises to overcome both pharmaceutical and clinical challenges. Yet, there are many challenges facing the translation from bench top to clinics. Hence, there is a continuous need to develop and improve upon biocompatibility and biodegradability of polymeric materials for therapeutically efficient NPs fabrications, to suit a variety of target applications, delivery approaches, and various tissues.

Poly α-esters are a wide group of synthetic polymers that are commonly used in various biomedical application for NPs formulations, such as *PL*. The versatile nature of *PL* has made it a very attractive candidate for many biomedical applications as formulating many NPs, MP, other drug carriers and successful loading of different drugs and macromolecules that many of them have been approved by the FDA for clinical use (68-70). The main drawbacks of *PL* NPs are the bulk hydrolytic degradation with accumulation of acidic products, causing a reduction of local pH at the site of drug action. This affects the stability of pH-sensitive drugs and the long degradation with repeated doses and local acidity promoting an inflammatory response (68). Thus, novel materials are under development to provide better alternatives for polymeric NPs applications. *PG* is such a novel polymer that was synthesized and characterized in LJMU laboratories. It has successfully been formulated into NPs, MPs, and drug conjugates for lung delivery with good aerosolization performance and deep lung delivery encapsulating many small drugs and macromolecules (34, 72, 74-78).

This project provided a detailed nanotoxicological evaluation of polymeric NPs formulated from the two polymers *PG* and *PL* using *in vitro* pulmonary cell lines. Different sizes and charges of NPs were successfully formulated into different sizes;

200 nm, 500 nm, 800 nm, and with different charges; negatively- and positively charged NPs using emulsification-solvent evaporation methods.

A stability and degradation studies were evaluated in different biological media. All NPs showed better stability in SFM than CM. *PL* NPs showed faster degradation with acidic pH changes, while *PG* NPs showed slower degradation with an alkaline pH slowly decreasing toward the neutrality by the end of 28 days. This denoted better suitability of *PG* NPs for lung delivery with lower acidic changes.

A nanotoxicological screen covered a variety of general cytotoxicity, inflammatory, genotoxicity and mechanistic cellular assays as well as visual confirmation via microscopy were performed to uncover the physicochemical dependent cytotoxicity after NPs cellular interactions. *PL* and *PG* had showed some differences due to faster rate of *PL* degradation but overall, *PG* showed biocompatible cellular responses that can be compared to *PL* at low concentrations as similar or better. The size increase was associated with a limited uptake for the larger sized NPs, hence lower cytotoxicity at low concentrations to smaller NPs, however, higher cytotoxicity at high concentrations. Negatively charged NPs were commonly reported to be more cytotoxic than their negative counterparts that were correlated to the larger size of positive NPs after dispersion in media that might denote limited uptake. The apoptosis especially the extrinsic pathway was the major cause of cell death for these NPs. Limited inflammatory response after THP-1 exposure that requires further *in vivo* translation to uncover the nature of this inflammatory reaction. These NPs didn't induce any genotoxicity nor any adverse effects on the TJs integrity. Active endocytosis mechanism was mainly the internalisation mechanisms. Visual confirmation of internalisation and co-localisation with lysosomes and mitochondria that confirmed the vesicular transport and possible therapeutic potentials to target subcellular targets.

Overall, these studies had explored the potential safe use of these polymeric NPs for lung delivery. *PG* showed better profile of slower degradation (can be used for sustained formulations), of less acidic changes (less risk of acidity and inflammatory stimulation), and biocompatible profile that can be explored for *in vivo* lung delivery.

Reference List

1. WHO. The top 10 causes of Death: World Health Organization; 2018 [cited 2018 September 15th]. Available from: http://www.who.int/news-room/fact-sheets/detail/the-top-10-causes-of-death.

2. Stocks J., Hislop A. Structure and Function of the respiratory system; Developmental Aspects and their relevance to Aerosol Therapy. In: Bisgaard H OC, Smaldone G C editor. Drug Delivery to the lungs. Marcel Dekker: Inc.: New York; 2002. p. 47-89.

3. Osman N., Kaneko K., Carini V., *et al.* Carriers for the targeted delivery of aerosolized macromolecules for pulmonary pathologies. Expert Opinion on Drug Delivery. 2018;15(8):821-34.

4. Weibel E. R. Chapter II - Organization of the Human Lung. In: Weibel ER, editor. Morphometry of the Human Lung: Academic Press; 1963. p. 4-9.

5. Weibel E. R. What makes a good lung? The morphometric basis of lung function. Swiss Medical Weekly. 2009;139(27):375-86.

6. Kunda N. K., Somavarapu S., Gordon S. B., *et al.* Nanocarriers targeting dendritic cells for pulmonary vaccine delivery. Pharm Res. 2013;30(2):325-41.

7. Kaneko K., Osman N., Carini V., *et al.* Overview of the Advantages and Disadvantages of Different Mucosal Sites for the Delivery of Nanoparticles. Mucosal Delivery of Drugs and Biologics in Nanoparticles. AAPS Advances in the Pharmaceutical Sciences Series. 41: Springer, Charm; 2020. p. 61-82.

8. Anderson C. F., Grimmett M. E., Domalewski C. J., *et al.* Inhalable nanotherapeutics to improve treatment efficacy for common lung diseases. WIREs Nanomedicine and Nanobiotechnology. 2020;12(1):e1586.

9. El-Sherbiny I. M., El-Baz N. M., Yacoub M. H. Inhaled nano- and microparticles for drug delivery. Global Cardiology Science Practice. 2015;21:56-88.

10. Gaul R., Ramsey J. M., Heise A., *et al.* Nanotechnology approaches to pulmonary drug delivery: Targeted delivery of small molecule and gene-based therapeutics to the lung. In: Grumezescu AM, editor. Design of Nanostructures for Versatile Therapeutic Applications: William Andrew Publishing; 2018. p. 221-53.

11. Osman N. M., Sexton D. W., Saleem I. Y. Toxicological assessment of nanoparticle interactions with the pulmonary system. Nanotoxicology. 2020;14(1):21-58.

12. Patton. J. S. Mechanisms of macromolecule absorption by the lungs. Advanced drug delivery reviews. 1996;19:3-36

13. Olsson B., Bondesson E., Borgström L., *et al.* Pulmonary Drug Metabolism, Clearance, and Absorption. In: Smyth HDC, Hickey AJ, editors. Controlled Pulmonary Drug Delivery. New York, NY: Springer New York; 2011. p. 21-50.

14. Mansour H. M., Rhee Y. S., Wu X. Nanomedicine In Pulmonary Delivery. International Journal Nanomedicine. 2009;4:299-319.

15. Rajaraman P. K., Choi J., Hoffman E. A., *et al.* Transport and deposition of hygroscopic particles in asthmatic subjects with and without airway narrowing. Journal of Aerosol Science. 2020:10-81.

16. Longest P. W., McLeskey Jr J. T., Hindle M. Characterization of nanoaerosol size change during enhanced condensational growth. Aerosol Science and Technology. 2010;44(6):473-83.

17. Hu J., Dong Y., Pastorin G., *et al.* Spherical agglomerates of pure drug nanoparticles for improved pulmonary delivery in dry powder inhalers. Journal of Nanoparticle Research. 2013;15(4):15-60. .

18. Chandel A., Goyal A. K., Ghosh G., *et al.* Recent advances in aerosolised drug delivery. Biomedicine & Pharmacotherapy. 2019;112:16-21.

19. Rangaraj N., Pailla S. R., Sampathi S. Insight into pulmonary drug delivery: Mechanism of drug deposition to device characterization and regulatory requirements. Pulmonary Pharmacology & Therapeutics. 2019;54:1-21.

20. Muralidharan P., Malapit M., Mallory E., *et al.* Inhalable nanoparticulate powders for respiratory delivery. Nanomedicine: Nanotechnology, Biology and Medicine. 2015;11(5):1189-99.

21. Attias Cohen S., Kingma P. S., Whitsett J. A., *et al.* S*P*-D loaded *PLGA* nanoparticles as drug delivery system for prevention and treatment of premature infant's lung diseases. International Journal of Pharmaceutics. 2020;585:19-87.

22. Byrne A. J., Mathie S. A., Gregory L. G., *et al.* Pulmonary macrophages: key Players in the innate defence of the airways. Thorax. 2015;70(12):1189-96.

23. Mohamed A., Pekoz A. Y., Ross K., *et al.* Pulmonary delivery of Nanocomposite Microparticles (NCMPs) incorporating miR-146a for treatment of COPD. International Journal of Pharmaceutics. 2019;569:18-24.

24. Kleinstreuer C., Zhang Z., Donohue J. F. Targeted drug-aerosol delivery in the human respiratory system. Annu Rev Biomed Eng. 2008;10:195-220.

25. Rodrigues T. C., Oliveira M. L. S., Soares-Schanoski A., *et al.* Mucosal immunization with PspA (Pneumococcal surface protein A)-adsorbed nanoparticles targeting the lungs for protection against pneumococcal infection. *PL*OS ONE. 2018;13(1):e0191692.

26. Sumio Chono, Tomoharu Tanino, Toshinobu Seki, *et al.* Influence of particle size on drug delivery to rat alveolar macrophages following pulmonary administration of ciprofloxacin incorporated into liposomes. Journal of Drug Targeting. 2006;14(8):557-66.

27. Mehta M., Deeksha, Sharma N., *et al.* Interactions with the macrophages: An emerging targeted approach using novel drug delivery systems in respiratory diseases. Chemico-Biological Interactions. 2019;304:10-9.

28. Pandey P., Mehta M., Shukla S., *et al.* Emerging Nanotechnology in Chronic Respiratory Diseases. In: Talegaonkar s. RMeNiHH, editor. Nanoformulations in Human Health. 20: Springer, Charm; 2020. p. 449-68.

29. Fröhlich E S.-B. S. Toxicological Assessment of Inhaled Nanoparticles: Role of in Vivo, ex Vivo, in Vitro, and in Silico Studies. International Journal of Molecular Sciences. 2014;15(3):4795-822.

30. Mo'tasem M. A., Obaidat R. M., Alnaief M., *et al.* Development, In Vitro Characterization, and In Vivo Toxicity Evaluation of Chitosan-Alginate Nanoporous Carriers Loaded with Cis*PL*atin for Lung Cancer Treatment. AAPS PharmSciTech. 2020;21(5):1-12.

31. Samaridou E., Alonso M. J. Nose-to-brain peptide delivery - The potential of nanotechnology. Bioorganic Medical Chemistry. 2018;26(10):2888-905.

32. Pontes J. F., Grenha A. Multifunctional nanocarriers for lung drug delivery. Nanomaterials. 2020;10(2):183.

33. Merisko-Liversidge E. M., Liversidge G. G. Drug nanoparticles: formulating poorly water-soluble compounds. Toxicolgical Pathology. 2008;36(1):43-8.

34. Tawfeek H. M., Evans A. R., Iftikhar A., *et al.* Dry powder inhalation of macromolecules using novel PEG-co-polyester microparticle carriers. International Journal Pharmarmaceutics. 2013;441(1-2):611-9.

35. Gaggar A., Chen J., Chmiel J. F., *et al.* Inhaled alpha1-proteinase inhibitor therapy in patients with cystic fibrosis. JOURNAL Cyst Fibros. 2016;15(2):227-33.

36. Depreter F. M., Pilcer, G., Amighi, K. Inhaled proteins: Challenges and perspectives. Int J Pharm. 2013;447(1):251- 80.

37. Chauhan R., Sood N. Biopharmaceuticals: New yet Natural. British Biotechnology Journal. 2016;14(1):1-19.

38. Kunda N. K., Alfagih I. M., Miyaji E. N., *et al.* Pulmonary dry powder vaccine of pneumococcal antigen loaded nanoparticles. International Journal of Pharmceuticals. 2015;495(2):903-12.

39. Yan Y., Zhou K., Xiong H., *et al.* Aerosol delivery of stabilized polyester-siRNA nanoparticles to silence gene expression in orthotopic lung tumors. Biomaterials. 2017;118:84-93.

40. Kim Y. K., Xing L., Chen B. A., *et al.* Aerosol delivery of programmed cell death protein 4 using polysorbitol-based gene delivery system for lung cancer therapy. JOURNAL Drug Target. 2014;22(9):829-38.

41. Rudolph C, Schillinger U, Ortiz A, *et al.* Aerosolized nanogram quantities of *PL*asmid DNA mediate highly efficient gene delivery to mouse airway epithelium. Molecular Therapy. 2005;12(3):493-501.

42. Mela´nia Babincova, Babinec P. Aerosolized VEGF in combination with intravenous magnetically targeted delivery of DNA–nanoparticle complex may increase efficiency of cystic fibrosis gene therapy. Med Hypotheses. 2006;67(4):10-20.

43. Yan G., Li A., Zhang A., *et al.* Polymer-Based Nanocarriers for Co-Delivery and Combination of Diverse Therapies against Cancers. Nanomaterials (Basel). 2018;8(2).

44. Costa-Gouveia J., Pancani E., Jouny S., *et al.* Combination therapy for tuberculosis treatment: pulmonary administration of ethionamide and booster co-loaded nanoparticles. Scientific Reports. 2017;7(1):5390.

45. Wang Y., Zhang H., Hao J., *et al.* Lung cancer combination therapy: co-delivery of paclitaxel and doxorubicin by nanostructured lipid carriers for synergistic effect. Drug delivery. 2016;23(4):1398-403.

46. Zhang M., Liu E., Cui Y., *et al.* Nanotechnology-based combination therapy for overcoming multidrug-resistant cancer. Cancer biology & medicine. 2017;14(3):212-27.

47. Sangtani A., Petryayeva E., Wu M., *et al.* Intracellularly Actuated Quantum Dot–Peptide–Doxorubicin Nanobioconjugates for Controlled Drug Delivery via the Endocytic Pathway. Bioconjugate Chemistry. 2018;29(1):136-48.

48. Zamboni W. C., Torchilin V., Patri A. K., *et al.* Best practices in cancer nanotechnology: perspective from NCI nanotechnology alliance. Clinical Cancer Research. 2012;18(12):3229-41.

49. Zimmer A. Drug Targeting Technology, Physical·Chemical·Biological Methods, Edited by Hans Schreier. ChemBioChem. 2002;3(6):581-.

50. Tan Y. F., Lao L. L., Xiong G. M., *et al.* Controlled-release nanotherapeutics: State of translation. JOURNAL Control Release. 2018;284:39-48.

51. Kalaydina R.-V., Bajwa K., Qorri B., *et al.* Recent advances in "smart" delivery systems for extended drug release in cancer therapy. International journal of nanomedicine. 2018;13:4727-45.

52. Zhou L W. H., Li Y. . Stimuli-Responsive Nanomedicines for Overcoming Cancer Multidrug Resistance. Theranostics. 2018; 8(4):1059-74. .

53. Heidi M Mansour, Yun-Seok Rhee, Wu X. Nanomedicine in pulmonary delivery. International journal of nanomedicine. 2009;4:299-319.

54. De Jong W. H., Borm P. J. Drug delivery and nanoparticles:applications and hazards. International Journal Nanomedicine. 2008;3(2):133-49.

55. Pilcer G., Amighi K. Formulation strategy and use of excipients in pulmonary drug delivery. International Journal Pharmceuticals. 2010;392(1-2):1-19.

56. Vilar G., Tulla-Puche J., Albericio F. Polymers and drug delivery systems. Current Drug Delivery. 2012;9(4):367-94.

57. Iyer R., Hsia C. C. W., Nguyen K. T. Nano-Therapeutics for the Lung: State-of-the-Art and Future Perspectives. Current Pharmaceutical Design. 2015;21(36):5233-44.

58. Chavda V. P. Chapter 4 - Nanobased Nano Drug Delivery: A Comprehensive Review. In: Mohapatra SS, Ranjan S, Dasgupta N, *et al.*, editors. Applications of Targeted Nano Drugs and Delivery Systems: Elsevier; 2019. p. 69-92.

59. Donaldson K., Stone V., Tran C. L., *et al.* Nanotoxicology. Occup Environ Med. 2004;61(9):727-8.

60. Lombardo D., Kiselev M. A., Caccamo M. T. Smart Nanoparticles for Drug Delivery Application: Development of Versatile Nanocarrier *PL*atforms in Biotechnology and Nanomedicine. Journal of Nanomaterials. 2019;2019:26.

61. Kumari A., Yadav S. K., Yadav S. C. Biodegradable polymeric nanoparticles based drug delivery systems. Colloids Surf B Biointerfaces. 2010;75(1):1-18.

62. Ulery B. D., Nair L. S., Laurencin C. T. Biomedical applications of biodegradable polymers. Journal of Polymer Science Part B: Polymer Physics. 2011;49(12):832-64.

63. Kumar S., Maiti P. Controlled biodegradation of polymers using nanoparticles and its application. RSC Advances. 2016;6(72):67449-80.

64. Prajapati S. K., Jain A., Jain A., *et al.* Biodegradable polymers and constructs: A novel approach in drug delivery. European Polymer Journal. 2019;120:109191.

65. Larrañaga A., Lizundia E. A review on the thermomechanical properties and biodegradation behaviour of polyesters. European Polymer Journal. 2019;121:109296.

66. Singh V., Tiwari M. Structure-Processing-Property Relationship of Poly(Glycolic Acid) for Drug Delivery Systems 1: Synthesis and Catalysis. International Journal of Polymer Science. 2010;2010:652719.

67. Mir M., Ahmed N., Rehman A. U. Recent applications of *PLGA* based nanostructures in drug delivery. Colloids Surf B Biointerfaces. 2017;159:217-31.

68. Swider E., Koshkina O., Tel J., *et al.* Customizing poly(lactic-co-glycolic acid) particles for biomedical applications. Acta Biomaterialia. 2018;73:38-51.

69. Bobo D., Robinson K. J., Islam J., *et al.* Nanoparticle-Based Medicines: A Review of FDA-Approved Materials and Clinical Trials to Date. Pharmceutical Research,. 2016;33(10):2373-87.

70. Essa D., Kondiah P. P. D., Choonara Y. E., *et al.* The Design of Poly(lactide-co-glycolide) Nanocarriers for Medical Applications. Frontiers in Bioengineering and Biotechnology. 2020;8(48).

71. Rezvantalab S., Drude N. I., Moraveji M. K., *et al. PLGA*-based nanoparticles in cancer treatment. Front Pharmacol. 2018;9:1260.

72. Thompson CJ H. D., Higgins S, Hutcheon, G.A., Rostron, C., Munday, D.L. Enzymatic synthesis and evaluation of new novel o-pentadecalactone polymers for the production of biodegradable microspheres. Journal Microencapsulation. 2006; 23:213–26.

73. Thompson C. J., Hansford, D., Higgins, S., Hutcheon, G. A., Rostron, C., Munday, D. L. Enzymatic synthesis and evaluation of new novel omega-pentadecalactone polymers for the production of biodegradable microspheres. Journal of Microencapsulation. 2006;23(2):213-26.

74. Kunda N. K., Alfagih I. M., Dennison S. R., *et al.* Bovine serum albumin adsorbed *PGA-co-PDL*nanocarriers for vaccine delivery via dry powder inhalation. Pharm Res. 2015;32(4):1341-53.

75. Thompson C. J., Hansford D., Munday D. L., *et al.* Synthesis and evaluation of novel polyester-ibuprofen conjugates for modified drug release. Drug Dev Ind Pharm. 2008;34(8):877-84.

76. Thompson C. J., Hansford D., Higgins S., *et al.* Evaluation of ibuprofen-loaded microspheres prepared from novel copolyesters. International Journal of Pharmaceutics. 2007;329(1-2):53-61.

77. Tawfeek H. M., Khidr S. H., Samy E. M., *et al.* Evaluation of biodegradable polyester-co-lactone microparticles for protein delivery. Drug Devision Industrial Pharmaceuticals. 2014;40(9):1213-22.

78. Tawfeek H. M. Evaluation of PEG and mPEG-co-(*PG*A-co-PDL) microparticles loaded with sodium diclofenac. Saudi Pharmaceutical Journal. 2013;21(4):387-97.

79. Mohamed A., Kunda N. K., Ross K., *et al.* Polymeric nanoparticles for the delivery of miRNA to treat Chronic Obstructive Pulmonary Disease (COPD). European Journal of Pharmaceutics and Biopharmaceutics. 2019;136:1-8.

80. Alfagih I., Kunda N., Alanazi F., *et al.* Pulmonary Delivery of Proteins Using Nanocomposite Microcarriers. J Pharm Sci. 2015;104(12):4386-98.

81. Kunda N. K., Alfagih I. M., Dennison S. R., *et al.* Dry powder pulmonary delivery of cationic *PGA-co-PDL*nanoparticles with surface adsorbed model protein. International Journal of Pharmceuticals. 2015;492(1-2):13-22.

82. Wang Y., Li P., Truong-Dinh Tran T., *et al.* Manufacturing techniques and surface engineering of polymer based nanoparticles for targeted drug delivery to cancer. Nanomaterials. 2016;6(2):26.

83. Essa D., Choonara Y. E., Kondiah P. P., *et al.* Comparative Nanofabrication of *PLGA*-Chitosan-PEG Systems Employing Microfluidics and Emulsification Solvent Evaporation Techniques. Polymers. 2020;12(9):1882.

84. Pillay V., Essa D., Kondiah P. P., *et al.* The design of poly (lactide-co-glycolide) nanocarriers for medical applications. Frontiers in Bioengineering and Biotechnology. 2020;8:48.

85. Kuzmov A., Minkoab T. Nanotechnology approaches for inhalation treatment of lung diseases. Journal of Controlled Release. 2015;219:500-18.

86. Takenaka S., Karg E., Roth C., *et al.* Pulmonary and systemic distribution of inhaled ultrafine silver particles in rats. Environ Health Perspect. 2001;109 Sup*PL* 4:547-51.

87. Hohenegger M. Novel and current treatment concepts using pulmonary drug delivery. Current Drug Delivery. 2010;16(22):2484-92.

88. Insmed. Insmed. Arikayce 2019 [cited 2018 8th October]. Available from: http://investor.insmed.com/news-releases/news-release-details/insmed-announces-fda-approval-arikaycer-amikacin-liposome.

89. Bou S., Wang X., Anton N., *et al.* Lipid-core/polymer-shell hybrid nanoparticles: synthesis and characterization by fluorescence labeling and electrophoresis. Soft Matter. 2020;16(17):4173-81.

90. Tahir N., Haseeb M. T., Madni A., *et al.* Lipid Polymer Hybrid Nanoparticles: A Novel Approach for Drug Delivery. In: Rajeev K NG, Rahul S., Prakash S. (eds), editor. Role of Novel Drug Delivery Vehicles in Nanobiomedicine: IntechOpen; 2019.

91. Parvathaneni V., Kulkarni N. S., Chauhan G., *et al.* Development of pharmaceutically scalable inhaled anti-cancer nanotherapy - Repurposing amodiaquine for non-small cell lung cancer (NSCLC). Mater Sci Eng C Mater Biol Ap*PL*. 2020;115:11-39.

92. Kalombo L., Lemmer Y., Semete-Makokotlela B., *et al.* Spray-Dried, Nanoencapsulated, Multi-Drug Anti-Tuberculosis Therapy Aimed at Once Weekly Administration for the Duration of Treatment. Nanomaterials. 2019;9(8):1167.

93. Vaidya B., Kulkarni N. S., Shukla S. K., *et al.* Development of inhalable quinacrine loaded bovine serum albumin modified cationic nanoparticles: Repurposing quinacrine for lung cancer therapeutics. International Journal of Pharmaceutics. 2020;577:89-95.

94. Ernst J., Klinger-Strobel M., Arnold K., *et al.* Polyester-based particles to overcome the obstacles of mucus and biofilms in the lung for tobramycin application under static and dynamic fluidic conditions. European Journal of Pharmaceutics and Biopharmaceutics. 2018;131:120-9.

95. Guo X., Zhang X., Ye L., *et al.* Inhalable microspheres embedding chitosan-coated *PLGA* nanoparticles for 2-methoxyestradiol. JOURNAL Drug Target. 2014;22(5):421-7.

96. Chishti N., Jagwani S., Dhamecha D., *et al.* Preparation, optimization, and In Vivo Evaluation of nanoparticle-based formulation for pulmonary delivery of anticancer drug. Medicina. 2019;55(6):294.

97. Jensen D. K., Jensen L. B., Koocheki S., *et al.* Design of an inhalable dry powder formulation of DOTA*P*-modified *PLGA* nanoparticles loaded with siRNA. Journal of Controlled Release. 2012;157(1):141-8.

98. Shukla S. K., Kulkarni N. S., Farrales P., *et al.* Sorafenib Loaded Inhalable Polymeric Nanocarriers against Non-Small Cell Lung Cancer. Pharmaceutical Research. 2020;37(3):67.

99. Wang X., Parvathaneni V., Shukla S. K., *et al.* Inhalable resveratrol-cyclodextrin complex loaded biodegradable nanoparticles for enhanced efficacy against non-small cell lung cancer. International Journal of Biological Macromolecules. 2020;164:638-50.

100. Elbatanony R. S., Parvathaneni V., Kulkarni N. S., *et al.* Afatinib-loaded inhalable *PLGA* nanoparticles for localized therapy of non-small cell lung cancer (NSCLC)-development and in-vitro efficacy. Drug Delivery Translation Research. 2020;2(8):1-17.

101. Kaye R. S., Purewal T. S., Alpar H. O. Simultaneously manufactured nano-in-micro (SIMANIM) particles for dry-powder modified-release delivery of antibodies. Journal of Pharmaceutical Sciences. 2009;98(11):4055-68.

102. Haque A. K. M. A., Dewerth A., Antony J. S., *et al.* Chemically modified hCFTR mRNAs recuperate lung function in a mouse model of cystic fibrosis. Scientific Reports. 2018;8(1):16776.

103. Alfagih I., Kunda N., Alanazi F., *et al.* Pulmonary Delivery of Proteins Using Nanocomposite Microcarriers. Journal of Pharmaceutical Sciences. 2015;104(12):4386-98.

104. Kunda N. K., Alfagih I. M., Dennison S. R., *et al.* Bovine Serum Albumin Adsorbed *PGA-co-PDL*Nanocarriers for Vaccine Delivery via Dry Powder Inhalation. Pharmaceutical Research. 2015;32(4):1341-53.

105. Muller A. Pulmonary delivery of resveratrol-loaded nanocomposite microparticles to treat lung cancer: Liverpool John Moores University; 2020.

106. Kunda N. K., Alfagih I. M., Miyaji E. N., *et al.* Pulmonary dry powder vaccine of pneumococcal antigen loaded nanoparticles. International Journal of Pharmaceutics. 2015;495(2):903-12.

107. Gill K. K., Nazzal S., Kaddoumi A. Paclitaxel loaded PEG(5000)-DSPE micelles as pulmonary delivery *PL*atform: formulation characterization, tissue distribution, Plasma pharmacokinetics, and toxicological evaluation. Eur J Pharm Biopharm. 2011;79(2):276-84.

108. Grenha A., Seijo B., Remuñán-López C. Microencapsulated chitosan nanoparticles for lung protein delivery. European Journal of Pharmaceutical Sciences. 2005;25(4-5):427-37.

109. Grenha A., Remuñán-López C., Carvalho E. L. S., *et al.* Microspheres containing lipid/chitosan nanoparticles complexes for pulmonary delivery of therapeutic proteins. European Journal of Pharmaceutics and Biopharmaceutics. 2008;69(1):83-93.

110. Grenha A., Grainger C. I., Dailey L. A., *et al.* Chitosan nanoparticles are compatible with respiratory epithelial cells in vitro. European Journal of Pharmaceutical Sciences. 2007;31(2):73-84.

111. Al-Qadi S., Grenha A., Carrión-Recio D., *et al.* Microencapsulated chitosan nanoparticles for pulmonary protein delivery: In vivo evaluation of insulin-loaded formulations. Journal of Controlled Release. 2012;157(3):383-90.

112. Hong S. H., Lee J. H., Jiang H. L., *et al.* Dual expression of shAkt1 and Pdcd4 suppresses lung tumorigenesis in K-rasLA1 mice. Anticancer Res. 2015;35(4):2015-9.

113. Ray A., Mandal A., Mitra A. K. Recent Patents in Pulmonary Delivery of Macromolecules. Recent Pat Drug Deliv Formul. 2015;9(3):225-36.

114. Al-Hallak K. M., Azarmi S., Anwar-Mohamed A., *et al.* Secondary cytotoxicity mediated by alveolar macrophages: a contribution to the total efficacy of nanoparticles in lung cancer therapy? European Journal of Pharmaceutics and Biopharmaceutics. 2010;76(1):112-9.

115. Zhong Q., da Rocha S. R. P. Poly(amidoamine) Dendrimer–Doxorubicin Conjugates: In Vitro Characteristics and Pseudosolution Formulation in Pressurized Metered-Dose Inhalers. Molecular Pharmaceutics. 2016;13(3):1058-72.

116. Kim H. W., Park I. K., Cho C. S., *et al.* Aerosol delivery of glucosylated polyethylenimine/phosphatase and tensin homologue deleted on chromosome 10 complex suppresses Akt downstream pathways in the lung of K-ras null mice. Cancer Res. 2004;64(21):7971-6.

117. Moraga-Espinoza D., Eshaghian E., Smyth H. D. C. Mass Median *PL*ume Angle: A novel approach to characterize *PL*ume geometry in solution based pMDIs. International Journal of Pharmaceutics. 2018;543(1-2):376-85.

118. Corcoran T. E., Niven R., Verret W., *et al.* Lung deposition and pharmacokinetics of nebulized cyclosporine in lung trans*PL*ant patients. Joural of Aerosol Medicine Pulmonary Drug Delivery. 2014;27(3):178-84.

119. Wang Y., Li J. Y., Leavey A., *et al.* Comparative Study on the Size Distributions, Respiratory Deposition, and Transport of Particles Generated from Commonly Used Medical Nebulizers. J Aerosol Med Pulm Drug Deliv. 2017;30(2):132-40.

120. de Boer A. H., Hagedoorn P., Hoppentocht M., *et al.* Dry powder inhalation: past, present and future. Expert Opinion on Drug Delivery. 2017;14(4):499-512.

121. Hoppentocht M., Hagedoorn P., Frijlink H. W., *et al.* Technological and practical challenges of dry powder inhalers and formulations. Advanced drug delivery reviews. 2014;75:18-31.

122. De Boer A. H., Gjaltema D., Hagedoorn P., *et al.* Characterization of inhalation aerosols: a critical evaluation of cascade impactor analysis and laser diffraction technique. Int J Pharm. 2002;249(1-2):219-31.

123. Labiris N. R., Dolovich M. B. Pulmonary drug delivery. Part I: physiological factors affecting therapeutic effectiveness of aerosolized medications. Br JOURNAL Clin Pharmacol. 2003;56(6):588-99.

124. Bisgaard H., O'Callaghan C., Smaldone G. Drug Delivery to the Lung. 1 ed. Bisgaard H, O'Callaghan, C, Smaldone, G (eds), editor: Taylor & Francis; 1999.

125. Tsapis N., Bennett D., Jackson B., *et al.* Trojan particles: large porous carriers of nanoparticles for drug delivery. Proc Natl Acad Sci U S A. 2002;99(19):12001-5.

126. Bohr A., Water J., Beck-Broichsitter M., *et al.* Nanoembedded microparticles for stabilization and delivery of drug-loaded nanoparticles. Current pharmaceutical design. 2015;21(40):5829-44.

127. Wang Y., Beck-Broichsitter M., Yang M., *et al.* Investigation of nanocarriers and excipients for preparation of nanoembedded microparticles. Int J Pharm. 2017;526(1-2):300-8.

128. Ely L., Roa W., Finlay W. H., *et al.* Effervescent dry powder for respiratory drug delivery. Eur J Pharm Biopharm. 2007;65(3):346-53.

129. Azarmi S., Löbenberg R., Roa W. H., *et al.* Formulation and in vivo evaluation of effervescent inhalable carrier particles for pulmonary delivery of nanoparticles. Drug development and industrial pharmacy. 2008;34(9):943-7.

130. Al-Hallak M. H., Sarfraz M. K., Azarmi S., *et al.* Distribution of effervescent inhalable nanoparticles after pulmonary delivery: an in vivo study. Ther Deliv. 2012;3(6):725-34.

131. Lewinski N., Colvin V., Drezek R. Cytotoxicity of nanoparticles. Small. 2008;4(1):26-49.

132. Heyder J. Deposition of inhaled particles in the human respiratory tract and consequences for regional targeting in respiratory drug delivery. Proc Am Thorac Soc. 2004;1(4):315-20.

133. Stein S. W., Thiel C. G. The History of Therapeutic Aerosols: A Chronological Review. Journal of aerosol medicine and pulmonary drug delivery. 2017;30(1):20-41.

134. Scherliess R., Etschmann C. DPI formulations for high dose applications - Challenges and opportunities. International Journal of Pharmaceutics. 2018;548(1):49-53.

135. Lim Y. H., Tiemann K. M., Hunstad D. A., *et al.* Polymeric nanoparticles in development for treatment of pulmonary infectious diseases. Wiley Interdiscip Rev Nanomed Nanobiotechnol. 2016;8(6):842-71.

136. Moore T. L., Rodriguez-Lorenzo L., Hirsch V., *et al.* Nanoparticle colloidal stability in cell culture media and impact on cellular interactions. Chemistry Society Reviews. 2015;44(17):6287-305.

137. Bello D., Warheit D. B. Biokinetics of engineered nano-TiO2 in rats administered by different exposure routes: implication for human health. Nanotoxicology. 2017;11(4):431-3.

138. Nierenberg D., Khaled A. R., Flores O. Formation of a protein corona influences the biological identity of nanomaterials. Rep Pract Oncol Radiother. 2018;23(4):300-8.

139. Monopoli M. P., Walczyk D., Campbell A., *et al.* Physical-chemical aspects of protein corona: relevance to in vitro and in vivo biological impacts of nanoparticles. Journal American Chemistry Society. 2011;133(8):2525-34.

140. Vilanova O., Mittag J. J., Kelly P. M., *et al.* Understanding the Kinetics of Protein-Nanoparticle Corona Formation. 2016;10(12):10842-50.

141. Vij N., Min T., Marasigan R., *et al.* Development of PEGylated *PLGA* nanoparticle for controlled and sustained drug delivery in cystic fibrosis. JOURNAL Nanobiotechnology. 2010;8:22.

142. Forest V., Vergnon J.-M., Pourchez J. Biological monitoring of inhaled nanoparticles in patients: an appealing approach to study causal link between human respiratory pathology and exposure to nanoparticles. Chemical Research in Toxicology. 2017;30(9):1655-60.

143. Bourquin J., Milosevic A., Hauser D., *et al.* Biodistribution, Clearance, and Long-Term Fate of Clinically Relevant Nanomaterials. Advanced Materials. 2018;30(19):e1704307.

144. Rinaldo M., Andujar P., Lacourt A., *et al.* Perspectives in Biological Monitoring of Inhaled Nanosized Particles. Ann Occup Hyg. 2015;59(6):669-80.

145. Kroon L. A. Drug interactions with smoking. Am JOURNAL Health Syst Pharm. 2007;64(18):1917-21.

146. Longmire M., Choyke P. L., Kobayashi H. Clearance properties of nano-sized particles and molecules as imaging agents: considerations and caveats. Nanomedicine (London, England). 2008;3(5):703-17.

147. Zhao Z., Ukidve A., Krishnan V., *et al.* Effect of physicochemical and surface properties on in vivo fate of drug nanocarriers. Adv Drug Deliv Rev. 2019.

148. Behzadi S., Serpooshan V., Tao W., *et al.* Cellular uptake of nanoparticles: journey inside the cell. Chemical Society Reviews. 2017;46(14):4218-44.

149. Donahue N. D., Acar H., Wilhelm S. Concepts of nanoparticle cellular uptake, intracellular trafficking, and kinetics in nanomedicine. Adv Drug Deliv Rev. 2019.

150. Abdelaziz H. M., Gaber M., Abd-Elwakil M. M., *et al.* Inhalable particulate drug delivery systems for lung cancer therapy: Nanoparticles, microparticles, nanocomposites and nanoaggregates. Journal of Controlled Release. 2018;269:374-92.

151. Accomasso L., Cristallini C., Giachino C. Risk Assessment and Risk Minimization in Nanomedicine: A Need for Predictive, Alternative, and 3Rs Strategies. Front Pharmacol. 2018;9(228).

152. Begines B., Ortiz T., Pérez-Aranda M., *et al.* Polymeric Nanoparticles for Drug Delivery: Recent Developments and Future Prospects. Nanomaterials. 2020;10(7):1403.

153. Bachler G., Losert S., Umehara Y., *et al.* Translocation of gold nanoparticles across the lung epithelial tissue barrier: Combining in vitro and in silico methods to substitute in vivo experiments. Partice Fibre Toxicology. 2015;12:18.

154. Chen R., Xu L., Fan Q., *et al.* Hierarchical pulmonary target nanoparticles via inhaled administration for anticancer drug delivery. Drug delivery. 2017;24(1):1191-203.

155. Lee D., Hong J. H. Nanoparticle-Mediated Therapeutic Application for Modulation of Lysosomal Ion Channels and Functions. Pharmaceutics. 2020;12(3):217.

156. Lee D. U., Park J.-Y., Kwon S., *et al.* Apoptotic lysosomal proton sponge effect in tumor tissue by cationic gold nanorods. Nanoscale. 2019;11(42):19980-93.

157. Wang T., Bai J., Jiang X., *et al.* Cellular uptake of nanoparticles by membrane penetration: a study combining confocal microscopy with FTIR spectroelectrochemistry. ACS Nano. 2012;6(2):1251-9.

158. Jameson C. J., Oroskar P., Song B., *et al.* Molecular Dynamics Studies of Nanoparticle Transport Through Model Lipid Membranes. Biomimetic Lipid Membranes: Fundamentals, Applications, and Commercialization: Springer; 2019. p. 109-65.

159. Manzanares D., Ceña V. Endocytosis: The Nanoparticle and Submicron Nanocompounds Gateway into the Cell. Pharmaceutics. 2020;12(4):371.

160. Uribe-Querol E., Rosales C. Phagocytosis: Our current understanding of a universal biological process. Frontiers in Immunology. 2020;11.

161. Hillaireau H., Couvreur P. Nanocarriers' entry into the cell: relevance to drug delivery. Cellular and Molecular Life Sciences. 2009;66(17):2873-96.

162. Champion J. A., Katare Y. K., Mitragotri S. Making polymeric micro- and nanoparticles of complex shapes. Proceedings of the National Academy of Sciences. 2007;104(29):11901-4.

163. Nelemans L. C., Gurevich L. Drug Delivery with Polymeric Nanocarriers—Cellular Uptake Mechanisms. Materials. 2020;13(2):366.

164. Champion J. A., Mitragotri S. Role of target geometry in phagocytosis. Proceedings of the National Academy of Sciences of the United States of America. 2006;103(13):4930-4.

165. Champion J. A., Mitragotri S. Role of target geometry in phagocytosis. Proceedings of the National Academy of Sciences. 2006;103(13):4930-4.

166. Bakand S., Hayes A. Toxicological Considerations, Toxicity Assessment, and Risk Management of Inhaled Nanoparticles. International Journal Molecular Sciences. 2016;17(6).

167. Susanne E., Thomas F. R. Modulation of dynamin function by small molecules. Biological Chemistry. 2018;399(12):1421-32.

168. Marie-Anais F., Mazzolini J., Bourdoncle P., *et al.* "Phagosome Closure Assay" to Visualize Phagosome Formation in Three Dimensions Using Total Internal Reflection Fluorescent Microscopy (TIRFM). Joural of Visualised Experiments. 2016(114):54470.

169. Joseph J. G., Liu A. P. Mechanical Regulation of Endocytosis: New Insights and Recent Advances. Advanced Biosystems. 2020;4:190-278.

170. Uribe-Querol E., Rosales C. Phagocytosis: Our Current Understanding of a Universal Biological Process. Frontiers in Immunology. 2020;11:1066.

171. Kumar A., Ahmad A., Vyawahare A., *et al.* Membrane Trafficking and Subcellular Drug Targeting Pathways. Front Pharmacol. 2020;11:629.

172. Park R. J., Shen H., Liu L., *et al.* Dynamin tri*PL*e knockout cells reveal off target effects of commonly used dynamin inhibitors. Journal of Cell Science. 2013;126(22):5305-12.

173. Foroozandeh P., Aziz A. A. Insight into Cellular Uptake and Intracellular Trafficking of Nanoparticles. Nanoscale research letters. 2018;13(1):339.

174. Canton J. Macropinocytosis: New Insights Into Its Underappreciated Role in Innate Immune Cell Surveillance. Frontiers in Immunology. 2018;9(2286):22-86.

175. Wang X., Chen Z., Mettlen M., *et al.* DASC, a sensitive classifier for measuring discrete early stages in clathrin-mediated endocytosis. eLife. 2020;9:e53686.

176. Kaksonen M., Roux A. Mechanisms of clathrin-mediated endocytosis. Nature reviews Molecular cell biology. 2018;19(5):313-26.

177. López-Hernández T., Puchkov D., Krause E., *et al.* Endocytic regulation of cellular ion homeostasis controls lysosome biogenesis. Nature Cell Biology. 2020:1-13.

178. Conner S. D., Schmid S. L. Regulated portals of entry into the cell. Nature. 2003;422(6927):37-44.

179. Pelkmans L., Kartenbeck J., Helenius A. Caveolar endocytosis of simian virus 40 reveals a new two-step vesicular-transport pathway to the ER. Nature Cell Biology. 2001;3(5):473-83.

180. Dauty E., Remy J. S., Zuber G., *et al.* Intracellular delivery of nanometric DNA particles via the folate receptor. Bioconjugated Chemistry. 2002;13(4):831-9.

181. Cohen A. W., Hnasko R., Schubert W., *et al.* Role of caveolae and caveolins in health and disease. Physiological reviews. 2004;84(4):1341-79.

182. Parton R. G., Del Pozo M. A. Caveolae as Plasma membrane sensors, protectors and organizers. Nature reviews Molecular cell biology. 2013;14(2):98-112.

183. Sezgin E., Levental I., Mayor S., *et al.* The mystery of membrane organization: composition, regulation and roles of lipid rafts. Nature reviews Molecular cell biology. 2017;18(6):361-74.

184. Shin S. W., Song I. H., Um S. H. Role of Physicochemical Properties in Nanoparticle Toxicity. Nanomaterials. 2015;5(3):1351-65.

185. Li Y., Cheng Q., Jiang Q., *et al.* Enhanced endosomal/lysosomal escape by distearoyl phosphoethanolamine-polycarboxybetaine lipid for systemic delivery of siRNA. JOURNAL Control Release. 2014;176:104-14.

186. Pan L., Liu J., Shi J. Cancer cell nucleus-targeting nanocomposites for advanced tumor therapeutics. Chemical Society Reviews. 2018;47(18):6930-46.

187. Li L., Li X., Wu Y., *et al.* Multifunctional Nucleus-targeting Nanoparticles with Ultra-high Gene Transfection Efficiency for In Vivo Gene Therapy. Theranostics. 2017;7(6):1633-49.

188. Chen Z. P., Li M., Zhang L. J., *et al.* Mitochondria-targeted drug delivery system for cancer treatment. JOURNAL Drug Target. 2016;24(6):492-502.

189. Salnikov V., Lukyanenko Y. O., Frederick C. A., *et al.* Probing the outer mitochondrial membrane in cardiac mitochondria with nanoparticles. Biophys JOURNAL. 2007;92(3):1058-71.

190. Eftekhari A. The application of novel mitochondria-targeted antioxidants: current strategies and future perspectives. Journal of Advanced Chemical and Pharmaceutical Materials. 2018;1(1):1-2.

191. Scott C. C., Vacca F., Gruenberg J. Endosome maturation, transport and functions. Semin Cell Dev Biol. 2014;31:2-10.

192. Elkin S. R., Lakoduk A. M., Schmid S. L. Endocytic pathways and endosomal trafficking: a primer. Wien Med Wochenschr. 2016;166(7-8):196-204.

193. Rothen-Rutishauser B., Bourquin J., Petri-Fink A. Nanoparticle-Cell Interactions: Overview of Uptake, Intracellular Fate and Induction of Cell Responses. Biological Responses to Nanoscale Particles: Springer; 2019. p. 153-70.

194. Xia T., Zhu Y., Mu L., *et al.* Pulmonary diseases induced by ambient ultrafine and engineered nanoparticles in twenty-first century. Natl Sci Rev. 2016;3(4):416-29.

195. Farnoud A. M., Nazemidashtarjandi S. Emerging investigator series: interactions of engineered nanomaterials with the cell Plasma membrane; what have we learned from membrane models? Environmental Science-Nano. 2019;6(1):13-40.

196. Yeh Y. C., Saha K., Yan B., *et al.* The role of ligand coordination on the cytotoxicity of cationic quantum dots in HeLa cells. Nanoscale. 2013;5(24):12140-3.

197. Leroueil P. R., Berry S. A., Duthie K., *et al.* Wide varieties of cationic nanoparticles induce defects in supported lipid bilayers. Nano letters. 2008;8(2):420-4.

198. Mecke A., Majoros I. J., Patri A. K., *et al.* Lipid Bilayer Disruption by Polycationic Polymers: The Roles of Size and Chemical Functional Group. Langmuir. 2005;21(23):10348-54.

199. Pang Y. T., Ge Z., Zhang B., *et al.* Pore formation induced by nanoparticles binding to a lipid membrane. Nanoscale. 2020;12(14):7902-13.

200. Mu Q., Jiang G., Chen L., *et al.* Chemical basis of interactions between engineered nanoparticles and biological systems. Chemistry Reviews. 2014;114(15):7740-81.

201. Jing B., Zhu Y. Disruption of Supported Lipid Bilayers by Semihydrophobic Nanoparticles. Journal of the American Chemical Society. 2011;133(28):10983-9.

202. Singh S. Zinc oxide nanoparticles impacts: Cytotoxicity, genotoxicity, developmental toxicity, and neurotoxicity. Toxicology Mechanisms and Methods. 2019;29(4):300-11.

203. Karlsson H. L., Cronholm P., Hedberg Y., *et al.* Cell membrane damage and protein interaction induced by copper containing nanoparticles—Importance of the metal release process. Toxicology. 2013;313(1):59-69.

204. Chu Z., Miu K., Lung P., *et al.* Rapid endosomal escape of prickly nanodiamonds: implication for gene delivery. Scientific Reports. 2015;5:11-61.

205. Hu Y., Litwin T., Nagaraja A. R., *et al.* Cytosolic delivery of membrane-impermeable molecules in dendritic cells using pH-responsive core-shell nanoparticles. Nano Lett. 2007;7(10):3056-64.

206. Ispanixtlahuatl-Meráz O., Schins R. P. F., Chirino Y. I. Cell type specific cytoskeleton disruption induced by engineered nanoparticles. Environmental Science: Nano. 2018;5(2):228-45.

207. Tarantola M., Schneider D., Sunnick E., *et al.* Cytotoxicity of metal and semiconductor nanoparticles indicated by cellular micromotility. ACS Nano. 2009;3(1):213-22.

208. Oh W.-K., Kim S., Yoon H., *et al.* Shape-Dependent Cytotoxicity and Proinflammatory Response of Poly(3,4-ethylenedioxythiophene) Nanomaterials. Small. 2010;6(7):872-9.

209. Fu X., Hosta-Rigau L., Chandrawati R., *et al.* Multi-Stimuli-Responsive Polymer Particles, Films, and Hydrogels for Drug Delivery. Chemistry Research. 2018;4(9):2084-107.

210. Kim K. S., Lee D., Song C. G., *et al.* Reactive oxygen species-activated nanomaterials as theranostic agents. Nanomedicine (London, England). 2015;10(17):2709-23.

211. Domej W., Oettl K., Renner W. Oxidative stress and free radicals in COPD--implication and relevance for treatment. International Journal Chronic Obstructive Pulmonary Disease. 2014;9:1207-24.

212. Sebag S. C., Koval O. M., Paschke J. D., *et al.* Mitochondrial CaMKII inhibition in airway epithelium protects against allergic asthma. JCI insight. 2017;2(3):e88297.

213. Dröge W. Free radicals in the physiological control of cell function. Physiol Rev. 2002;82(1):47-95.

214. Koppenol W. H. The Haber-Weiss cycle--70 years later. Redox Rep. 2001;6(4):229-34.

215. Anttila S., Hukkanen J., Hakkola J., *et al.* Expression and localization of CYP3A4 and CYP3A5 in human lung. American Journal Respiratory Cell Molecular Biology. 1997;16(3):242-9.

216. Sabido O., Figarol A., Klein J.-P., *et al.* Quantitative Flow Cytometric Evaluation of Oxidative Stress and Mitochondrial Impairment in RAW 264.7 Macrophages after Exposure to Pristine, Acid Functionalized, or Annealed Carbon Nanotubes. Nanomaterials. 2020;10(2):319.

217. Howard D., Sebastian S., Le Q. V.-C., *et al.* Chemical Mechanisms of Nanoparticle Radiosensitization and Radioprotection: A Review of Structure-Function Relationships Influencing Reactive Oxygen Species. International Journal of Molecular Sciences. 2020;21(2):579.

218. Cho Y.-L., Tan H. W. S., Saquib Q., *et al.* Dual role of oxidative stress-JNK activation in autophagy and apoptosis induced by nickel oxide nanoparticles in human cancer cells. Free Radical Biology and Medicine. 2020;153:173-86.

219. Nemmar A., Al-Salam S., Beegam S., *et al.* Aortic Oxidative Stress, Inflammation and DNA Damage Following Pulmonary Exposure to Cerium Oxide Nanoparticles in a Rat Model of Vascular Injury. Biomolecules. 2019;9(8):376.

220. Xu L., Zhao M., Gao W., *et al.* Polymeric nanoparticles responsive to intracellular ROS for anticancer drug delivery. Colloids Surf B Biointerfaces. 2019;181:252-60.

221. Joshi-Barr S., de Gracia Lux C., Mahmoud E., *et al.* Ex*PL*oiting oxidative microenvironments in the body as triggers for drug delivery systems. Antioxidant Redox Signalling. 2014;21(5):730-54.

222. Yang B., Chen Y., Shi J. Reactive Oxygen Species (ROS)-Based Nanomedicine. Chemical Reviews. 2019;119(8):4881-985.

223. Saifi M. A., Khan W., Godugu C. Cytotoxicity of Nanomaterials: Using Nanotoxicology to Address the Safety Concerns of Nanoparticles. Pharm Nanotechnol. 2018;6(1):3-16.

224. Pathak R. K., Kolishetti N., Dhar S. Targeted nanoparticles in mitochondrial medicine. Wiley Interdiscip Rev Nanomed Nanobiotechnol. 2015;7(3):315-29.

225. Weissig V. From serendipity to mitochondria-targeted nanocarriers. Pharm Res. 2011;28(11):2657-68.

226. D'Souza G. G., Rammohan R., Cheng S. M., *et al.* DQAsome-mediated delivery of *PL*asmid DNA toward mitochondria in living cells. JOURNAL Control Release. 2003;92(1-2):189-97.

227. Xu J., Shamul J. G., Wang H., *et al.* Targeted Heating of Mitochondria Greatly Augments Nanoparticle-Mediated Cancer Chemotherapy. Advanced healthcare materials. 2020;9(14):181-200.

228. Doak S. H., Dusinska M. NanoGenotoxicology: present and the future. Mutagenesis. 2016;32(1):1-4.

229. Singh N., Nelson B. C., Scanlan L. D., *et al.* Exposure to Engineered Nanomaterials: Impact on DNA Repair Pathways. Int J Mol Sci. 2017;18(7):1515.

230. *PL*atel A., Carpentier R., Becart E., *et al.* Influence of the surface charge of *PLGA* nanoparticles on their in vitro genotoxicity, cytotoxicity, ROS production and endocytosis. JOURNAL Ap*PL* Toxicol. 2016;36(3):434-44.

231. Tulinska J., Kazimirova A., Kuricova M., *et al.* Immunotoxicity and genotoxicity testing of *PLGA*-PEO nanoparticles in human blood cell model. Nanotoxicology. 2015;9(sup1):33-43.

232. Kazimirova A., Magdolenova Z., Barancokova M., *et al.* Genotoxicity testing of *PLGA*-PEO nanoparticles in TK6 cells by the comet assay and the cytokinesis-block micronucleus assay. Mutat Res. 2012;748(1-2):42-7.

233. Reuter S., Gupta S. C., Chaturvedi M. M., *et al.* Oxidative stress, inflammation, and cancer: how are they linked? Free Radicals Biology Medicines. 2010;49(11):1603-16.

234. Wong J., Magun B. E., Wood L. J. Lung inflammation caused by inhaled toxicants: a review. International Journal Chronic Obstructive Pulmonary Disease. 2016;11:1391-401.

235. Chen L., Deng H., Cui H., *et al.* Inflammatory responses and inflammation-associated diseases in organs. Oncotarget. 2017;9(6):7204-18.

236. Braakhuis H. M., Park M. V., Gosens I., *et al.* Physicochemical characteristics of nanomaterials that affect pulmonary inflammation. Part Fibre Toxicol. 2014;11:18.

237. Thomas C., Rawat A., Hope-Weeks L., *et al.* Aerosolized *PL*A and *PLGA* nanoparticles enhance humoral, mucosal and cytokine responses to hepatitis B vaccine. Mol Pharm. 2011;8(2):405-15.

238. Fittschen C., Sandhaus R., Worthen G., *et al.* Bacterial lipopolysaccharide enhances chemoattractant-induced elastase secretion by human neutrophils. Journal of leukocyte biology. 1988;43(6):547-56.

239. Demento S. L., Eisenbarth S. C., Foellmer H. G., *et al.* Inflammasome-activating nanoparticles as modular systems for optimizing vaccine efficacy. Vaccine. 2009;27(23):3013-21.

240. Mohammadinejad R., Moosavi M. A., Tavakol S., *et al.* Necrotic, apoptotic and autophagic cell fates triggered by nanoparticles. Autophagy. 2019;15(1):4-33.

241. Tang D., Kang R., Berghe T. V., *et al.* The molecular machinery of regulated cell death. Cell Res. 2019;29(5):347-64.

242. Julien O., Wells J. A. Caspases and their substrates. Cell Death & Differentiation. 2017;24(8):1380-9.

243. Mohammadinejad R., Moosavi M. A., Tavakol S., *et al.* Necrotic, apoptotic and autophagic cell fates triggered by nanoparticles. Autophagy. 2019;15(1):4-33.

244. Garcia-Mouton C., Hidalgo A., Cruz A., *et al.* The Lord of the Lungs: The essential role of pulmonary surfactant upon inhalation of nanoparticles. European Journal of Pharmaceutics and Biopharmaceutics. 2019;144:230-43.

245. Jakobsson J. K. F., Aaltonen H. L., Nicklasson H., *et al.* Altered deposition of inhaled nanoparticles in subjects with chronic obstructive pulmonary disease. BMC pulmonary medicine. 2018;18(1):129.

246. Xabi M., Cristiane de Souza C., Claus-Michael L. Overcoming the pulmonary barrier: new insights to improve the efficiency of inhaled therapeutics. European Journal of Nanomedicine. 2014;6(3):157-69.

247. Boegh M., Nielsen H. M. Mucus as a barrier to drug delivery–understanding and mimicking the barrier properties. Basic & clinical pharmacology & toxicology. 2015;116(3):179-86.

248. Lai S. K., Wang Y.-Y., Hanes J. Mucus-penetrating nanoparticles for drug and gene delivery to mucosal tissues. Advanced drug delivery reviews. 2009;61(2):158-71.

249. Vaghasiya K., Sharma A., Ray E., *et al.* Methods to Characterize Nanoparticles for Mucosal Drug Delivery. In: Muttil P. KNeMDoDaBiNAAitPR, editor. Mucosal Delivery of Drugs and Biologics in Nanoparticles. 41: Springer; 2020. p. 27-57.

250. Djekic L., Martinovic M. In Vitro, Ex Vivo and In Vivo Methods for Characterization of Bioadhesiveness of Drug Delivery Systems. Bioadhesives in Drug Delivery. 2020:57-98.

251. Mura S., Hillaireau H., Nicolas J., *et al.* Influence of surface charge on the potential toxicity of *PLGA* nanoparticles towards Calu-3 cells. International journal of nanomedicine. 2011;6:2591-605.

252. Hu G., Jiao B., Shi X., *et al.* Physicochemical Properties of Nanoparticles Regulate Translocation across Pulmonary Surfactant Monolayer and Formation of Lipoprotein Corona. ACS Nano. 2013;7(12):10525-33.

253. Partikel K., Korte R., Stein N. C., *et al.* Effect of nanoparticle size and PEGylation on the protein corona of *PLGA* nanoparticles. European Journal of Pharmaceutics and Biopharmaceutics. 2019;141:70-80.

254. Raesch S. S., Tenzer S., Storck W., *et al.* Proteomic and Lipidomic Analysis of Nanoparticle Corona upon Contact with Lung Surfactant Reveals Differences in Protein, but Not Lipid Composition. ACS Nano. 2015;9(12):11872-85.

255. Hidalgo A., Cruz A., Pérez-Gil J. Pulmonary surfactant and nanocarriers: Toxicity versus combined nanomedical applications. Biochimica et Biophysica Acta (BBA) - Biomembranes. 2017;1859(9, Part B):1740-8.

256. Schneider C. S., Xu Q., Boylan N. J., *et al.* Nanoparticles that do not adhere to mucus provide uniform and long-lasting drug delivery to airways following inhalation. Sci Adv. 2017;3(4):e1601556.

257. Zhang B., Lung P. S., Zhao S., *et al.* Shape dependent cytotoxicity of *PLGA*-PEG nanoparticles on human cells. Scientific Reports. 2017;7(1):1-8.

258. Mlika M., Adigun R., Gossman W. G. Silicosis (Coal Worker Pneumoconiosis). StatPearls [Internet]: StatPearls Publishing; 2020.

259. Yoo J.-W., Mitragotri S. Polymer particles that switch shape in response to a stimulus. Proceedings of the National Academy of Sciences. 2010;107(25):11205-10.

260. Truong N. P., Whittaker M. R., Mak C. W., *et al.* The importance of nanoparticle shape in cancer drug delivery. Expert Opin Drug Deliv. 2015;12(1):129-42.

261. Mittal G., Sahana D., Bhardwaj V., *et al.* Estradiol loaded *PLGA* nanoparticles for oral administration: effect of polymer molecular weight and copolymer composition on release behavior in vitro and in vivo. Journal of Controlled Release. 2007;119(1):77-85.

262. Fonseca C., Simoes S., Gaspar R. Paclitaxel-loaded *PLGA* nanoparticles: preparation, physicochemical characterization and in vitro anti-tumoral activity. Journal of Controlled Release. 2002;83(2):273-86.

263. Song X., Zhao Y., Wu W., *et al. PLGA* nanoparticles simultaneously loaded with vincristine sulfate and verapamil hydrochloride: systematic study of particle size and drug entrapment efficiency. International Journal of Pharmaceutics. 2008;350(1-2):320-9.

264. Grabowski N., Hillaireau H., Vergnaud J., *et al.* Surface coating mediates the toxicity of polymeric nanoparticles towards human-like macrophages. International Journal of Pharmaceutics. 2015;482(1-2):75-83.

265. Vetten M. A., Gulumian M. Interference of Gold Nanoparticles with In vitro Endotoxin Detection Assays. Current Nanoscience. 2020;16(2):204-13.

266. Oostingh G. J., Casals E., Italiani P., *et al.* Problems and challenges in the development and validation of human cell-based assays to determine nanoparticle-induced immunomodulatory effects. Particle and Fibre Toxicology. 2011;8(1):8.

267. Li Y., Boraschi D. Endotoxin contamination: a key element in the interpretation of nanosafety studies. Nanomedicine (London, England). 2016;11(3):269-87.

268. Limbach L. K., Li Y., Grass R. N., *et al.* Oxide nanoparticle uptake in human lung fibroblasts: effects of particle size, agglomeration, and diffusion at low concentrations. Environ Sci Technol. 2005;39(23):9370-6.

269. Drescher D., Orts-Gil G., Laube G., *et al.* Toxicity of amorphous silica nanoparticles on eukaryotic cell model is determined by particle agglomeration and serum protein adsorption effects. Anal Bioanal Chem. 2011;400(5):1367-73.

270. Gatoo M. A., Naseem S., Arfat M. Y., *et al.* Physicochemical Properties of Nanomaterials: Im*PL*ication in Associated Toxic Manifestations. BioMed Research International. 2014;2014:8.

271. Wu L., Zhang J., Watanabe W. Physical and chemical stability of drug nanoparticles. Advanced drug delivery reviews. 2011;63(6):456-69.

272. Donaldson K., Borm P. J., Castranova V., *et al.* The limits of testing particle-mediated oxidative stress in vitro in predicting diverse pathologies; relevance for testing of nanoparticles. Part Fibre Toxicol. 2009;6:13.

273. Sayes C. M., Warheit D. B. Characterization of nanomaterials for toxicity assessment. Wiley Interdiscip Rev Nanomed Nanobiotechnol. 2009;1(6):660-70.

274. Mourdikoudis S., Pallares R. M., Thanh N. T. K. Characterization techniques for nanoparticles: comparison and complementarity upon studying nanoparticle properties. Nanoscale. 2018;10(27):12871-934.

275. Joris F., Manshian B. B., Peynshaert K., *et al.* Assessing nanoparticle toxicity in cell-based assays: influence of cell culture parameters and optimized models for bridging the in vitro-in vivo gap. Chemistry Society Reviews. 2013;42(21):8339-59.

276. Sakagami M. In vitro, ex vivo and in vivo methods of lung absorption for inhaled drugs. Advanced drug delivery reviews. 2020;In Press.

277. Nahar K., Gupta N., Gauvin R., *et al.* In vitro, in vivo and ex vivo models for studying particle deposition and drug absorption of inhaled pharmaceuticals. European Journal of Pharmaceutical Sciences. 2013;49(5):805-18.

278. Gordon S., Daneshian M., Bouwstra J., *et al.* Non-animal models of epithelial barriers (skin, intestine and lung) in research, industrial applications and regulatory toxicology. Altex. 2015;32(4):327-78.

279. Braakhuis H. M., He R., Vandebriel R. J., *et al.* An Air-liquid Interface Bronchial Epithelial Model for Realistic, Repeated Inhalation Exposure to Airborne Particles for Toxicity Testing. JoVE (Journal of Visualized Experiments). 2020(159):e61210.

280. Sayes C. M., Reed K. L., Warheit D. B. Assessing toxicity of fine and nanoparticles: comparing in vitro measurements to in vivo pulmonary toxicity profiles. Toxicol Sci. 2007;97(1):163-80.

281. Grainger C. I., Greenwell L. L., Lockley D. J., *et al.* Culture of Calu-3 Cells at the Air Interface Provides a Representative Model of the Airway Epithelial Barrier. Pharmaceutical Research. 2006;23(7):1482-90.

282. Hiemstra P. S., Grootaers G., van der Does A. M., *et al.* Human lung epithelial cell cultures for analysis of inhaled toxicants: Lessons learned and future directions. Toxicology in Vitro. 2018;47:137-46.

283. Reeves S. R., Barrow K. A., White M. P., *et al.* Stability of gene expression by primary bronchial epithelial cells over increasing passage number. BMC pulmonary medicine. 2018;18(1):91-143.

284. Papazian D., Würtzen P. A., Hansen S. W. Polarized airway epithelial models for immunological co-culture studies. International archives of allergy and immunology. 2016;170(1):1-21.

285. Rayner R. E., Makena P., Prasad G. L., *et al.* Optimization of normal human bronchial epithelial (NHBE) cell 3D cultures for in vitro lung model studies. Scientific Reports. 2019;9(1):1-10.

286. Reus A. A., Maas W. J., Jansen H. T., *et al.* Feasibility of a 3D human airway epithelial model to study respiratory absorption. Toxicol In Vitro. 2014;28(2):258-64.

287. Tenenbaum-Katan J., Artzy-Schnirman A., Fishler R., *et al.* Biomimetics of the pulmonary environment in vitro: A microfluidics perspective. Biomicrofluidics. 2018;12(4):042209.

288. Rasmussen K., Rauscher H., Kearns P., *et al.* Developing OECD test guidelines for regulatory testing of nanomaterials to ensure mutual acceptance of test data. Regul Toxicol Pharmacol. 2019;104:74-83.

289. Li M., Byron P. R. Tobramycin disposition in the rat lung following airway administration. Journal of Pharmacology and Experimental Therapeutics. 2013;347(2):318-24.

290. Kim Y. H., Boykin E., Stevens T., *et al.* Comparative lung toxicity of engineered nanomaterials utilizing in vitro, ex vivo and in vivo approaches. J Nanobiotechnology. 2014;12(1):47.

291. Dumigan A., Fitzgerald M., Santos J. S.-P. G., *et al.* A Porcine Ex Vivo Lung Perfusion Model To Investigate Bacterial Pathogenesis. mBio. 2019;10(6):e02802-19.

292. Ross J. T., Nesseler N., Lee J.-W., *et al.* The ex vivo human lung: research value for translational science. JCI insight. 2019;4(11).

293. Slama A., Raber C., Hedderich C., *et al.* Im*PL*ementation of an experimental isolated lung perfusion model on surgically resected human lobes. Scientific Reports. 2019;9(1):12-93.

294. Liu G., Betts C., Cunoosamy D. M., *et al.* Use of precision cut lung slices as a translational model for the study of lung biology. Respiratory Research. 2019;20(1):162.

295. Oberdorster G., Kuhlbusch T. A. J. In vivo effects: Methodologies and biokinetics of inhaled nanomaterials. NanoImpact. 2018;10:38-60.

296. Myatt G. J., Ahlberg E., Akahori Y., *et al.* In silico toxicology protocols. Regulatory Toxicology and Pharmacology. 2018;96:1-17.

297. Nel A., Xia T., Meng H., *et al.* Nanomaterial toxicity testing in the 21st century: use of a predictive toxicological approach and high-throughput screening. Chemistry Research. 2013;46(3):607-21.

298. Wagnera A. M., Granb, M. P., Peppasa, N. A. Designing the new generation of intelligent biocompatible carriers for protein and peptide delivery. Acta Pharmaceutica Sinica B. 2018.

299. Congcong Lin, Xue Zhang, Hubiao Chen, *et al.* Dual-ligand modified liposomes provide effective local targeted delivery of lung-cancer drug by antibody and tumor lineage-homing cell-penetrating peptide. Drug delivery. 2018;25(1):256-66.

300. Suzuki H., Ueno K., Mizumoto T., *et al.* Self-micellizing solid dispersion of cyclosporine A for pulmonary delivery: Physicochemical, pharmacokinetic and safety assessments. European Journal of Pharmaceutics Sciences. 2017;96:107-14.

301. Qiu T. A., Clement P. L., Haynes C. L. Linking nanomaterial properties to biological outcomes: analytical chemistry challenges in nanotoxicology for the next decade. Chem Commun (Camb). 2018;54(91):12787-803.

302. Raies A. B., Bajic V. B. In silico toxicology: computational methods for the prediction of chemical toxicity. Wiley interdisci*PL*inary reviews Computational molecular science. 2016;6(2):147-72.

303. Marin E., Briceño M. I., Caballero-George C. Critical evaluation of biodegradable polymers used in nanodrugs. International journal of nanomedicine. 2013;8:30-71.

304. Okada M. Chemical syntheses of biodegradable polymers. Progress in Polymer Science. 2002;27(1):87-133.

305. Chaudhary A. K., Beckman, E. J., Russell, A. J. Rational Control of Polymer Molecular Weight and Dispersity during Enzyme-Catalyzed Polyester Synthesis in Supercritical Fluids. Journal of the American Chemical Society. 1995;117(13):3728-33.

306. Namekawa S., Uyama, H., Kobayashi, S. Enzymatic Synthesis of Polyesters from Lactones, Dicarboxylic Acid Divinyl Esters, and Glycols through Combination of Ring-Opening Polymerization and Polycondensation. Biomacromolecules. 2000;1(3):335-8.

307. Kobayashi S., Uyama, H. In vitro polyester synthesis via enzymatic polymerization. Current Organic Chemistry. 2002;6(2):209-22.

308. Kobayashi S., Takeya, K., Suda, S., Uyama, H. Lipase-catalyzed ring-opening polymerization of medium-size lactones to polyesters. Macromolecular Chemistry and Physics. 1998;199(8):1729-36.

309. Uyama H., Kikuchi, H., Takeya, K., Hoshi, N., Kobayashi, S. Immobilized lipase showing high catalytic activity toward enzymatic ring-opening polymerization of macrolides. Chemistry Letters. 1996(2):107-8.

310. Kobayashi S. Lipase-catalyzed polyester synthesis - A green polymer chemistry. Proceedings of the Japan Academy Series B-Physical and Biological Sciences. 2010;86(4):338-65.

311. Margolin A. L., Crenne, J., Klibanov, A. M. Stereoselective oligomerizations catalyzed by lipases in organic solvents. Tetrahedron Letters. 1987;28(15):1607-9.

312. Therisod M., Klibanov, A. M. Facile enzymatic preparation of monoacylated sugars in pyridine. Journal of the American Chemical Society. 1986;108(18):5638-40.

313. Uyama H., Klegraf, E., Wada, S., Kobayashi, S. Regioselective polymerization of sorbitol and divinyl sebacate using lipase catalyst. Chemistry Letters. 2000(7):800-1.

314. Iftikhar A. Enzymatic synthesis and evaluation of biodegradable polyesters for microparticulate drug delivery: Liverpool John Moores University; 2011.

315. Namekawa S., Uyama H., Kobayashi S. Enzymatic synthesis of polyesters from lactones, dicarboxylic acid divinyl esters, and glycols through combination of ring-opening polymerization and polycondensation. Biomacromolecules. 2000;1(3):335-8.

316. Tawfeek H. M., Abdellatif A. A. H., Dennison T. J., *et al*. Colonic delivery of indometacin loaded *PGA-co-PDL*microparticles coated with Eudragit L100-55 from fast disintegrating tablets. International Journal of Pharmaceutics. 2017;531(1):80-9.

317. Gaskell E. E., Hobbs G., Rostron C., *et al.* Encapsulation and release of α-chymotrypsin from poly(glycerol adipate-co-ω-pentadecalactone) microparticles. Journal of Microencapsulation. 2008;25(3):187-95.

318. Lu L., Garcia C. A., Mikos A. G. In vitro degradation of thin poly(DL-lactic-co-glycolic acid) films. JOURNAL Biomed Mater Res. 1999;46(2):236-44.

319. Marques M. R., Loebenberg R., Almukainzi M. Simulated biological fluids with possible application in dissolution testing. Dissolution Technol. 2011;18(3):15-28.

320. Sharma S., Parmar A., Kori S., *et al. PLGA*-based nanoparticles: A new paradigm in biomedical applications. TrAC Trends in Analytical Chemistry. 2016;80:30-40.

321. McCall R. L., Sirianni R. W. *PLGA* nanoparticles formed by single-or double-emulsion with vitamin E-T*PG*S. JoVE (Journal of Visualized Experiments). 2013(82):e51015.

322. Iqbal M., Zafar N., Fessi H., *et al.* Double emulsion solvent evaporation techniques used for drug encapsulation. International Journal of Pharmaceutics. 2015;496(2):173-90.

323. Blehn G. F., Ernsberger M. L. Polyvinyl Alcohol as an Emulsifying Agent. Industrial & Engineering Chemistry. 1948;40(8):1449-53.

324. Jensen D. K., Jensen L. B., Koocheki S., *et al.* Design of an inhalable dry powder formulation of DOTA*P*-modified *PLGA* nanoparticles loaded with siRNA. J Control Release. 2012;157(1):141-8.

325. Campbell R. B., Balasubramanian S. V., Straubinger R. M. Phospholipid-cationic lipid interactions: influences on membrane and vesicle properties. Biochimica et Biophysica Acta (BBA) - Biomembranes. 2001;1512(1):27-39.

326. Hagigit T., Nassar T., Behar-Cohen F., *et al.* The influence of cationic lipid type on in-vitro release kinetic profiles of antisense oligonucleotide from cationic nanoemulsions. European Journal of Pharmaceutical Sciences. 2008;70(1):248-59.

327. Simberg D., Weisman S., Talmon Y., *et al.* DOTAP (and other cationic lipids): chemistry, biophysics, and transfection. Crit Rev Ther Drug Carrier Syst. 2004;21(4):257-317.

328. Bose R. J., Arai Y., Ahn J. C., *et al.* Influence of cationic lipid concentration on properties of lipid-polymer hybrid nanospheres for gene delivery. International Journal Nanomedicine. 2015;10:5367-82.

329. Mainardes R. M., Evangelista R. C. *PLGA* nanoparticles containing praziquantel: effect of formulation variables on size distribution. International Journal of Pharmaceutics. 2005;290(1):137-44.

330. Honary S., Zahir F. Effect of zeta potential on the properties of nano-drug delivery systems-a review (Part 2). Tropical Journal of Pharmaceutical Research. 2013;12(2):265-73.

331. Arvizo R. R., Miranda O. R., Thompson M. A., *et al.* Effect of nanoparticle surface charge at the Plasma membrane and beyond. Nano letters. 2010;10(7):2543-8.

332. Fröhlich E. The role of surface charge in cellular uptake and cytotoxicity of medical nanoparticles. International journal of nanomedicine. 2012;7:5577-91.

333. He C., Hu Y., Yin L., *et al.* Effects of particle size and surface charge on cellular uptake and biodistribution of polymeric nanoparticles. Biomaterials. 2010;31(13):3657-66.

334. Cedervall T., Lynch I., Lindman S., *et al.* Understanding the nanoparticle–protein corona using methods to quantify exchange rates and affinities of proteins for nanoparticles. Proceedings of the National Academy of Sciences. 2007;104(7):2050-5.

335. Lundqvist M., Stigler J., Elia G., *et al.* Nanoparticle size and surface properties determine the protein corona with possible implication for biological impacts. Proceedings of the National Academy of Sciences. 2008;105(38):14265-70.

336. Monopoli M. P., Åberg C., Salvati A., *et al.* Biomolecular coronas provide the biological identity of nanosized materials. Nature Nanotechnology. 2012;7(12):779-86.

337. Walkey C. D., Olsen J. B., Guo H., *et al.* Nanoparticle size and surface chemistry determine serum protein adsorption and macrophage uptake. Journal of the American Chemical Society. 2012;134(4):2139-47.

338. Zhang Y., Wu J. L., Lazarovits J., *et al.* An analysis of the binding function and structural organization of the protein corona. Journal of the American Chemical Society. 2020;142(19):8827-36.

339. Hickey J. W., Santos J. L., Williford J.-M., *et al.* Control of polymeric nanoparticle size to improve therapeutic delivery. J Control Release. 2015;219:536-47.

340. Liu N., Tang M., Ding J. The interaction between nanoparticles-protein corona complex and cells and its toxic effect on cells. Chemosphere. 2020;245:125624.

341. Docter D., Westmeier D., Markiewicz M., *et al.* The nanoparticle biomolecule corona: lessons learned–challenge accepted? Chemical Society Reviews. 2015;44(17):6094-121.

342. Van Hong Nguyen B.-J. L. Protein corona: a new approach for nanomedicine design. International journal of nanomedicine. 2017;12:31-7.

343. Wang J., Feng S.-S., Wang S., *et al.* Evaluation of cationic nanoparticles of biodegradable copolymers as siRNA delivery system for hepatitis B treatment. International Journal of Pharmaceutics. 2010;400(1):194-200.

344. Chen X., Gao C. Influences of surface coating of *PLGA* nanoparticles on immune activation of macrophages. Journal of Materials Chemistry B. 2018;6(14):2065-77.

345. Partikel K., Korte R., Mulac D., *et al.* Serum type and concentration both affect the protein-corona composition of *PLGA* nanoparticles. Beilstein Journal of Nanotechnology. 2019;10(1):1002-15.

346. Calas A., Uzu G., Martins J. M., *et al.* The importance of simulated lung fluid (SLF) extractions for a more relevant evaluation of the oxidative potential of particulate matter. Scientific Reports. 2017;7(1):1-12.

347. Menon J. U., Ravikumar P., Pise A., *et al.* Polymeric nanoparticles for pulmonary protein and DNA delivery. Acta Biomaterialia. 2014;10(6):2643-52.

348. Engineer C., Parikh J., Raval A. Review on hydrolytic degradation behavior of biodegradable polymers from controlled drug delivery system. Trends in Biomaterials & Artificial Organs. 2011;25(2):23-45.

349. Kumskova N., Ermolenko Y., Osipova N., *et al.* How subtle differences in polymer molecular weight affect doxorubicin-loaded *PLGA* nanoparticles degradation and drug release. Journal of Microencapsulation. 2020;37(3):283-95.

350. Hussein A. S., Abdullah N., Ahmadun F. R. In vitro degradation of poly (D, L-lactide-co-glycolide) nanoparticles loaded with linamarin. IET Nanobiotechnol. 2013;7(2):33-41.

351. Polloni A. E., Chiaradia V., Figura E. M., *et al.* Polyesters from macrolactones using commercial lipase NS 88011 and Novozym 435 as biocatalysts. Applied biochemistry and biotechnology. 2018;184(2):659-72.

352. Rescignano N., Tarpani L., Romani A., *et al.* In-vitro degradation of *PLGA* nanoparticles in aqueous medium and in stem cell cultures by monitoring the cargo fluorescence spectrum. Polymer Degradation and Stability. 2016;134:296-304.

353. Swider E., Maharjan S., Houkes K., *et al.* Förster Resonance Energy Transfer-Based Stability Assessment of *PLGA* Nanoparticles in Vitro and in Vivo. ACS Applied Bio Materials. 2019;2(3):1131-40.

354. Fischer H., Widdicombe J. H. Mechanisms of acid and base secretion by the airway epithelium. JOURNAL Membr Biol. 2006;211(3):139-50.

355. Fischer H. Function of Proton Channels in Lung Epithelia. Wiley interdisci*PL*inary reviews Membrane transport and signaling. 2012;1(3):247-58.

356. Capasso M., DeCoursey T. E., Dyer M. J. pH regulation and beyond: unanticipated functions for the voltage-gated proton channel, HVCN1. Trends Cell Biol. 2011;21(1):20-8.

357. Kato Y., Ozawa S., Miyamoto C., *et al.* Acidic extracellular microenvironment and cancer. Cancer cell international. 2013;13(1):1-8.

358. Groos E., Walker L., Masters J. R. Intravesical chemotherapy. Studies on the relationship between pH and cytotoxicity. Cancer. 1986;58(6):1199-203.

359. Smith S., Martin P., Edwards R. Tumour pH and response to chemotherapy: an in vivo 31P magnetic resonance spectroscopy study in non-Hodgkin's lymphoma. The British journal of radiology. 1991;64(766):923-8.

360. Hamaguchi R., Narui R., Wada H. Effects of Alkalization Therapy on Chemotherapy Outcomes in Metastatic or Recurrent Pancreatic Cancer. Anticancer Res. 2020;40(2):873-80.

361. Izumi H., Torigoe T., Ishiguchi H., *et al.* Cellular pH regulators: potentially promising molecular targets for cancer chemotherapy. Cancer treatment reviews. 2003;29(6):541-9.

362. Dai Y., Xu C., Sun X., *et al.* Nanoparticle design strategies for enhanced anticancer therapy by ex*PL*oiting the tumour microenvironment. Chemical Society Reviews. 2017;46(12):3830-52.

363. Faber S. C., McCullough S. D. Through the Looking Glass: In Vitro Models for Inhalation Toxicology and Interindividual Variability in the Airway. Application In Vitro Toxicology. 2018;4(2):115-28.

364. Monteiro-Riviere N. A., Inman A. O., Zhang L. W. Limitations and relative utility of screening assays to assess engineered nanoparticle toxicity in a human cell line. Toxicol Ap*PL* Pharmacol. 2009;234(2):222-35.

365. Stoddart M. J. Cell viability assays: introduction. Methods Mol Biol. 2011;740:1-6.

366. Dhawan A., Sharma V. Toxicity assessment of nanomaterials: methods and challenges. Anal Bioanal Chem. 2010;398(2):589-605.

367. Jesus S., Schmutz M., Som C., *et al.* Hazard Assessment of Polymeric Nanobiomaterials for Drug Delivery: What Can We Learn From Literature So Far. Frontiers in Bioengineering and Biotechnology. 2019;7(261).

368. Singh A. V., Laux P., Luch A., *et al.* Review of emerging concepts in nanotoxicology: opportunities and challenges for safer nanomaterial design. Toxicology Mechanisms and Methods. 2019;29(5):378-87.

369. d'Angelo I., Quaglia F., Ungaro F. *PLGA* carriers for inhalation: where do we stand, where are we headed? Therapeutic Delivery. 2015;6(10):1139-44.

370. Mir M., Ahmed N., Rehman A. u. Recent applications of *PLGA* based nanostructures in drug delivery. Colloids and Surfaces B: Biointerfaces. 2017;159:217-31.

371. Al-Nasiry S., Geusens N., Hanssens M., *et al.* The use of Alamar Blue assay for quantitative analysis of viability, migration and invasion of choriocarcinoma cells. Human Reproduction. 2007;22(5):1304-9.

372. Gu W., Zhang S., Li Y., *et al.* [Study on cytotoxicity of respiratory system exposed to fine particulate matter by real time cell analyze and Alamar Blue]. Wei Sheng Yan Jiu. 2016;45(5):829-33.

373. Eruslanov E., Kusmartsev S. Identification of ROS using oxidized DCFDA and flow-cytometry. Methods Mol Biol. 2010;594:57-72.

374. Lorscheidt S., Lamprecht A. Safety assessment of nanoparticles for drug delivery by means of classic in vitro assays and beyond. Expert Opinion on Drug Delivery. 2016;13(11):1545-58.

375. Kong C., Miao F., Wu Y., *et al.* Oxycodone suppresses the apoptosis of hippocampal neurons induced by oxygen-glucose deprivation/recovery through caspase-dependent and caspase-independent pathways via κ- and δ-opioid receptors in rats. Brain Research. 2019;1721:146319.

376. Sivandzade F., Bhalerao A., Cucullo L. Analysis of the Mitochondrial Membrane Potential Using the Cationic JC-1 Dye as a Sensitive Fluorescent Probe. Bio-protocol. 2019;9(1):e3128.

377. Decker T., Lohmann-Matthes M.-L. A quick and simple method for the quantitation of lactate dehydrogenase release in measurements of cellular cytotoxicity and tumor necrosis factor (TNF) activity. Journal of Immunological Methods. 1988;115(1):61-9.

378. Witika B. A., Makoni P. A., Matafwali S. K., *et al.* Biocompatibility of Biomaterials for Nanoencapsulation: Current Approaches. Nanomaterials. 2020;10(9):1649.

379. Allen M., Millett P., Dawes E., *et al.* Lactate dehydrogenase activity as a rapid and sensitive test for the quantification of cell numbers in vitro. Clinical Materials. 1994;16(4):189-94.

380. Hiebl B., Peters S., Gemeinhardt O., *et al.* Impact of serum in cell culture media on in vitro lactate dehydrogenase (LDH) release determination. Journal of Cellular Biotechnology. 2017;3:9-13.

381. Klezovitch O., Edelstein C., Scanu A. M. Stimulation of Interleukin-8 Production in Human THP-1 Macrophages by Apolipoprotein(a): EVIDENCE FOR A CRITICAL INVOLVEMENT OF ELEMENTS IN ITS C-TERMINAL DOMAIN. Journal of Biological Chemistry. 2001;276(50):46864-9.

382. Kamiloglu S., Sari G., Ozdal T., *et al.* Guidelines for cell viability assays. Food Frontiers. 2020;1(3):332-49.

383. Kumar G., Degheidy H., Casey B. J., *et al.* Flow cytometry evaluation of in vitro cellular necrosis and apoptosis induced by silver nanoparticles. Food and chemical toxicology. 2015;85:45-51.

384. Grabowski N., Hillaireau H., Vergnaud J., *et al.* Toxicity of surface-modified *PLGA* nanoparticles toward lung alveolar epithelial cells. International Journal of Pharmaceutics. 2013;454(2):686-94.

385. Lecoeur H., de Oliveira-Pinto L. M., Gougeon M.-L. Multiparametric flow cytometric analysis of biochemical and functional events associated with apoptosis and

oncosis using the 7-aminoactinomycin D assay. Journal of Immunological Methods. 2002;265(1):81-96.

386. Shaulov-Rotem Y., Merquiol E., Weiss-Sadan T., *et al.* A novel quenched fluorescent activity-based probe reveals caspase-3 activity in the endoplasmic reticulum during apoptosis. Chemical Science. 2016;7(2):1322-37.

387. Prabhakar U. E. E., Miller B.E., Davis H.M. Multiplexed Cytokine Sandwich Immunoassays Clinical Applications In: Microarrays in Clinical Diagnostics. Methods in Molecular Medicine™, vol 114. Humana Press. Joos T.O. FPe, editor: Humana Press; 2005.

388. Prabhakar U., Eirikis E., Reddy M., *et al.* Validation and comparative analysis of a multiplexed assay for the simultaneous quantitative measurement of Th1/Th2 cytokines in human serum and human peripheral blood mononuclear cell culture supernatants. Journal of Immunological Methods. 2004;291(1):27-38.

389. Kellar K. L., Douglass J. P. Multiplexed microsphere-based flow cytometric immunoassays for human cytokines. Journal of Immunological Methods. 2003;279(1):277-85.

390. Langie S., Azqueta A., Collins A. The comet assay: past, present, and future. Frontiers in Genetics. 2015;6(1):5-26.

391. Ostling O., Johanson K. J. Microelectrophoretic study of radiation-induced DNA damages in individual mammalian cells. Biochemical and Biophysical Research Communications. 1984;123(1):291-8.

392. Liao W., McNutt M. A., Zhu W.-G. The comet assay: A sensitive method for detecting DNA damage in individual cells. Methods. 2009;48(1):46-53.

393. Olive P. L., Banath J. P., Durand R. E. Heterogeneity in radiation-induced DNA damage and repair in tumor and normal cells measured using the "comet" assay. Radiat Res. 1990;122(1):86-94.

394. Jesus S., Schmutz M., Som C., *et al.* Hazard assessment of polymeric nanobiomaterials for drug delivery: what can we learn from literature so far. Frontiers in Bioengineering and Biotechnology. 2019;7:261.

395. Rampersad S. N. Multiple applications of Alamar Blue as an indicator of metabolic function and cellular health in cell viability bioassays. Sensors (Basel, Switzerland). 2012;12(9):12347-60.

396. Prabha S., Arya G., Chandra R., *et al.* Effect of size on biological properties of nanoparticles employed in gene delivery. Artificial Cells, Nanomedicine, and Biotechnology. 2016;44(1):83-91.

397. Xiong S., George S., Yu H., *et al.* Size influences the cytotoxicity of poly (lactic-co-glycolic acid) (*PLGA*) and titanium dioxide (TiO2) nanoparticles. Arch Toxicol. 2013;87(6):1075-86.

398. Yasar H., Biehl A., De Rossi C., *et al.* Kinetics of mRNA delivery and protein translation in dendritic cells using lipid-coated *PLGA* nanoparticles. Journal Nanobiotechnology. 2018;16(1):1-72.

399. Grabowski N., Hillaireau H., Vergnaud-Gauduchon J., *et al.* Surface-Modified Biodegradable Nanoparticles' Impact on Cytotoxicity and Inflammation Response on a Co-Culture of Lung Epithelial Cells and Human-Like Macrophages. Journal of Biomedical Nanotechnology. 2016;12(1):135-46.

400. Fulda S., Gorman A. M., Hori O., *et al.* Cellular Stress Responses: Cell Survival and Cell Death. International Journal of Cell Biology. 2010;10:52-74.

401. Pizzinga M., Harvey R. F., Garland G. D., *et al.* The cell stress response: extreme times call for post-transcriptional measures. WIREs RNA. 2020;11(3):e1578.

402. Roces CB H. M., Schmidt ST, Christensen D, Perrie Y. . Investigating Prime-Pull Vaccination through a Combination of Parenteral Vaccination and Intranasal Boosting. Vaccines. 2020;8(1):10.

403. Gratton S. E. A., Ropp P. A., Pohlhaus P. D., *et al.* The effect of particle design on cellular internalization pathways. Proceedings of the National Academy of Sciences of the United States of America. 2008;105(33):11613-8.

404. Magnani N. D., Marchini T., Calabró V., *et al.* Role of mitochondria in the redox signaling network and its outcomes in high impact inflammatory syndromes. Frontiers in Endocrinology. 2020;11(4):56-67.

405. Di Meo S., Reed T. T., Venditti P., *et al.* Role of ROS and RNS Sources in Physiological and Pathological Conditions. Oxidative Medicine and Cellular Longevity. 2016;2016:1245049.

406. Venditti P., Di Meo S. The role of reactive oxygen species in the life cycle of the mitochondrion. International Journal of Molecular Sciences. 2020;21(6):2173.

407. Forrester S. J., Kikuchi D. S., Hernandes M. S., *et al.* Reactive Oxygen Species in Metabolic and Inflammatory Signaling. Circulation Research. 2018;122(6):877-902.

408. Karanam G., Arumugam M. K. Reactive oxygen species generation and mitochondrial dysfunction for the initiation of apoptotic cell death in human hepatocellular carcinoma He*PG*2 cells by a cyclic dipeptide Cyclo (-Pro-Tyr). Molecular Biology Reports. 2020(5):47-59.

409. Testa M. P., Alvarado O., Wournell A., *et al.* Screening assay for oxidative stress in a feline astrocyte cell line, G355-5. JoVE (Journal of Visualized Experiments). 2011(53):e2841.

410. Gogvadze V., Orrenius S., Zhivotovsky B. Mitochondria in cancer cells: what is so special about them? Trends Cell Biol. 2008;18(4):165-73.

411. Liew S. S., Qin X., Zhou J., *et al.* Smart Design of Nanomaterials for Mitochondria-Targeted Nanotherapeutics. Angewandte Chemie International Edition.1(1):3-43.

412. Stevanović M., Pavlović V., Nunić J., *et al.* ROS-inducing potential, influence of different porogens and in vitro degradation of poly (D, L-lactide-co-glycolide)-based material. Express polymer letters. 2011;5(11):996-1008.

413. Yin Win K., Feng S.-S. Effects of particle size and surface coating on cellular uptake of polymeric nanoparticles for oral delivery of anticancer drugs. Biomaterials. 2005;26(15):2713-22.

414. Singh R. P., Ramarao P. Accumulated polymer degradation products as effector molecules in cytotoxicity of polymeric nanoparticles. Toxicol Sci. 2013;136(1):131-43.

415. Hu J., Liu S. Modulating intracellular oxidative stress via engineered nanotherapeutics. Journal of Controlled Release. 2020;319:333-43.

416. Huang P., Feng L., Oldham E. A., *et al.* Superoxide dismutase as a target for the selective killing of cancer cells. Nature. 2000;407(6802):390-5.

417. Narayanan D., Ma S., Özcelik D. Targeting the redox landscape in cancer therapy. Cancers. 2020;12(7):17-60.

418. Fotakis G., Timbrell J. A. In vitro cytotoxicity assays: comparison of LDH, neutral red, MTT and protein assay in hepatoma cell lines following exposure to cadmium chloride. Toxicol Lett. 2006;160(2):171-7.

419. Jones C. F., Grainger D. W. In vitro assessments of nanomaterial toxicity. Advanced drug delivery reviews. 2009;61(6):438-56.

420. Oparka M., Walczak J., Malinska D., *et al.* Quantifying ROS levels using CM-H2DCFDA and HyPer. Methods. 2016;109:3-11.

421. Figueroa D., Asaduzzaman M., Young F. Real time monitoring and quantification of reactive oxygen species in breast cancer cell line MCF-7 by 2′, 7′–dichlorofluorescin diacetate (DCFDA) assay. Journal of pharmacological and toxicological methods. 2018;94:26-33.

422. Chennoufi R., Trinh N.-D., Simon F., *et al.* InterPlay between Cellular Uptake, Intracellular Localization and the Cell Death Mechanism in Triphenylamine-Mediated Photoinduced Cell Death. Scientific Reports. 2020;10(1):68-81.

423. Li X., Zhao Y., Yin J., *et al.* Organic fluorescent probes for detecting mitochondrial membrane potential. Coordination Chemistry Reviews. 2020;420:213419.

424. Chapman J., Ng Y. S., Nicholls T. J. The Maintenance of Mitochondrial DNA Integrity and Dynamics by Mitochondrial Membranes. Life. 2020;10(9):164.

425. Perry S. W., Norman J. P., Barbieri J., *et al.* Mitochondrial membrane potential probes and the proton gradient: a practical usage guide. Biotechniques. 2011;50(2):98-115.

426. Bulthuis E. P., Adjobo-Hermans M. J., Willems P. H., *et al.* Mitochondrial morphofunction in mammalian cells. Antioxid Redox Signal. 2019;30(18):2066-109.

427. Xu H., Martinoia E., Szabo I. Organellar channels and transporters. Cell calcium. 2015;58(1):1-10.

428. Zorova L. D., Popkov V. A., *PL*otnikov E. Y., *et al.* Mitochondrial membrane potential. Analytical biochemistry. 2018;552:50-9.

429. Kroemer G., Galluzzi L., Brenner C. Mitochondrial membrane permeabilization in cell death. Physiological reviews. 2007;87(1):99-163.

430. Zorov D. B., Juhaszova M., Sollott S. J. Mitochondrial reactive oxygen species (ROS) and ROS-induced ROS release. Physiological reviews. 2014;94(3):909-50.

431. Wacquier B., Combettes L., Dupont G. Dual dynamics of mitochondrial permeability transition pore opening. Scientific Reports. 2020;10(1):1-10.

432. Murphy M. P. How mitochondria produce reactive oxygen species. The Biochemical journal. 2009;417(1):1-13.

433. Rezvantalab S., Drude N. I., Moraveji M. K., *et al.* *PLGA*-Based Nanoparticles in Cancer Treatment. Front Pharmacol. 2018;9(1260).

434. Ikeda G., Matoba T., Nakano Y., *et al.* Nanoparticle-mediated targeting of cyclosporine A enhances cardioprotection against ischemia-reperfusion injury through inhibition of mitochondrial permeability transition pore opening. Scientific Reports. 2016;6:20467.

435. Ishikita A., Matoba T., Ikeda G., *et al.* Nanoparticle-mediated delivery of mitochondrial division inhibitor 1 to the myocardium protects the heart from ischemia-reperfusion injury through inhibition of mitochondria outer membrane permeabilization: a new therapeutic modality for acute myocardial infarction. Journal of the American Heart Association. 2016;5(7):e003872.

436. Balakrishnan K., Casimeer S. C., Ghidan A. Y., *et al.* Bioformulated Hesperidin-Loaded *PLGA* Nanoparticles Counteract the Mitochondrial-Mediated Intrinsic Apoptotic Pathway in Cancer Cells. Journal of Inorganic and Organometallic Polymers and Materials. 2020;12(6):56-76.

437. Marrache S., Dhar S. Engineering of blended nanoparticle *PL*atform for delivery of mitochondria-acting therapeutics. Proceedings of the National Academy of Sciences. 2012;109(40):16288-93.

438. Marrache S., Pathak R. K., Dhar S. Detouring of cis*PL*atin to access mitochondrial genome for overcoming resistance. Proceedings of the National Academy of Sciences. 2014;111(29):10444-9.

439. Nassir A. M., Shahzad N., Ibrahim I. A., *et al.* Resveratrol-loaded *PLGA* nanoparticles mediated programmed cell death in prostate cancer cells. Saudi Pharmaceutical Journal. 2018;26(6):876-85.

440. Velichkovska M., Surnar B., Nair M., *et al.* Targeted mitochondrial COQ10 delivery attenuates Antiretroviral-drug-induced senescence of neural progenitor cells. Molecular Pharmaceutics. 2018;16(2):724-36.

441. Salvioli S., Ardizzoni A., Franceschi C., *et al.* JC-1, but not DiOC6(3) or rhodamine 123, is a reliable fluorescent probe to assess delta psi changes in intact cells: implication for studies on mitochondrial functionality during apoptosis. FEBS Lett. 1997;411(1):77-82.

442. Fan X., Hussien R., Brooks G. A. H2O2-induced mitochondrial fragmentation in C2C12 myocytes. Free Radic Biol Med. 2010;49(11):1646-54.

443. Chan F. K.-M., Moriwaki K., De Rosa M. J. Detection of necrosis by release of lactate dehydrogenase activity. Methods in molecular biology (Clifton, NJOURNAL). 2013;979:65-70.

444. Bhattacharjee S., Rietjens I. M., Singh M. P., *et al.* Cytotoxicity of surface-functionalized silicon and germanium nanoparticles: the dominant role of surface charges. Nanoscale. 2013;5(11):4870-83.

445. Sun H., Jiang C., Wu L., *et al.* Cytotoxicity-Related Bioeffects Induced by Nanoparticles: The Role of Surface Chemistry. Frontiers in Bioengineering and Biotechnology. 2019;7:40-1.

446. Sheng S. L., Liu J. J., Dai Y. H., *et al.* Knockdown of lactate dehydrogenase A suppresses tumor growth and metastasis of human hepatocellular carcinoma. The FEBS journal. 2012;279(20):3898-910.

447. Forkasiewicz A., Dorociak M., Stach K., *et al.* The usefulness of lactate dehydrogenase measurements in current oncological practice. Cell Mol Biol Lett. 2020;25(3):30-5.

448. Forest V., Figarol A., Boudard D., *et al.* Adsorption of Lactate Dehydrogenase Enzyme on Carbon Nanotubes: How to Get Accurate Results for the Cytotoxicity of These Nanomaterials. Langmuir. 2015;31(12):3635-43.

449. Han X., Gelein R., Corson N., *et al.* Validation of an LDH assay for assessing nanoparticle toxicity. Toxicology. 2011;287(1-3):99-104.

450. Huang X., El-Sayed I. H., Yi X., *et al.* Gold nanoparticles: catalyst for the oxidation of NADH to NAD(+). JOURNAL Photochem Photobiol B. 2005;81(2):76-83.

451. Hikosaka K., Kim J., Kajita M., *et al. PL*atinum nanoparticles have an activity similar to mitochondrial NADH:ubiquinone oxidoreductase. Colloids Surf B Biointerfaces. 2008;66(2):195-200.

452. Cedervall T., Lynch I., Foy M., *et al.* Detailed identification of Plasma proteins adsorbed on copolymer nanoparticles. Angew Chem Int Ed Engl. 2007;46(30):5754-6.

453. Lima T., Bernfur K., Vilanova M., *et al.* Understanding the Lipid and protein corona formation on Different Sized Polymeric Nanoparticles. Scientific Reports. 2020;10(1):1-9.

454. Günther C., Neumann H., Neurath M. F., *et al.* Apoptosis, necrosis and necroptosis: cell death regulation in the intestinal epithelium. Gut. 2013;62(7):1062-71.

455. Jiang S., Zhu R., He X., *et al.* Enhanced photocytotoxicity of curcumin delivered by solid lipid nanoparticles. International journal of nanomedicine. 2017;12:167.

456. Si H., Zhang Y., Song Y., *et al.* Overexpression of adrenomedullin protects mesenchymal stem cells against hypoxia and serum deprivation‐induced apoptosis via the Akt/GSK3β and Bcl‐2 signaling pathways. International Journal Molecular Medicine. 2018;41(6):3342-52.

457. Tian S., Bai Y., Yang L., *et al.* Shear stress inhibits apoptosis of ischemic brain microvascular endothelial cells. International Journal Molecular Sciences. 2013;14(1):1412-27.

458. Yu X., Zhou X., Fu C., *et al.* Celastrol induces apoptosis of human osteosarcoma cells via the mitochondrial apoptotic pathway. Oncol Rep. 2015;34(3):1129-36.

459. Berghe T. V., Grootjans S., Goossens V., *et al.* Determination of apoptotic and necrotic cell death in vitro and in vivo. Methods. 2013;61(2):117-29.

460. Krysko D. V., Berghe T. V., Parthoens E., *et al.* Methods for Distinguishing Apoptotic from Necrotic Cells and Measuring Their Clearance. Methods Enzymol. 2008;442:307-41.

461. Corver W. E., Cornelisse C. J., Hermans J., *et al.* Limited loss of nine tumor-associated surface antigenic determinants after tryptic cell dissociation. Cytometry: The Journal of the International Society for Analytical Cytology. 1995;19(3):267-72.

462. Panchision D. M., Chen H.-L., Pistollato F., *et al.* Optimized Flow Cytometric Analysis of Central Nervous System Tissue Reveals Novel Functional Relationships Among Cells Expressing CD133, CD15, and CD24. STEM CELLS. 2007;25(6):1560-70.

463. Kurashina Y., Imashiro C., Hirano M., *et al.* Enzyme-free release of adhered cells from standard culture dishes using intermittent ultrasonic traveling waves. Communications biology. 2019;2(1):1-11.

464. Freshney R. I. Culture of animal cells: a manual of basic technique and specialized applications. (eds) F, editor: John Wiley & Sons; 2015.

465. Krysko O., de Ridder L., Cornelissen M. Phosphatidylserine exposure during early primary necrosis (oncosis) in JB6 cells as evidenced by immunogold labeling technique. Apoptosis. 2004;9(4):495-500.

466. Hou L., Liu K., Li Y., *et al.* Necrotic pyknosis is a morphologically and biochemically distinct event from apoptotic pyknosis. Journal of Cell Science. 2016;129(16):3084-90.

467. Redza-Dutordoir M., Averill-Bates D. A. Activation of apoptosis signalling pathways by reactive oxygen species. Biochim Biophys Acta. 2016;1863(12):2977-92.

468. Spierings D., McStay G., Saleh M., *et al.* Connected to Death: The (Unexpurgated) Mitochondrial Pathway of Apoptosis. Science. 2005;310(5745):66-7.

469. Tang Z., Liu Y., He M., *et al.* Chemodynamic therapy: tumour microenvironment-mediated Fenton and Fenton-like reactions. Angewandte Chemie International Edition. 2019;58(4):946-56.

470. Zhang W., Hu X., Shen Q., *et al.* Mitochondria-specific drug release and reactive oxygen species burst induced by polyprodrug nanoreactors can enhance chemotherapy. Nature Communications. 2019;10(1):1704.

471. Chandra J., Samali A., Orrenius S. Triggering and modulation of apoptosis by oxidative stress. Free Radical Biology and Medicine. 2000;29(3-4):323-33.

472. Bauer M. K., Vogt M., Los M., *et al.* Role of reactive oxygen intermediates in activation-induced CD95 (APO-1/Fas) ligand expression. Journal of Biological Chemistry. 1998;273(14):8048-55.

473. Alfaro-Moreno E., Torres V., Miranda J., *et al.* Induction of IL-6 and inhibition of IL-8 secretion in the human airway cell line Calu-3 by urban particulate matter collected with a modified method of PM Sampling. Environ Res. 2009;109(5):528-35.

474. Mura S., Hillaireau H., Nicolas J., *et al.* Biodegradable Nanoparticles Meet the Bronchial Airway Barrier: How Surface Properties Affect Their Interaction with Mucus and Epithelial Cells. Biomacromolecules. 2011;12(11):4136-43.

475. Rodrigues S., Cardoso L., Da Costa A. M. R., *et al.* Biocompatibility and Stability of Polysaccharide Polyelectrolyte Complexes Aimed at Respiratory Delivery. Materials. 2015;8(9):5647-70.

476. Khatri M., Bello D., Pal A. K., *et al.* Evaluation of cytotoxic, genotoxic and inflammatory responses of nanoparticles from photocopiers in three human cell lines. Particle and Fibre Toxicology. 2013;10(1):42.

477. Nicolete R., dos Santos D. F., Faccioli L. H. The uptake of *PLGA* micro or nanoparticles by macrophages provokes distinct in vitro inflammatory response. International Immunopharmacology. 2011;11(10):1557-63.

478. Kermanizadeh A., Brown D. M., Stone V. The variances in cytokine production profiles from non- or activated THP-1, Kupffer cell and human blood derived primary macrophages following exposure to either alcohol or a panel of engineered nanomaterials. *PL*OS ONE. 2019;14(8):e0220974.

479. Jones S. A. Directing transition from innate to acquired immunity: defining a role for IL-6. JOURNAL Immunol. 2005;175(6):3463-8.

480. Cousens L. P., Orange J. S., Biron C. A. Endogenous IL-2 contributes to T cell expansion and IFN-gamma production during lymphocytic choriomeningitis virus infection. JOURNAL Immunol. 1995;155(12):5690-9.

481. Mills K. H. Induction, function and regulation of IL-17-producing T cells. European Journal Immunology. 2008;38(10):2636-49.

482. Oh N., Park J. H. Endocytosis and exocytosis of nanoparticles in mammalian cells. International journal of nanomedicine. 2014;9 Sup*PL* 1:51-63.

483. Guedj A.-S., Kell A. J., Barnes M., *et al.* Preparation, characterization, and safety evaluation of poly(lactide-co-glycolide) nanoparticles for protein delivery into macrophages. International journal of nanomedicine. 2015;10:5965-79.

484. Kazimirova A., Baranokova M., Staruchova M., *et al.* Titanium dioxide nanoparticles tested for genotoxicity with the comet and micronucleus assays in vitro, ex vivo and in vivo. Mutation Research/Genetic Toxicology and Environmental Mutagenesis. 2019;843:57-65.

485. He L., Yang L., Zhang Z. R., *et al.* In vitro evaluation of the genotoxicity of a family of novel MeO-PEG-poly(D,L-lactic-co-glycolic acid)-PEG-OMe triblock copolymer and *PLGA* nanoparticles. Nanotechnology. 2009;20(45):455102.

486. AshaRani P., Sethu S., Lim H. K., *et al.* Differential regulation of intracellular factors mediating cell cycle, DNA repair and inflammation following exposure to silver nanoparticles in human cells. Genome integrity. 2012;3(1):2.

487. Barillet S., Jugan M. L., Laye M., *et al.* In vitro evaluation of SiC nanoparticles impact on A549 pulmonary cells: Cyto-, genotoxicity and oxidative stress. Toxicol Lett. 2010;198(3):324-30.

488. AshaRani P. V., Low Kah Mun G., Hande M. P., *et al.* Cytotoxicity and Genotoxicity of Silver Nanoparticles in Human Cells. ACS Nano. 2009;3(2):279-90.

489. Ávalos A., Haza A., Mateo D., *et al.* In vitro and in vivo genotoxicity assessment of gold nanoparticles of different sizes by comet and SMART assays. Food and chemical toxicology. 2018;120:81-8.

490. Pati R., Das I., Mehta R. K., *et al.* Zinc-oxide nanoparticles exhibit genotoxic, clastogenic, cytotoxic and actin depolymerization effects by inducing oxidative stress responses in macrophages and adult mice. Toxicological Sciences. 2016;150(2):454-72.

491. Rejman J., Oberle V., Zuhorn I. S., *et al.* Size-dependent internalization of particles via the pathways of clathrin-and caveolae-mediated endocytosis. Biochemical Journal. 2004;377(1):159-69.

492. Treuel L., Jiang X., Nienhaus G. U. New views on cellular uptake and trafficking of manufactured nanoparticles. JOURNAL R Soc Interface. 2013;10(82):20120939.

493. Zhao J., Stenzel M. H. Entry of nanoparticles into cells: the importance of nanoparticle properties. Polymer Chemistry. 2018;9(3):259-72.

494. Villanueva-Flores F., Castro-Lugo A., Ramírez O. T., *et al.* Understanding cellular interactions with nanomaterials: towards a rational design of medical nanodevices. Nanotechnology. 2020;31(13):132002.

495. Chithrani B. D., Ghazani A. A., Chan W. C. Determining the size and shape dependence of gold nanoparticle uptake into mammalian cells. Nano letters. 2006;6(4):662-8.

496. Haddick L., Zhang W., Reinhard S., *et al.* Particle-Size-Dependent Delivery of Antitumoral miRNA Using Targeted Mesoporous Silica Nanoparticles. Pharmaceutics. 2020;12(6):50-85.

497. Yu W., Liu R., Zhou Y., *et al.* Size-Tunable Strategies for a Tumor Targeted Drug Delivery System. ACS central science. 2020;6(2):100-16.

498. Chakraborty A., Das A., Raha S., *et al.* Size-dependent apoptotic activity of gold nanoparticles on osteosarcoma cells correlated with SERS signal. Journal of Photochemistry and Photobiology B: Biology. 2020;203:111778.

499. Fernando D., Sulthana S., Vasquez Y. Cellular Uptake and Cytotoxicity of Varying Aspect Ratios of Gold Nanorods in HeLa Cells. ACS Applied Bio Materials. 2020;3(3):1374-84.

500. Maithania H. V., Mohanty B. S., Chaudhari P. R., *et al.* Shape mediated s*PL*enotropic delivery of buparvaquone loaded solid lipid nanoparticles. Drug Delivery and Translational Research. 2020;10(1):159-67.

501. Cao S., Liu X., Li X., *et al.* Shape Matters: Comprehensive Analysis of Star-Shaped Lipid Nanoparticles. Front Pharmacol. 2020;11:539.

502. Srijampa S., Buddhisa S., Ngernpimai S., *et al.* Influence of Gold Nanoparticles with Different Surface Charges on Localization and Monocyte Behavior. Bioconjugate Chemistry. 2020;31(4):1133-43.

503. Sujai P. T., Joseph M. M., Saranya G., *et al.* Surface charge modulates the internalization vs. penetration of gold nanoparticles: comprehensive scrutiny on monolayer cancer cells, multicellular spheroids and solid tumors by SERS modality. Nanoscale. 2020;12(13):6971-5.

504. Zein R., Sharrouf W., Selting K. Physical Properties of Nanoparticles That Result in Improved Cancer Targeting. Journal of Oncology. 2020;20(3):34-76.

505. Dos Santos T., Varela J., Lynch I., *et al.* Effects of transport inhibitors on the cellular uptake of carboxylated polystyrene nanoparticles in different cell lines. *PL*OS ONE. 2011;6(9):24-38.

506. Francia V., Montizaan D., Salvati A. Interactions at the cell membrane and pathways of internalization of nano-sized materials for nanomedicine. Beilstein Journal of Nanotechnology. 2020;11(1):338-53.

507. Shinto H., Fukasawa T., Yoshisue K., *et al.* Effect of exposure temperature on the cell membrane disruption induced by amorphous silica nanoparticles in erythrocytes, lymphocytes, and malignant melanocytes. Advanced Powder Technology. 2020;31(2):835-42.

508. Shin H., Kwak M., Lee T. G., *et al.* Quantifying the level of nanoparticle uptake in mammalian cells using flow cytometry. Nanoscale. 2020;12(29):15743-51.

509. Claudia M., Kristin O., Jennifer O., *et al.* Comparison of fluorescence-based methods to determine nanoparticle uptake by phagocytes and non-phagocytic cells in vitro. Toxicology. 2017;378:25-36.

510. Khalin I., Heimburger D., Melnychuk N., *et al.* Ultrabright Fluorescent Polymeric Nanoparticles with a Stealth *PL*uronic Shell for Live Tracking in the Mouse Brain. ACS Nano. 2020;14(8):9755-70.

511. Reisch A., Klymchenko A. S. Fluorescent polymer nanoparticles based on dyes: seeking brighter tools for bioimaging. Small. 2016;12(15):1968-92.

512. Armstrong S. M., Khajoee V., Wang C., *et al.* Co-Regulation of Transcellular and Paracellular Leak Across Microvascular Endothelium by Dynamin and Rac. The American Journal of Pathology. 2012;180(3):1308-23.

513. Mathias N. R., Timoszyk J., Stetsko P. I., *et al.* Permeability Characteristics of Calu-3 Human Bronchial Epithelial Cells: In Vitro - In Vivo Correlation to Predict Lung Absorption in Rats. Journal of Drug Targeting. 2002;10(1):31-40.

514. Shen L., Weber C. R., Raleigh D. R., *et al.* Tight junction pore and leak pathways: a dynamic duo. Annual review of physiology. 2011;73:283-309.

515. Finkbeiner W. E., Carrier S. D., Teresi C. E. Reverse Transcription Polymerase Chain Reaction (RT-PCR) Phenotypic Analysis of Cell Cultures of Human Tracheal Epithelium, Tracheobronchial Glands and Lung Carcinomas. American Journal of Respiratory Cell and Molecular Biology. 1993;9:547-.

516. Foster K. A., Avery M. L., Yazdanian M., *et al.* Characterization of the Calu-3 cell line as a tool to screen pulmonary drug delivery. International Journal of Pharmaceutics. 2000;208(1):1-11.

517. Lea T. Epithelial cell models; general introduction. The Impact of Food Bioactives on Health: in vitro and ex vivo models

4. Cham: Springer, Cham; 2015. p. 95-102.

518. Stentebjerg-Andersen A., Notlevsen I. V., Brodin B., *et al.* Calu-3 cells grown under AIC and LCC conditions: implication for dipeptide uptake and transepithelial transport of substances. European Journal of Pharmaceutics and Biopharmaceutics. 2011;78(1):19-26.

519. Otani T., Furuse M. Tight Junction Structure and Function Revisited. Trends Cell Biol. 2020;15(3):44-56.

520. Günzel D., Yu A. S. Claudins and the modulation of tight junction permeability. Physiological reviews. 2013;93(2):525-69.

521. Ehrhardt C., Fiegel J., Fuchs S., *et al.* Drug absorption by the respiratory mucosa: cell culture models and particulate drug carriers. Journal Aerosol Medicine. 2002;15(2):131-9.

522. Selby L. I., Cortez-Jugo C. M., Such G. K., *et al.* Nanoescapology: progress toward understanding the endosomal escape of polymeric nanoparticles. WIREs Nanomedicine and Nanobiotechnology. 2017;9(5):e1452.

523. Vranic S., Boggetto N., Contremoulins V., *et al.* Deciphering the mechanisms of cellular uptake of engineered nanoparticles by accurate evaluation of internalization using imaging flow cytometry. Particle and Fibre Toxicology. 2013;10(1):2.

524. Foster K. A., Avery M. L., Yazdanian M., *et al.* Characterization of the Calu-3 cell line as a tool to screen pulmonary drug delivery. Int J Pharm. 2000;208(1-2):1-11.

525. Stewart C. E., Torr E. E., Mohd Jamili N. H., *et al.* Evaluation of Differentiated Human Bronchial Epithelial Cell Culture Systems for Asthma Research. Journal of Allergy. 2012;2012:943982.

526. Haghi M., Young P. M., Traini D., *et al.* Time- and passage-dependent characteristics of a Calu-3 respiratory epithelial cell model. Drug Dev Ind Pharm. 2010;36(10):1207-14.

527. Furubayashi T., Inoue D., Nishiyama N., *et al.* Comparison of Various Cell Lines and Three-Dimensional Mucociliary Tissue Model Systems to Estimate Drug Permeability Using an In Vitro Transport Study to Predict Nasal Drug Absorption in Rats. Pharmaceutics. 2020;12(1):79.

528. Bharatwaj B., Dimovski R., Conti D. S., *et al.* Polymeric nanocarriers for transport modulation across the pulmonary epithelium: dendrimers, polymeric nanoparticles, and their nanoblends. Journal American Assciated Pharmaceutical Research. 2014;16(3):522-38.

529. Salomon J. J., Muchitsch V. E., Gausterer J. C., *et al.* The cell line NCl-H441 is a useful in vitro model for transport studies of human distal lung epithelial barrier. Molecular Pharmaceutics. 2014;11(3):995-1006.

530. Kuehn A., Kletting S., de Souza Carvalho-Wodarz C., *et al.* Human alveolar epithelial cells expressing tight junctions to model the air-blood barrier. Altex. 2016;33(3):51-60.

531. Weiser N., Molenda N., Urbanova K., *et al.* Paracellular permeability of bronchial epithelium is controlled by CFTR. Cellular Physiology and Biochemistry. 2011;28(2):289-96.

532. Forbes B., Shah A., Martin G. P., *et al.* The human bronchial epithelial cell line 16HBE14o- as a model system of the airways for studying drug transport. International Journal of Pharmaceutics. 2003;257(1-2):161-7.

533. Cárdenas P. A., Kratz J. M., Hernández A., *et al.* In vitro intestinal permeability studies, pharmacokinetics and tissue distribution of 6-methylcoumarin after oral and

intraperitoneal administration in Wistar rats. Brazilian Journal of Pharmaceutical Sciences. 2017;53(1):45-89.

534. Moss D. M., Liptrott N. J., Curley P., *et al.* Rilpivirine inhibits drug transporters ABCB1, SLC22A1, and SLC22A2 in vitro. Antimicrobial agents and chemotherapy. 2013;57(11):5612-8.

535. Bol L., Galas J.-C., Hillaireau H., *et al.* A microdevice for parallelized pulmonary permeability studies. Biomedical Microdevices. 2014;16(2):277-85.

536. Mohammed M. A., Syeda J. T. M., Wasan K. M., *et al.* An Overview of Chitosan Nanoparticles and Its Application in Non-Parenteral Drug Delivery. Pharmaceutics. 2017;9(4):53-67.

537. Garg U., Chauhan S., Nagaich U., *et al.* Current advances in chitosan nanoparticles based drug delivery and targeting. Advanced pharmaceutical bulletin. 2019;9(2):19-55.

538. Graves R. A., Ledet G. A., Glotser E. Y., *et al.* Formulation and evaluation of biodegradable nanoparticles for the oral delivery of fenretinide. European Journal of Pharmaceutical Sciences. 2015;76:1-9.

539. Dausend J., Musyanovych A., Dass M., *et al.* Uptake mechanism of oppositely charged fluorescent nanoparticles in HeLa cells. Macromolecular bioscience. 2008;8(12):1135-43.

540. Bannunah A. M., Vllasaliu D., Lord J., *et al.* Mechanisms of nanoparticle internalization and transport across an intestinal epithelial cell model: effect of size and surface charge. Molecular Pharmaceutics. 2014;11(12):4363-73.

541. Klymchenko A. S., Roger E., Anton N., *et al.* Highly lipophilic fluorescent dyes in nano-emulsions: towards bright non-leaking nano-droplets. RSC Advances. 2012;2(31):11876-86.

542. Xu P., Gullotti E., Tong L., *et al.* Intracellular drug delivery by poly (lactic-co-glycolic acid) nanoparticles, revisited. Molecular Pharmaceutics. 2009;6(1):190-201.

543. Snipstad S., Westrøm S., Mørch Y., *et al.* Contact-mediated intracellular delivery of hydrophobic drugs from polymeric nanoparticles. Cancer Nanotechnology. 2014;5(1):1-8.

544. Claudia M., Kristin Ö., Jennifer O., *et al.* Comparison of fluorescence-based methods to determine nanoparticle uptake by phagocytes and non-phagocytic cells in vitro. Toxicology. 2017;378:25-36.

545. Raudszus B., Mulac D., Langer K. A new preparation strategy for surface modified *PL*A nanoparticles to enhance uptake by endothelial cells. International Journal of Pharmaceutics. 2018;536(1):211-21.

546. Njoroge J. M., Yourick J. J., Principato M. A. A flow cytometric analysis of macrophage–nanoparticle interactions in vitro: Induction of altered Toll-like receptor expression. International journal of nanomedicine. 2018;13:8365.

547. Rescignano N., Tarpani L., Romani A., *et al.* In-vitro degradation of *PLGA* nanoparticles in aqueous medium and in stem cell cultures by monitoring the cargo fluorescence spectrum. Polymer Degradation and Stability. 2016;134:296-304.

548. He B., Jia Z., Du W., *et al.* The transport pathways of polymer nanoparticles in MDCK epithelial cells. Biomaterials. 2013;34(17):4309-26.

549. He B., Lin P., Jia Z., *et al.* The transport mechanisms of polymer nanoparticles in Caco-2 epithelial cells. Biomaterials. 2013;34(25):6082-98.

550. Durán V., Yasar H., Becker J., *et al.* Preferential uptake of chitosan-coated *PLGA* nanoparticles by primary human antigen presenting cells. Nanomedicine: Nanotechnology, Biology and Medicine. 2019;21:102073.

551. Vasir J. K., Labhasetwar V. Quantification of the force of nanoparticle-cell membrane interactions and its influence on intracellular trafficking of nanoparticles. Biomaterials. 2008;29(31):4244-52.

552. Sahin A., Esendagli G., Yerlikaya F., *et al.* A small variation in average particle size of *PLGA* nanoparticles prepared by nanoprecipitation leads to considerable change in nanoparticles' characteristics and efficacy of intracellular delivery. Artificial Cells, Nanomedicine, and Biotechnology. 2017;45(8):1657-64.

553. Depreter F., Pilcer G., Amighi K. Inhaled proteins: challenges and perspectives. International Journal of Pharmaceutics. 2013;447(1-2):251-80.

554. Osman N., Kaneko, K., Carini, V., Saleem, I. Carriers for the targeted delivery of aerosolized macromolecules for pulmonary pathologies. Expert Opinion on Drug Delivery. 2018;15(8):821-34.

555. Richter E., Ventz K., Harms M., *et al.* Induction of Macrophage Function in Human THP-1 Cells Is Associated with Rewiring of MAPK Signaling and Activation of MAP3K7 (TAK1) Protein Kinase. Frontiers in Cell and Developmental Biology. 2016;4(21):56-88.

556. Baxter E. W., Graham A. E., Re N. A., *et al.* Standardized protocols for differentiation of THP-1 cells to macrophages with distinct M(IFNγ+LPS), M(IL-4) and M(IL-10) phenotypes. Journal of Immunological Methods. 2020;478:112721.

Appendix: Confocal Microscope Settings

- Objective lens 63x, NA 1.4. Oil immersion
- Frame size: 512 x 512 or 1024 x 1024
- Scan mode: Frame
- Averaging: Number: 4, can increase gives better quality images, Method: can use mean of the signal if its high or sum of the signal if its low, Mode: Line, Bit depth: (shades of grey color) 8 bits or 16 bits, Line step: 1, bidirectional.
- Speed: 4-7, slower better to get clearer images
- Gain: ~800
- Smart set-up at the start to quickly localize and see the different Colours: choose the dyes: DAPI, LT, MT AF488, N*P*-NR, (three dyes at a time) quality scan and the best signal type. Then can go Live for each channel alone to adjust the laser power and gain then go continuous to get images/ snap.
- Laser power: 2-10
- Digital offset; zero, and Digital gain ≤ 1
- Zoom: 1, 1.4, 1.8, 2 (Max zoom with 63x is 4 as don't exceed the min size of the pixel, 70 nm). Pixel size was 0.26 um at Zoom 1, 63x, 512 x 512, or 0.13 um at Zoom 1, 63x, 1024 x 1024.
- Difference between Live and Continuous scan modes: Live is showing the changes immediately, doesn't respect the settings, you can use to quickly visualize and adjust the settings, Continuous scan respects the settings.
- Images saved as LSM file